

Fluorescent toolboxes for reaction monitoring in microscopy and on the single-molecule level

Dissertation
zur Erlangung des Grades
des Doktors der Naturwissenschaften
der Naturwissenschaftlich-Technischen Fakultät III
Chemie, Pharmazie, Bio- und Werkstoffwissenschaften
der Universität des Saarlandes

Von

Dipl. Chem. Marcel Wirtz

Saarbrücken

Februar 2015

Tag des Kolloquiums: 27.03.2015

Dekan: Prof. Dr.-Ing. Dirk Bähre

Berichterstatter: Prof. Dr. Gregor Jung

Prof. Dr. Uli Kazmaier

.....

.....

Vorsitz: Prof. Dr. Claus Jacob

Akad. Mitarbeiter: Dr. Josef Zapp

Meinem Mann Markus Ettelbrück,
meinen Eltern Monika und Peter Wirtz,
meiner Schwester und Schwager Christina und Aidan Doyle,
meiner Schwester Bernadette Wirtz,
meinen Großeltern Katharina und Ludwig Wirtz

to

Mary Doyle

One of the loveliest persons I know,
unfortunately there was no more time

Danksagung

Ein großes Dankeschön gebührt **Prof. Gregor Jung** für die Möglichkeit, dieses spannende Themengebiet in seinem Arbeitskreis bearbeiten zu können. Ebenfalls möchte ich mich für das Vertrauen bedanken, dass er in mich gesetzt hat und für seinen schier grenzenlosen Optimismus, für die vielen motivierenden Gespräche und seine weitreichende Unterstützung, mit der es möglich war die gesetzten Ziele zu erreichen. Außerdem möchte ich Ihm für seine Stresstoleranz danken, die bei einem ungeduldigen Mitarbeiter tagesweise gefordert wird.

Ich danke auch **Prof. Uli Kazmaier** dafür, dass er diese Arbeit so schnell begutachtet und für seine tollen Vorlesungen, die mir die Werkzeuge für das Gelingen dieser Aufgaben vermittelt haben.

Ich möchte auch **Prof. Dirk-Peter Hertel**, **Prof. Oliver Trapp**, **Dr. Arina Rybina** und **Dr. Carolin Lang** für die tolle Zusammenarbeit in den letzten Jahren danken. Es war nicht nur ein Forschungsverbund, der sehr produktiv zusammengearbeitet hat, vielmehr ist ein engerer persönlicher Kontakt entstanden, den ich sehr schätze und der mir auch sehr am Herzen liegt. Die Projekttreffen waren aus diesen Gründen immer Motivationsschub für neue Aufgaben und eine erfrischende Abwechslung im Forschungsalltag.

Ich möchte auch meinen Arbeitskollegen und Bachelor-Studenten danken, die mir die zeitintensive Forschungsarbeit angenehmer gestaltet haben und mich dabei durch fruchtbare Diskussionen, ihr naturwissenschaftliches Know-how und ihre Arbeit unterstützt haben. Hier möchte ich besonders **Philipp Rebmann** herausstellen, der mich als Betreuer in seiner Bachelor Arbeit „ertragen“ musste.

Ich möchte auch meinen Kommilitonen und Freunden danken, die mich auf meinem bisherigen Weg unterstützt haben. Immer wenn die Forschung frustrierte, waren sie für mich da und haben mich wieder aufgebaut, um die bestehenden Hürden zu meistern.

Besonders möchte ich **Björn Finkler** nennen, mit dem ich über fachliches wie außerfachliches sprechen konnte und der immer ein offenes Ohr für Probleme hat. Er sagt seine ehrliche Meinung und man kann sich immer auf ihn verlassen. Ebenfalls möchte ich **Tobias Uhl** danken, der mich seit meiner Gymnasialzeit als treuer Freund begleitet und mit dem man durch dick und dünn gehen kann. **Achim Pitz**, **Erwin Conrad** und **Frank Schultze**

sind ebenfalls tolle Freunde, die mir immer mit Ihrer Lebenserfahrung und mit Rat und Tat zur Seite stehen. Ich möchte mich noch bei meinen beiden lieben Damen bedanken, **Kathrin Omlor** und **Caroline Wern**. Diese beiden bezaubernden Ladies schaffen es einem nach einem frustrierenden Tag ein Sonnenschein-Lächeln auf das Gesicht zu zaubern. Last but not least möchte ich **Thomas Kronenberger** und **Birgit Bernardi** danken, beide stehen mir immer als Freunde zur Seite und haben mir nicht nur die Musik, sondern auch viele praktische Dinge für das alltägliche Leben vermittelt. Darüber hinaus zeigte mir **Thomas**, wie man strukturiert an ein Problem herangeht und es zielorientiert löst. Vielen Dank euch beiden für die tolle Freundschaft

Neben meinen Freunden gilt mein größter Dank meiner Familie. Zu allererst meinen Eltern **Monika** und **Peter Wirtz** die mir diesen Weg überhaupt erst ermöglichten, mich mit fachlichem Knowhow sowie seelisch und moralisch immer unterstützen. Neben meinen Eltern waren meine Schwestern **Christina Doyle** und **Bernadette Wirtz** sowie meinem Schwager **Aidan Doyle** meine Stütze in Studium und Promotion. Alle haben mich in den schweren Phasen aufgebaut und mir geholfen weiter zu machen, auch wenn es einmal aussichtslos erschien. Sie haben mir dabei geholfen die Herausforderungen aus vielen Blickwinkeln zu betrachten, mir andere Denk- und Sichtweisen zu eröffnen und wenn es nötig war, mir nochmal den Kopf zurecht rücken. Es ist toll eine solche Familie im Hintergrund zu haben auf die man sich 150%ig verlassen kann.

Außerdem möchte ich meinen Schwiegereltern in Spe, **Jürgen** und **Uschi Ettelbrück**, danken, dafür, dass sie mir immer die Daumen drücken, mitfiebern und mich unterstützen, wenn wichtige Herausforderungen anstehen.

Mein letzter und größter Dank gebührt meinem Mann **Markus Ettelbrück**. Ohne seine Unterstützung, sein Verständnis, seine Hilfe hätte ich diesen Meilenstein in meinem Leben sicherlich nicht so gemeistert. Er half mir wo er konnte, baute mich immer wieder auf wenn ich zweifelte und war immer dann der Fels in der Brandung, wenn ein Sturm nahte und ich nicht standhaft erschien. Vielen Dank dafür mein größter Schatz der Welt.

Table of contents

Danksagung	I
Table of contents	III
1. Abstract	1
2. General Part	3
2.1. Introduction	3
2.1.1. <i>Single-molecule experiments for reaction monitoring</i>	3
2.1.2. <i>Objective target</i>	7
2.2. Reaction monitoring with fluorescent methods	8
2.2.1. <i>Fluorogenic visualization concepts (scheme 3 A)</i>	9
2.2.2. <i>Reaction monitoring using physical processes between a fluorophore and a second component (scheme 3 B)</i>	14
2.2.3. <i>Ratiometric single-molecule reaction monitoring (scheme 3 C)</i>	17
2.3. Fluorescent dyes.....	22
2.3.1. <i>Fluorescent dye classes</i>	22
2.3.2. <i>BODIPY dyes</i>	28
3. Epoxidation reaction^[1]	41
4. Cu^I-catalyzed azide-alkyne cyclization (CuAAC) - Click reaction^[4]	47
5. Metathesis reaction	54
6. Summary	62
7. Appendix	66
7.1. Epoxidation reaction.....	66
7.1.1. <i>General Experimental</i>	66
7.1.2. <i>Probe synthesis and analytical characterization</i>	67
7.1.3. <i>Spectra</i>	70
7.2. Cu ^I -catalyzed azide-alkyne cyclization (CuAAC) - Click reaction.....	89
7.2.1. <i>BODIPY derivatives and azides used for click reactions</i>	89
7.2.2. <i>Background signal in microscopy experiments</i>	90
7.2.3. <i>Comparison of alkyne-BODIPY and click transformation</i>	90
7.2.4. <i>Influence of the copper moiety onto fluorescence in microscopy</i>	91

Table of contents

7.2.5. General Experimental.....	95
7.2.7. Spectral data	108
7.3. Metathesis reaction	124
7.3.1. Further reactivity study of BODIPYlidene compound (2).....	124
7.3.2. Control experiments revealing reaction selectivity.....	125
7.3.3. Detailed description of the used kinetic model.....	127
7.3.4. ¹⁹ F-NMR kinetic analysis of α -vinyl BODIPY (1) and α -styryl BODIPY (3) formation.....	129
7.3.5. General Experimental.....	131
7.3.6. Synthetic procedures and characterization data.....	134
7.3.7. Spectra.....	139
8. Literature	146
9. List of abbreviations	161
10. Scientific contributions.....	162
Scientific journals.....	162
Scientific conferences.....	162
Poster presentations.....	162
Oral presentations.....	163

1. Abstract

Progress in research and chemical industry can be achieved with fundamental knowledge about organic reaction mechanisms delivered by spectroscopy. Single-molecule methods represent a new approach, which allow concurrent following of molecular processes and different reaction pathways in one experiment^[1-3]. For these techniques, fluorophores can be used which include reactive targets as part of the chromophore ("participant approach")^[3]. In this work, such fluorophores are presented containing double or triple bonds as reactive centers. Selective reactions at these structural motifs form new dyes with different optical parameters. These changes in fluorescence wavelength are used for reaction monitoring. Following the well-investigated epoxidation reaction by hypsochromic emission wavelength shift, a new detection method was introduced^[1]. Cu⁺ catalyzed azide-alkyne cycloadditions (CuAAC) firstly enabled reaction monitoring by a bathochromic shift of fluorescence wavelength via expanding the fluorophore^[4]. At last, the metathesis reaction was visualized on single-molecule level. Therefore, a metathesis reagent was synthesized, where the chromophore is located at a Ruthenium center as carbene. This compound represents a multichromophoric, fluorogenic metathesis intermediate^[5]. Reaction monitoring with fluorescence methods ranging from ensemble measurements to single-molecule experiments can only be enabled synthesizing described fluorophore systems.

Fortschritt in Forschung und chemischer Industrie kann durch die genaue Kenntnis der Mechanismen chemischer Umsetzungen mittels Spektroskopie erreicht werden. Die einzelmolekülspektroskopischen Methoden stellen eine neuen Möglichkeit dar, die es erlaubt gleichzeitig molekulare Prozesse und verschiedene Reaktionspfade in einem Experiment zu beobachten^[1,2]. Für diese Techniken können Fluorophore benutzt werden, die reaktive Gruppen als Teil des Chromophoren aufweisen^[3]. In dieser Arbeit werden Fluorophore vorgestellt, die Doppel- und Dreifachbindungen als reaktive Zentren besitzen. Selektive Reaktionen an diesen Struktureinheiten bilden neue Farbstoffe mit unterschiedlichen optischen Eigenschaften. Die neue Detektionsmethode wurde an der gut untersuchten Epoxidierungsreaktion mittels Blauverschiebung der

Emissionswellenlänge vorgestellt^[1]. Die Kupfer(I) katalysierte Azid-Alkin Zykoaddition ermöglichte zum ersten mal die Reaktionsverfolgung durch eine Rotverschiebung der Emissionswellenlänge mittels Erweiterung des Fluorophoren^[4]. Zuletzt wurde die Metathese-Reaktion auf Einzelmolekülebene visualisiert. Dafür wurde eine Metathese Reagenz synthetisiert, das den Chromophoren an einem Ruthenium-Zentrum als Carben angebracht hat. Diese Verbindung stellt ein multichromophores, fluorogenes Metathese Intermediat dar^[5]. Die Synthese solcher Farbstoff-Systeme ermöglicht die Reaktionsverfolgung mittels Fluoreszenzmethoden von Ensemble- bis hin zu Einzelmolekülexperimenten.

2. General Part

2.1. Introduction

2.1.1. Single-molecule experiments for reaction monitoring

The information about reaction mechanisms can lead to fundamental improvements in organic chemistry. Increased yield, selectivity or specificity can only be achieved, if all reaction steps are known and understood. Accordingly, reaction conditions or catalysts can be optimized achieving a more economical reaction balance^[6-8]. Various spectroscopic experiments^[9-11] have been successful in identifying the transformation steps. Kinetic data^[12-14] can be extracted by tracking the change of specific signals over time. Two different techniques can be used identify the origin of these changes. Extrinsic methods require a marker to be attached to the transformed molecule. Kinetic data can be obtained by monitoring the marker molecule's significant parameters (e.g. vibrational bands, NMR signals, diffusion time...) as its environment changes during the reaction ("spectator approach")^[15,16]. In an intrinsic method, the reaction monitoring system generally includes

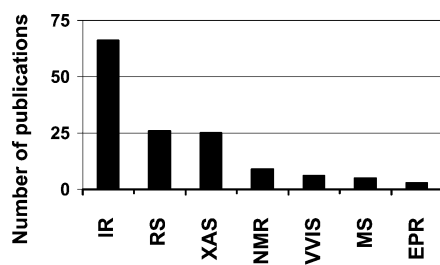


figure 1:
Numbers of publications for in situ reaction mechanism investigation for every spectroscopy method. [applied from^[21]]

specific reactive sides, which generate the required signals ("participant approach"). The benefit of the intrinsic method is that it permits the direct correlation of transformation and experimental signals^[17-20].

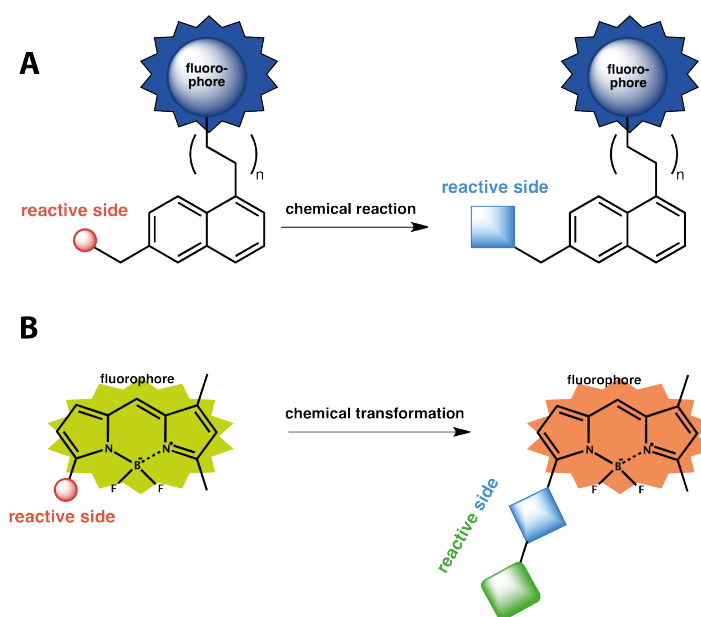
Currently, the two most used spectroscopy tools for reaction monitoring are IR and Raman spectroscopy (figure 1)^[21]. Both methods can be applied, if groups with specific vibration signals are transformed.

The reaction progress can be visualized by the change of specific absorption bands (e.g. of carbon-oxygen double bonds or amide bonds)^[22]. Other methods also exist, outside of vibrational spectroscopy, which can be used for mechanistic investigations. Oxidation states or coordinative states can be analyzed by XAS^[21]. In NMR experiments, changes of significant chemical shifts (e.g. ¹H: carbene-H, alkyne-H, double bond signals or ³¹P: Phosphine ligand signals, etc.) are correlated with the reactions progress. Consequently, information about the reaction steps and kinetics can be determined from the resulting data^[23-25]. UV-Vis absorption spectroscopy^[26,27] is a related method. As part of this approach,

a change in the component's absorption bands is required during the reaction^[21,26,27]. An entire reaction mechanism can be revealed through a combination of different spectroscopic experiments^[18,20,28].

Branching out from these common methods, reaction monitoring with fluorescence spectroscopy represents a new approach. Ensemble measurements provide a summarized view of a reaction^[1,29,30] and the resulting kinetic data can be analyzed to reveal applicability to single-molecule investigations. In microscopic experiments, one reaction participant has to be immobilized which, in turn, represents the particular reactive side. Single fluorescence signal traces of individual reactive centers can be monitored. Every possible reaction trajectory can be visualized through the analysis of this data. Furthermore, the frequency of each pathway and the transformations, which have taken place, can be illustrated. Consequently, it is possible to determine fast upstream processes or molecular changes (*e.g.* ligand diffusion, conformational reorganization, etc.) in the formation of a reactive state. This information is difficult to obtain within a single experiment, in conjunction with another spectroscopic investigation, due to time resolution or missing experimental focus (*e.g.* missing specific marker). Single-molecule fluorescence spectroscopy (SMFS) methods are analytical tools for the visualization of complete reaction mechanisms. These investigations include all possible pathways within a single experiment, on a molecule by molecule basis and as every chemist would wish for, with high time resolution and statistical validation^[1,3,31].

A well-characterized reaction-specific fluorophore system is required for single-molecule experiments^[1,3-5,32,33], as complete structural information must be ensured for all possible fluorescent states. Starting compounds, intermediates and products should be synthesized separately and completely characterized (NMR, X-ray, MS, UV-Vis, fluorescence,...)^[1,4,5]. The single-molecule experimental setup can be configured (excitation lasers, emission filters, dichroitic mirrors, etc.)^[33-36] using the data obtained from optical spectroscopy. Structural elucidation combined with appropriate fluorescence data enable single-molecule fluorescence signal assignment to the molecular interpretation in reaction progress. For these investigations, the fluorophore and the reactive group have to be connected. This combination can be achieved via two different techniques:



**scheme 1: Schematic visualization of fluorescent reaction monitoring systems:
A: "spectator" and B: "participant" approach.**

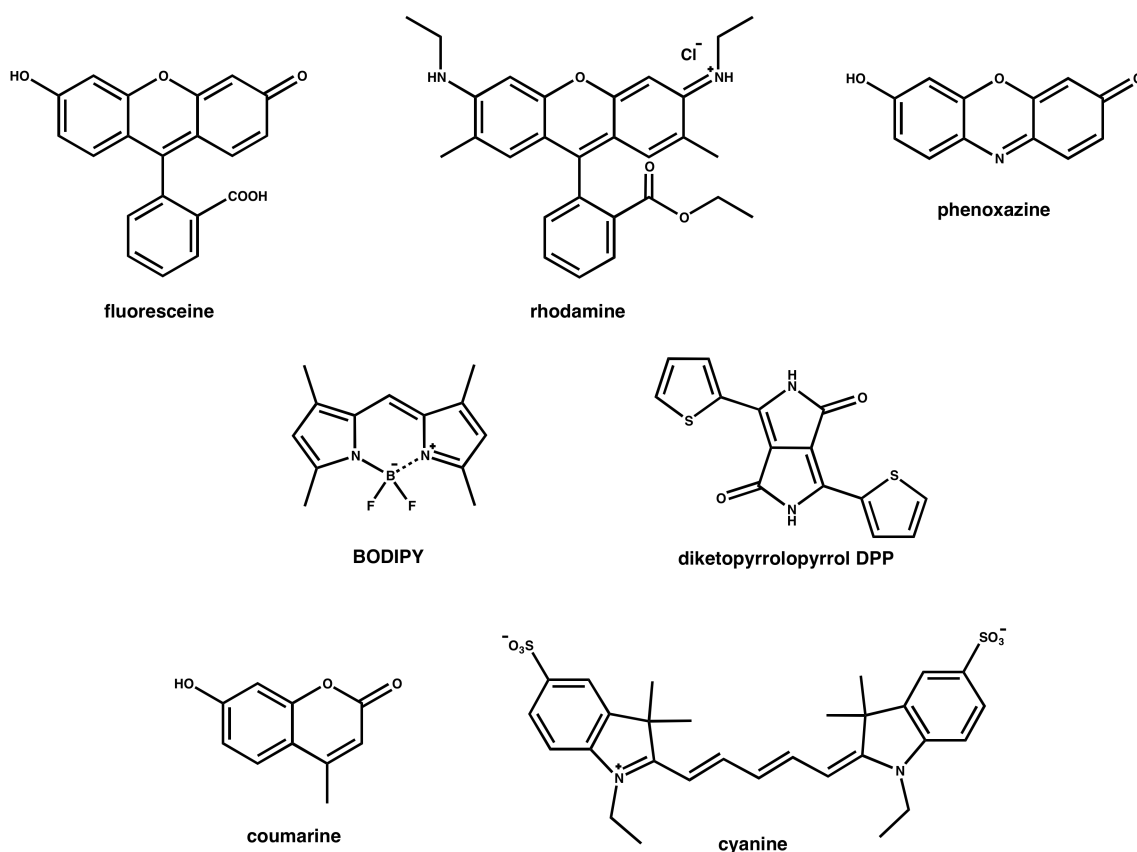
- A. The fluorophore and the reactive molecule can be linked via an inert molecular bridge (e.g. an alkyne chain). The fluorophore is not part of the reaction, he only accompanies the reactants. Any fluorophore can be used as label. Reaction details can be obtained using energy transfer processes like Förster Resonance Energy Transfer (FRET) between two fluorophores, fluorescence quenching, fluorophore orientation or by changing parameters like diffusion time. This type of fluorophore tagging is called the "spectator approach"^[3] and is used in single-molecule spectroscopy, indicating protein folding^[37,38], in-vivo enzyme kinetics^[39–42], protein-protein interactions^[43,44], chemical processes^[35,45] or polymeric orientation^[46,47] (scheme 1 **A**).
- B. The other possibility is the "participant approach" and is described in scheme 1 **B**. The reactive moiety is included in the chromophoric unit. The regiospecific reaction forms a new dye with different optical properties. Consequently, reaction tracking is facilitated through gradually shifting spectroscopic parameters (e.g. such as emission wavelength) as the reaction progresses (scheme 1 **B**).^[1,2,4,5,32]

Fluorescence reaction monitoring does not only require fluorescence labeling. The different microscopic approaches utilize cover glasses where reactive centers or fluorophores have to be immobilized. Therefore, physical absorption or covalent bonding

can be used^[37]. Macroscopic networks like polymers or enzymes are located on surfaces via Van-der Waals interaction. Reactive components can be located at the polymeric backbone or side chains as reactive derivatization accessible for reaction partners (e.g. azide functionalized agarose beads^[4]^[32]). Fluorophores, covalently bound onto the surface, have to be attached via a chemical reaction. Silanes are most commonly employed for surface functionalization because they can react with free hydroxy groups of the siloxane in condensation reaction^[1,5,48]. These silanes comprise of the desired reactive moieties for reaction monitoring, as different alkenes^[5] or fluorescent, reactive dyes for "participant approach"^[1].

Both immobilization strategies are used in single-molecule investigations^[3]. Localization via physical adsorption limits the experimental application because the addition of solved reaction partners annihilates the Van-der Waals attraction^[4]. Then, the adsorbed molecules have the ability to diffuse away out of the adjusted focus. For this reason, monitoring reactions of the same molecule is extremely difficult. This drawback can be circumvented through the use of covalent bonding. The molecule is located at the surface, so the addition or even exchange of reagents can be easily applied^[1,5,29]. The difficulty lies within the siloxane preparation and the condensation reaction conditions due to the instability of the introduced reactive groups.

The fluorophores administered require very specific optical properties. The optical fluorophore characteristics required for single-molecule experiments^[45,49-51] include a high fluorescence quantum yield, high photostability, sharp absorption and emission bands and large Stokes shifts. A large variety of usable dyes exist (scheme 2), which fulfill most of the necessary requirements.



scheme 2: A variety of fluorophores usable in microscopy and single-molecule experiments^[52].

BODIPY dyes represent the best combination of all prerequisite factors (see chapter 2.3)^[53–55]. Looking beyond the optical properties, the chemical access to this dye class is relatively straightforward. The scaffold synthesis reveals moderate yields and a lot of chemical transformations exist at the core. These dyes are highly soluble in organic solvents, are unaffected by their environment and exhibit an uncharged chromophore^[52,56–59].

2.1.2. Objective target

The chromophoric system is the most important element of a single-molecule reaction investigation. The different optical properties of the fluorophores specify the existing experimental setup and the known localization procedures limit their molecular structure. Appropriate dye systems, which enable selective reaction visualization, are missing. The biggest insights into transformations and the most data are achieved via the “participant approach”. Therefore, appropriate, stable fluorophores are required.

The chromophores have to contain one side for immobilization and one selective, specific structural motif, where the reaction can proceed. The starting compounds, intermediates and final products of a reaction have to be synthesized separately, in sufficient quantity, to assign optical properties (e.g. fluorescence wavelength) and structure.

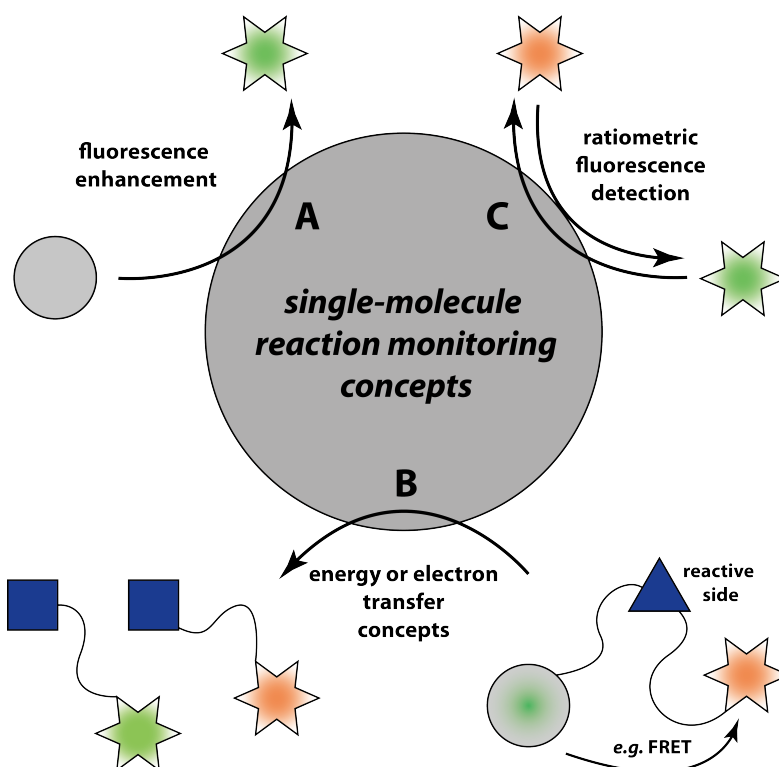
In this work, three different fluorescent systems were synthesized to investigate three different reactions. The first one enables the monitoring of an epoxidation reaction, based on the work of Alex Schmitt^[60]. Next, triple bond derivatized BODIPYs were used for the investigation of Cu⁺ catalyzed alkyne-azide cyclization (CuAAC). The starting compound and corresponding triazole product were synthesized. Then, the structural information of both molecules was estimated, so that their optical parameters could be compared. Both emission maxima were separated enabling fluorescence reaction visualization of triazole formation via Click reaction. The knowledge of both emission signals enabled the assignment of starting substrate and formed product in microscopic reaction visualization. A more complex system was developed for tracking the metathesis reaction, which required the synthesis of the starting compound, the final product and a reactive carbene intermediate of a cross metathesis. The isolation and characterization of the reactive Ruthenium-BODIPYlidene metathesis reagent was the most challenging aspect of this investigation.

The single-molecule spectroscopic techniques could be adapted for visualization of three different chemical reactions using these fluorophore systems. These investigations permitted the observation of different reaction pathways and the collection of missing mechanistic information.

2.2. Reaction monitoring with fluorescent methods

Fluorescence methods were first applied to monitor enzymatic transformations^[61,62]. In such studies fluorogenic probes were converted to strongly fluorescent molecules (scheme 3 A)^[63,64]. Energy or electron transfer concepts provide another approach usable for tracking (scheme 3 B)^[65-67]. Enzymes were immobilized on cover glasses and solutions of reactive fluorogenic or profluorescent substrates were added. The reactive sides of enzymes could be located and transformations could be visualized by analyzing fluorescent bursts with their emission time trace^[68]. The ratiometric concept provides the most important insights into reaction monitoring. At the catalytic center of the enzyme, the chromophore is transformed during the reaction, which results in a different emission wavelength. The relative change in emission intensity of both species reveal the associated kinetic data^[69,70].

In enzymology, these methods are often used because it is possible to identify the location of the reactive centers and intensity-time analysis delivers the required catalytic turnover rates. This approach has been established as the standard method for characterizing enzyme activity and is now being transferred for use in the characterization of chemical reactions^[68,71].



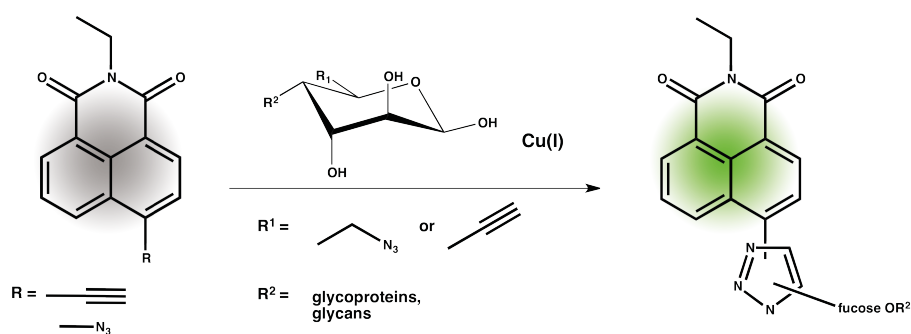
scheme 3: Different methods used for reaction monitoring in ensemble and single-molecule measurements.

2.2.1. Fluorogenic visualization concepts (scheme 3 A)

Reaction monitoring with fluorogenic probes only enables product formation signal tracking. In this approach, starting compounds are non-fluorescent or the emission signal is suppressed by transfer processes. During the reaction, this pre-fluorescent state is discarded and a fluorescence signal is observed.

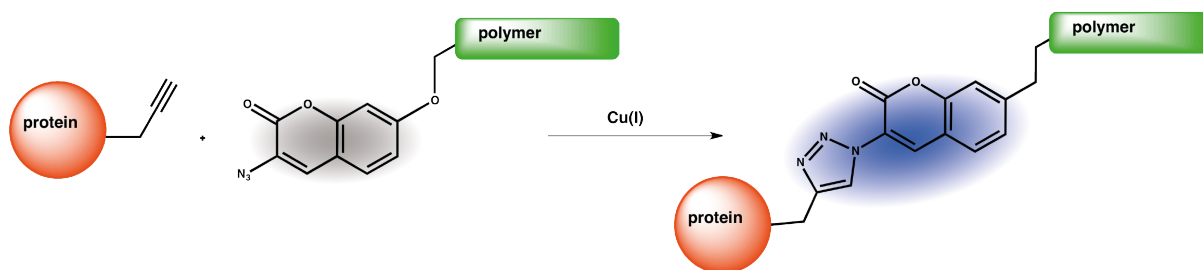
Ensemble measurements

Click reactions were often visualized by ensemble fluorescence enhancement methods^[72-75]. One approach involves the use of probes, which only exhibit fluorescence in the UV range of the electromagnetic spectrum^[76]. They applied an alkyne functionalized 1,8-naphthalimide, which slightly observes fluorescence in the UV region. These compounds were coupled with a corresponding 6-modified fucose. Fluorescence increase was established by formation of triazole moiety^[76].



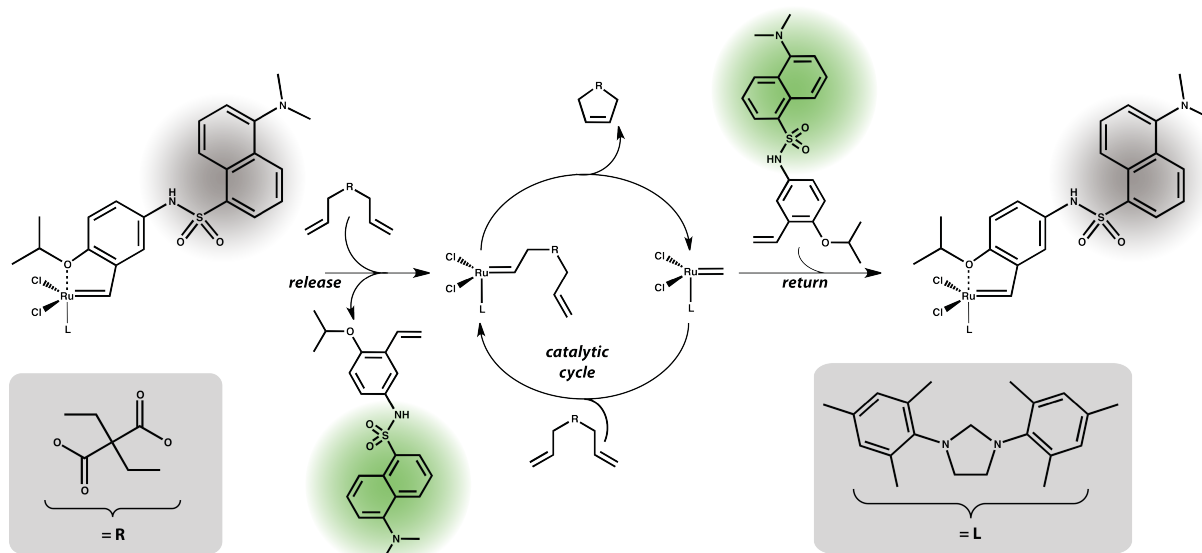
scheme 4: Fluorogenic click reaction by Sawa et al.^[76].

Another approach consists of quenching the substrate fluorescence using energy transfer processes, e.g. in the click reaction^[77,78]. The triazole ring is formed during the reaction, which results in the emergence of a fluorescence signal. A Coumarine and a BODIPY derivative served as chromophores.



scheme 5: Fluorogenic click reaction with quenched fluorophores as starting compounds. Dirks et al. used this approach for combination of a protein and a polymer compound^[77].

Not only CuAAC reactions can be visualized through the application of fluorescence enhancement methods. Metathesis can also be illustrated using fluorescence enhancement. The first fluorogenic metathesis catalyst was synthesized by Plenio et al.^[79]. A chromophore was added to a Hoveyda-Grubbs catalyst to estimate the significance of the release-return mechanism in olefin metathesis. The mechanism, investigated by Hoveyda et al.^[80], describes the formation of the reactive species of a metathesis catalyst with a styrenyl isopropyl ether ligand in the initiation steps of the reaction.



scheme 6: Release-return initiation mechanism for Hoveyda-Grubbs catalysts^[80] adapted to the investigations by Plenio et al.^[79].

Plenio et al. synthesized an analogue catalyst, where a quenched dansyl dye was located at the carbenoid side (scheme 6)^[79]. In the first initiation step, the coordinately attached carbene ether was released via an exchange through the olefin compound. The ligand separation from the metal center restored the fluorescence of the included dansyl chromophore. A fluorescence signal could be detected (scheme 6 “release”). Through this ligand separation, a reactive 14 valence electron complex was formed. This reactive species entered the catalytic cycle and performed a metathesis reaction (scheme 6 “catalytic cycle”). According to Hoveyda, the unreactive catalyst state was restored by rearrangement of the benzylidene ether ligand. This behavior should reduce the emission signal from dansyl dye in fluorescence analysis due to re-approved quenching (scheme 6 “return”).

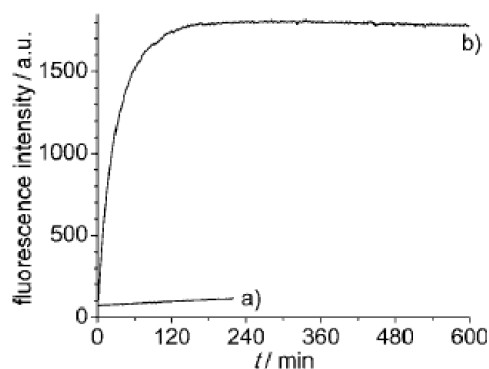


figure 2: Fluorescence intensity behavior of Plenio's metathesis catalyst in ensemble measurements: a) in toluene solution b) during RCM [traces applied from ^[79]]

Similar signal behavior was not found in the aftermath of the metathesis reaction. Instead, the fluorescence intensity remained almost constant (figure 2 b). Consequently, the return mechanism seemed not to be as revalent in the reaction mechanism^[79].

The monitoring of reactions using fluorogenic methods are not limited to use in ensemble measurements. Single-molecule investigations also exist using the same approach.

Single-molecule investigations

Roeflaers et al. visualized first reactions with a fluorogenic reaction system^[36]. A catalyzed ester hydrolysis and a transesterification reaction were both monitored using hydroxide crystals. Fluoresceine diacetate served as a fluorogenic probe and a lithium-aluminium-hydroxide single crystal fulfilled both the roles of a catalyst and an immobilized reactive side. Analysis of the appearance of single bursts, revealed that transesterification reactions are catalyzed at the outer crystal plane instead of hydrolysis, which is catalyzed by lateral crystal faces^[36].

Esfandiari et al. investigated the ligand exchange at a platinum metal center with a pre-fluorescent probe^[29]. They synthesized an aqua platinum complex including a BODIPY chromophore. This molecule could react with a sulfur-functionalized surface to permit real time imaging of a Pt-S ligand exchange. Variations in the ligand sphere were made visible by the emerging fluorescence. A cover glass was surface-substituted containing alternating stripes, one with and one without sulfur. After the addition of the platinum complex, the sulfur molecules transferred to the palladium metal and were bound to the surface. Excitation revealed single-molecule fluorescence (figure 3)^[29].

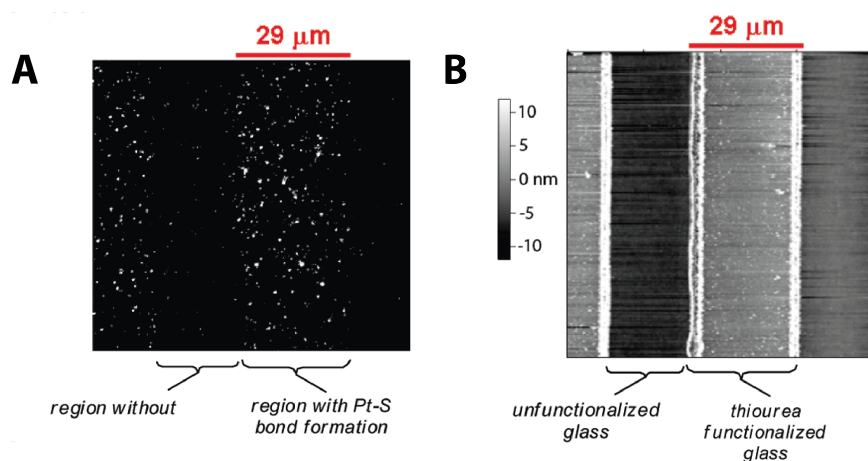


figure 3: Single-molecule experiment for visualization of H₂O - S ligand exchange at Pt complexes [applied from ^[29]].

Hofkens, Roeffaers and coworkers published a fluorogenic approach for detection of an oxirane formation^[2]. This group presented the epoxidation of a BODIPY double bond via *tert*-butylperoxide, which was catalyzed by Ti-MCM-41 (a mesoporous titano silica supporting material). They synthesized a phenyl-butadienyl-substituted BODIPY probe, which could be epoxidized at two alternating double bonds (figure 4).

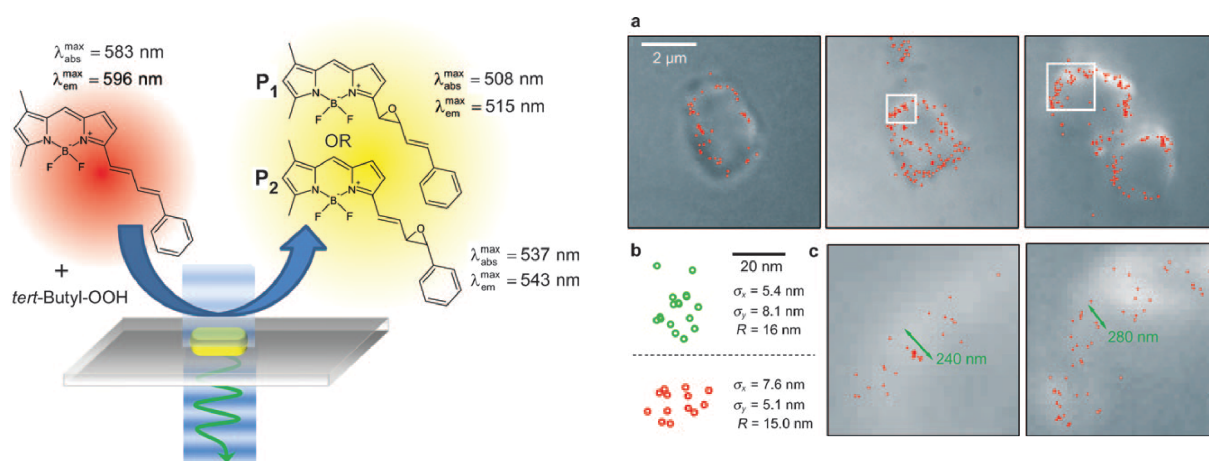


figure 4: Epoxidation of phenylbutadienyl-BODIPY with *tert*-butylperoxide catalyzed by Ti-MCM-41. [adapted from ^[2]]

Epoxidation shortens the chromophoric unit resulting in a hypsochromic fluorescence wavelength shift of about 50 to 80 nm. Visualization via total internal reflection fluorescence (TIRF) microscopy was established by locating the peroxide containing supporting material on a cover glass surface. The focal plane was investigated by suppressing emissions from catalytic events at its top or bottom. Detection of the epoxide product formed, using fluorescence enhancement, revealed the active side of the Ti-MCM-41 catalyst. The investigations showed that product formation mainly takes place at the outer sphere of a Ti-MCM-41 particle^[81].

Pre-fluorescent methods can also be used to determine molecular orientation. Mecking et al. established the synthesis of a Hoveyda type metathesis catalyst by including a fluorescence label. The perylene diimide tag is located at the aryloxy moiety, which is transferred onto the reactive partners. This catalyst was used for synthesis of polyethylene nanoparticles. In the last step, the perylene moiety is transferred onto the polyethylene chain. Using defocus patterns in single-molecule analysis, the orientation of the nanoparticles can be estimated (figure 5)^[82].

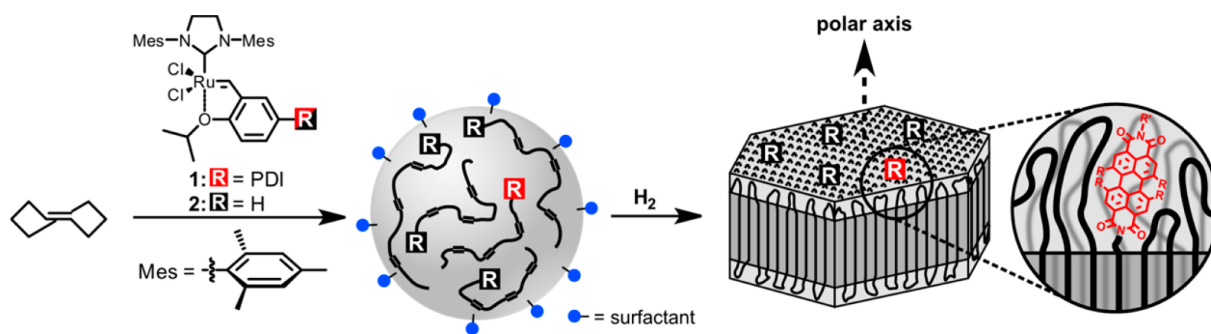


figure 5: PE nano crystal synthesis using perylene diimide substituted metathesis catalyst.
[applied from ^[82]]

Fluorescence enhancement methods only deliver information about specific reaction steps depending on the tailored pre-fluorescent system. Complete monitoring from the initiation to final product formation cannot be examined in its entirety. A more detailed insight into reaction behavior can be achieved using physical processes.

2.2.2. Reaction monitoring using physical processes between a fluorophore and a second component (scheme 3 B)

Different physical interactions can be observed between a fluorophore and another compound. The fluorescence signal of two fluorophores depends on their distance and their spectral overlap. Resonance energy transfer (RET) occurs (figure 6 top); if both molecules are spatially close and their optical bands exhibit spectral overlap. This interaction relies on the physical phenomenon of dipole - dipole interaction between a donor (D) and an acceptor molecule (A). The donor molecule D is treated as an oscillating dipole, which starts oscillating after absorbing light energy. A second dipole with a similar resonance frequency represents the acceptor molecule (A). This second molecule oscillation is initiated via interaction with the first one. As a result, the emission signal of the acceptor molecule A is observed. Such energy transfers occur without the appearance of a photon. RET is also known as Förster resonance energy transfer (FRET)^[83].

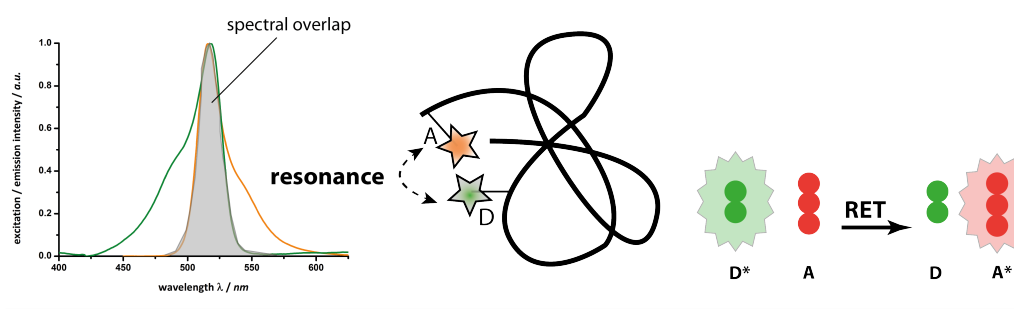
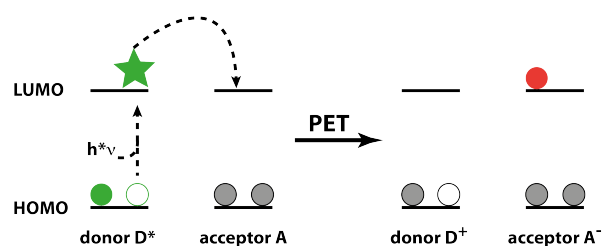
resonance energy transfer**photoinduced electron transfer**

figure 6: Comparison of resonance energy transfer (RET) [top] and photoinduced electron transfer (PET) [bottom]^[83].

Fluorescence quenching can occur via a photoinduced electron transfer (PET) from an electron donor to an acceptor (figure 6 bottom). In contrast to RET, this mechanism involves the transfer of a particle between two components. An electron of the donor molecule is excited into the LUMO by light absorption. This electron is transferred in the acceptor LUMO, which contains a similar orbital energy (figure 6 bottom). Generally, a fluorophore acts as acceptor and no fluorescence can be observed because of missing relaxation possibility. If the fluorophore is an electron rich compound, it can also act as a donor. In this case, no emission signal can be detected because of the missing electron (photooxidation)^[83], which has already been transferred.

Compared to fluorescence enhancement methods, resonance energy transfer or photoinduced electron transfer approaches enable monitoring of *reversible* reactions or processes. Therefore, these concepts are often used in biology to visualize active center coordination dynamics, different protein folding states or molecular information by distance measuring^[83–91]. Various examples of these methods have been transferred for use on chemical processes.

Ensemble measurements

Blum et al. used transfer processes for quantification of ligand exchange at Pt complexes^[30]. Two different functionalized fluorophores were synthesized, a green FRET

donor bearing a diphenylphosphine moiety and a red FRET acceptor with an allylchloride ligand. These compounds were used for synthesis of a bis-allyl BODIPY palladium chloride dimer. This palladium complex was mixed with the FRET donor and an exchange at the metal center was established. The optical properties of both chromophores were not influenced by palladium. A decrease in intensity of the green and an increasing intensity of the red BODIPY was observed by monitoring the intensity signals of the two BODIPY chromophores. This observation resulted from the proceeding FRET and consequently, the ligand exchange rates could be determined (figure 7)^[30] from this data.

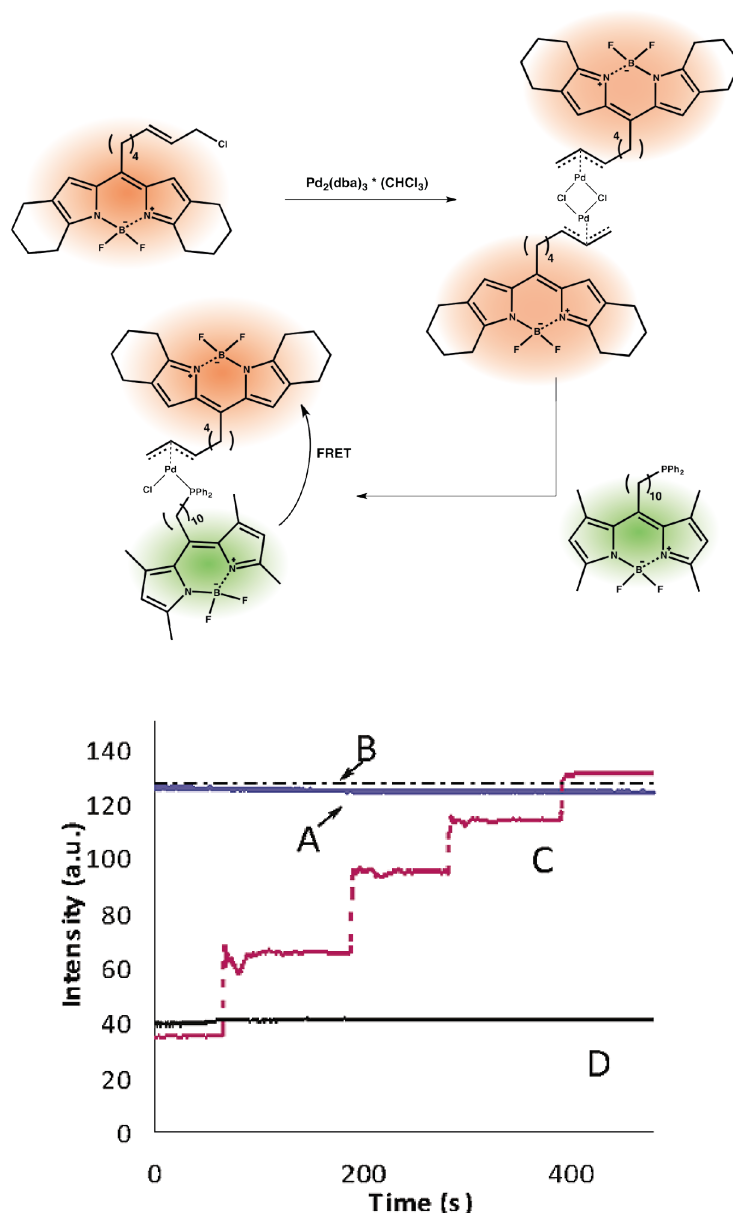


figure 7: Allyl-phosphine ligand exchange investigation using FRET on palladium complex -
A: Addition of green BODIPY achieving full exchange and maximum signal intensity of red BODIPY;
B: Theoretical maximum intensity for full ligand exchange;
C: Stepwise addition of green BODIPY showing correlated intensity increase of the red BODIPY;
D: Blank experiment. [traces applied out of ^[30]

Single-molecule investigations

Another approach towards single-molecule reaction dynamic analysis via electron transfer processes was presented by Hertel et al.^[35,45]. This involved a fluorophore and a Cu^{2+} binding ligand being immobilized on a surface with a DNA backbone. Consequently, the fluorescence signal intensity trace could be monitored until photobleaching. Fluorophore and ligand were in close proximity, so coordinated Cu^{2+} induced fluorescence quenching. The emission time trace of single reactive centers visualized reversible association and dissociation behavior by continuous switching fluorescence intensities (figure 8)^[45].

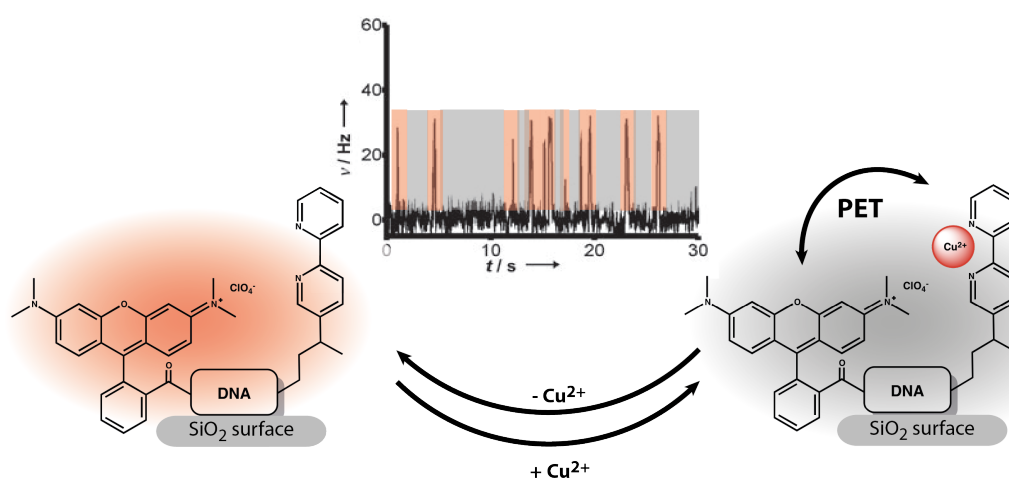


figure 8: Single-molecule analysis of Cu^{2+} - Bipy bonding behavior with photoinduced electron transfer. Single-molecule timetrace with appropriate signals are illustrated in the middle of the figure. [traces applied from ^[35]].

Energy or electron transfer approaches provide an overview of a reversible reaction. During these transformations, specified systems can reveal single molecular processes. Complete reaction monitoring including formation of a reactive state or an intermediate could hardly be analyzed. Therefore, ratiometric probes are needed, where the fluorescence signal is directly correlated with the reaction process.

2.2.3. Ratiometric single-molecule reaction monitoring (scheme 3 C)

Fluorescent probes used in conversion experiments show a direct change of the emission signal from the first compound into the signal of the second, characterized by an isosbestic or isoemissive point. Therefore, a fluorophore has to be converted at a reactive side or intermolecular effects like FRET have to be used.

Ensemble measurements

Such intermolecular effects between two fluorophores were used by Hensle et al. for visualization of gold catalysis in ensemble measurements. A FRET pair bridged with a triple bond and a functional side for cyclization was synthesized. Adding Au catalyst, a cyclization reaction cleaves the two chromophores and consequently, the energy transfer ceases to continue. The green fluorescence signal increases and the reaction can be observed by monitoring ratiometric changes in the signal (figure 9) [92].

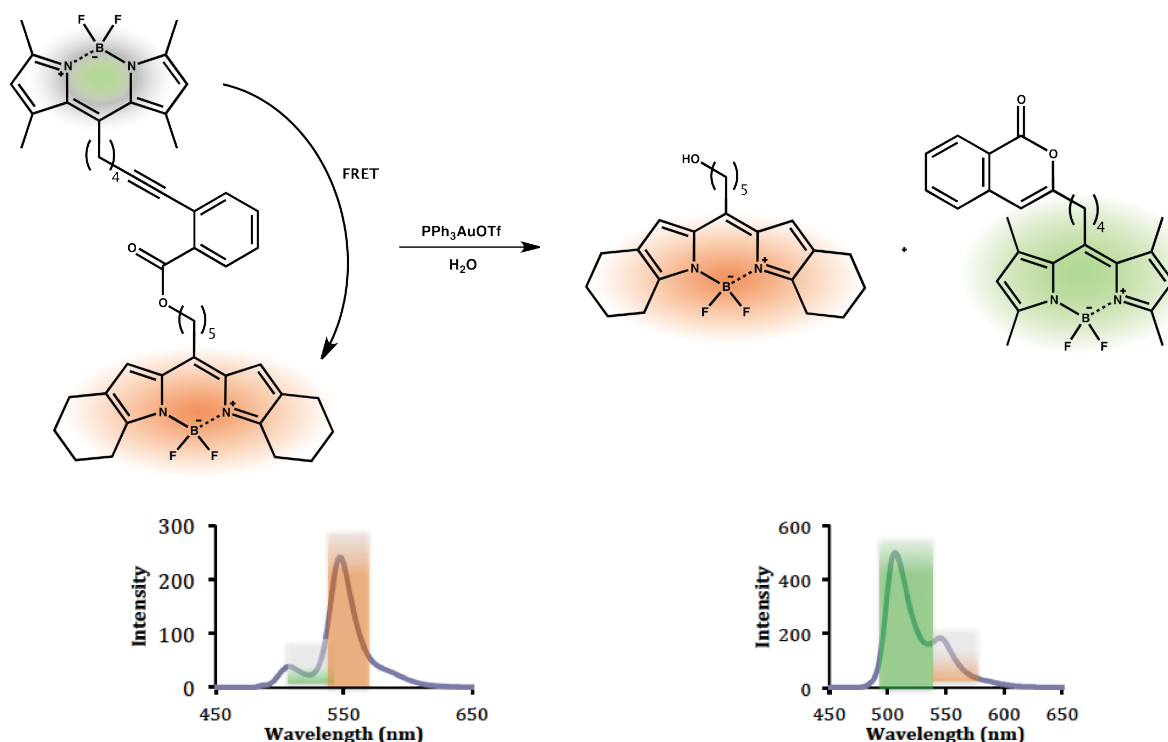


figure 9: Visualization of Au catalyzed cyclization using FRET [traces applied from [92]].

Another ratiometric technique, which involved visualizing the CuAAC click reaction was provided by Bunz et al. [93]. Different diethynylbenzothiadiazoles were synthesized observing a fluorescence emission signal near $\lambda_{\text{em}} \approx 440$ nm. Click reaction with different PEG azides elongates the chromophoric unit and shifts the emission maximum bathochromically about 65 nm to the green region of the electromagnetic spectrum ($\lambda_{\text{em}} \approx 510$ nm). These PEG substituted ditriazolbenzothiadiazole serve as water-soluble chromophores for ion detection by fluorescence quenching and ratiometric absorbance shift [93].

Single-molecule investigations

The first ratiometric reaction visualized on single-molecule level was the photooxidation of terrylene^[32]. Terrylene was immobilized into a *p*-terphenyl crystal to gain insight in the process of photobleaching. The fluorescence intensity time traces of single terrylene molecules were analyzed in different atmospheres (air, oxygen, argon). Several time traces were extracted and showed that the “on” times of the fluorophores decreased with increasing oxygen concentrations. In air, single-molecule analysis revealed an abrupt decrease of the terrylene fluorescence signal. After a dark state a brighter fluorescence returned. The fluorescence spectra, revealed a blue shifted emission signal (figure 10) both before and after the observed dark state. This shift was explained by photooxidation of an aromatic double bond in terrylene, forming a non-fluorescent endoperoxide followed by rearrangement to the final fluorescent diperoxide (figure 10)^[32].

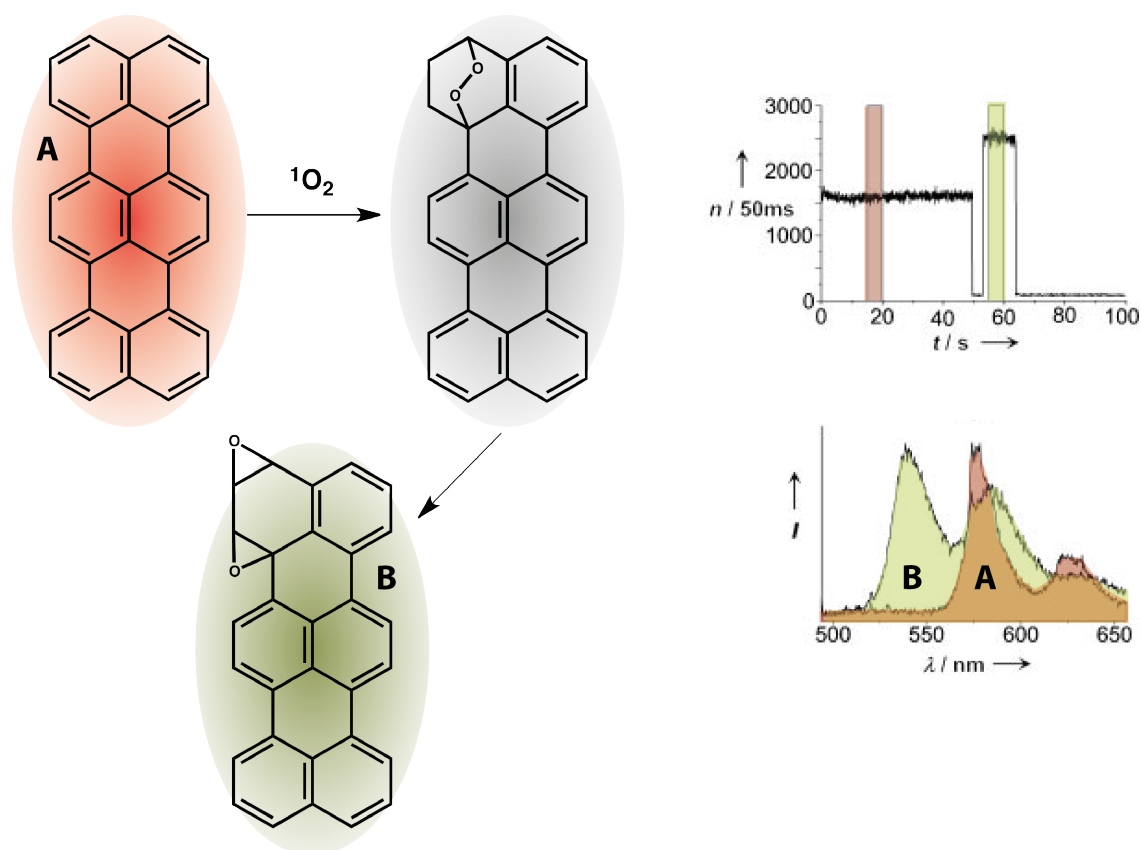


figure 10: Photooxidation on single-molecule level visualized by Basché et al [graphs applied from ^[32]].

A similar outcome was reached by Vosch et al. in photooxidation experiments of terrylenediimide (TDI)^[94]. This compound was immobilized in a polystyrene film and investigated on single-molecule level. Excitation with laser light at $\lambda_{\text{ex}} = 633 \text{ nm}$ showed single-molecule fluorescence. In the next step, this area was photobleached ($\lambda_{\text{ex}} = 633 \text{ nm}$, 16 kWcm^{-2} , 1 s per pixel). Analyzing the same section with an excitation wavelength of $\lambda_{\text{ex}} =$

480 nm, a single-molecule fluorescence with a hypsochromic shift about $\Delta\lambda = 80$ nm was observed again (figure 11). Emission spectra of single pixels revealed multiple species hypsochromic shifted with excellent photophysical properties^[32]. These products resemble smaller analogues of perylene dye class, such as PDI or PMI, which are formed via photo oxidation.

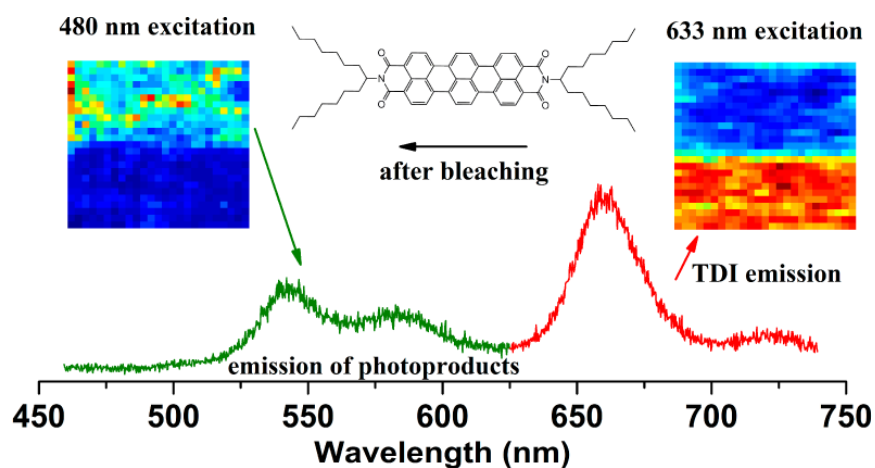


figure 11: Ratiometric photooxidation of TDI to perylene analogues visualized on single-molecule level and in ensemble measurements [applied from ^[94]].

Therefore, a ratiometric photooxidation reaction was observed on single-molecule level which was also validated via ensemble measurements.

Ratiometric reaction monitoring systems enable simple data interpretation because fluorescence signals are directly correlated with the reaction progress. So, the relative data reveal kinetic parameters such as conversion rates. On single-molecule level, the optical separation of the starting compound and the product facilitate reaction monitoring with a multi-channel setup. Unfortunately, the number of usable, selective chromophores for such investigations is limited.

Fluorescence methods can provide insight in different reaction types depending on the specific test system employed. Fluorogenic concepts only enable the visualization of individual reaction steps as opposed to the complete transformations. Further insight into reaction dynamics can be provided using fluorophore systems, which observe transfer processes like FRET or PET. It is not possible to analyze the entire reaction with a single fluorophore system with such approaches in a single experiment. Ratiometric probes show the possibility to correlate conversion with emission signal behavior. Therefore, fluorophores have to be part of the reaction, as shown in the epoxidation of terylene.

Ensemble experiments only produce averaged data from the reaction progress. As a result of these investigations, the application of a fluorophore system on single-molecule experiments can be estimated. Single-molecule methods facilitate a detailed view of the transformation mechanism. Immobilized fluorophore, which contain specific sites where the investigated reaction can proceed, are required. The alteration of optical parameters, such as the changes to the fluorescence wavelength during transformation, combined with a convenient experimental setup, allows reaction monitoring on single-molecule level.

Such investigations enable a detailed determination of reaction mechanisms including association and dissociation processes without various experiments. A major benefit of this approach is that there is a relatively high time resolution, *e.g.* fluorescence methods even can resolve proton transfer reactions^[95-97]. Consequently, processes could be observed, which were not possible via other methods such as NMR. Using a proper fluorophore system, nearly all possible reactions trajectories can be investigated. The frequency of different events provides a statistical validation of the particular reaction pathway. The sensitivity of this method facilitates a precise examination of the reaction because the behavior of every single molecule is observed. Consequently, a transformation can be completely characterized including all its possible trajectory pathways. The necessary kinetic information can be extracted by means of reaction time traces. Single-molecule reaction analysis provides a powerful tool for mechanistic investigations to visualize specific transformation states. For a detailed chemical interpretation and verification of the data obtained, further structure elucidating tools should be included during analysis. Therefore, usable dyes with specific characteristics are required. In the next chapter, chromophores, which can be used for such experiments are summarized.

2.3. Fluorescent dyes

Most fluorescent organic molecules are characterized by a delocalized π -electron system containing small HOMO – LUMO gaps. Electrons can be excited from HOMO to LUMO using light absorption and return to the former state emitting a photon^[83,98].

2.3.1. Fluorescent dye classes

The structural motifs of most fluorescent dyes contain alternating double bonds and fused unsaturated ring systems. The resulting different molecular structures enable a classification of the dyes. Some of these fluorophore families are listed in figure 12, where the number of synthetic publications is correlated with their use in single-molecule applications.

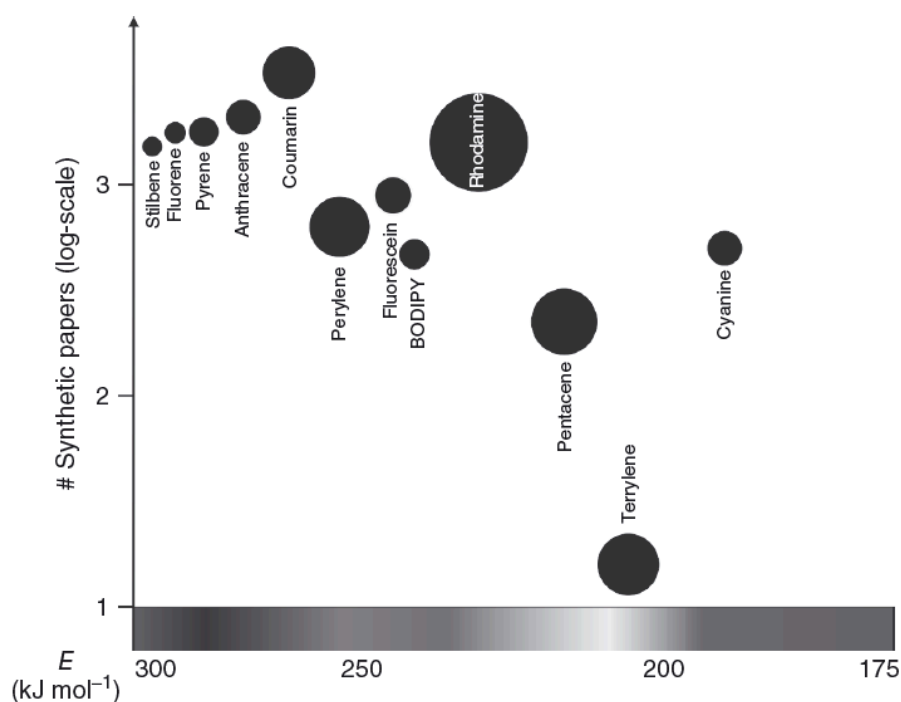


figure 12: Quantitative visualization of a Web-of-Science research - number of synthetic publications for different dye families correlated with citation frequency in single-molecule investigations visualized by filled area combined with corresponding emission energy [applied from^[99]].

The major synthetic access is found for fluorophores emitting high energetic photons (Stilben, Fluorene, Pyrene, Anthracene). In contrast, these molecules exhibit a minor application in single-molecule studies due to high background fluorescence at these excitation wavelength. These unwanted signals are caused by impurities and scattering effects in the blue region of the electromagnetic spectrum. In addition, these dyes mostly

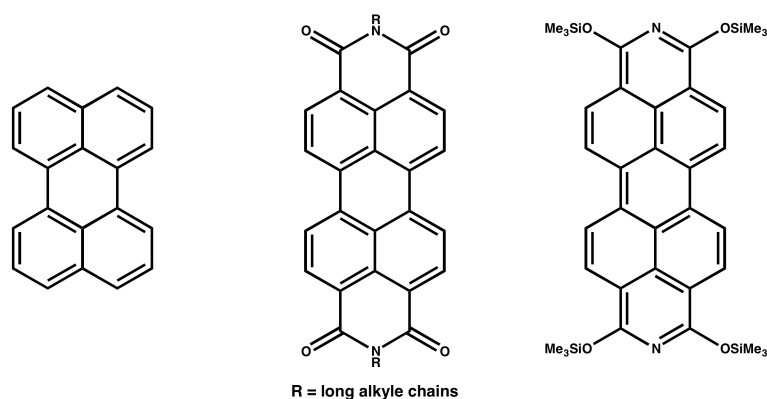
have inappropriate optical characteristics for single-molecule investigations^[100]. Terrylene or Pentacene, as orange emitting fluorophores and photophysically stable dyes, are similarly restrictive in their use, because of their limited synthetic approaches. There is currently no possible way to synthesize such molecules, so that they can be tailored for specific reactions. The favored dyes in single-molecule chemistry show a fluorescence signal with larger wavelength compared to the blue region of the electromagnetic spectrum. These fluorophores exhibit a large Stokes shift, a high brightness ($\epsilon > 50000 \text{ M}^{-1}\text{cm}^{-1}$, $QY > 0,1$), a high photostability, low aggregational tending and various formation and transformation abilities facilitating structural elucidation^[49,52,88]. The dyes with the highest application tendency in single-molecule chemistry consist of Perylene, Coumarin, Cyanine, Fluorescein, Rhodamine and BODIPY dyes^[99]. A comparison of these favored chromophores is listed in table 1 and further discussed.

table 1: Comparison of different fluorophores with their characteristics suitable for single-molecule applications according to literature and experimental experience (+ appropriate, o moderate, - inappropriate).

	λ_{fl} SM	QY	PS	synth. access	chem. modif.	purifi- cation	$\Delta\lambda$ react.	pH sens.	solu- bility
Perylene	+ [101]	+ [102,103]	+ [102]	- [104]	- [105]	-	-	-	- [106]
Coumarin	-/o [107]	o [108,109]	+ [110]	+ [111-114]	o [52]	+	-	+ [108]	+
Cyanine	+ [115]	o [115]	+ [116,117]	+ [52]	o [115]	o	-	o [118]	o
Fluores- cein	o [119]	+/o [120,121]	o [122]	+ [52]	+ [52]	o [123-125]	+	+ [125]	o
Rhoda- mine	+ [126]	+ [126,127]	+ [128,129]	+ [52]	+ [128,130]	o [131]	+	- [129]	o
BODIPY	o [132]	+ [133]	+ [134]	+ [133,135- 137]	+ [138]	+	+	- [139]	+

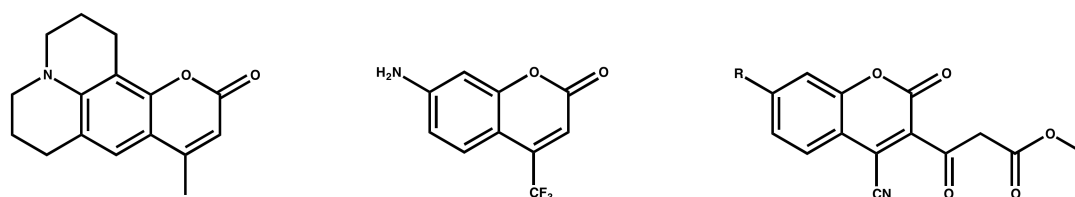
Perylene dyes (scheme 7) exhibit excellent quantum yields^[102,103] and photostabilities^[102]. Furthermore, an ideal optical detection window proposes their usage in single-molecule

investigations. Any pH sensibility is not observable because of absent functionalities. A problem of these dyes is their inconvenient solubility in most solvents^[106] because of π - π stacking and formation of J-aggregates^[140]. Furthermore, synthetic access is very limited^[104]. Substitutions only include bromination at the perylene core or different moieties at the nitrogen or oxygen positions in case of perylene-diimides^[105]. Therefore, synthetic access for cross-coupling reactions is possible but restricted purification procedures complicate the isolation of a single species, required for single-molecule investigations. Transformations at the chromophore don't induce great spectral changes in the emission signals because small size variation at a large chromophore doesn't show a great impact on the energies of the valence orbitals.



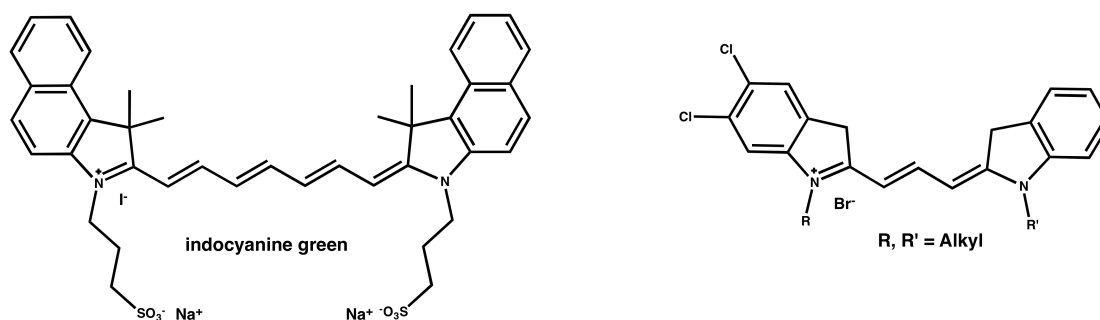
scheme 7: Different Perylene dyes.

Coumarin derivatives (scheme 8) can be synthesized by numerous different reactions. Common purification methods enable isolation of a pure compound^[111–114]. As laser dyes, these fluorophores reveal high photostabilities^[108,109] but only moderate fluorescence quantum yields^[110]. Compared to other dye classes, only few transformations exist after the establishment of the chromophore^[52]. These dyes are soluble in the most solvents. In a protic environment, a sensitivity to pH is observable^[108]. Furthermore, the emission bands of these dyes are generally quite broad compared to other fluorophores. Optical separation of the maxima of the different species e.g. in ratiometric conversion is complicated.



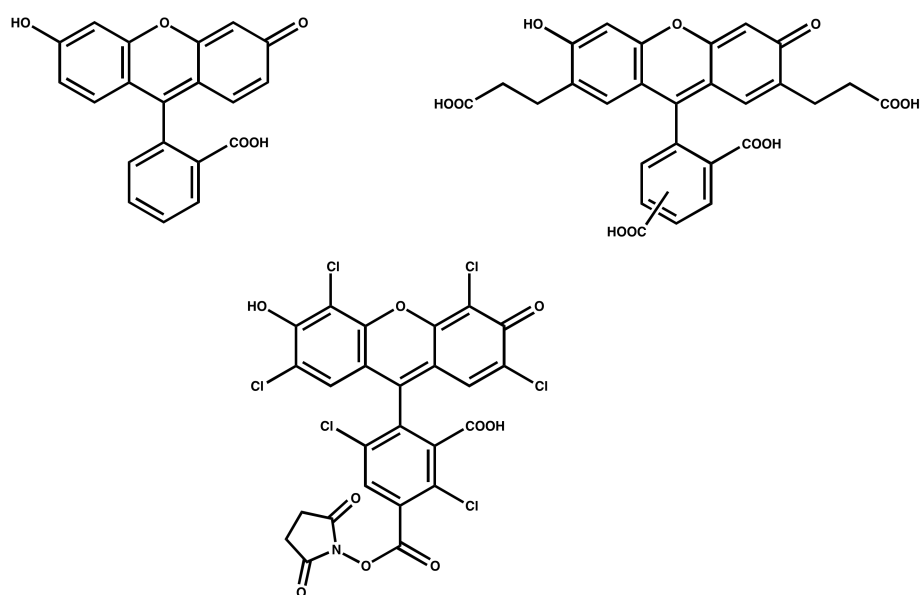
scheme 8: Different Coumarin dyes.

Another dye class, the Cyanine dyes (scheme 9), are often used as laser dyes, which exemplify their excellent photostability^[116,117]. Different synthetic routes for chromophore formation are published^[52], but synthetic modifications at the core are limited^[115]. Most derivatives exhibit a moderate quantum yield^[115] because of their flexible, alternating double bonds. They are used as pH sensors, which illustrate their characteristic pH sensitivity^[118]. The dyes exhibit moderate solubility and purification properties, which restrict their access through synthetic means. Additionally, small structural changes to the chromophoric unit in an examined reaction, exhibited very little influence on the optical parameters due to the size of the molecules.



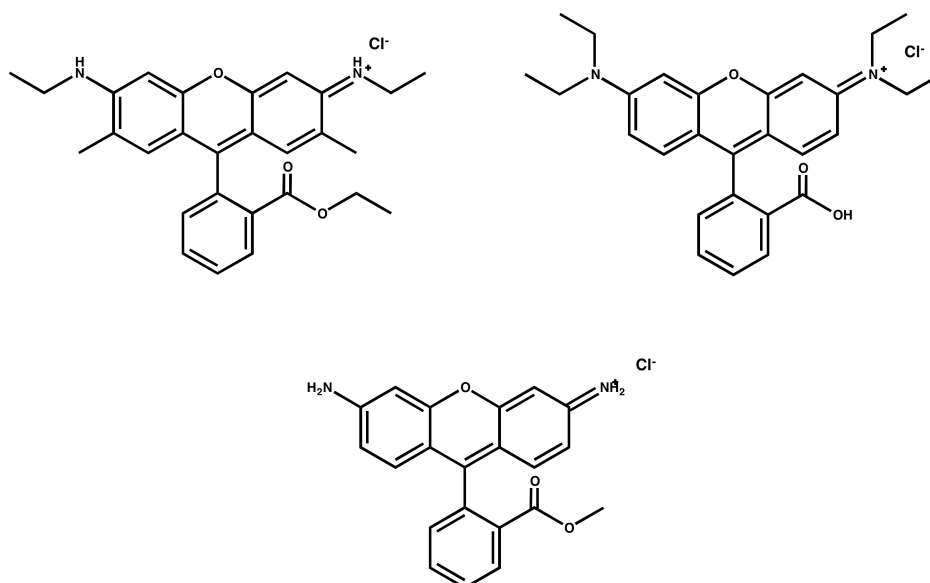
scheme 9: Different Cyanine dyes.

Fluoresceine dyes have various possible strategies for chromophore formation or post-modification^[52] combined with changes in optical parameters suitable for optical separation. Moreover, crystallization is a typical work-up procedure for Fluoresceins enabling structural elucidation (scheme 10)^[123-125]. Moderate quantum yields^[120,121] and photostabilities^[122] were found for different derivatives. The solubility of these dyes is limited to polar solvents depending on how they are modified. This behavior complicates chemical purification. These dyes are often used as fluorescent pH sensors, revealing their proton sensitivity^[125].



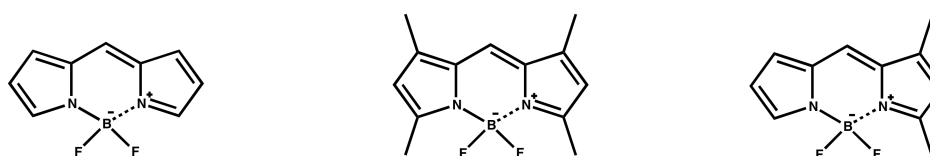
scheme 10: Different Fluorescein dyes.

Rhodamine derivatives (scheme 11) are structural isomers to fluoresceins. They are preferred to fluoresceins in single-molecule spectroscopy because of their excellent fluorescence quantum yield^[126,127] and their photostability^[128,129]. Their emission range is located between orange and red in the visible light spectrum and changes in the chromophoric unit make the emission band suitable for optical separation. Similar to fluoresceins, the synthetic access^[52] and the chemical post-modification properties^[128,130] have been thoroughly investigated. Rhodamines show a reduced pH sensitivity compared to fluorescein derivatives^[129]. Their use is undermined by its molecular charge, which limits its potential solubility. This molecular characteristic complicates the work up procedures as well. Most of the different species could only be separated by crystallization, which requires greater amounts of substance^[131].



scheme 11: Different Rhodamine dyes.

BODIPY fluorophores (scheme 12) exhibit high fluorescence quantum yields^[133] combined with a high photostability^[134]. The chromophore can be easily synthesized^[133,135–137] and modified^[138] after chromophore formation. These dyes can be dissolved in nearly all organic solvents. Therefore, typical organic purification procedures facilitate single compound isolation. Structure elucidation is easily reached, as these fluorophores form excellent crystals for X-ray determination^[4]. The fluorescence range lies between green and red^[54], depends on modifications and is unaffected by the proton concentration. Excitation of green compounds can sometimes show increased background fluorescence in comparison to rhodamines because of the optical detection window^[5].



scheme 12: Different BODIPY dyes.

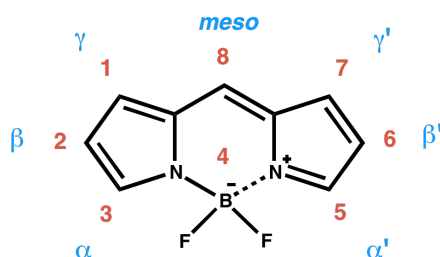
The use of the different fluorophores depends on the respective scientific target. The Coumarin derivatives mainly emit in the blue region of the electromagnetic spectrum (figure 12)^[115]. Hence, the successful realization of single-molecule experiments is quite difficult to accomplish because of perturbing background effects caused by high excitation energies. The other fluorophores exhibit adequate emission signal ranges. Perylene derivatives exhibit favored optical properties but their synthetic and clean up limitations disfavor their usability in single-molecule approaches. Cyanin chromophores are more easily synthesized as Perylene compounds, but the poor post-modification and

isolation properties also restrict their potential use. Fluorescein derivatives allow post-modification and easy structural determination, but their spectral characteristics are not optimal. Therefore, rhodamine dyes, which are the most stable analogues to fluoresceins, could be used in such experiments. A limitation resides in the difficult chemical cleaning procedures required to establish a usable clarity for single-molecule investigations.

BODIPY dyes offer the best alternative to the presented fluorophores for single-molecule reaction systems. Different synthetic approaches, modification possibilities and work up procedures exist for tailoring a fluorophore with the ideal optical characteristics in the required purity. Therefore, BODIPY dyes are used as fluorophores for the detection systems in further single-molecule reaction monitoring experiments. A closer look at their synthetic approaches and their chemistry is illustrated in the following section.

2.3.2. BODIPY dyes

Treibs and Kreuzer first described these fluorophores in 1968^[141]. The symmetrical core contains four different positions, α , β , γ and *meso* (appropriate numeration according to scheme 13), which can be used for functionalization^[54,142–144].



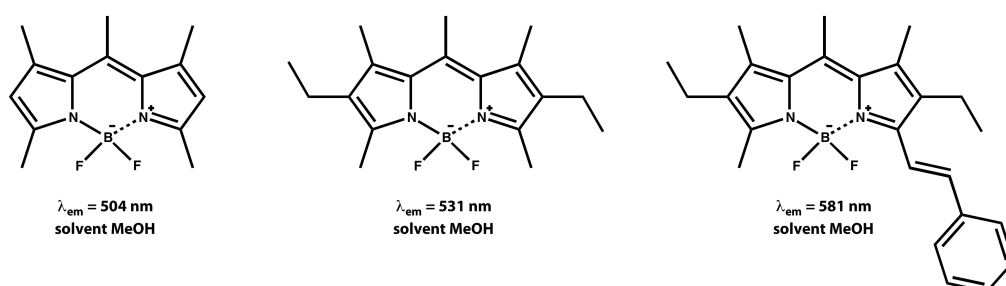
scheme 13: Glossary of BODIPY positions^[54,142–144].

Optical properties

Influence of electronic effects on fluorescence

These small molecules offer interesting optical characteristics for microscopic and single-molecule applications. Beside high fluorescence quantum yield^[54], high photostability^[134], sharp fluorescence peaks^[145] and small Stokes shift^[146], they are insensitive to pH and polarity^[145,146]. These qualities explain their use in cell markers^[147], fluorescent switches^[148,149], light harvesters^[150], cation sensors^[151] and in many more applications^[152]. In solution, they resist aggregation and their uncomplicated chemical access facilitate the synthesis of specific fluorophores required for reaction monitoring^[55].

The optical properties of the BODIPY dyes can also be changed by chromophore substitution. Different groups can be introduced, which influence the electron density in the ground state S_0 and the excited state S_1 , via inductive or mesomeric effects, depending on their positions^[153]. If the S_1 state is stabilized via charge transfer, the LUMO energy level is lowered, so that the energy gap between HOMO and LUMO is reduced. This behavior results in a bathochromic shift of fluorescence signal (scheme 14). Taking the opposite approach, the electronic effects stabilize the ground state and the energy of the HOMO is lowered. Consequently, the difference between HOMO and LUMO is increased resulting in a hypsochromic fluorescence wavelength shift^[153].

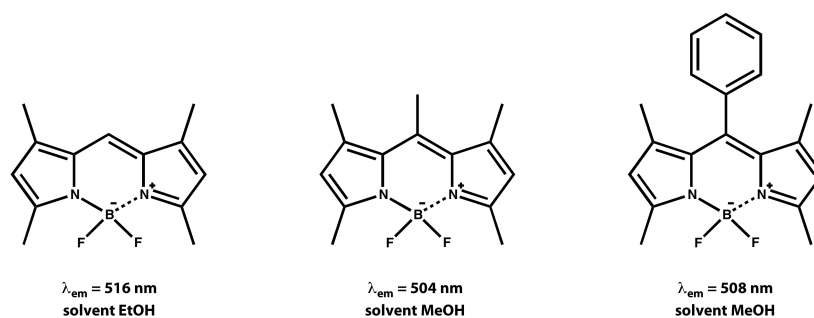


scheme 14: Different substituted BODIPYs show substitution influence onto the emission wavelength. The influence depends on the substitution position^[153].

Extending the π -system of BODIPY dyes via unsaturated and/or aromatic groups, the HOMO and LUMO orbitals of the BODIPY and the substituent are conjugated. This connection leads to a smaller energy differences between the ground and the excited state and results in the observation of a bathochromic fluorescence shift (scheme 14). Such an influence on the orbitals depends on the environment of the chromophore (solvent, impurities...) and the substitution position^[153,154].

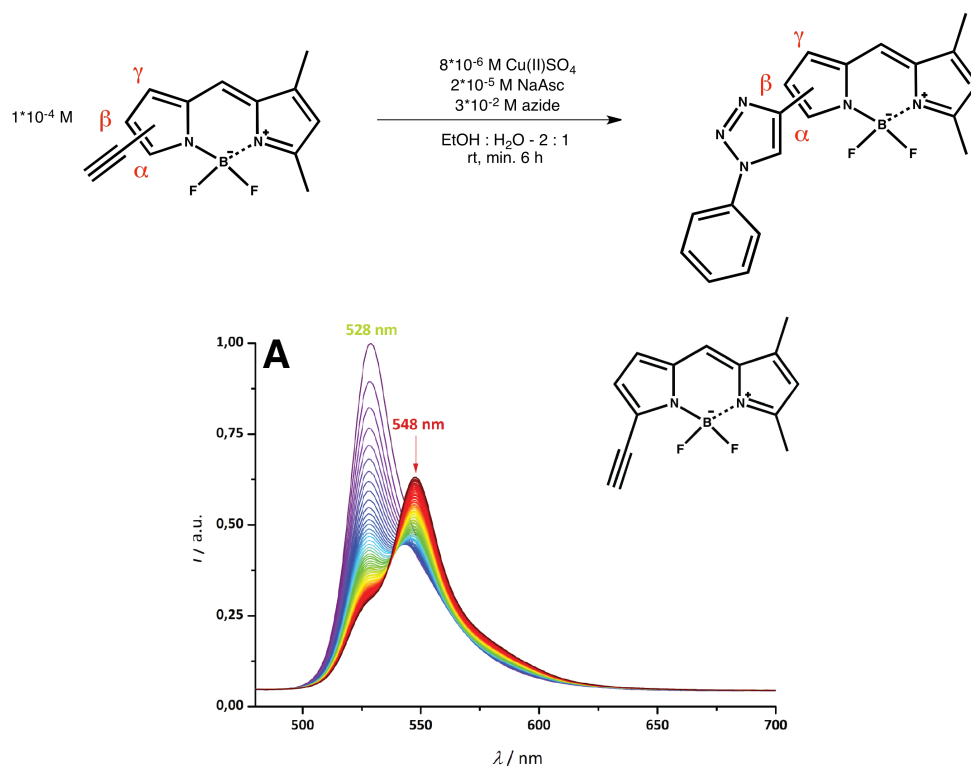
Influence of substitution position on fluorescence

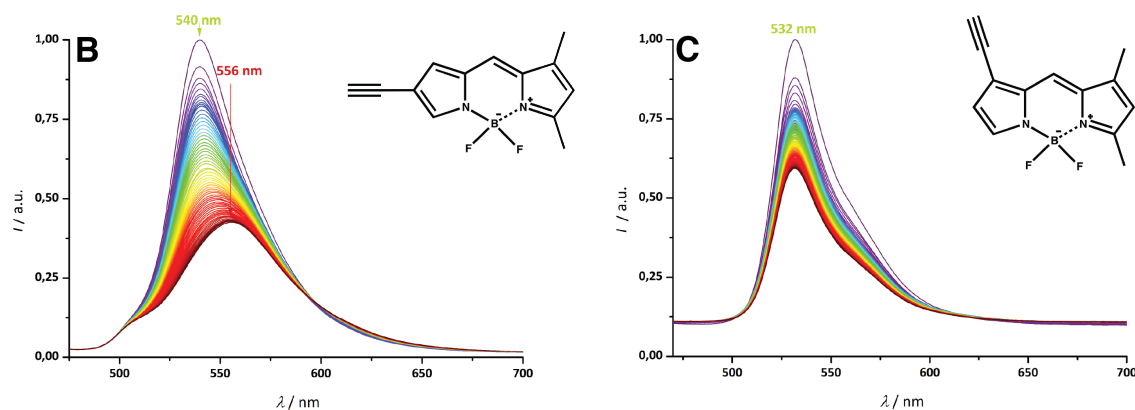
Derivatization on α , β , γ or *meso* position has a different influence on the HOMO and LUMO orbitals of the BODIPY compound. Therefore, the substitution position has to be chosen carefully, in order to produce the required change in optical properties. In scheme 15, different *meso* substitutions are shown, which can have a restricted influence on the optical properties, depending on the group^[155-158] used.



scheme 15: Different BODIPY derivatives showing substitution influence onto optical properties^[155–158].

The influence of a substitution at positions α , β or γ was examined in conversion experiments using the appropriate synthesized alkyne BODIPYs. These dyes were transformed via click reaction to the corresponding triazole compounds. The positional influence on optical properties can be visualized (scheme 16) with this substitution. The starting compound for α and γ differ slightly in their emission wavelength ($\Delta\lambda_{fl} = 4 \text{ nm}$) and both show a typical sharp BODIPY peak form. The β -ethynyl compound possesses a larger bathochromic shift compared to the other derivatives ($\Delta\lambda_{fl \alpha-\beta} = 12 \text{ nm}$; $\Delta\lambda_{fl \gamma-\beta} = 8 \text{ nm}$), but this species contains much broader spectra ($\Delta\lambda_{FWHM \alpha \text{ compound}} = 22 \text{ nm} \leftrightarrow \Delta\lambda_{FWHM \beta \text{ compound}} = 42 \text{ nm}$) compared to the structural isomers.





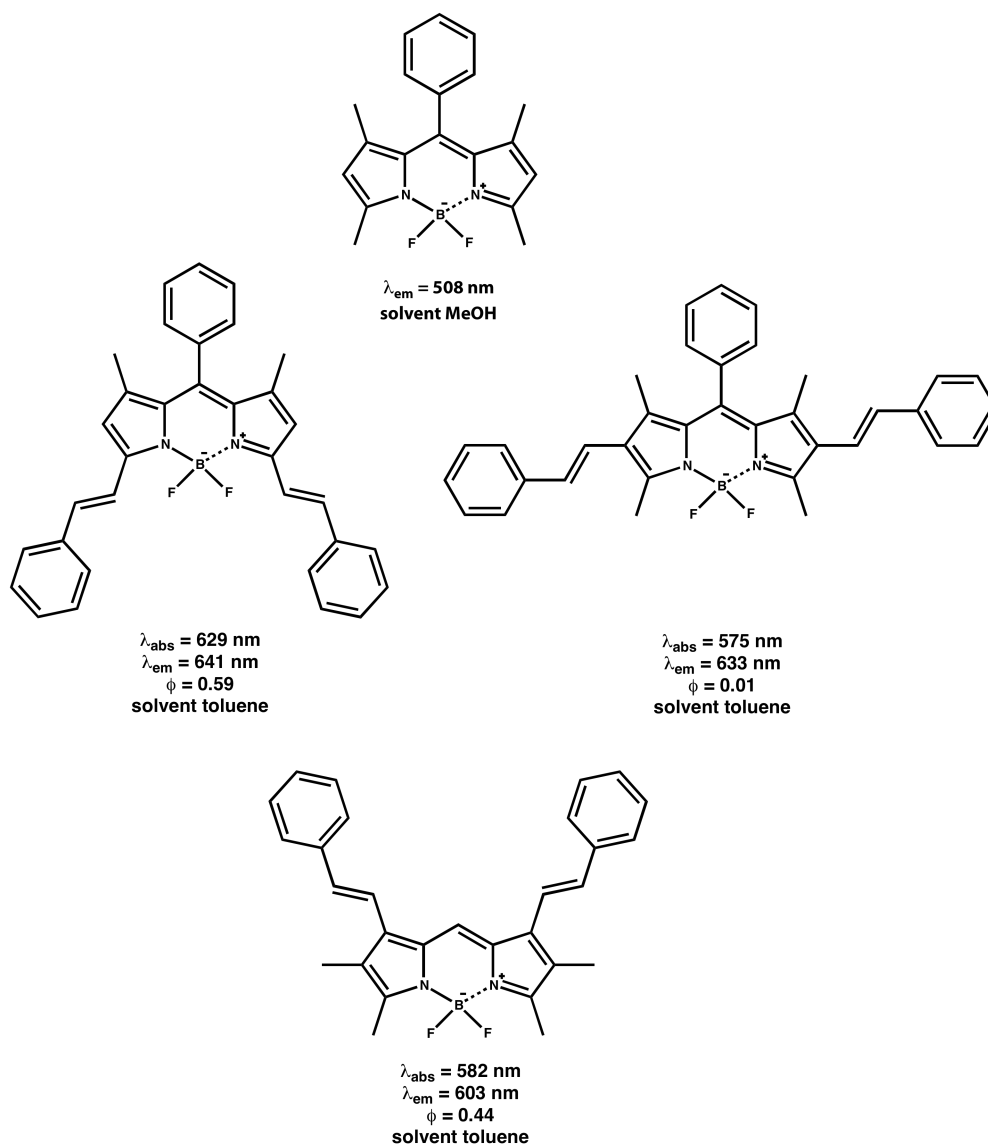
scheme 16: Analysis of BODIPY's fluorescence properties via reaction monitoring upon substitution on different BODIPY core positions.

Transformation of the alkyne to triazole moiety induces a bathochromic shift in fluorescence wavelength due to the elongation of the HOMO and LUMO orbitals and the corresponding energy gap attenuation. Using α -ethynyl BODIPY, a ratiometric change in emission signal via an isoemissive point is observed as containing distinct spectra. These optical properties facilitate both kinetic data extraction and reaction monitoring.

In contrast to the α -isomer, the conversion of γ -ethynyl BODIPY to the corresponding triazole does not show a change in fluorescence wavelength. The decomposition rate is much slower compared to the other components. The intensity of the emission band is reduced due to the BODIPY's decomposition. Analyzing fluorescence lifetime shows an increase from 4.7 ns to 5.7 ns, which is comparable to previously published results^[56]. This observation is an indication of a proceeding reaction, but the starting compound and the final product can not be spectrally separated, because of a weaker interaction between the valence orbitals of BODIPY and alkyne moiety. As a consequence, no further reaction visualizations are possible with γ -substituted BODIPY's.

Similar to the α -substituted fluorophore, the formation of the β -triazole BODIPY could also be monitored by a small bathochromic shift. In contrast to the α - and γ -BODIPY, the spectra became much broader ($\Delta\lambda_{FWHM} = 42 \text{ nm} \rightarrow 60 \text{ nm}$). These optical parameters circumvent kinetic data extraction because of a wide spectral overlap of both species. Therefore, α -substituted BODIPY derivatives, with their convenient optical properties, are the best reactive dye alternatives in fluorescence reaction analysis.

These investigations were confirmed by Shen et al. using different optically characterized distyryl-substituted BODIPYs (scheme 17)^[159].



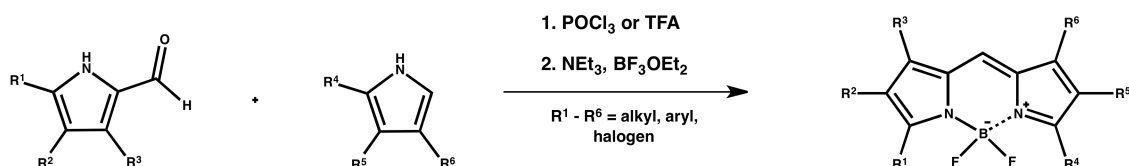
scheme 17: Influence of BODIPY core substitution on different positions^[159].

As seen before, these results clearly show, that the α position can cause a sufficient bathochromic shift and results in the maximum brightness level. Therefore, derivatization at this carbon atom is the most suitable side for derivatization chemistry at the BODIPY core.

Chemical access

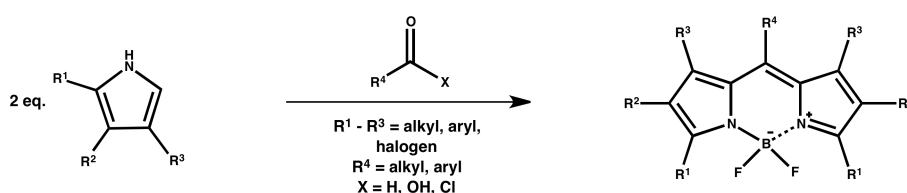
BODIPY dyes can be synthesized via three different ways:

- A. Unsymmetrical BODIPYs are prepared by carrying out an acid catalyzed condensation reaction of a pyrrole carbonyl compound with a second pyrrole compound. Forming the dipyrromethene scaffold, deprotonation and complexation produces the required compound (scheme 18)^[53].



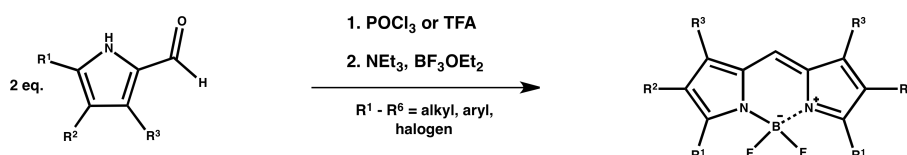
scheme 18: Synthetic approach to unsymmetrical BODIPY compounds^[53].

- B. Symmetrical BODIPYs can be formed via the condensation of a pyrrole compound with an aromatic aldehyde, acid or acid chloride under formation of corresponding pyrromethene precursor. Subsequent oxidization, deprotonation and complexation, with boron trifluoride diethyl etherate yields the required BODIPY chromophore (scheme 19)^[53].



scheme 19: Synthetic procedure forming symmetrical BODIPYs^[53].

- C. Another synthetic pathway for symmetric BODIPYs is described in a condensation reaction of two pyrrole carbaldehydes. In a one-pot condensation-decarbonylation reaction, the corresponding dipyrromethene is formed. After deprotonation and complexation the chromophore can be isolated (scheme 20)^[160].

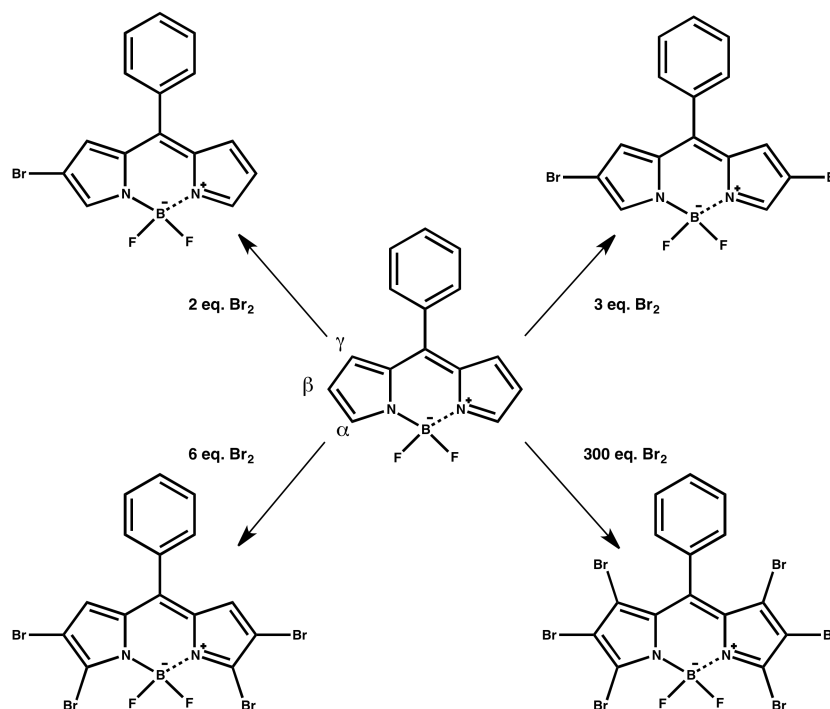


scheme 20: Synthetic procedure forming symmetrical BODIPYs using pyrrole carbaldehydes^[160].

Using these synthetic routes, BODIPY scaffolds can be formed and the desired groups for further transformations can be introduced. Route A only yields unsymmetrical fluorophores without substituents in *meso* position. This synthetic access is the most suitable for BODIPY derivatives, used for reaction monitoring, because only *one* reactive moiety in α position can be formed. Double transformation or side reactions at a second reactive center (created in B and C, both with and without, substitution in the *meso* position) are prevented.

Introduction of chemical groups at the BODIPY core

BODIPY dyes can be transformed using nucleophilic substitutions, Knoevenagel condensations or cross-coupling reactions^[53,56,58,161–163]. Metal catalyzed transformations provide efficient synthetic tools for derivatization of molecules, especially BODIPY dyes^[135,164,165]. Therefore, halogenated precursors are needed. The bromination potential of BODIPY compounds was investigated by Jiao et al. using *meso* phenyl BODIPY^[166]. This compound was transformed with different amounts of bromine, yielding the subsequent brominated species. One β -position is substituted with 2 equivalents of bromine. Increasing the amount of bromine, further sides can be substituted until every free position at the BODIPY core is derivatized (scheme 21). These investigations visualize the reactivity at the formed BODIPY core ($\beta > \alpha > \gamma$)^[166].

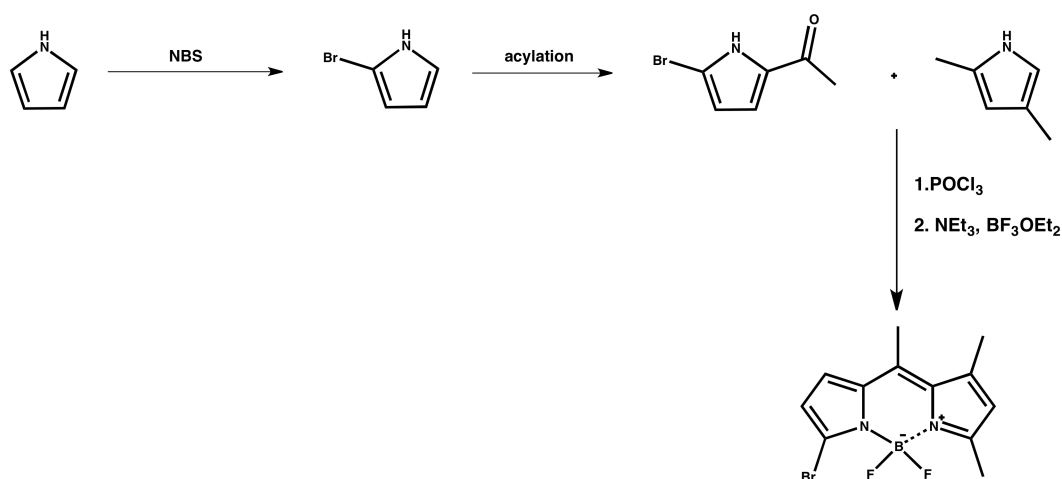


scheme 21: Bromination of BODIPY scaffold^[166].

***a* position**

The most commonly used derivatization of BODIPY dyes takes place at positions 3 and 5 (scheme 13). Preventing β substitution (scheme 21), direct halogenation at these carbon atoms, is only possible by using the uncomplexed dipyrromethene core^[58]. Treatment with NCS or NBS successfully produces the symmetrical double halogenated compounds. Subsequent oxidation, deprotonation and complexation form the desired fluorophore^[58]. If

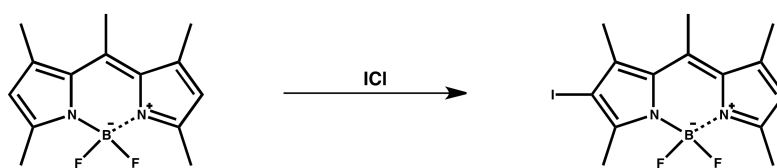
unsymmetrical, mono-halogenated BODIPYs are required, the synthesis of the corresponding pyrrole compounds is necessary. Bromination of pyrrole and the subsequent formation of a carbonyl group, provides the synthetic building block required for the construction of unsymmetrical halogenated BODIPYs. This conclusion was also reached in a publication by Leen et al. (scheme 22)^[56,58,167].



scheme 22: Formation of single α halogenated, unsymmetrical BODIPYs according to Leen et al.^[56,58].

β position

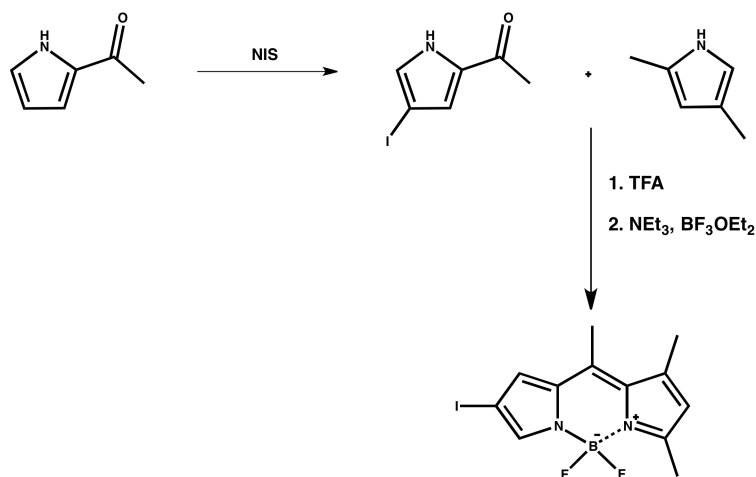
Functionalization at positions 2 and 6 seem much easier. Treatment with bromine (scheme 21) or iodine monochloride leads to selective halogenation. This procedure was presented by Ziessel et al. (scheme 23)^[168].



scheme 23: Iodation of BDP 546 in β position^[168].

Another halogenation approach involves the use of iodic acid and iodine. Yogo et al. used this method in their investigation of singlet oxygen production^[169] to achieve the iodination of the tetramethyl BODIPY in β position.

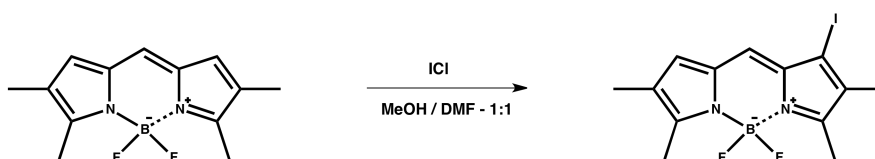
If unsymmetrical BODIPYs are needed, the synthesis of the appropriate pyrrole is necessary. Leen et al. synthesized 4-iodo pyrrolyl methylketone for the purpose of β -iodo BODIPY synthesis (scheme 24)^[56,58,170].



scheme 24: Synthesis of unsymmetrical halogenated BODIPY^[56,58,170].

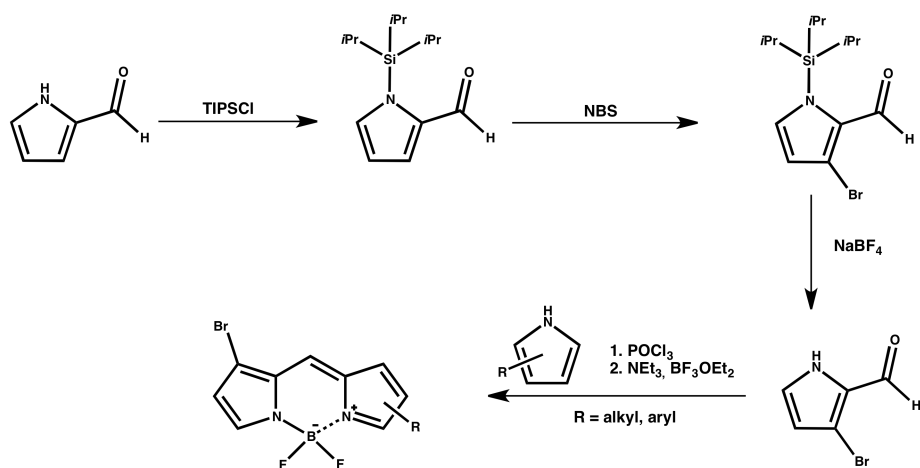
***γ* position**

BODIPYs with substituents at the γ position are rarely used because of their limited synthetic approach. Only a few examples are known. In these examples, the 1 and/or 7 position at the scaffold is directly substituted. If selective derivatization in γ and γ' is required, other positions have to be protected with inert groups. Then, halogenation at these carbon atoms can be established (scheme 25)^[171].



scheme 25: Iodation of γ position^[171].

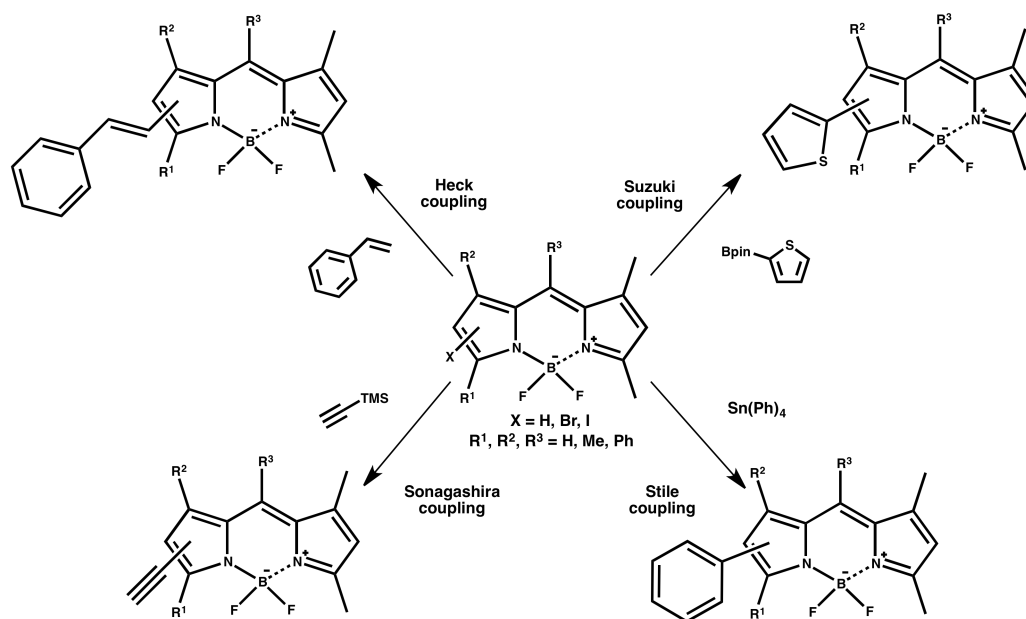
Jiao et al. presented another possible approach involving the use of 300 equivalents of bromine (scheme 21)^[166]. BODIPYs functionalized in γ position without any protective groups can only be achieved, if suitable pyrrole molecules are available in the scaffold formation process. So, 5-bromo pyrrole can be synthesized using bulky protective groups at the nitrogen atom to block the ortho positions. Further treatment with NBS leads to unselective formation of the target compound^[167,172]. Then, the required fluorophore could be subsequently formed with the synthesized building block (scheme 26).



scheme 26: Synthetic route to γ brominated BODIPY compounds.

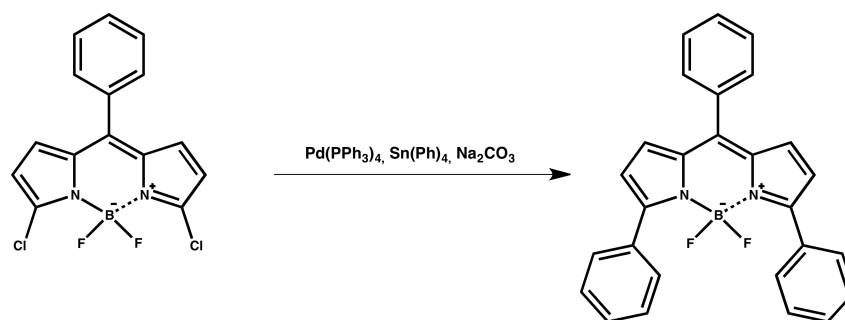
Cross-coupling reactions using BODIPY dyes

The previously presented reactive compounds could also be converted using cross coupling reactions (scheme 27)^[56,58,163].



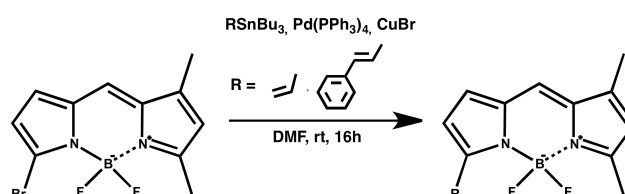
scheme 27: Overview of different cross-coupling reactions on BODIPY chromophores^[56,58,163–165].

Using Stille couplings, phenyl moieties can be directly attached onto the chromophoric unit^[163].



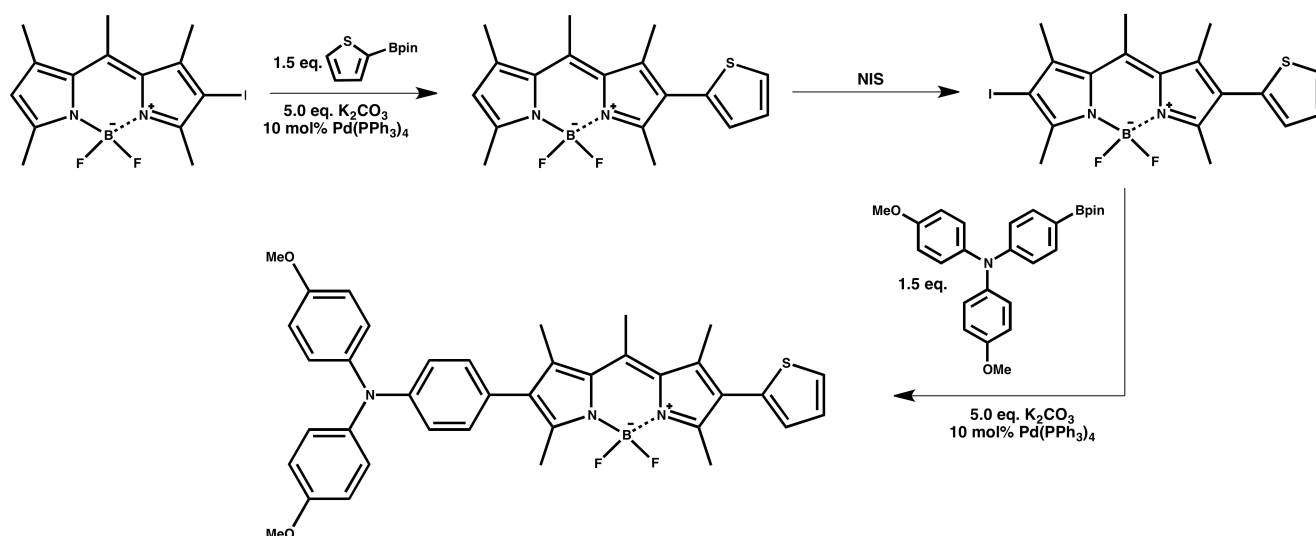
scheme 28: Stille reaction for BODIPY derivatization^[163].

Rohand et al. showed that BODIPY chromophores could be elongated via phenyl moieties. In comparison to commonly used synthetic routes, cross-coupling reactions enable a facile, economical synthetic access. Reactive moieties, which permit reaction monitoring using the “participant approach”, can be added by exchanging the organo tin reagents for tributylvinyl- or tributylstyryl tin^[5].



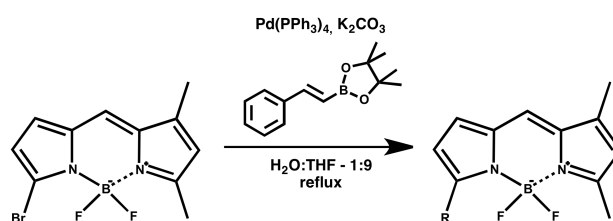
scheme 29: Synthesis of α -vinyl and α -styryl BODIPY used for metathesis reaction monitoring^[5].

Not only Stille reactions enable derivatization with metal catalyzed reactions. Suzuki types show similar reactivity. Using different boron acid pinacol esters, Bonnier et al. also synthesized light harvesting BODIPY fluorophores^[173]. The Suzuki reaction is therefore used twice to form a double functionalized system.



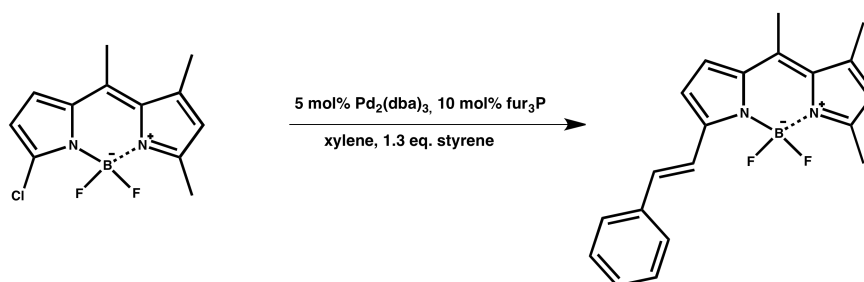
scheme 30: Synthesis of a light harvesting system via double Suzuki reaction^[173].

Additionally, this synthesis technique was chosen for the formation of styryl BODIPY. *Trans*-phenylvinyl boronic acid pincole ester was used as coupling reagent to accomplish compound derivatization in the Suzuki reaction, as a “greener” alternative to the Stille approach.



scheme 31: Green synthesis of α -styryl BODIPY used in metathesis visualization.

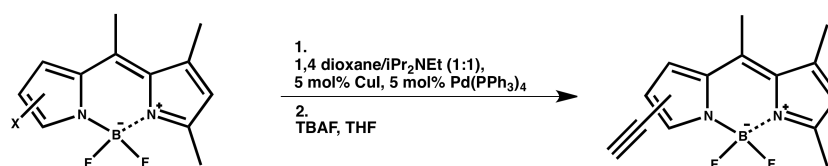
Leen et al. achieved the visualization of Heck type reactions on BODIPY compounds too^[56]. They used different cross coupling approaches, expanding the visible range of the fluorophores. The chromophoric unit was elongated with these reactions. Consequently, bathochromic fluorescence shifts were established^[56].



scheme 32: Heck reaction on BODIPY dyes visualized by Leen and coworkers^[56].

Not only halogenated BODIPY chromophores can be used for Heck reactions. Burgess et al. showed how the β -position of tetramethyl BODIPY can be directly functionalized without halogenation^[174]. Here, an oxidant, heat or microwave radiation is used.

Triple bond compounds can be introduced directly into BODIPY chromophores using Sonogashira coupling. Boens et al. describe transition metal catalyzed C – C bond formations on α and β position of the BODIPY core^[56].



scheme 33: Ethynyl BODIPY synthesis by Boens et al^[56].

A similar strategy was used in the synthesis of the different ethynyl substituted BODIPY compounds^[4].

The metal catalyzed reactions presented here, provide a high functional group tolerance, mild reaction conditions and a broad spectrum of transformation abilities. In comparison to metal catalyzed reactions, general chromophore extensions by Knoevenagel condensation^[135,175] or nucleophilic attack^[57,58,163] exhibit less yields and more side reactions because of harsh conditions. Therefore, cross coupling reactions serve as well-suited, synthetic tools for BODIPY functionalization. Because of these advantages, such transformations were used for the synthesis of single-molecule fluorophores systems. BODIPYs (with double bonds bearing different moieties, triple bonds and carbenoids) were used in the examination of the three different reactions: epoxidation, triazole formation and metathesis.

3. Epoxidation reaction^[1]

In the past two decades, single-molecule fluorescence spectroscopy (SMFS) has been employed to resolve heterogeneities in solid state physics, biophysics and for localization studies with high spatial resolution^[33,176–181]. Although the notation “molecule” is inherently connected to chemistry, applications of SMFS to reaction dynamics were rare, despite the early report of observed self-sensitized photo-oxidation of single terrylene molecules hosted in a *p*-terphenyl crystal^[32]. So far, single-molecule methods are mostly used to investigate catalytic turnover of enzymes^[182–184]. Only recently, SMFS has been applied to study heterogeneous catalysis. The cleavage of fluorogenic esters was used to investigate and map the spatial distribution of active catalytic sites for ester hydrolysis on crystal particles^[36,185] and to characterize the catalytic behavior of individual enzymes^[186]. With a similar approach, catalytic redox-reaction of fluorogenic substrates have been studied at the surface of gold nanoparticles^[187] and titanasilicate zeolites^[188]. Aiming at progress in studying heterogeneous organometallic reactions, the kinetics of ligand-exchange at platinum has been studied on the molecular level^[189]. Recently, the high spatial localization accuracy of SMFS allowed for distinguishing homogeneous catalysis from surface reactions^[34]. All mentioned single-molecule studies share the same experimental approach in which individual chemical reactions are distinguished by the occurrence of single fluorescent spots, *e.g.* due to the conversion of ubiquitous leuco-dyes or quenched substrates into brightly fluorescing product molecules. Here, light emission appears during the last event in a succession of elementary reaction steps. We have shown earlier that a reversible complexation of metal ions can be characterized with SMFS by immobilizing a fluorescently labeled ligand^[190]. Binding of a metal ion leads to specific fluorescence quenching of the ligand such that the forward chemical process (complexation) and the reverse reaction (dissociation) can be quantitatively studied by recording fluorescence trajectories of single ligand molecules.

A similar approach was used to observe the reversible redox-reaction of immobilized perylene diimide dyes^[191]. In the present work we expanded this concept to the more general case of irreversible reactions. In order to observe the initial and final state we had to make sure that the reactive group was part of the chromophoric structure^[175]. More specifically, we were interested in following the conversion of a single substrate molecule along its reaction pathway to the final product during the well known epoxidation reaction

on a double bond with *m*-chloroperbenzoic acid (*m*CPBA)^[192].

Here, the course of the reaction is embedded by the disappearance of the fluorescent substrate and the appearance of the fluorescent product. The experimentally most convenient and reliable indicator of a completed reaction is the change of the emission color^[2,32]. Besides the design of an appropriate probe molecule for epoxidation, where we could rely on previous experiments with BODIPY dyes^[2,193], other challenges have to be overcome. For maintenance of single-molecule conditions during the whole reaction, the fluorescent substrate is less abundant by several orders than in experiments with fluorogenic substrates but the concentration of the co-reagent prevails in large excess. Continuous observation until reactive collision takes place can be achieved using less mobile or even immobile substrates. Finally, the substrate must fluoresce until the reaction proceeds hence demanding a photo-stable fluorophore without addition of stabilizers. In the following, we present a system, which fulfills the mentioned requirements. To probe the epoxidation reaction with SMFS, we designed the fluorescent probe oxy-allyl BDP **(1)** (1-Methyl-(*E*)-3-(2-allyloxy)styryl-4,4'-difluoro-bora-3a,4a-diaza-(*s*)-indacene) consisting of a BODIPY core expanded by an oxy-allyl styryl unit (figure 13 a). Its synthesis followed the conventional Knoevenagel-like condensation^[54,55].

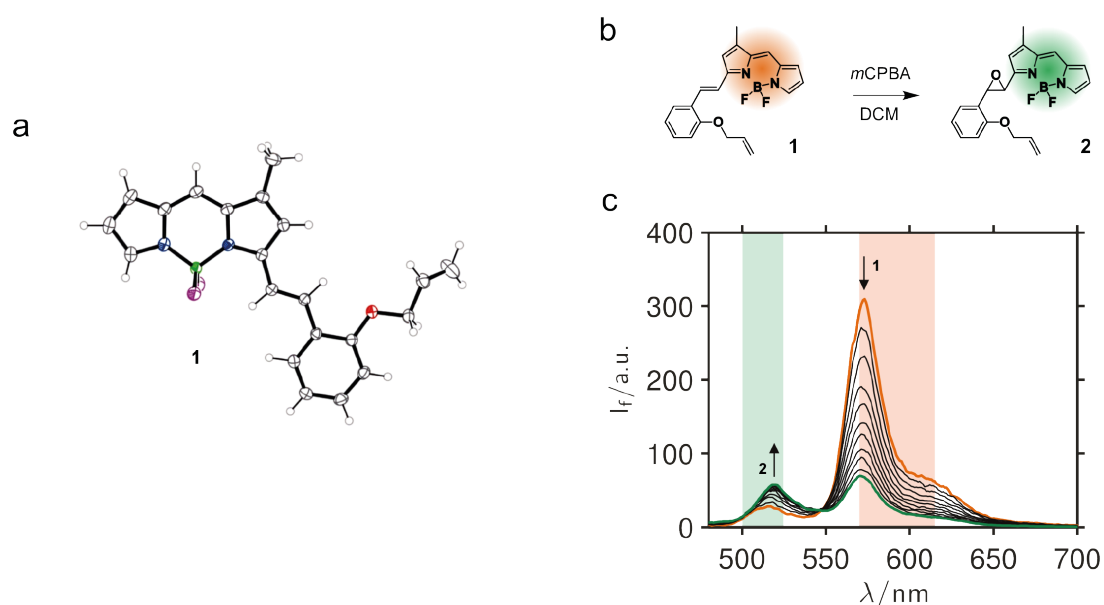


figure 13: Epoxidation of (1) with 200fold excess of *m*CPBA yields (2) with significantly changed emission properties. a, Crystal structure of the substrate oxy-allyl BDP (1). b-c, Epoxidation of (1) (red line) with *m*CPBA to the product (2) (green line) can be followed as a spectral shift in fluorescence emission. The green and red shaded areas signify the wavelength range of the emission filters used in single-molecule experiments for product and substrate detection respectively. Emission spectra were recorded after addition of 200fold excess of *m*CPBA (~0.2 mM) over 6 h with an excitation wavelength of 470 nm.

The previously introduced styryl-BODIPY system has already shown promising results in epoxidation reactions^[193], while here the additional tagging with an oxy-allylic residue serves as linker for covalent surface binding (figure 14 a). This latter moiety is not expanding the chromophoric π -system resulting in almost indistinguishable spectral properties compared to the formerly studied system. Furthermore, the missing conjugation ensures that surface binding minimizes influences on the electronic properties of the substrate.

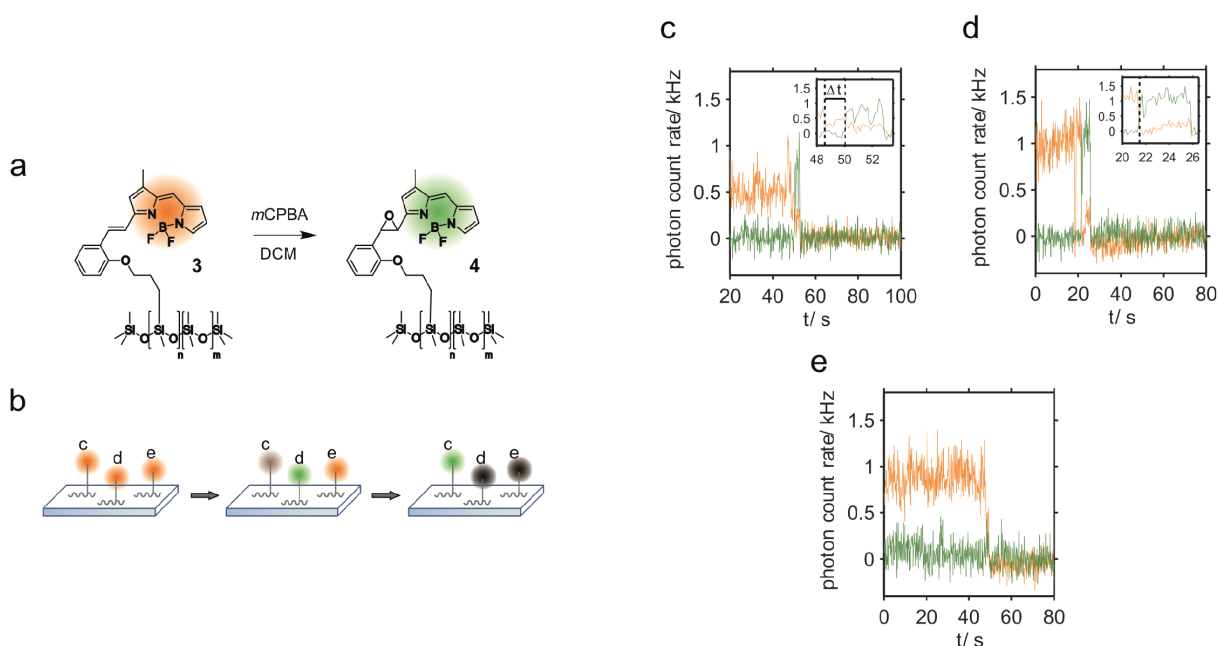


figure 14: Proposed reaction of immobilised (3) and characteristic signatures of the different reactions and reaction pathways observed in time-resolved single-molecule experiments. a, Reaction scheme of the epoxidation of immobilised (3) to (4). b, Schematic representation of the three different conversions observed in single-molecule experiments. c-e, Single-molecule traces of substrate (570-615 nm, yellow) and product emission (500-525 nm, green) recorded at 7.4 Hz show specific features that are characteristic for substrate conversion via a dim intermediate state (c), immediate conversion (d), and photo-bleaching of (3).

Epoxidation of the yellow fluorescent BODIPY moiety ($\lambda_{em} = 572$ nm) with *m*CPBA in excess leads to formation of (2) with green fluorescence ($\lambda_{em} = 518$ nm) due to shortening of the chromophoric unit (figure 13 b)^[2,193]. The blue shift of the emission by roughly 50 nm as a result of the transformation provides the required color change by which the initial substrate (1) and the reaction product (2) can be unambiguously assigned in a two-channel detection scheme. The overall performance remains unchanged when the dye is immobilized.

For single-molecule experiments (1) was first covalently attached to polysiloxane polymer HMPS (hydridomethyldimethyl-poly-siloxane) via hydrosilylation of the allylic double

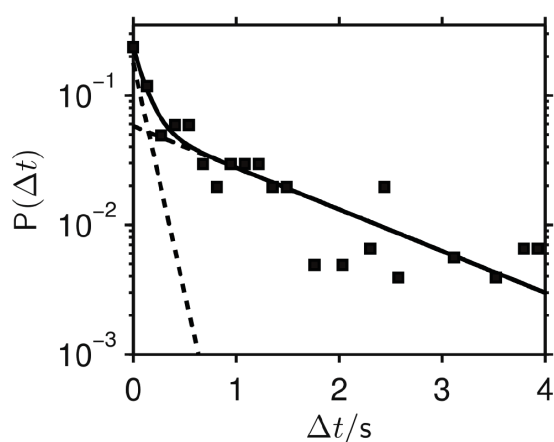
bond^[194,195]. Resulting labeled polymer was immobilized on a glass cover slide. We tested different solvents for their suitability in SMFS and found DCM being the most suitable for the epoxidation reaction while toluene and ethylacetate showed rather high fluorescence background. Reactions of individual substrate molecules (**3**) with *m*CPBA (0.2 mM) in DCM to oxidized product (**4**) were recorded on a TIRF microscope equipped with simultaneous laser excitation at 532 and 488 nm (figure 14 a, b). Dual-color detection in the wavelength ranges of 570-615 nm for the yellow and 500-525 nm for the green fluorescence (figure 13 b) is realized by an emCCD camera operated at a frame rate of 7.4 Hz, *i.e.* 1/135 ms⁻¹. The immobilized probes exhibit a photo-stability sufficient for extended observation periods (up to one minute, compare to figure 14 e). Moreover, the marginal hydrogenation of the double bond during preparation leading to initially green fluorescent spots was used to prove perfect alignment of the two detection channels.

Epoxidation was initiated by addition of *m*CPBA (0.2 mM) in DCM. Immediately after sealing with a second cover slide the sample was placed on the microscope for image acquisition (~2 min). In total, we acquired 1595 single-molecule traces, which were manually inspected and categorized in three relevant classes (figure 14 b). The traces in figure 14 c-e show the background corrected fluorescence emission recorded in the substrate (yellow) and the product channel (green). More than 90 % of single-molecule traces showed a loss of substrate emission in a single frame without change to product emission. We attribute this behaviour to photo-bleaching of individual substrate molecules or oxidative destruction of the chromophoric system as side reaction. The latter is also observed in ensemble experiments (figure 13 c). However, a relatively high percentage of traces (115 traces, *i.e.* ~7 %) exhibit a clear spectral shift of the emission from substrate to product channel (figure 13 b).

Again, we observed that product emission is always terminated in a single frame due to photo-bleaching (figure 14 c and d) clearly indicating the single-molecule nature of the investigated system. We emphasize at this point the well-known benefits of single-molecule techniques for investigating chemical reactions in which significant trajectories can be selected specifically. Design of our experiments and spectral detection ranges strongly suggest that the spectral shift observed in single-molecule experiments signifies conversion of the double bond in (**3**) to an epoxide in (**4**) (figure 14 c, d). The more than 20fold increased probability is a clear indication that the observed spectral shift in presence of *m*CPBA occurs due to epoxidation of the exocyclic double bond leaving the

chromophoric BODIPY core intact, in good agreement with previous findings^[2,193]. Epoxidation by *m*CPBA is assumed to proceed most probably in a concerted reaction^[192] via a single transition state within a few picoseconds and thus far below the time resolution of the image acquisition. Most trajectories obeyed this expected immediate conversion from yellow to green fluorescence. However, long lasting dim states were frequently observed during conversion (figure 14 c). Therefore, we collected the lag time Δt (figure 14 c inset) of the dim states in a histogram. figure 15 a shows a semi-logarithmic plot of the probability densities, which we obtained by normalisation of the histogram.

a



b

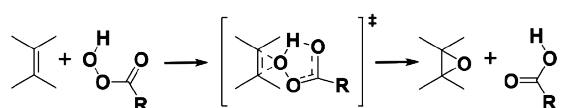


figure 15: a, Normalised probability histogram of the lag time Δt that is fitted best by a double exponential model with time constants of 0.12 s (75%) and 1.4 s (25%). b, Reaction scheme of the concerted epoxidation mechanism as proposed by Barlett^[192].

The simplest model that fitted the data with equally distributed fit residuals was a bi-exponential function that yielded two time constants of 120 ms and 1.4 s and amplitudes of 75% and 25%, respectively. This corroborates that the two time constants reflect two distinguishable reaction pathways yielding the same product (**4**). The more abundant reaction path, which can be attributed to the lifetime below our instrumental response time is compatible with the widely accepted, concerted reaction mechanism (figure 15 b). The intermediate state with the lifetime of roughly 1 s demands, however, for an alternative explanation. The lifetime of the intermediate state does not depend on the overall progress of the reaction in the ensemble. It is therefore unlikely that reaction pathways are caused by side-products, which would accumulate with time.

In this study, epoxidation of an immobilised BODIPY substrate by *m*CPBA was monitored at the single-molecule level. Single-molecule transients show significant lag times during

chemical transformation of involved double bond signalled by a shift in emission wavelength. Kinetic analysis results in two different lag times (120 ms and 1.4 s) indicative of two distinct reaction pathways. The shorter one is below the time-resolution of our instrument and corresponds to the well-known concerted mechanism occurring on picosecond-time scale. The slower one strongly indicates a transient intermediate formed upon epoxidation of the conjugated double bond with *m*CPBA. Although our current data allows distinguishing the two pathways, we can only speculate on its nature.

We could exclude light-driven dim states by additional experiments at higher excitation intensity, which gave similar results. Thus, possible explanations for the intermediate state could be alternative reaction pathways. A radical intermediate is improbable as those are usually not associated with fluorescence emission and might not explain the weak emission we observe. Alternatively, an extended mechanism involving protonated epoxide as intermediate has been proposed and discussed already by different authors in the 1990s^[196]. This pathway was also supported recently by quantum chemical calculations^[197]. The transient nature of the proposed intermediate, however, imposes practical limitations for its experimental verification so far and might be fully understood with support of theoretical calculations estimating the energetic profiles of reaction pathways and intermediates.

In conclusion, we visualized the irreversible conversion of a substrate into a product by means of single-molecule detection. We provide a versatile experimental setup comprising probe design, immobilization and experimental conditions for single-molecule experiments that have high potential to study the wealth of organic reactions at double bonds. Interpretation of our experiments is based on the correlation between the spectral shifts observed in bulk and at single-molecule level indicative for a reaction of the double bond. Reaction details will be fully understood with additional chemical analysis. We further envision design of similar fluorescent probes where different specific reactions occurring can be directly observed and studied by means of single-molecule techniques. Such a toolbox has high potential opening new perspectives on observing, understanding and ultimately controlling chemical reactions^[40]. Beyond that, direct observation of the stochastic nature of chemical reactions provides a new way for perceiving, conceiving and realizing chemistry.

This work was part of a collaboration of Saarland University and Heidelberg University. The contributions from Dr. Arina Rybina and Dr. Carolin Lang are gratefully acknowledged.

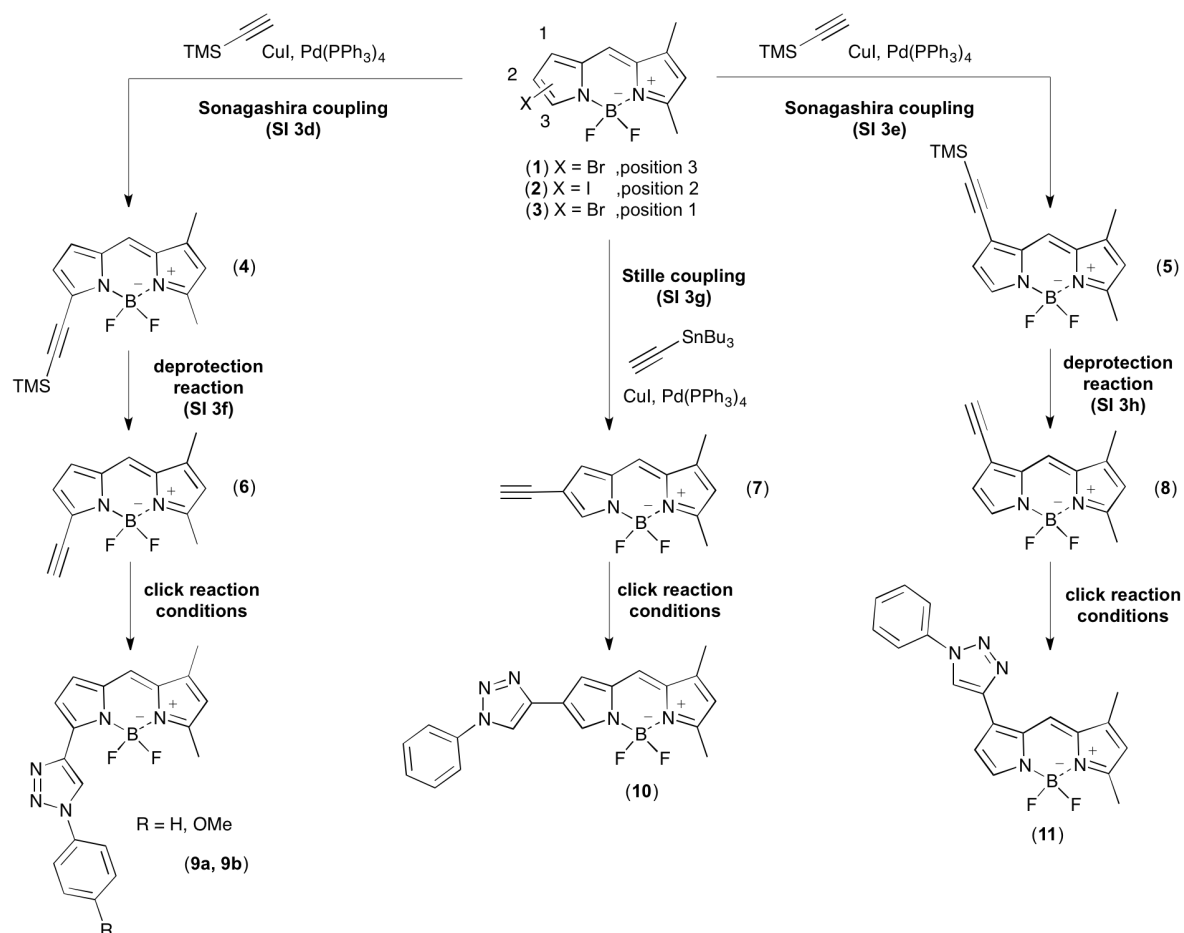
4. Cu^I-catalyzed azide-alkyne cyclization (CuAAC) - Click reaction^[4]

In 2001, B. Sharpless defined click reactions as transformations being compatible with a wide variety of functional groups.^[198] A prototypic example is Huisgen's 1,3-dipolar cycloaddition of azides with alkynes by Cu^I catalysis^[199–205]. Especially the development of fluorogenic substrates on its basis stimulated applications in the life science and greatly expanded the application range^[39,73,206,205,207–216]. A different approach relies on chromophores expanded by a reactive moiety, which undergo a distinct spectral shift during the transformation^[1,175]. In our contribution, we report such a chromophore-containing, "dual-color" reactive BODIPY probe. The presented substrate, undergoing a distinct bathochromic fluorescence shift and thus reducing background signal during CuAAC, allows for following the reaction by spectral and time-resolved fluorescence microscopy^[1,74,78,175,206,207,217–219].

Our interest in click chemistry arose only recently, when we realized that only few fluorogenic substrates with negligible background fluorescence exist for microscopic applications^[74,78,206,207,217]. For reaction monitoring by means of fluorescence, a shift in emission wavelength describes the most convenient approach for signal tracking^[1,32,94,175]. BODIPY dyes were chosen as scaffold due to their convenient optical properties and easy accessibility via condensation of two pyrroles^[52–54]. The benefit of the here proposed reactive probes is twofold: on the one hand, red-shifted electronic spectra of the product lead to unprecedented fluorescence enhancement. Thus, some of the noticed limitations in sensitivity can be overcome without the need of a second chromophore as energy-transfer acceptor^[74]. On the other hand, suchlike two-color emissive, reactive probes can act as "molecular chameleons" and are examples among more general attempts to visualize single-molecule chemistry on a microscopic scale^[3,32,33,92,94,220].

Consequently, the reactive group has to be part of the chromophoric system changing its size (participant approach)^[3]. As any conjugated ring system, *i.e.* here the triazole after the click reaction, is oriented perpendicular to the chromophore plane when in the *meso* position and thus not conjugated to the latter, fluorescence shifts will be very small or even hypsochromic^[29,54,92]. Derivatisation of α , β , or γ position (scheme 34), should therefore induce a presumably bathochromic change in wavelength^[1,54]. Accordingly we

first investigated the most suitable position on an unsymmetrical BODIPY core for reaction monitoring (scheme 34).



scheme 34: Synthesis of reactive probes for CuAAC-click reaction conditions: 10^{-4} M BODIPY, $8 \cdot 10^{-6}$ M CuSO₄, $2 \cdot 10^{-5}$ M NaAsc, $3 \cdot 10^{-2}$ M phenyl azide, EtOH:H₂O – 2:1, rt, min. 6 h (Appendix 7.2.6 for further details).

All BODIPY compounds were synthesized according to existing procedures^[56,58,171,221,222]. UV-Vis and fluorescence spectroscopic characterization of all components was done (table 2; figure 16; Appendix 7.2.6). CuAAC was investigated at micromolar dye concentration. Under these conditions, almost stoichiometric amounts of Cu^{II} and ascorbic acid were employed and large excess of the azide is added for establishing reasonable conversion kinetics. The reaction process was measured following fluorescence signal of each alkyne compound and the corresponding reaction product. Excitation of weakly absorbing, spectrally broad higher excitation states at 415 nm ensured that all chromophores could be excited at the same time despite unknown spectral shifts during the conversion.

table 2: Spectroscopic details of the favored dyes (see Appendix 7.2.6 for data of all compounds).

compound	$\lambda_{\text{abs}} / \text{nm}$	$\lambda_{\text{ex}} / \text{nm}$	$\lambda_{\text{em}} / \text{nm}$	$\tau / \text{ns (DCM)}$	Φ (DCM)
α -TMSAc-BODIPY (4)	529	529	540	5.3	1.00 – 0.02
α -Ethynyl-BODIPY (6)	518	518	529	6.5	0.89 \pm 0.02
Click product (9)	544	544	555	6.1	0.73 \pm 0.05

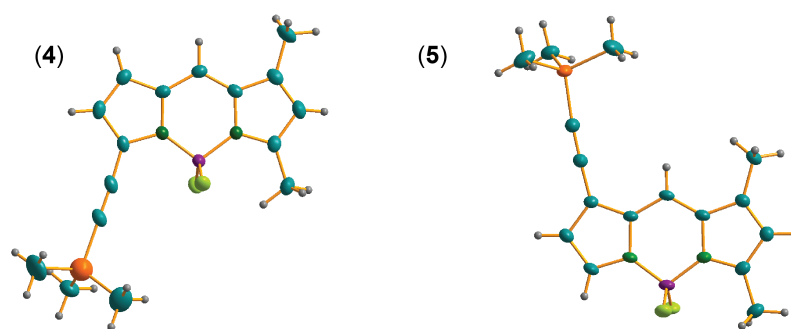


figure 16: X-ray crystallographic structures of the stabilized precursors of two ethynyl BODIPYs. The fluorescent alkynes (6) – (8) did not withstand crystallization without decomposition but were unambiguously identified in NMR by formation of the characteristic alkyne-H signal at $\delta = 3.1 - 3.6$ ppm (Appendix 7.2.3)^[56,171].

Conversions of the different substrates are compared (figure A9). First, the reaction of α -ethynyl BODIPY (6) with phenyl azide was investigated. A change in fluorescence wavelength from $\lambda = 528$ nm of (6) to $\lambda = 548$ nm of the product is visible. The spectral shift is large enough for spectral separation, as the spectra are rather narrow ($\Delta\lambda_{\text{FWHM}} \approx 20$ nm) over the whole course. At 538 nm an isoemissive point appears after approximately 2 hours. β -ethynyl BODIPY (7) was converted under same conditions. Despite a noticeable spectral shift during the reaction from $\lambda_{\text{em}} = 540$ nm to $\lambda_{\text{em}} = 556$ nm (figure A9), this change is smaller. Additionally, due to overlapping emission spectra, which even become broader during the reaction ($\Delta\lambda_{\text{FWHM}} \approx 42$ nm \rightarrow 60 nm)^[56], an optical separation appeared in vain. We therefore excluded compound (7) from further investigations. The third investigated compound (8), exhibits optical properties similar to compound (6). During the conversion, no optical shift is detected, but the emission band of γ -ethynyl BODIPY (8) slowly diminished (figure A9). For verifying that any reaction except from decomposition

of the BODIPY compound (**8**) occurred, fluorescence lifetime analysis was performed at the beginning and after 24 h. A prolongation from $\tau_{fl(\mathbf{8})} = 4.7$ ns to $\tau_{fl(\text{corr. product})} = 5.7$ ns (both in EtOH/H₂O) indicated a successful conversion, in agreement with previously noticed fluorescence lifetime prolongations due to substitution at this position^[171]. We conclude from these experimental data that CuAAC of compound (**8**) hardly affects the steady-state spectroscopic properties and (**8**) was consequently discarded from further experiments. As a result of the comparison, (**6**) exhibits the optimal parameters for reaction monitoring. For further improving optical separation, three different azide moieties, benzyl azide, phenyl azide and anisyl azide, were tested for conversion (figure A9). Every species is expected to enlarge the chromophoric system by a different amount. Comparison of the resulting spectra reveals, however, that only the triazole ring as common structural element, is sufficient to shift the emission by roughly 20 nm to the red. Exhibiting the largest fluorescence change, anisyl azide was used for following the kinetics (figure 17 A). After some initial reduction due to putative Cu^I-acetylide formation, the fluorescence intensity of the starting compound diminished in the same manner as the product fluorescence emerged (figure 17 A, inset: kinetic analysis of substrate conversion and product formation¹). A suchlike isoemissive point at $\lambda_{em} = 540$ nm was already found in

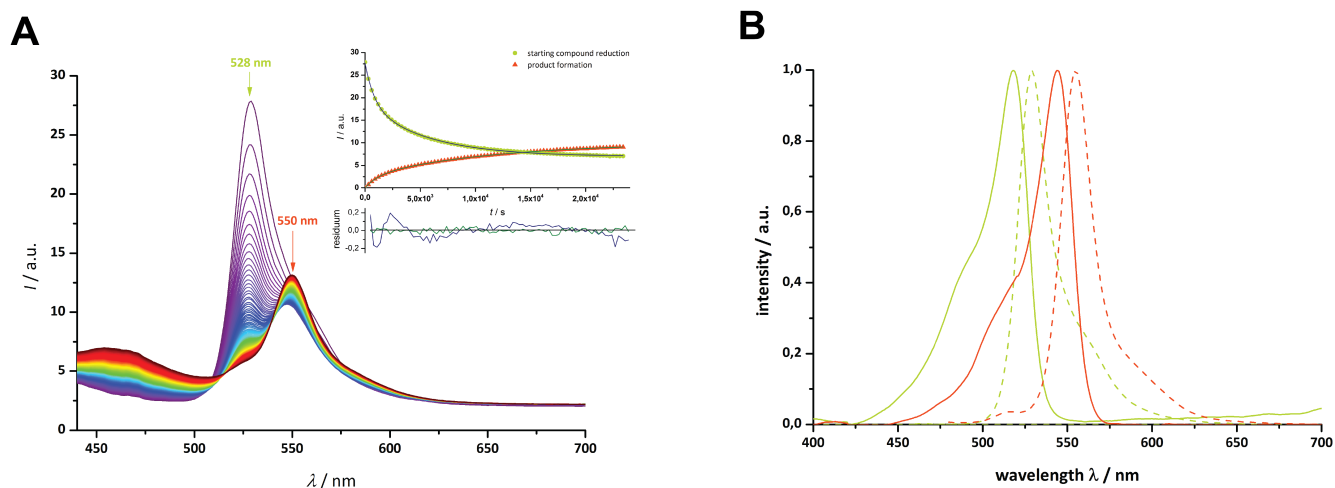


figure A9 after the initial phase.

figure 17: A: Conversion of (6**) with anisyl azide to (**9b**) (reaction progress over 6 h, spectra taken every 5 min); B: Comparison of compounds (**6**) and (**9b**).**

¹ α -ethynyl BODIPY depletion: $k_{SC-1} = 1,17 \cdot 10^{-3} \text{ s}^{-1}$, $k_{SC-2} = 1,77 \cdot 10^{-4} \text{ s}^{-1}$
 product formation: $k_{P-1} = 0,86 \cdot 10^{-3} \text{ s}^{-1}$, $k_{P-2} = 0,87 \cdot 10^{-4} \text{ s}^{-1}$

A closer inspection of the kinetics is obtained by a biexponential fit function. It is interesting to note that no time lag for product formation was found indicating, partially, rather rapid Cu^I-acetylide formation. The analysis yields rate-constants, which were slightly larger for the substrate depletion than for the product emergence². Evidence for a side reaction is provided by appearance of a hypsochromically shifted emission band at $\lambda_{em} = 470$ nm concomitant with product formation. The broad emission band was traced back to BODIPY-decomposition, that was only noticed under the use of anisyl azide. We learn, however, from these kinetic experiments that a successful visualization of the conversion appears feasible in microscopy between 15 min and 2 h. After reaction completion, the product was isolated, identified by its typical ¹H NMR signal ($\delta = 8.83$ ppm)^[223] and subsequently characterized by optical spectroscopy (table 2, Appendix 7.2.6, figure A38, A39, A45). A bathochromic shift of 26 nm with respect to the substrate (figure 17 B) is observed. Both molecules slightly differ in their fluorescence lifetimes as well (table 2).

² α -ethynyl BODIPY depletion: $k_{SC-1} = 1,17 * 10^{-3} s^{-1}$, $k_{SC-2} = 1,77 * 10^{-4} s^{-1}$
product formation: $k_{P-1} = 0,86 * 10^{-3} s^{-1}$, $k_{P-2} = 0,87 * 10^{-4} s^{-1}$

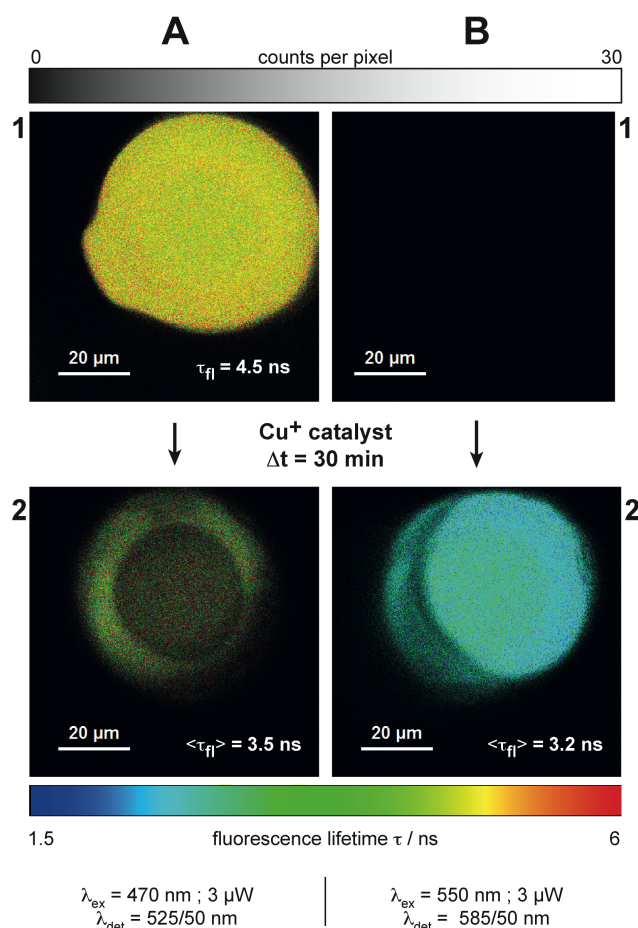


figure 18: Visualization of click reaction between α -ethynyl BODIPY (6) and azide agarose on a glass surface with corresponding fluorescence lifetimes; column A: excitation with $\lambda_{ex} = 470 \text{ nm}$ @ 20 MHz, emission filter $\lambda_{det} = 525/50 \text{ nm}$; column B: excitation with $\lambda_{ex} = 550 \text{ nm}$ @ 80 MHz, emission filter $\lambda_{det} = 585/50 \text{ nm}$. Time lag between 1 and 2 is 30 min.

The obtained spectroscopic characteristics from ensemble measurements can be exploited for microscopic visualization (figure 18). Commercially available azide-functionalized agarose beads were adsorbed on a glass slide. The first detection channel uses excitation with a pulsed diode laser at $\lambda_{ex} = 470 \text{ nm}$ and $\lambda_{det} = 525/50 \text{ nm}$, thus ensuring detection of the starting compound (6) (column A, figure 18). A second channel only addresses the triazole product by means of a pulsed fiber laser operating at $\lambda_{ex} = 550 \text{ nm}$ and $\lambda_{det} = 585/50 \text{ nm}$. Background fluorescence was negligible (figure A10, A14).

α -ethynyl BODIPY (6) was added (figure 18, 1st row). Green emission shows BODIPY accumulation within the bead. τ_{fl} over all pixels is 4.5 ns, distinctly reduced compared to the lifetime of BODIPY (6) in the solvent ($\tau_{fl}(\text{EtOH}) = 5.6 \text{ ns}$).

In agreement with the control experiment (figure A14), this is the result of a changed micro-environment, e.g. an altered refractive index^[224]. Analyzing the same bead with $\lambda_{ex} = 550 \text{ nm}$, no signal was noticed. This result hints to negligible light-induced AAC, as B1 was

recorded immediately after A1.

After addition of CuSO₄/NaAsc in H₂O, green fluorescence is visible deriving from unreacted α -ethynyl BODIPY adsorbed to the agarose network (averaged lifetime $\langle\tau_{fl}\rangle = 3.5$ ns, A2). Noteworthy, the control experiment (figure A14) exhibited the same tendency in lifetime reduction. We therefore attribute this common shortening to the locally increased concentration of cuprous and cupric ions as triazole compounds are known for their good complexation behavior of Cu^I[225]. Fluorescence in the product channel (figure 18 B2), which was not detected in the control experiment, perfectly matches the spectroscopic behavior found in the cuvette experiments. Together with an even further reduced fluorescence lifetime (averaged lifetime $\langle\tau_{fl}\rangle = 3.2$ ns), these findings unambiguously proved triazole formation.

In our work, we established a fluorescent reaction system for studying CuAAC and its visualization by fluorescence microscopy. Fluorophores bearing C-C triple bonds at different positions as target for click chemistry were synthesized and characterized. It turned out that the α -position at the BODIPY core is most sensitive for following CuAAC by fluorescence spectroscopy (figure 17). Comparison of several azide moieties revealed that only the triazole ring is mostly responsible for the bathochromic fluorescence shift by more than 20 nm. Finally, we visualized the click reaction using azide agarose (figure 18). A careful combination of excitation and detection conditions easily separates product and substrate fluorescence. After catalyst addition, fluorophores located within the beads changed their emission color from green to yellow as in the cuvette experiment.

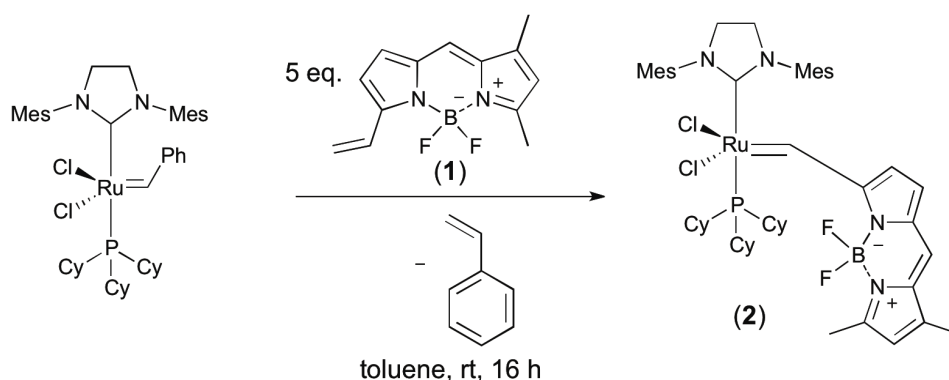
A two-color fluorescent probe for investigating CuAAC is presented. Due to the distinct bathochromic shift, our compound considered as fluorogenic substrate for application in heterogeneous catalysis, when only the product is excited^[33]. It should be noted that exactly these latter features are the main advantages over all other yet available substrates for single-molecule chemistry investigation, where the chromophore extension was shortened leading to a hypsochromic shift^[1,32,94]. The presented data serve as basis for ongoing single-molecule experiments and will be continued similarly to previous work^[1].

5. Metathesis reaction

A Ruthenium-carbene complex was synthesized, where the chromophore is directly connected to the metal center. Therefore, metathesis reaction introduces a boron dipyrromethene (BODIPY) compound into the target molecule. The formation of two compounds with distinguishable fluorescence properties starting from styrene could be analyzed in cuvette experiments and was confirmed with ^{19}F -NMR. The presented fluorogenic compound enables fluorescence labeling of terminal double bonds and by adjusting the exposure conditions single-molecule trajectories could be recorded. We foresee application of this colorization scheme in material sciences, where combination with super-resolution can be achieved.

The metathesis reaction represents a milestone in chemical history because of different reaction types and a broad variety of compatible functionalities^[226–231]. The employed Mo / Ru catalysts differ in stability, selectivity and activity^[232]. Over the last two decades, catalysts were further optimized by substituting phosphine-ligands with *e.g.* N-heterocyclic carbenes^[23,233–241]. Despite systematic mechanistic studies, several questions concerning polymer chain growth and orientation still remained unanswered^[34,82,242]. Recently, single-molecule fluorescence techniques have been employed paving new ways for investigating catalytic reactions. For instance, the synthesis of carbenes bearing a fluorescence label enabled single-molecule studies of polymer orientation^[82] and investigation of metathesis mechanisms in ensemble measurements^[79]. Fluorescently labeled monomers proved homogeneous catalysis during polymer formation^[34]. However, visualization of the elementary steps of the catalytic cycle has not yet been attempted. For this long-time purpose, we synthesized a metathesis complex bearing a fluorophore as carbene unit. Thus, the fluorophore moiety is directly bound to the reactive center and therefore quenched in its fluorescence emission. Consequently, the quenched fluorophore is now part of the metathesis reaction enabling observation of two-color, fluorogenic turnover (participant approach)^[2,3,34]. In the following, we exemplify the use of the BODIPYlidene compound (**2**) for monitoring the simultaneous formation of two optically different products and for tagging terminal double bonds in microscopy. Derivatives of Ruthenium-based metathesis catalysts compounds are generally

synthesized combining a precursor like 2nd generation Grubbs catalyst and an olefin unit in excess, *i.e.* α -vinyl-BODIPY (**1**) in scheme 35^[235,243].



scheme 35: Synthesis of BODIPYlidene Ruthenium metathesis reagent (2).

The equilibrium is shifted towards product formation by removal of volatile styrene. Careful work-up procedures allowed isolation of dark blue crystals of the BODIPYlidene Ruthenium metathesis reagent (**2**). Spectroscopic analysis exhibit absorption at $\lambda_{\text{abs}}(\text{toluene}) = 612 \text{ nm}$ (figure 19 A) and missing emission indicates fluorescence quenching ($\tau_{\text{fl}} \leq 80 \text{ ps}$, $\lambda_{\text{ex}} = 600 \text{ nm}$, $\lambda_{\text{det}} = 650 - 720 \text{ nm}$, Appendix 7.3.6) due to the binding to the Ruthenium center. This is in agreement with a recent publication which describes quenching of BODIPY fluorescence by various transition metals including Ru(II)^[244]. Isolation of the blue-colored BODIPYlidene complex was not possible using 1st generation Grubbs catalyst as starting compound because of rapid decomposition into α -carbonyl BODIPY^[245]. The stability of the compound (**2**) presented here is much higher, although intrinsic decomposition was observed on the time-scale of several hours^[246].

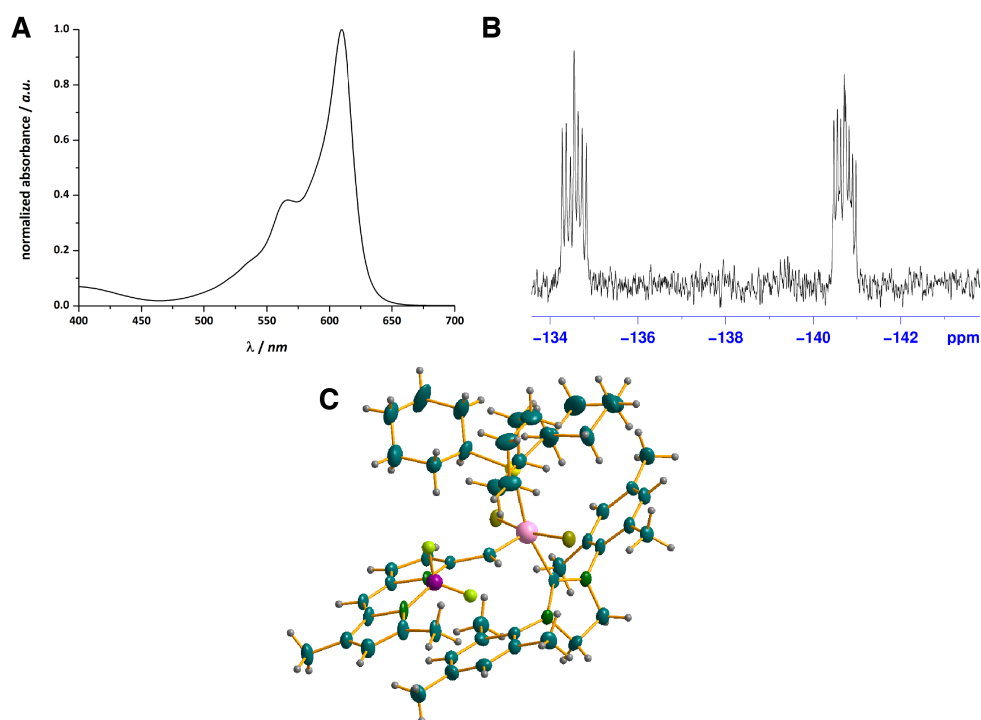


figure 19: A: UV/Vis spectrum of BODIPYlidene Ru metathesis reagent (**2**). No doubtless fluorescence emission was noticed, which could be attributed to (**2**); B: ^{19}F -NMR of the catalyst showing two non-equivalent fluorine atoms with germinal F-F-coupling ($^2J_{\text{F-F}} = 102$ Hz) and quartett splitting by coupling with ^{11}B ($J_{^{19}\text{F-}^{11}\text{B}} = 34$ Hz) of (**2**); C: crystal structure of BODIPYlidene reagent (**2**).

The BODIPYlidene metathesis compound (**2**) was analyzed by ^1H -NMR, ^{19}F -NMR and X-ray crystallography (figure 19 B, C, Appendix 7.3.7). Aside of the common BODIPY signals in the usual aromatic range, a carbenoide H appeared at $\delta = 21.7$ ppm (figure A56). Interestingly, this characteristic signal is among the most downfield-shifted 2nd generation Grubbs catalyst carbenoide signal ($\delta = 19.16$ ppm) for the available carbenoide derivatised compounds^[237]. The extended electron density of the carbene bearing BODIPY can be made responsible for this additional screening^[247]. The ^{19}F -NMR of the complex showed two signals of the two fluorine atoms of the BF_2 -group ($\delta = -134.6$ and -140.7 ppm) with germinal coupling ($^2J_{\text{F-F}} = 102$ Hz), together with the ^{19}F - ^{11}B coupling ($J_{^{19}\text{F-}^{11}\text{B}} = 34$ Hz), thus providing strong evidence for a fixed BODIPY moiety. The carbene including binding angle (C-C-Ru) was determined by X-ray diffraction (figure 19 C) and was found to be slightly larger (133.4°) than the ideal sp^2 hybridization.

Metathesis catalysts transfer their carbene moiety onto olefins during the catalytic cycle^[242]. In our case, the BODIPYlidene chromophore is turned into a fluorescent species. The conversion with *cis*-stilbene solely yields α -styryl BODIPY (**3**) which was characterized

previously (see Appendix, 7.3.1)^[193]. As any alkene can bind with two different steric orientations, more than one product is expected with styrene as co-substrate (figure 20).

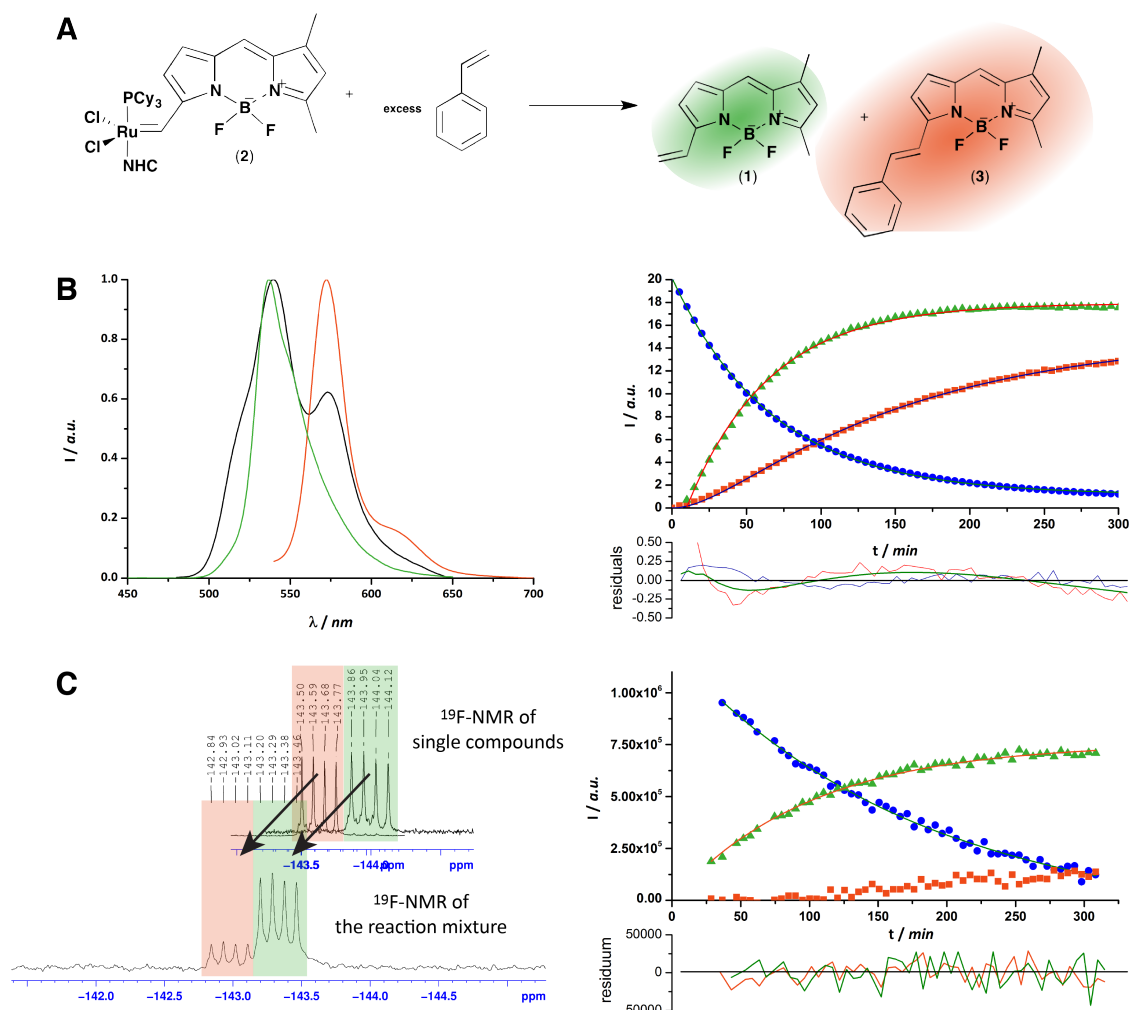


figure 20: A: Conversion of freshly distilled styrene with (2); B: On the left: fluorescence emission spectra (0.3 μM) of (1) (green), (3) (orange) and the diluted mixture after the reaction (black). On the right: in-situ kinetics of formation of (1) (green), (3) (orange) and decomposition of reagent (2) (blue), monitored by UV/Vis for (2) and fluorescence emission spectroscopy for (1) and (3) (30 μM; ratio (2) : styrene ~ 1 : 1000; solvent toluene); C: On the left: ¹⁹F-NMR spectra (12 mM) of (1) (green), (3) (orange) and the diluted mixture after the reaction (black). On the right: in-situ kinetics of formation of (1) (green), (3) (orange) and decomposition of reagent (2) (blue), monitored by NMR spectroscopy (ratio (2) to styrene 1 : 100; figure A50, solvent deuterio chloroform). Data are fitted by a consecutive reaction model on the basis of pseudo-first order behavior (Appendix, 7.3.3). Please note that the concentration of styrene was slightly different in both experiments runs (see Appendix 7.3.4, 7.3.5 for details), the shift in ¹⁹F-NMR upon addition of styrene presumably results from a different solvent composition and is also observed for (2).

The generation of (3) followed the kinetics of sequential reaction (2) → intermediate → (3) (see table 3 for time constants and Appendix 7.3.3-5 for details of the analysis). According to the kinetic analysis, formation of an intermediate, which could be the putative Ruthenacyclobutane derivative, turned out to be more rapid than its decomposition. The same kinetic behavior was also observed in the reaction of (2) with stilbene and with diphenyl-

butadiene. In the latter case, **(3)** and another product with an even further red-shifted emission was observed (see Appendix 7.3.1).

Formation of **(1)** showed similar kinetics for the second process, *i.e.* intermediate decay with a distinctly faster, not resolvable initial reaction. It should be mentioned that an exact analysis of the latter kinetics is aggravated by reabsorption effects, slow intrinsic decomposition of **(2)** and putative long-term consumption of **(1)** with release of volatile ethene. However, dilution of the sample taken after 24 h, indicated formation of **(1)** and **(3)** according to their fluorescence (figure 20 B).

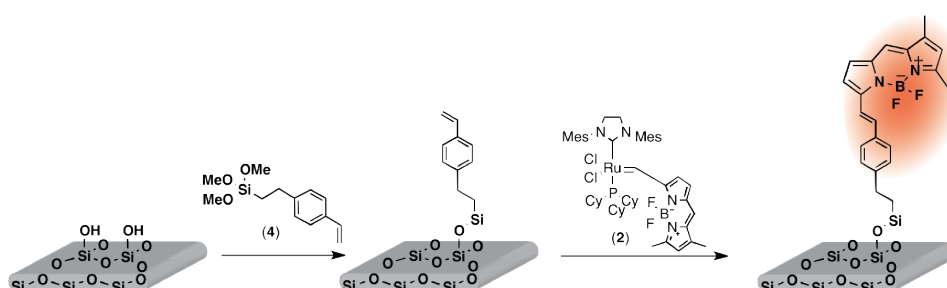
The reaction of metathesis reagent **(2)** with freshly distilled styrene in excess yields α -vinyl BODIPY **(1)** and α -styryl BODIPY **(3)** in a ratio of 4:1 (α -vinyl : α -styryl), as estimated by ^{19}F -NMR signal integration (figure A52). As the large excess of styrene hid all specific signals of **(1)** and **(3)** in ^1H -NMR, ^{19}F -NMR studies provided quantitative insight into reaction kinetics solely of BODIPY compounds (figure 20 C). The formation of α -styryl compound **(3)** was slower compared to fluorescence measurements, which could be a sign of some inhibition. Despite these differences, the outcome of both spectroscopic assays resembles each other: Whereas **(2)** seems to be directly converted to **(1)**, the formation of products with internal double bonds is delayed. We conclude that the general behavior, *i.e.* the decomposition of **(2)** and formation of **(1)** and **(3)**, is similar for both spectroscopic assays. Formation of **(1)** and **(3)** as products was unambiguously confirmed by optical and magnetic resonance spectroscopy (figure 20 B, C, table 3, figure A51). A unified kinetic and mechanistic picture by which **(3)** is formed, however, remains hidden yet.

table 3: Comparison of the kinetic data estimated from optical spectroscopy and ^{19}F -NMR experiments. Please note that the condition of both experiments were different.

	decomposition of compound (2) / min ⁻¹	formation of compound (1) / min ⁻¹	formation of compound (3) / min ⁻¹
optical measurements	$k_1 = 1.18 * 10^{-2}$	$k_1 = 1.81 * 10^{-2}$	$k_1 = 7.02 * 10^{-3}$ $k_2 = 3.66 * 10^{-2}$
^{19}F-NMR measurement	$k_1 = 5.55 * 10^{-3}$	$k_1 = 1.00 * 10^{-2}$	-/-

For demonstrating the reactivity of metathesis reagent **(2)** towards terminal double-bonds, a cover slide modified with styryl units is briefly exposed (~10s) to a solution of compound **(2)** (1 μM) in toluene and afterwards washed several times with the same solvent (analytical grade). The siloxane layer was prepared via gas phase silylation reaction

(scheme 36, see Appendix) using styrylethenyl-trimethoxysilane and a freshly cleaned (see Appendix) cover glass^[48,248].



scheme 36: Immobilization procedure for demonstrating reactivity of (2) towards terminal alkenes.

In this model case, the BODIPYlidene metathesis reagent (2) is supposed to be converted to corresponding α -styryl BODIPY (3) during exposure, according to the accepted mechanism, elongated by a linker to the surface^[242]. The formation of fluorescence was detected in an appropriate analysis channel, which was chosen by comparison with the spectroscopic data from ensemble spectroscopy (figure 21, $\lambda_{\text{ex}} = 550 \text{ nm}$, $\lambda_{\text{det}} = 560 - 610 \text{ nm}$). As any solvent and (2) were carefully removed, fluorescence can only emerge after complete sequence (2) \rightarrow Ruthena-cyclobutane \rightarrow (3), during exposure with (2). No fluorescence was detected without double-bond functionalization or without addition of (2) (see Appendix 7.3.2). Exposure of (2) dissolved in toluene onto functionalized surfaces allows for visualizing silane distribution (figure 21 A).

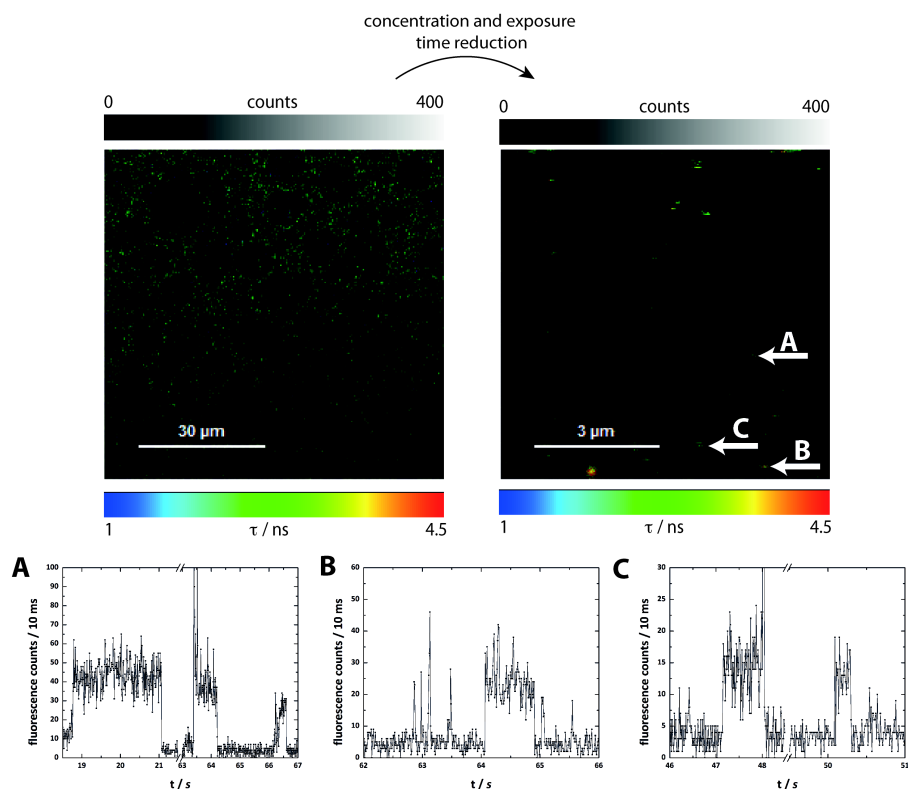


figure 21: FLIM images of styrylsiloxane functionalized surface treated with BODIPYlidene metathesis reagent (2). Different concentrations (A: 100 μ M; B: 100nM) and exposure times (A: 30 s; B: 3 s) show a related reactivity of (2). (256x256 pixel, 5 ms pixel dwell time, laser intensity: 1.41 kW*cm⁻² @ λ_{ex} = 550 nm).

Obviously, gas phase deposition of (4) results in circular structures of about 10 mm diameter, which might also reflect reactivity heterogeneities of the glass surface towards silanization. Noteworthy, there are hardly any other methods for visualizing monolayers of terminal bonds. FLIM (fluorescence lifetime imaging microscopy) showed reduction of the fluorescence lifetime of (3) when bound to the surface ($\tau_{fl} = 4.9$ ns \rightarrow $\tau_{fl} = 2.8$ ns), which could also be the result of the altered surrounding (air-glass interface) compared to solution. The coverage could be adjusted by reducing the reagent concentration from 100 mM to 100 nM and the contact dwell time finally yielding individual molecules as proven by single-molecule trajectories (figure 21 A - C)^[36,37,49,249,250].

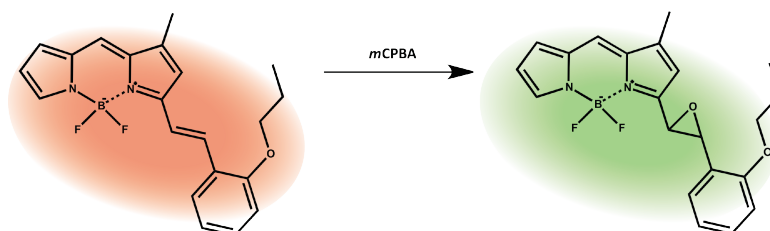
In summary, we synthesized and characterized fluorogenic BODIPYlidene Ruthenium complex (2). The presented compound has unique properties because a fluorophore is directly attached to the reactive metal center. Therefore, the formed reaction products emit different colors depending on the conjugation length and, thus, on the particular reaction they underwent. We demonstrate that reaction of (2) with a terminal double bond functionalized surface leads to single-molecule signals of immobilized orange fluorescent BODIPY units as a putative result of half a catalytic cycle during metathesis. We therefore

envision the usage of such fluorogenic, multicolor probes for unraveling the regioselectivity of chemical reaction on single-molecule level. Our experiments exemplify the potential of such fluorogenic complexes also for material sciences^[82] where terminal double bonds can be made visible in fluorescence microscopy down to the conditions of super-resolution^[35].

6. Summary

In this work, different fluorophores with double and triple bonds were presented. These dyes were used in single-molecule and microscopy approaches for reaction monitoring with changing optical properties.

The widely-investigated epoxidation reaction was used to survey reaction monitoring with the single-molecule approach. This reaction and the corresponding concerted mechanism proposed by Bartlett in 1950 is widely accepted and has been published in numerous chemistry textbooks^[192,251,252]. Consequently, the mechanistic processes derived from single-molecule analysis could be compared against preexisting literature on an extensively investigated chemical reaction. Single-molecule investigations were conducted with TIRF microscopy using an immobilized, orange BODIPY chromophore. The chromophore was elongated via Knoevenagel condensation forming a styryl moiety. The isolated double bond represents the reactive side of the fluorophore. This structural motif reacted with *m*CPBA to the corresponding oxirane and shortened the expanded π -electron system. Therefore, a hypsochromic shift was detected. This change in fluorescence signal was used for reaction monitoring (scheme 37).



scheme 37: Epoxidation of BODIPY synthesized for ensemble measurements^[1].

Initial investigations used ensemble measurements to gather information on the product formed and the reaction constants^[193]. On the basis of this data, it was then possible to investigate the reaction system on a single-molecule level. Immobilization was achieved via a second, external double bond combined with a reactive siloxane polymer. Single-molecule investigations revealed the known concerted mechanism^[192]. Furthermore, a second occurring reaction pathway could be detected via a transient intermediate, which, up until now, could only be estimated via theoretical calculations^[1,196,197].

The single-molecule method was further optimized by using a different optical detection window in a second reaction.

Cu^+ catalyzed alkyne-azide cyclization (CuAAC) has already been investigated using fluorescence methods. These investigations used fluorogenic systems, where the emission signal is created during product formation. These concepts were used for the investigation of ion binding^[74] or *in vivo* imaging^[207,253] (chapter 2.2). In contrast to these studies, the approach presented here enables *complete* reaction monitoring, from the starting compound to the final product including a bathochromic fluorescence shift for the first time. Therefore, triple bond derivatized BODIPYs were combined with several azides. Examining the chromophoric unit in different positions revealed the best structural isomer for such investigations. A variety of used azides show, that the triazole moiety is solely responsible for wavelength shift. When azide functionalized agarose beads are adsorbed onto a cover glass, the reaction progress can be observed on microscopic scale using optically separated channels^[4]. Such a bathochromic, eye-visible shift in emission wavelength was firstly used for reaction monitoring, reducing background fluorescence through a change of the optical detection window (figure 22).

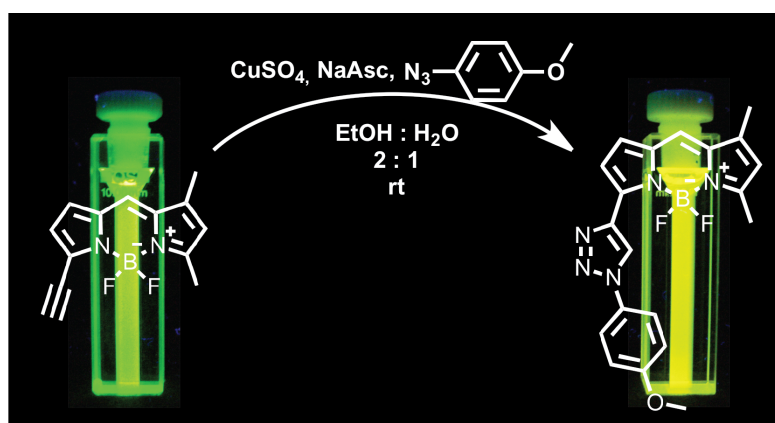


figure 22: Transformation of α -ethynyl BODIPY to α -triazol BODIPY via CuAAC. Reaction monitoring was firstly established using a bathochromic fluorescence shift (green to orange)^[4].

In the next step, the previously discussed techniques are combined to develop a detection system for metathesis reaction. The catalytic cycle can be visualized with the use of these fluorophores in single-molecule experiments.

Up until now, mechanistically, the coordinative behavior at the Ruthenium catalyst has not been clearly examined. The newly designed reaction system included only one external, reactive double bond, usable in single-molecule studies. A vinyl-BODIPY is transferred to the corresponding styryl derivative by cross metathesis. Again, a bathochromic wavelength shift is utilized for reaction visualization preventing background fluorescence.

The usability of the fluorophores was determined by combination of UV-Vis – fluorescence spectroscopy and NMR. Looking beyond the development of a visualization concept and the structural elucidation of the different compounds, a metathesis reaction intermediate could be synthesized and completely characterized. This compound represents a multichromophoric, fluorogenic metathesis reagent. The chromophore is located as a carbene unit and can be transferred onto molecules with an external double bond. Consequently, BODIPY dyes can be formed through a reaction with different conjugated olefins, which can be distinguished by their optical properties (figure 23). This characteristic is observable in NMR, ensemble and single-molecule investigations^[5].

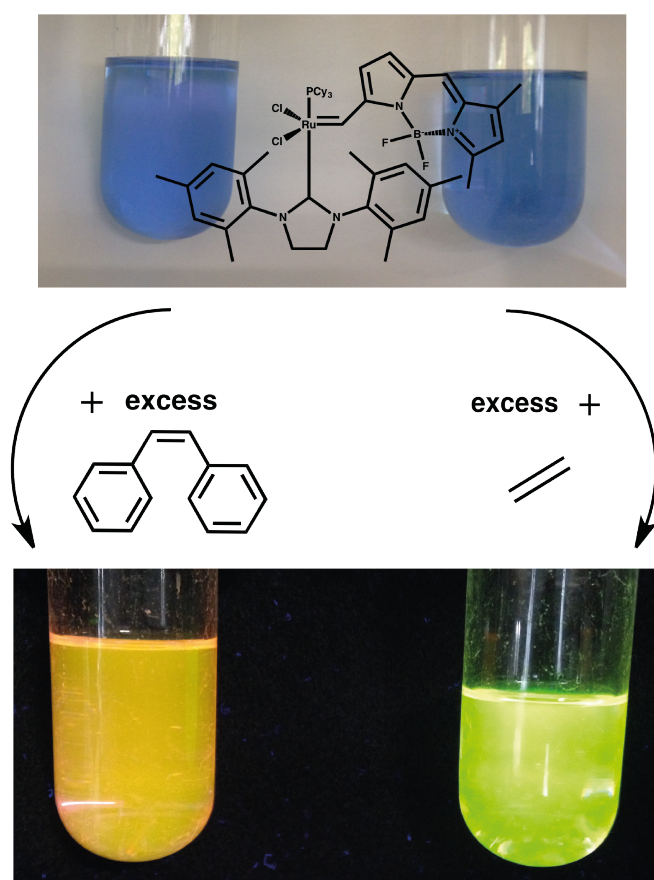


figure 23: Visualization of metathesis reaction: BODIPY metathesis reagent forms two different BODIPY chromophores depending on the conjugation length of the corresponding alkene^[5].

In contrast to previous work by A. Schmitt^[60], the metathesis reaction could be visualized with a regioselective, fluorescent system. It was possible to isolate the reaction intermediates formed and fluorogenic, multichromophoric behavior could be observed. Kinetic data could be extracted by two different spectroscopic methods, NMR and fluorescence ensemble measurements. Additionally, it was shown, that the characteristics

could be transferred on single-molecule level. This information is essential for further single-molecule mechanistic investigations.

7. Appendix

7.1. Epoxidation reaction

7.1.1. General Experimental

Chemicals and solvents

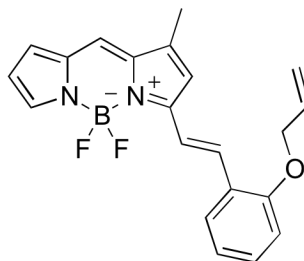
All starting materials and deuterated solvents were obtained from different commercial suppliers and used without further purification unless otherwise stated. Solvents for bulk and single-molecule experiments (tetrahydrofuran - THF and dichloromethane - DCM) had HPLC-grade quality. Anhydrous THF was prepared using an MBRAUN MB SCS-800 solvent purification system. All other solvents were dried under literature known procedures. Air- and moisture-sensitive reactions were conducted in oven-dried glassware by using standard Schlenk techniques under an inert atmosphere of N₂ or Ar.

Analytical and spectral techniques

¹H NMR spectra were recorded using Bruker Avance 300 (300 MHz) and Bruker Avance 400 (400 MHz) spectrometers. ¹³C NMR spectra were recorded using Bruker Avance 300 (75 MHz) and Bruker Avance 400 (100 MHz) spectrometers. Chemical shifts are reported in parts per million (ppm) and were calibrated to the residual signals of the deuterated solvents, coupling constants (J) are indicated in Hz. IR spectra were recorded on a Nicolet 6700 FT-IR with smart iTR ATR device (Thermo, San Jose, CA). Crystal structures were determined by Dr. V. Huch, Institute of inorganic chemistry, Saarland University, using the X8 ApexII X-ray diffractometer. Absorption and emission spectra were recorded with a Cary 500 Scan UV-Vis spectrometer and a Cary Eclipse 500 fluorescence spectrometer in dark quartz glass cuvettes. If not mentioned otherwise, the relative quantum yield Φ_f was determined with respect to two standard dyes (ATTO 565 and Sulforhodamine 101). HPLC-MS measurements were performed on an Agilent Technologies 1200 HPLC equipped with a binary solvent pump, autosampler, membrane solvent degasser, DAD detector and quadrupole mass spectrometer with APCI source. Separations were performed on a LiChrospher 100 RP-18e column (LiChroCART 250-4, particle size 5 μ m). Solvents (*n*-hexane and DCM) had HPLC-grade quality. Reactions were monitored using Silica on TLC PET-foils with a layer thickness of 0.25 mm and a pore size of 60 Å. Silica gel with a pore size of 0.040 – 0.063 mm as technical grade was used for column chromatography.

7.1.2. Probe synthesis and analytical characterization

Preparation of oxy-allyl BDP (1)



1-Methyl-(E)-3-(2-allyloxy)-styryl-4,4'-difluoro-bora-3a,4a-diaza-(s)-indacene

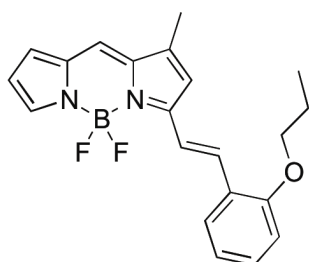
1,3-Dimethyl-4,4'-difluoro-bora-3a,4a-diaza-(S)-indacene (220 mg, 1.00 mmol, 1.00 eq) and *o*-allyloxybenzaldehyde (178 mg, 1.10 mmol, 1.10 eq) were added to anhydrous toluene (60 ml). The reaction mixture was heated to reflux. Immediately piperidine (851 mg, 10.0 mmol, 10.0 eq) and glacial acetic acid (600 mg, 10.0 mmol, 10.0 eq) were added. After refluxing for 2 h, the solvent was removed *in vacuo* and residues were purified by double column chromatography (DCM:hexane = 1:1, DCM:toluene = 1:1) to yield **1** as a violet solid (36.4 mg, 10 %).

¹H-NMR (400 MHz, CDCl₃, 298 K): δ = 7.85 (d, J = 16 Hz, 1 H), 7.75 (dd, J = 7.9, 1.6 Hz, 1 H), 7.70 (d, J = 16 Hz, 1 H), 7.67 (s, 1 H), 7.32 (m, 1 H), 7.14 (s, 1 H), 7.01 (t, J = 7.5 Hz, 1 H), 6.91 (d, J = 7.8 Hz, 1 H), 6.90 (s, 1 H), 6.78 (s, 1 H), 6.45 (m, 1 H), 6.15 (ddt, J = 17.3, 10.5, 5.3 Hz, 1 H), 5.46 (dq, J = 17.3, 1.6 Hz, 1 H), 5.35 (dq, J = 10.5, 1.3 Hz, 1 H), 4.64 (dt, J = 5.1, 1.4 Hz, 2 H), 2.30 (s, 3 H).

¹³C-NMR (100 MHz, CDCl₃, 298 K): δ = 159.7, 156.8, 144.5, 138.3, 138.0, 135.0, 133.0, 131.1, 127.8, 125.4, 125.1, 122.6, 121.1, 118.6, 117.7, 117.4, 116.1, 112.4, 69.3, 11.4.

Crystal structure see spectra section.

Absorption and emission maxima $\lambda_{\text{abs}} = 561 \text{ nm}$, $\lambda_{\text{em}} = 572 \text{ nm}$. $\Phi_f = 1.0$.

Preparation of oxy-propyl BDP (1')

1-Methyl-(E)-3-(2-propoxy)-styryl-4,4'-difluoro-bora-3a,4a-diaza-(s)-indacene.

(1') was synthesized following the procedure for (1) using *o*-propoxy- instead of *o*-allyloxy-benzaldehyde. 36.6 mg (0.1 mmol, 10 %) of a dark violet solid were isolated.

¹H-NMR (400 MHz, C₆D₆, 298 K): δ = 8.47 (d, J = 16 Hz, 1 H), 7.79 (d, J = 16 Hz, 1 H), 7.77 (s, 1 H), 7.59 (dd, J = 7.8, 1.8 Hz, 1 H), 7.03 (dt, J = 7.8, 1.8 Hz, 1 H), 6.72 (dt, J = 7.8, 1.8 Hz, 1 H), 6.55 (d, J = 3.8 Hz, 1 H), 6.50 (d, J = 7.8, 1.8 Hz, 1 H), 6.39 (s, 1 H), 6.30 (s, 1 H), 6.16 (m, 1 H), 3.52 (t, J = 6.5 Hz, 2 H), 1.74 (m, 2 H), 1.60 (s, 3 H), 0.93 (t, J = 6.5 Hz, 3 H).

¹³C-NMR (100 MHz, C₆D₆, 298 K): δ = 160.5, 158.5, 144.4, 139.5, 138.5, 136.4, 133.8, 131.4, 129.8, 125.8, 123.3, 121.5, 120.6, 117.6, 116.6, 112.6, 110.6, 70.4, 23.1, 11.3, 11.1.

Crystal structure see spectra section

Absorption and emission maxima λ_{abs} = 561 nm, λ_{em} = 573 nm. Φ_f = 0.99.

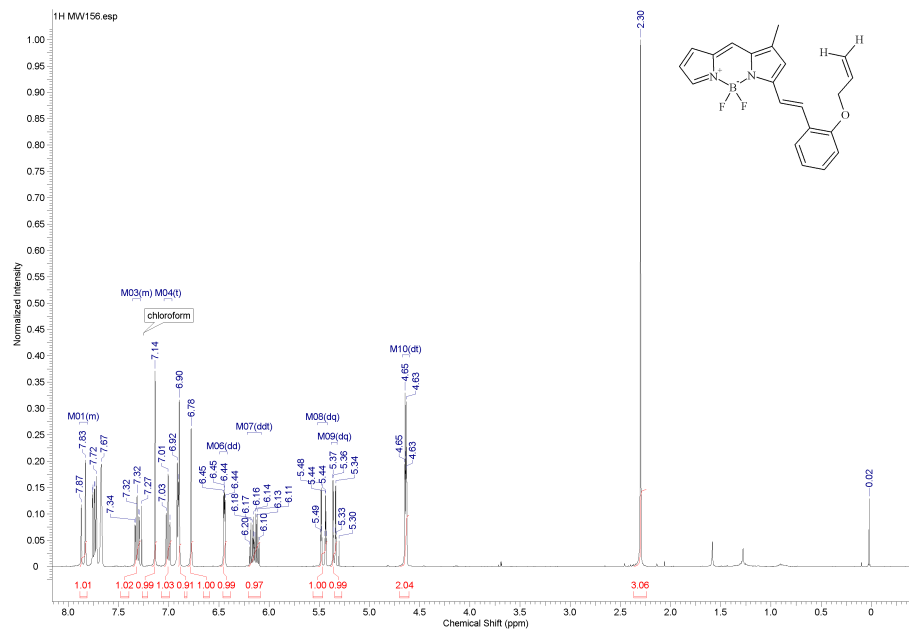
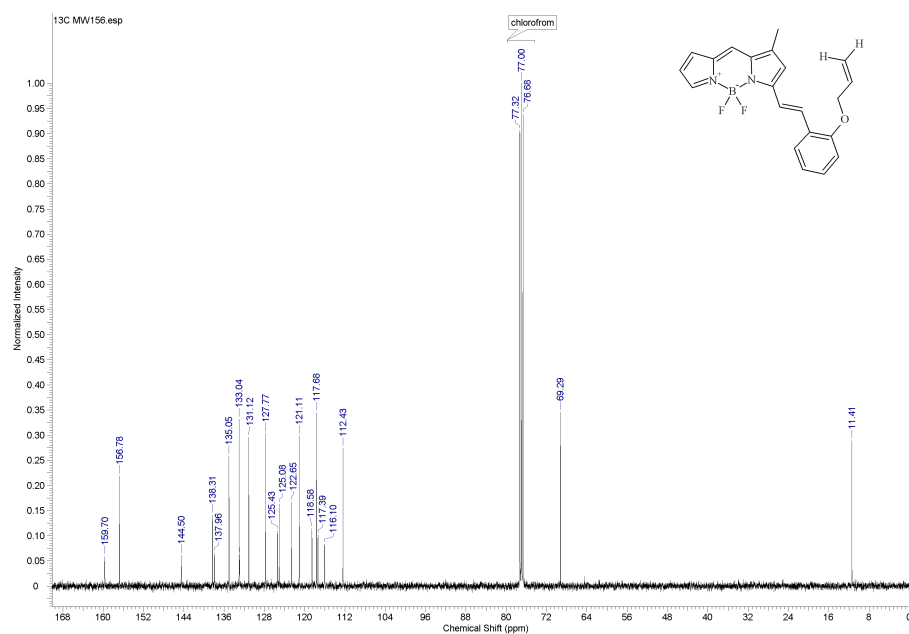


figure A4: TLC of the reaction mixture of reference compound (**1'**) with *m*CPBA. Only one green fluorescent product is formed in the reaction.

Epoxidation of (**1'**) with *m*CPBA was carried out to test for formation of fluorescent products. The correlation between the green fluorescence and the formed epoxide is shown by thin-layer chromatography (TLC) analysis in figure A4. The analogue substrate (**1'**) of the immobilized HMPS-BDP (**3**) also shows the blue-shift after epoxidation. The substrate spot is shown on top of the TLC together with a marginally existing green contamination from the synthesis. One product spot of the reaction with *m*CPBA is clearly shown below these spots. The green fluorescent stipple point, which is visible in the reaction mixture, presumably arises from a catalyzed addition to the TLC support material; it is completely immobile in any solvent.

7.1.3. Spectra

Spectra and detailed data of 1-methyl-3-(2-allyloxy)-styryl-4,4'-difluoro-bora-3a,4a-diaza-(s)-indacene (1)

figure A1: ¹H-NMR spectrum of (1).figure A2: ¹³C-NMR spectrum of (1).

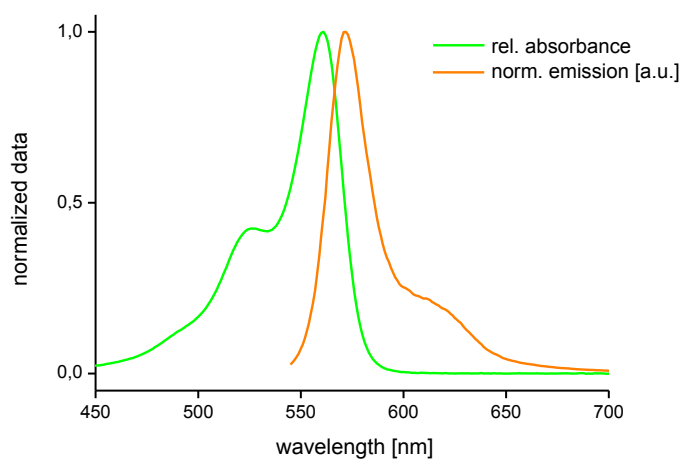


figure A3: UV-Vis- and emission-spectrum of **(1)**.

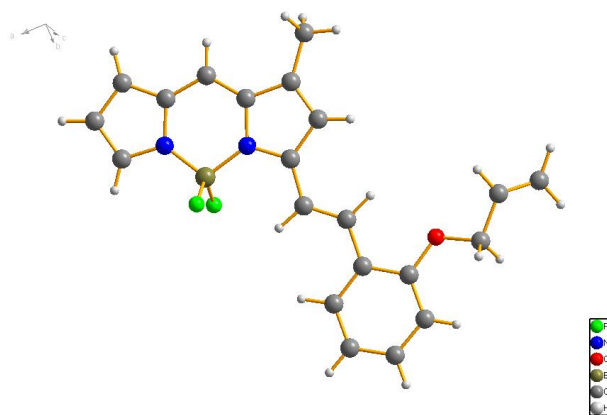


figure A4: crystal structure of **(1)**.

table A1: Crystal data and structure refinement for oxy-ally-BDP **(1)**

Empirical formula	C ₂₁ H ₁₉ B F ₂ N ₂ O	
Formula weight	364.19	
Temperature	150(2) K	
Wavelength	0.71073 Å	
Crystal system	Monoclinic	
Space group	P2(1)/n	
Unit cell dimensions	a = 10.6423(14) Å	α = 90°.
	b = 16.417(2) Å	β = 110.783(8)°.
	c = 11.1796(14) Å	γ = 90°.
Volume	1826.1(4) Å ³	
Z	4	

Appendix

Density (calculated)	1.325 Mg/m ³
Absorption coefficient	0.095 mm ⁻¹
F(000)	760
Crystal size	0.56 x 0.30 x 0.10 mm ³
Theta range for data collection	2.27 to 31.51°.
Index ranges	-15<=h<=10, -20<=k<=24, -16<=l<=16
Reflections collected	23205
Independent reflections	6013 [R(int) = 0.0300]
Completeness to theta = 31.51°	98.8 %
Absorption correction	None
Max. and min. transmission	0.9904 and 0.9486
Refinement method	Full-matrix least-squares on F ²
Data / restraints / parameters	6013 / 0 / 320
Goodness-of-fit on F ²	1.013
Final R indices [I>2sigma(I)]	R1 = 0.0462, wR2 = 0.1127
R indices (all data)	R1 = 0.0752, wR2 = 0.1295
Largest diff. peak and hole	0.401 and -0.198 e.Å ⁻³

table A2: Atomic coordinates ($\times 10^4$) and equivalent isotropic displacement parameters ($\text{\AA}^2 \times 10^3$) for oxy-ally-BDP (**1**). $U(eq)$ is defined as one third of the trace of the orthogonalized U^{ij} tensor.

	x	y	z	U(eq)
F(1)	11453(1)	1084(1)	2368(1)	34(1)
F(2)	12359(1)	114(1)	3865(1)	33(1)
N(1)	11794(1)	-244(1)	1641(1)	25(1)
N(2)	10001(1)	0(1)	2550(1)	22(1)
O(1)	7326(1)	1863(1)	5865(1)	34(1)
B(1)	11440(1)	260(1)	2639(1)	24(1)
C(1)	12941(1)	-192(1)	1373(1)	30(1)
C(2)	12882(2)	-729(1)	396(1)	34(1)
C(3)	11647(2)	-1121(1)	46(1)	33(1)
C(4)	10971(1)	-819(1)	833(1)	26(1)

Appendix

C(5)	9708(1)	-999(1)	899(1)	26(1)
C(6)	9236(1)	-606(1)	1738(1)	23(1)
C(7)	7976(1)	-673(1)	1937(1)	25(1)
C(8)	8006(1)	-112(1)	2849(1)	26(1)
C(9)	9267(1)	308(1)	3211(1)	23(1)
C(10)	9745(1)	972(1)	4095(1)	25(1)
C(11)	9022(1)	1293(1)	4746(1)	23(1)
C(12)	9444(1)	1956(1)	5666(1)	22(1)
C(13)	10698(1)	2341(1)	5993(1)	28(1)
C(14)	11091(1)	2937(1)	6923(1)	33(1)
C(15)	10234(1)	3152(1)	7563(1)	32(1)
C(16)	8970(1)	2801(1)	7245(1)	27(1)
C(17)	8568(1)	2216(1)	6287(1)	23(1)
C(18)	6481(1)	1941(1)	6613(1)	27(1)
C(19)	5304(1)	1394(1)	6015(1)	31(1)
C(20)	4060(2)	1582(1)	5803(2)	55(1)
C(21)	6861(2)	-1239(1)	1234(2)	35(1)

table A3: Bond lengths [\AA] and angles [$^\circ$] for oxy-ally-BDP (**1**).

F(1)-B(1)	1.3871(16)
F(2)-B(1)	1.3931(16)
N(1)-C(1)	1.3593(16)
N(1)-C(4)	1.3827(17)
N(1)-B(1)	1.5392(17)
N(2)-C(9)	1.3496(15)
N(2)-C(6)	1.3962(15)
N(2)-B(1)	1.5587(17)
O(1)-C(17)	1.3650(15)
O(1)-C(18)	1.4345(15)
C(1)-C(2)	1.389(2)
C(2)-C(3)	1.389(2)
C(3)-C(4)	1.4083(18)

Appendix

C(4)-C(5)	1.4045(19)
C(5)-C(6)	1.3723(17)
C(6)-C(7)	1.4396(18)
C(7)-C(8)	1.3656(18)
C(7)-C(21)	1.4922(18)
C(8)-C(9)	1.4335(18)
C(9)-C(10)	1.4373(17)
C(10)-C(11)	1.3408(17)
C(11)-C(12)	1.4550(16)
C(12)-C(13)	1.4030(17)
C(12)-C(17)	1.4118(16)
C(13)-C(14)	1.3802(19)
C(14)-C(15)	1.390(2)
C(15)-C(16)	1.3886(19)
C(16)-C(17)	1.3879(17)
C(18)-C(19)	1.4934(19)
C(19)-C(20)	1.296(2)
C(1)-N(1)-C(4)	108.01(11)
C(1)-N(1)-B(1)	126.53(11)
C(4)-N(1)-B(1)	125.44(10)
C(9)-N(2)-C(6)	107.80(10)
C(9)-N(2)-B(1)	127.47(10)
C(6)-N(2)-B(1)	124.73(10)
C(17)-O(1)-C(18)	119.38(10)
F(1)-B(1)-F(2)	108.97(10)
F(1)-B(1)-N(1)	110.00(10)
F(2)-B(1)-N(1)	110.72(10)
F(1)-B(1)-N(2)	109.78(10)
F(2)-B(1)-N(2)	110.28(10)
N(1)-B(1)-N(2)	107.07(10)
N(1)-C(1)-C(2)	109.82(13)
C(3)-C(2)-C(1)	106.86(12)

Appendix

C(2)-C(3)-C(4)	107.63(12)
N(1)-C(4)-C(5)	120.33(11)
N(1)-C(4)-C(3)	107.68(12)
C(5)-C(4)-C(3)	132.00(13)
C(6)-C(5)-C(4)	121.76(12)
C(5)-C(6)-N(2)	120.60(11)
C(5)-C(6)-C(7)	131.00(12)
N(2)-C(6)-C(7)	108.34(10)
C(8)-C(7)-C(6)	106.65(11)
C(8)-C(7)-C(21)	128.12(12)
C(6)-C(7)-C(21)	125.20(12)
C(7)-C(8)-C(9)	107.90(11)
N(2)-C(9)-C(8)	109.29(11)
N(2)-C(9)-C(10)	121.89(11)
C(8)-C(9)-C(10)	128.79(11)
C(11)-C(10)-C(9)	122.69(12)
C(10)-C(11)-C(12)	125.86(12)
C(13)-C(12)-C(17)	117.98(11)
C(13)-C(12)-C(11)	123.16(11)
C(17)-C(12)-C(11)	118.84(10)
C(14)-C(13)-C(12)	121.40(12)
C(13)-C(14)-C(15)	119.33(13)
C(16)-C(15)-C(14)	121.01(12)
C(17)-C(16)-C(15)	119.38(12)
O(1)-C(17)-C(16)	123.83(11)
O(1)-C(17)-C(12)	115.37(10)
C(16)-C(17)-C(12)	120.79(11)
O(1)-C(18)-C(19)	106.58(10)
C(20)-C(19)-C(18)	125.35(15)

Appendix

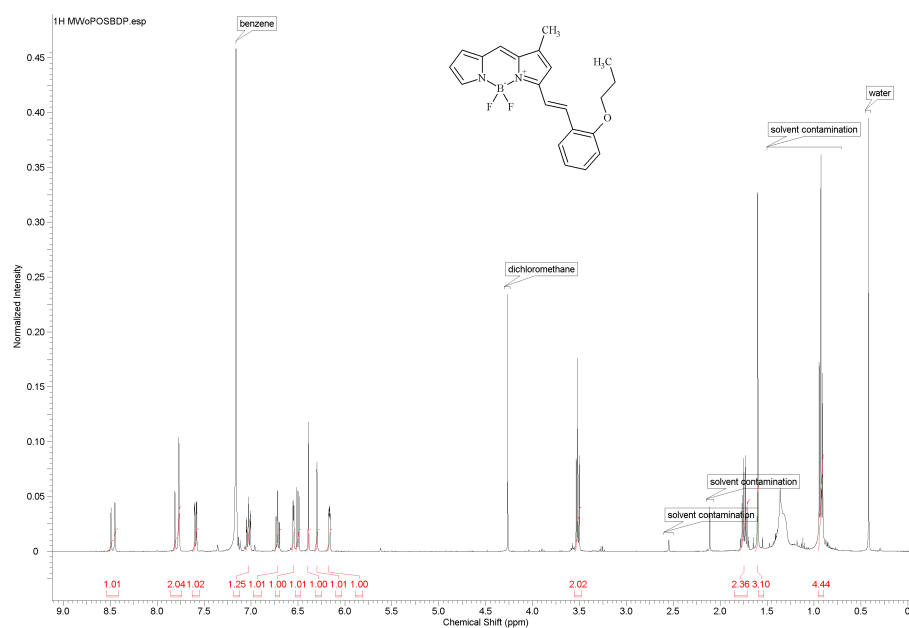
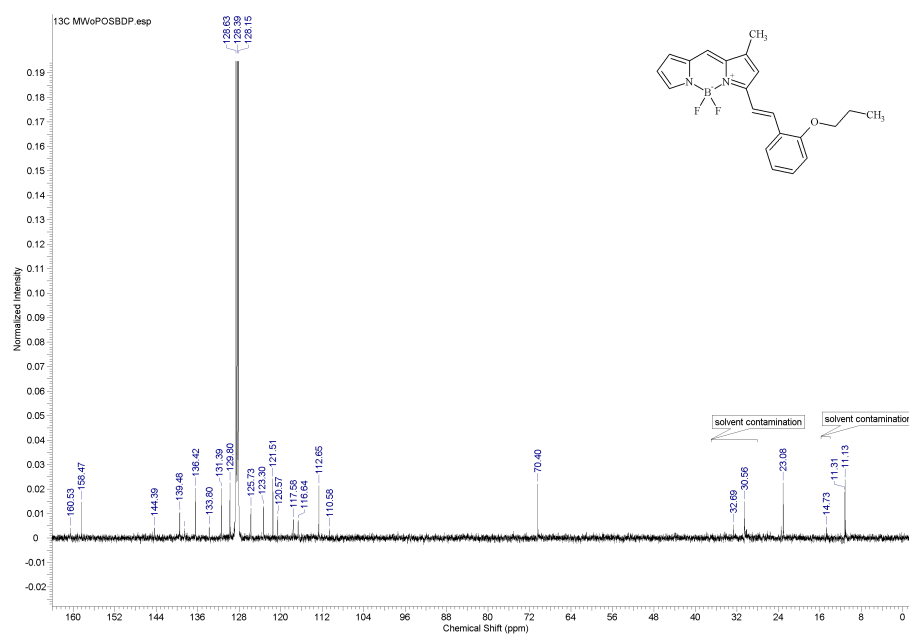
table A4: Anisotropic displacement parameters ($\text{\AA}^2 \times 10^3$) for oxy-ally-BDP (1). The anisotropic displacement factor exponent takes the form: $-2p^2[h^2 a^{*2}U^{11} + \dots + 2 h k a^* b^* U^{12}]$

	U ¹¹	U ²²	U ³³	U ²³	U ¹³	U ¹²
F(1)	39(1)	21(1)	51(1)	-1(1)	26(1)	-3(1)
F(2)	26(1)	43(1)	28(1)	-7(1)	7(1)	2(1)
N(1)	27(1)	24(1)	26(1)	1(1)	12(1)	3(1)
N(2)	25(1)	19(1)	22(1)	-1(1)	10(1)	0(1)
O(1)	25(1)	45(1)	36(1)	-16(1)	16(1)	-8(1)
B(1)	23(1)	23(1)	28(1)	-2(1)	12(1)	0(1)
C(1)	29(1)	32(1)	32(1)	3(1)	15(1)	4(1)
C(2)	38(1)	38(1)	32(1)	4(1)	20(1)	12(1)
C(3)	41(1)	32(1)	27(1)	-1(1)	15(1)	10(1)
C(4)	32(1)	23(1)	25(1)	0(1)	11(1)	5(1)
C(5)	32(1)	22(1)	24(1)	-1(1)	8(1)	2(1)
C(6)	27(1)	20(1)	22(1)	1(1)	8(1)	0(1)
C(7)	26(1)	24(1)	25(1)	1(1)	8(1)	-2(1)
C(8)	25(1)	28(1)	26(1)	0(1)	10(1)	-1(1)
C(9)	24(1)	22(1)	22(1)	1(1)	10(1)	1(1)
C(10)	24(1)	25(1)	26(1)	-3(1)	10(1)	-1(1)
C(11)	23(1)	24(1)	22(1)	0(1)	8(1)	1(1)
C(12)	22(1)	22(1)	22(1)	0(1)	8(1)	2(1)
C(13)	25(1)	31(1)	32(1)	-4(1)	13(1)	-1(1)
C(14)	27(1)	35(1)	37(1)	-8(1)	12(1)	-7(1)
C(15)	35(1)	28(1)	31(1)	-8(1)	10(1)	-3(1)
C(16)	30(1)	27(1)	27(1)	-4(1)	13(1)	3(1)
C(17)	22(1)	24(1)	24(1)	-1(1)	8(1)	1(1)
C(18)	26(1)	28(1)	30(1)	0(1)	14(1)	2(1)
C(19)	31(1)	30(1)	36(1)	2(1)	15(1)	-1(1)
C(20)	32(1)	39(1)	92(1)	0(1)	21(1)	-3(1)
C(21)	33(1)	35(1)	33(1)	-4(1)	8(1)	-9(1)

Appendix

table A5: Hydrogen coordinates ($\times 10^4$) and isotropic displacement parameters ($\text{\AA}^2 \times 10^3$) for oxy-ally-BDP (**1**).

	x	y	z	U(eq)
H(1)	13626(17)	179(10)	1832(15)	34(4)
H(2)	13586(18)	-810(11)	20(17)	44(5)
H(3)	11281(16)	-1523(11)	-626(16)	41(5)
H(4)	9157(16)	-1410(10)	345(15)	35(4)
H(5)	7307(15)	-22(9)	3199(14)	28(4)
H(6)	10657(17)	1175(10)	4208(16)	40(4)
H(7)	8117(15)	1054(9)	4615(14)	29(4)
H(8)	11329(17)	2172(10)	5572(15)	38(4)
H(9)	11952(18)	3184(11)	7128(17)	47(5)
H(10)	10502(17)	3540(11)	8212(17)	41(4)
H(11)	8373(16)	2973(10)	7664(15)	35(4)
H(12)	6989(17)	1791(11)	7491(16)	42(5)
H(13)	6201(16)	2509(10)	6602(15)	36(4)
H(14)	5474(18)	853(12)	5711(17)	48(5)
H(15)	3280(20)	1205(13)	5384(19)	60(6)
H(16)	3880(30)	2141(18)	6080(30)	105(9)
H(17)	6140(20)	-1211(13)	1590(20)	65(6)
H(18)	7180(20)	-1796(16)	1290(20)	75(7)
H(19)	6450(20)	-1107(12)	350(20)	58(6)

Spectra and detailed data of 1-methyl-3-(2-propoxy)-styryl-4,4'-difluoro-bora-3a,4a-diaza-(s)-indacene (1')figure A5: ¹H-NMR spectrum of (**1'**).figure A6: ¹³C-NMR spectrum of (**1'**).

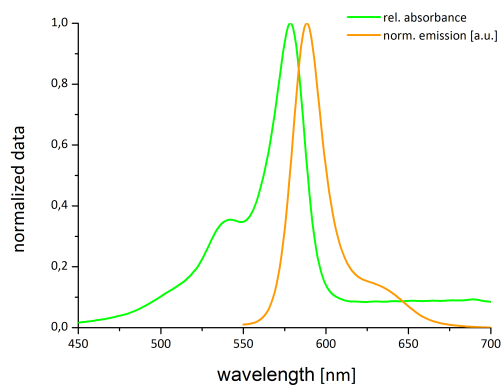


figure A7: UV-Vis- and emission spectrum of (1').

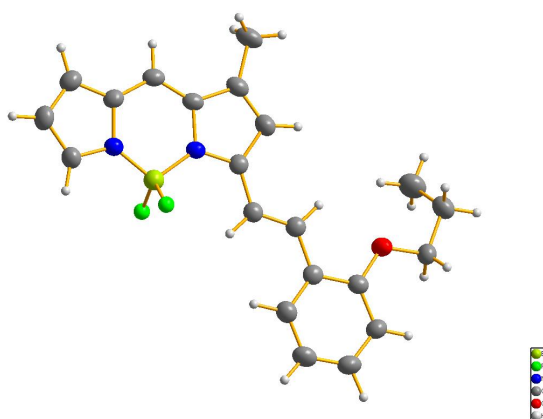


figure A8: crystal structure of (1').

table A6: Crystal data and structure refinement for (1')

Empirical formula	C ₂₁ H ₂₄ B F ₂ N ₂ O	
Formula weight	369.23	
Temperature	293(2) K	
Wavelength	0.71073 Å	
Crystal system	Monoclinic	
Space group	P2(1)/c	
Unit cell dimensions	a = 9.074(4) Å	α = 90°.
	b = 10.884(8) Å	β = 99.90(5)°.
	c = 19.675(8) Å	γ = 90°.
Volume	1914.2(18) Å ³	
Z	4	
Density (calculated)	1.281 Mg/m ³	
Absorption coefficient	0.091 mm ⁻¹	

Appendix

F(000)	780
Crystal size	0.43 x 0.25 x 0.08 mm ³
Theta range for data collection	2.81 to 28.04°.
Index ranges	-11<=h<=11, -14<=k<=14, -25<=l<=25
Reflections collected	17572
Independent reflections	4561 [R(int) = 0.0967]
Completeness to theta = 28.04°	98.5 %
Absorption correction	None
Max. and min. transmission	0.9927 and 0.9617
Refinement method	Full-matrix least-squares on F ²
Data / restraints / parameters	4561 / 0 / 317
Goodness-of-fit on F ²	0.802
Final R indices [I>2sigma(I)]	R1 = 0.0392, wR2 = 0.0787
R indices (all data)	R1 = 0.1008, wR2 = 0.0932
Largest diff. peak and hole	0.165 and -0.253 e.Å ⁻³

table A7: Atomic coordinates ($\times 10^4$) and equivalent isotropic displacement parameters ($\text{\AA}^2 \times 10^3$) for (**1'**). $U(eq)$ is defined as one third of the trace of the orthogonalized U^i tensor.

	x	y	z	U(eq)
B(1)	11797(2)	7247(2)	10208(1)	34(1)
F(1)	12631(1)	8212(1)	10546(1)	51(1)
F(2)	12491(1)	6836(1)	9667(1)	50(1)
N(1)	10176(1)	7707(1)	9910(1)	31(1)
N(2)	11641(1)	6187(1)	10707(1)	33(1)
C(1)	9773(2)	8649(1)	9470(1)	32(1)
C(2)	8177(2)	8718(2)	9326(1)	38(1)
C(3)	7610(2)	7790(2)	9677(1)	38(1)
C(4)	8866(2)	7138(2)	10057(1)	32(1)
C(5)	8936(2)	6170(2)	10504(1)	35(1)
C(6)	10300(2)	5682(2)	10842(1)	35(1)
C(7)	10629(2)	4738(2)	11326(1)	43(1)
C(8)	12181(2)	4662(2)	11493(1)	48(1)

Appendix

C(9)	12764(2)	5554(2)	11103(1)	41(1)
C(10)	10848(2)	9424(2)	9207(1)	35(1)
C(11)	10460(2)	10361(2)	8772(1)	35(1)
C(12)	11468(2)	11172(2)	8466(1)	34(1)
C(13)	13032(2)	11115(2)	8646(1)	41(1)
C(14)	13949(2)	11920(2)	8360(1)	47(1)
C(15)	13325(2)	12806(2)	7893(1)	46(1)
C(16)	11776(2)	12886(2)	7694(1)	41(1)
C(17)	10864(2)	12066(2)	7981(1)	35(1)
O(1)	9338(1)	12064(1)	7815(1)	45(1)
C(18)	8631(2)	12889(2)	7289(1)	41(1)
C(19)	6972(2)	12643(2)	7204(1)	52(1)
C(20)	6547(3)	11331(2)	6998(2)	63(1)
C(21)	6002(2)	7469(2)	9685(1)	51(1)

table A8: Bond lengths [\AA] and angles [$^\circ$] for (**1'**).

B(1)-F(1)	1.395(2)
B(1)-F(2)	1.400(2)
B(1)-N(2)	1.537(2)
B(1)-N(1)	1.568(2)
N(1)-C(1)	1.351(2)
N(1)-C(4)	1.414(2)
N(2)-C(9)	1.360(2)
N(2)-C(6)	1.402(2)
C(1)-C(2)	1.429(2)
C(1)-C(10)	1.451(2)
C(2)-C(3)	1.372(3)
C(2)-H(1)	0.988(18)
C(3)-C(4)	1.438(2)
C(3)-C(21)	1.504(2)
C(4)-C(5)	1.367(3)
C(5)-C(6)	1.405(2)

Appendix

C(5)-H(2)	0.983(18)
C(6)-C(7)	1.397(3)
C(7)-C(8)	1.393(3)
C(7)-H(3)	1.00(2)
C(8)-C(9)	1.396(3)
C(8)-H(4)	0.96(2)
C(9)-H(5)	1.005(19)
C(10)-C(11)	1.339(2)
C(10)-H(6)	0.970(19)
C(11)-C(12)	1.472(2)
C(11)-H(7)	0.969(17)
C(12)-C(13)	1.404(2)
C(12)-C(17)	1.407(2)
C(13)-C(14)	1.393(3)
C(13)-H(8)	1.02(2)
C(14)-C(15)	1.383(3)
C(14)-H(9)	0.97(2)
C(15)-C(16)	1.395(3)
C(15)-H(10)	1.02(2)
C(16)-C(17)	1.400(2)
C(16)-H(11)	0.98(2)
C(17)-O(1)	1.367(2)
O(1)-C(18)	1.436(2)
C(18)-C(19)	1.509(3)
C(18)-H(12)	0.951(19)
C(18)-H(13)	1.020(18)
C(19)-C(20)	1.516(3)
C(19)-H(14)	0.97(2)
C(19)-H(15)	1.02(2)
C(20)-H(16)	0.97(3)
C(20)-H(17)	1.04(2)
C(20)-H(18)	0.95(3)

Appendix

C(21)-H(21A)	0.9600
C(21)-H(21B)	0.9600
C(21)-H(21C)	0.9600
C(21)-H(21D)	0.9600
C(21)-H(21E)	0.9600
C(21)-H(21F)	0.9600
F(1)-B(1)-F(2)	108.95(14)
F(1)-B(1)-N(2)	111.31(15)
F(2)-B(1)-N(2)	110.37(14)
F(1)-B(1)-N(1)	109.54(14)
F(2)-B(1)-N(1)	109.50(15)
N(2)-B(1)-N(1)	107.15(13)
C(1)-N(1)-C(4)	108.60(13)
C(1)-N(1)-B(1)	127.95(13)
C(4)-N(1)-B(1)	123.43(13)
C(9)-N(2)-C(6)	106.35(14)
C(9)-N(2)-B(1)	127.20(13)
C(6)-N(2)-B(1)	126.45(13)
N(1)-C(1)-C(2)	108.70(14)
N(1)-C(1)-C(10)	123.01(14)
C(2)-C(1)-C(10)	128.29(16)
C(3)-C(2)-C(1)	108.43(16)
C(3)-C(2)-H(1)	127.2(10)
C(1)-C(2)-H(1)	124.3(10)
C(2)-C(3)-C(4)	107.03(14)
C(2)-C(3)-C(21)	128.64(16)
C(4)-C(3)-C(21)	124.33(16)
C(5)-C(4)-N(1)	121.46(14)
C(5)-C(4)-C(3)	131.28(14)
N(1)-C(4)-C(3)	107.24(14)
C(4)-C(5)-C(6)	122.42(15)
C(4)-C(5)-H(2)	119.8(11)

Appendix

C(6)-C(5)-H(2)	117.8(11)
C(7)-C(6)-N(2)	109.09(15)
C(7)-C(6)-C(5)	131.97(15)
N(2)-C(6)-C(5)	118.94(15)
C(8)-C(7)-C(6)	107.08(16)
C(8)-C(7)-H(3)	126.7(11)
C(6)-C(7)-H(3)	126.2(12)
C(7)-C(8)-C(9)	107.01(18)
C(7)-C(8)-H(4)	125.4(11)
C(9)-C(8)-H(4)	127.5(11)
N(2)-C(9)-C(8)	110.48(16)
N(2)-C(9)-H(5)	117.3(11)
C(8)-C(9)-H(5)	132.1(11)
C(11)-C(10)-C(1)	123.48(16)
C(11)-C(10)-H(6)	121.1(11)
C(1)-C(10)-H(6)	115.5(11)
C(10)-C(11)-C(12)	127.19(16)
C(10)-C(11)-H(7)	120.3(10)
C(12)-C(11)-H(7)	112.5(10)
C(13)-C(12)-C(17)	117.41(15)
C(13)-C(12)-C(11)	122.88(16)
C(17)-C(12)-C(11)	119.71(14)
C(14)-C(13)-C(12)	121.24(18)
C(14)-C(13)-H(8)	123.2(10)
C(12)-C(13)-H(8)	115.6(10)
C(15)-C(14)-C(13)	120.16(17)
C(15)-C(14)-H(9)	124.0(12)
C(13)-C(14)-H(9)	115.7(12)
C(14)-C(15)-C(16)	120.47(18)
C(14)-C(15)-H(10)	121.6(11)
C(16)-C(15)-H(10)	117.9(11)
C(15)-C(16)-C(17)	118.98(18)

Appendix

C(15)-C(16)-H(11)	119.1(11)
C(17)-C(16)-H(11)	121.9(11)
O(1)-C(17)-C(16)	123.37(16)
O(1)-C(17)-C(12)	114.90(14)
C(16)-C(17)-C(12)	121.73(15)
C(17)-O(1)-C(18)	118.64(13)
O(1)-C(18)-C(19)	106.37(15)
O(1)-C(18)-H(12)	110.5(12)
C(19)-C(18)-H(12)	112.2(10)
O(1)-C(18)-H(13)	108.2(10)
C(19)-C(18)-H(13)	110.6(9)
H(12)-C(18)-H(13)	108.9(15)
C(18)-C(19)-C(20)	113.53(18)
C(18)-C(19)-H(14)	106.5(12)
C(20)-C(19)-H(14)	110.2(12)
C(18)-C(19)-H(15)	105.1(12)
C(20)-C(19)-H(15)	114.4(12)
H(14)-C(19)-H(15)	106.5(17)
C(19)-C(20)-H(16)	113.4(14)
C(19)-C(20)-H(17)	111.0(13)
H(16)-C(20)-H(17)	106.6(19)
C(19)-C(20)-H(18)	112.3(15)
H(16)-C(20)-H(18)	110(2)
H(17)-C(20)-H(18)	102(2)
C(3)-C(21)-H(21A)	109.5
C(3)-C(21)-H(21B)	109.5
H(21A)-C(21)-H(21B)	109.5
C(3)-C(21)-H(21C)	109.5
H(21A)-C(21)-H(21C)	109.5
H(21B)-C(21)-H(21C)	109.5
C(3)-C(21)-H(21D)	109.5
H(21A)-C(21)-H(21D)	141.1

Appendix

H(21B)-C(21)-H(21D)	56.3
H(21C)-C(21)-H(21D)	56.3
C(3)-C(21)-H(21E)	109.5
H(21A)-C(21)-H(21E)	56.3
H(21B)-C(21)-H(21E)	141.1
H(21C)-C(21)-H(21E)	56.3
H(21D)-C(21)-H(21E)	109.5
C(3)-C(21)-H(21F)	109.5
H(21A)-C(21)-H(21F)	56.3
H(21B)-C(21)-H(21F)	56.3
H(21C)-C(21)-H(21F)	141.1
H(21D)-C(21)-H(21F)	109.5
H(21E)-C(21)-H(21F)	109.5

table A8: Anisotropic displacement parameters ($\text{\AA}^2 \times 10^3$) for ($\mathbf{1}'$). The anisotropic displacement factor exponent takes the form: $-2p^2[h^2 a^{*2}U^{11} + \dots + 2 h k a^* b^* U^{12}]$

	U ¹¹	U ²²	U ³³	U ²³	U ¹³	U ¹²
B(1)	28(1)	36(1)	37(1)	-1(1)	4(1)	-1(1)
F(1)	38(1)	42(1)	65(1)	6(1)	-12(1)	-10(1)
F(2)	39(1)	65(1)	52(1)	9(1)	22(1)	10(1)
N(1)	26(1)	36(1)	30(1)	0(1)	5(1)	-1(1)
N(2)	29(1)	36(1)	34(1)	2(1)	4(1)	-1(1)
C(1)	35(1)	34(1)	28(1)	-2(1)	4(1)	1(1)
C(2)	33(1)	46(1)	34(1)	-1(1)	0(1)	4(1)
C(3)	28(1)	50(1)	34(1)	-7(1)	3(1)	0(1)
C(4)	28(1)	39(1)	31(1)	-6(1)	6(1)	-5(1)
C(5)	32(1)	42(1)	33(1)	-4(1)	9(1)	-6(1)
C(6)	36(1)	36(1)	33(1)	0(1)	8(1)	-4(1)
C(7)	46(1)	43(1)	41(1)	4(1)	10(1)	-4(1)
C(8)	51(1)	45(1)	45(1)	10(1)	2(1)	5(1)
C(9)	37(1)	42(1)	43(1)	4(1)	2(1)	3(1)
C(10)	35(1)	37(1)	32(1)	0(1)	4(1)	1(1)

Appendix

C(11)	35(1)	38(1)	30(1)	-2(1)	4(1)	-1(1)
C(12)	36(1)	34(1)	31(1)	-5(1)	6(1)	-1(1)
C(13)	36(1)	44(1)	40(1)	-1(1)	1(1)	0(1)
C(14)	33(1)	53(1)	54(1)	-4(1)	5(1)	-6(1)
C(15)	40(1)	46(1)	54(1)	0(1)	14(1)	-8(1)
C(16)	41(1)	40(1)	45(1)	5(1)	11(1)	-3(1)
C(17)	33(1)	40(1)	33(1)	-3(1)	6(1)	-1(1)
O(1)	31(1)	56(1)	46(1)	18(1)	4(1)	0(1)
C(18)	39(1)	42(1)	43(1)	10(1)	6(1)	4(1)
C(19)	38(1)	60(1)	56(2)	8(1)	6(1)	8(1)
C(20)	43(1)	74(2)	69(2)	-2(2)	0(1)	-6(1)
C(21)	28(1)	73(1)	49(1)	-5(1)	3(1)	-2(1)

table A9: Hydrogen coordinates ($\times 10^4$) and isotropic displacement parameters ($\text{\AA}^2 \times 10^{-3}$) for (**1'**).

	x	y	z	U(eq)
H(21A)	5950	6684	9902	76
H(21B)	5464	7436	9221	76
H(21C)	5564	8084	9939	76
H(21D)	5369	8119	9473	76
H(21E)	5854	7366	10154	76
H(21F)	5754	6719	9435	76
H(1)	7605(18)	9322(16)	9011(10)	43(5)
H(2)	8010(20)	5775(16)	10586(10)	49(5)
H(3)	9890(20)	4215(18)	11511(11)	59(6)
H(4)	12730(20)	4066(18)	11798(11)	55(6)
H(5)	13820(20)	5824(17)	11090(10)	57(6)
H(6)	11890(20)	9223(17)	9368(10)	52(5)
H(7)	9414(19)	10544(15)	8609(9)	42(5)
H(8)	13436(19)	10441(17)	8985(11)	50(5)
H(9)	15010(20)	11846(18)	8532(11)	68(6)
H(10)	13970(20)	13416(18)	7684(11)	57(6)

Appendix

H(11)	11360(20)	13522(18)	7367(11)	55(6)
H(12)	8874(19)	13717(18)	7415(10)	45(5)
H(13)	9017(18)	12694(15)	6844(10)	39(5)
H(14)	6680(20)	12837(18)	7645(12)	57(6)
H(15)	6480(20)	13290(20)	6861(12)	71(7)
H(16)	7060(30)	10730(20)	7315(14)	83(8)
H(17)	6810(20)	11130(20)	6515(13)	70(7)
H(18)	5500(30)	11200(20)	6928(13)	91(8)

7.2. Cu^I-catalyzed azide-alkyne cyclization (CuAAC) - Click reaction

7.2.1. BODIPY derivatives and azides used for click reactions

Visualizing click reactions on BODIPYs, α -, β - and γ -ethynyl BODIPY were converted to the three different triazole products. Reaction monitoring was established in ensemble measurements. Out of these experiments, the compound with ideal optical characteristics for microscopy experiments was chosen, α -ethynyl BODIPY (**6**) (figure A9).

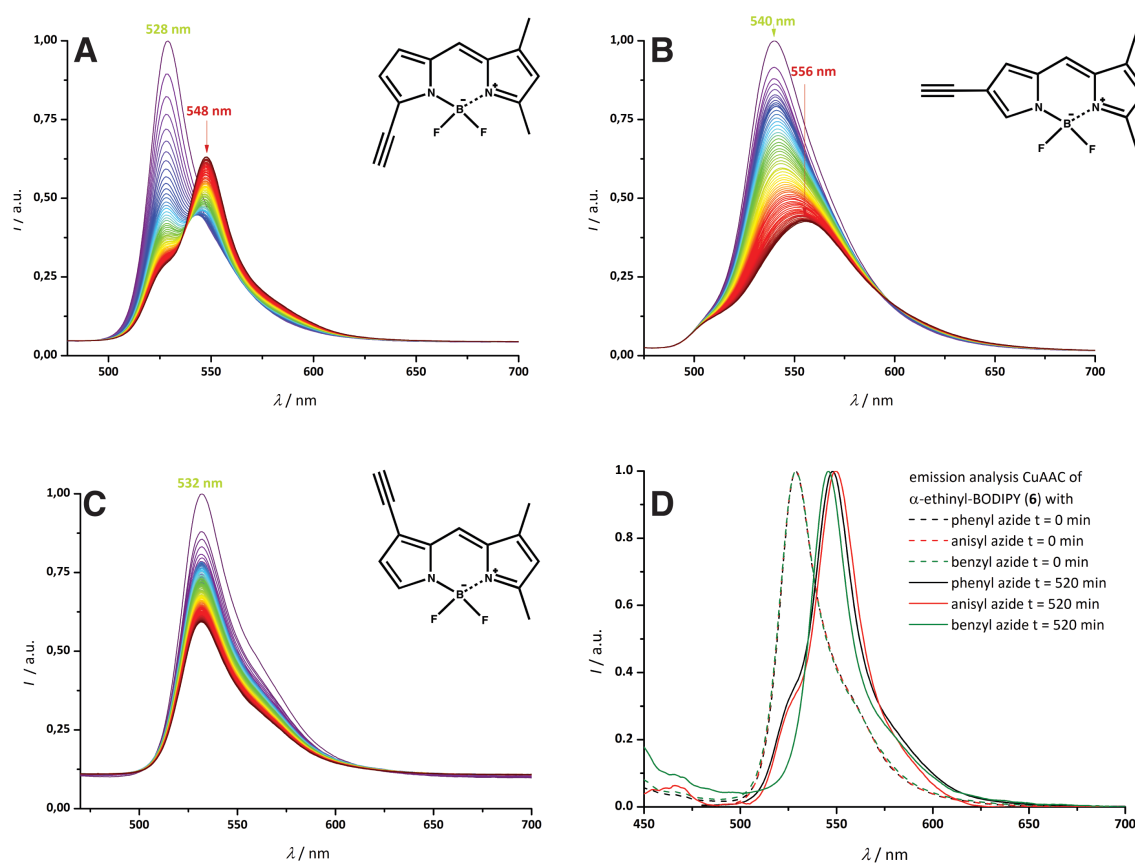


figure A9: Reaction monitoring of different derivatized alkyne BODIPY dyes in CuAAC with phenyl azide and optical comparison of different used azide moieties. Spectra are collected every five minutes over a period of 11 hours. **A:** α -derivative; **B:** β -derivative; **C:** γ -derivative; **D:** comparison of starting compound and triazole product.

7.2.2. Background signal in microscopy experiments

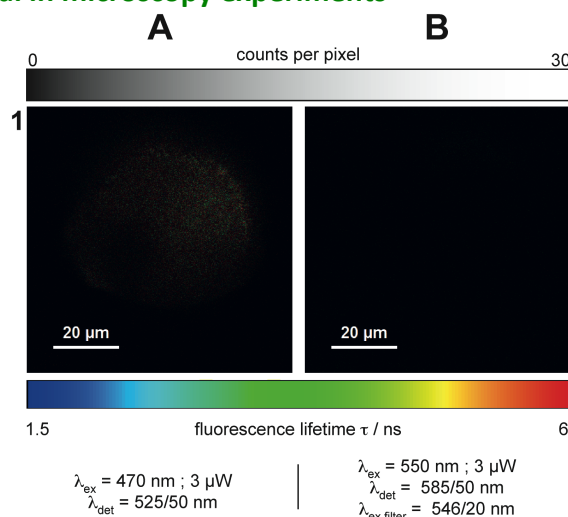


figure A10: Immobilized azide agarose beads without any fluorophore, before figure 18: **A**: minor background fluorescence in green detection channel; **B**: no background fluorescence in orange detection channel.

7.2.3. Comparison of alkyne-BODIPY and click transformation

The alkyne BODIPY compounds (**6**) – (**8**) could not be crystallized because of decomposition in solid state. The identification of these compounds was only possible using mass spectroscopy and the typical $^1\text{H-NMR}$ shift of the aromatic alkyne moiety, normally localized about $\gamma = 3.10$ ppm.

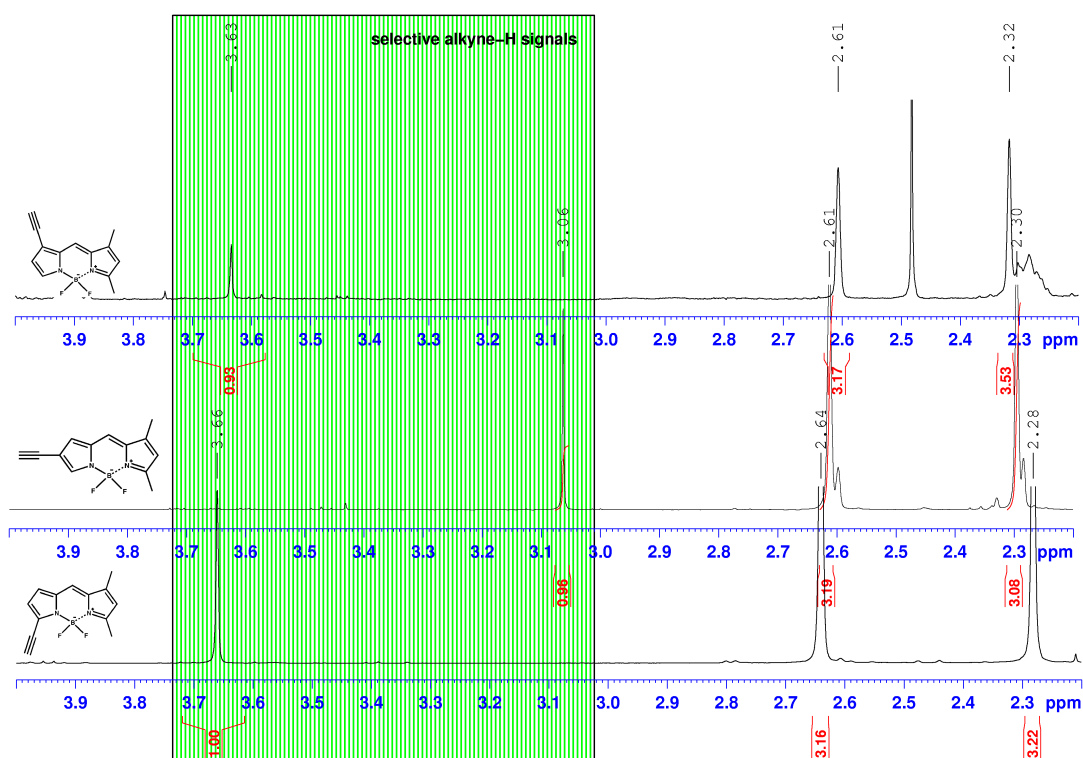


figure A11: Compendium of α , β and γ -ethynyl BODIPY alkyne-H signals.

All alkyne-H signals show a typical chemical shift for aromatic triple bond moieties (figure A11)^[254]. Comparing the α -ethynyl BODIPY (**6**) signal range with click product (**9b**), alkyne-H signal vanished (3.66 ppm) and the methoxy group signal emerges (3.89 ppm). These changes in chemical shift (0.23 ppm) and integration and the typical triazole-H formation at 8.83 ppm^[223] show product formation (figure A12).

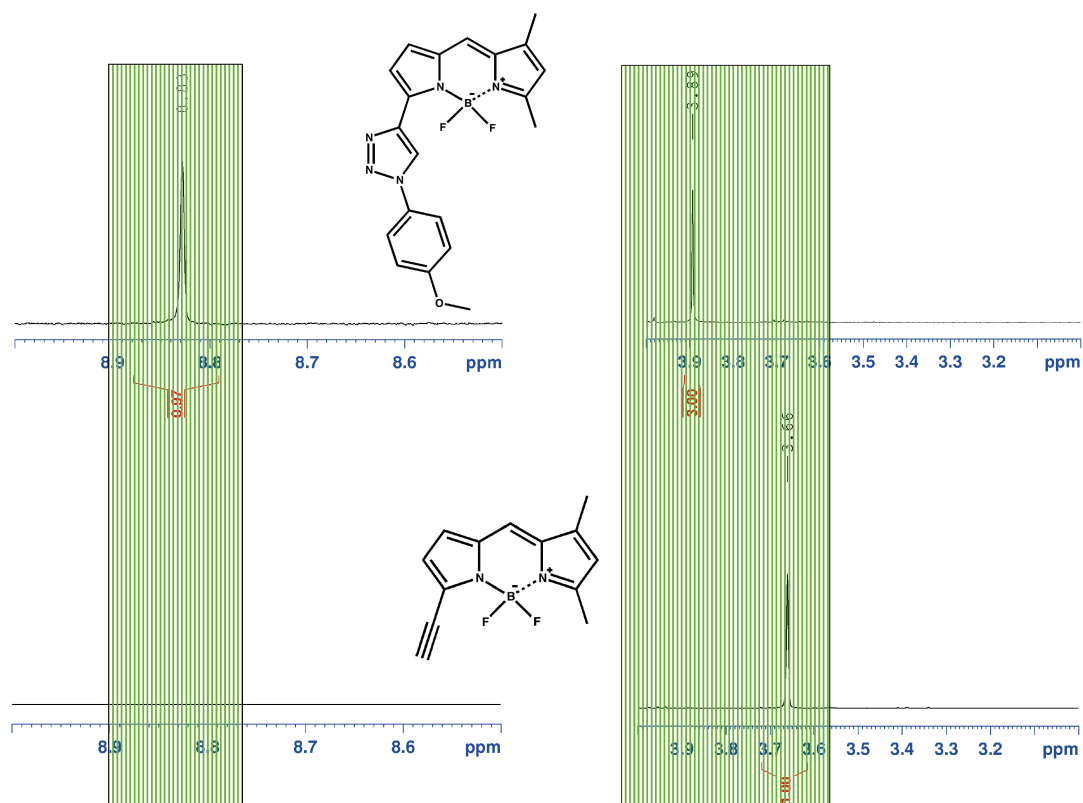


figure A12: ¹H-NMR comparison of characteristic signals of (**6**) and (**9b**).

7.2.4. Influence of the copper moiety onto fluorescence in microscopy

In conversion FLIM images (figure 18), a reduction of fluorescence lifetime is detected. A quenching process, induced by different copper species and the changed environment could be the reason. Proving this assumption, a second FLIM experiment was conducted: unsubstituted 5,7-dimethyl-4,4'-difluoro-bora-3a,4a-diaza-(s)-indacene-BODIPY^[134] is used as lifetime tracer and phenylacetylene as triple-bond-compound for coupling (figure A13).

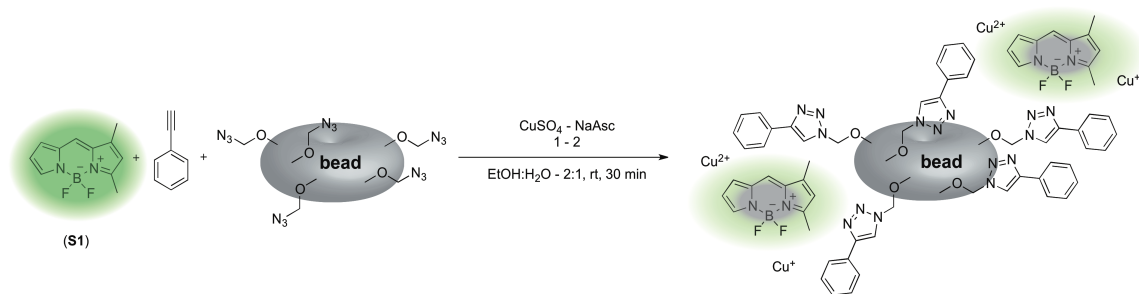


figure A13: FLIM control experiment – molecular description.

In the reaction, phenylacetylene is connected on azide agarose in presence of the non-reactive BODIPY compound. The stepwise fluorescence lifetime development of the unreactive dye shows environmental change and quenching induced by Cu-species (figure A14, table A10).

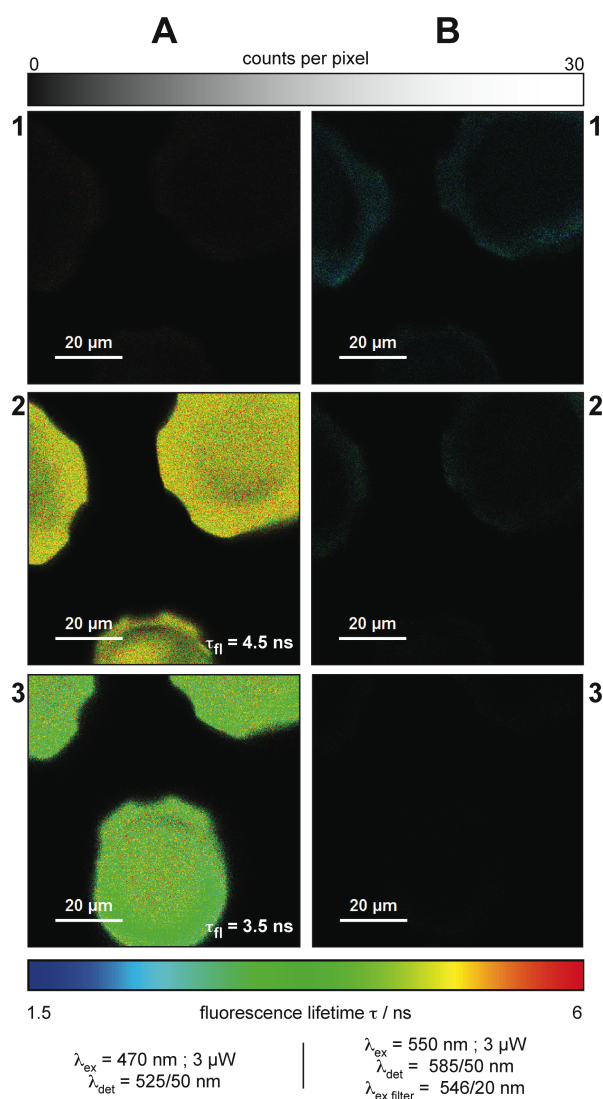
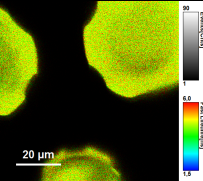
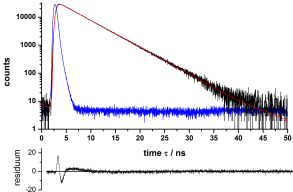
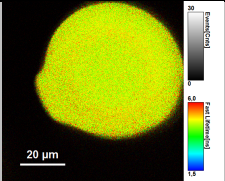
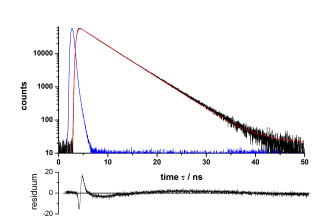
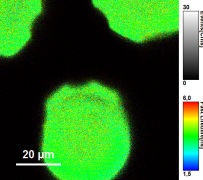
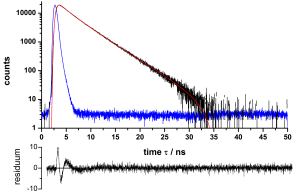
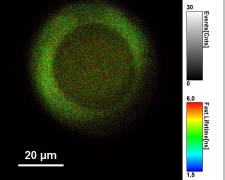
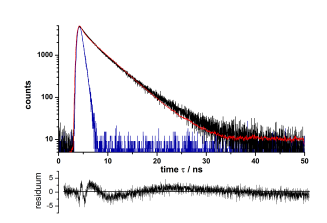
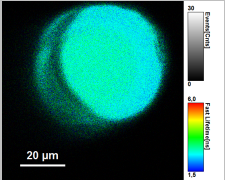
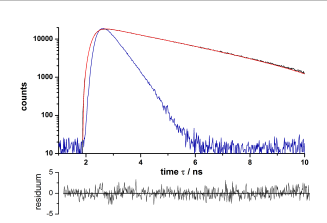


figure A14: FLIM images showing the influences of environmental changes and copper onto fluorescence lifetime: **A**: excitation with $\lambda_{\text{ex}} = 470 \text{ nm}$ @ 20 MHz, emission filter $\lambda_{\text{det}} = 525/50 \text{ nm}$ only detection BODIPY; **B**: excitation with $\lambda_{\text{ex}} = 550 \text{ nm}$ @ 80 MHz, emission filter $\lambda_{\text{det}} = 585/50 \text{ nm}$ only showing background fluorescence of agarose.

Quenching visualization was established with the same setup used for reaction monitoring. In figure A14-A1 and -B1 no chromophore was added, only background fluorescence of the agarose network is visible. Next (figure A14-2), a mixture of unsubstituted BODIPY (**S1**) and phenylacetylene is added. With an excitation wavelength $\lambda_{\text{ex}} = 470$ nm the green fluorescence of the BODIPY compound is detected (figure A14-A2). The fluorescence lifetime has already reduced about 1 ns because of the changed environment (table A10).^[224] Adding the reactive cuprous ion, the transformation starts and the phenyltriazole is formed. Parallel to product formation, the lifetime of the chromophore reduced again about 1 ns (figure A14-A3, table A10). Using $\lambda_{\text{ex}} = 550$ nm, only background fluorescence is visible (figure A14-B3).

table A10: fluorescence lifetime analysis of control experiment (figure A14) and reaction monitoring (figure 18).

FLIM control experiment (figure A14)			FLIM reaction progress (figure 18)		
FLIM image	τ_{fl} (over all pixels) / ns	lifetime histogram over all pixels reconvolution fit	FLIM image	τ_{fl} (over all pixels) / ns	lifetime histogram over all pixels reconvolution fit
 <p>$\lambda_{ex} = 470 \text{ nm},$ $\lambda_{det} = 525/50 \text{ nm}$</p>	4.5		 <p>$\lambda_{ex} = 470 \text{ nm},$ $\lambda_{det} = 525/50 \text{ nm}$</p>	<4.5>	
 <p>$\lambda_{ex} = 470 \text{ nm},$ $\lambda_{det} = 525/50 \text{ nm}$</p>	3.5		 <p>$\lambda_{ex} = 470 \text{ nm},$ $\lambda_{det} = 525/50 \text{ nm}$</p>	<3.5>	
			 <p>$\lambda_{ex} = 550 \text{ nm},$ $\lambda_{det} = 585/50 \text{ nm}$</p>	3.2	

Consequently, the fluorescence lifetime of chromophores changes twice:

- First, the lifetime reduces with transfer into the agarose matrix
- A second change results from the reaction conditions of CuAAC.

7.2.5. General Experimental

Chemicals and solvents

All chemicals and solvents were obtained from different suppliers (Sigma-Aldrich, Merck, Acros Organics, Alfa-Aesar, Apollo Scientific, TCI, Carbolution Chemicals, Combi Blocks, ABI). They were used without further purification. Solvents for spectroscopy investigations were used in HPLC or spectroscopic grade. Anhydrous solvents and pyrrole starting compounds were bought or prepared under literature-known procedures^[53,54,58,167,255–257].

Analytical instruments and measurement techniques

i. NMR-spectra:

NMR spectra were recorded in deuterated solvents as noted in experimental procedures using a Bruker Avance 400 (400 MHz) spectrometer according (nucleus frequency see table A11).

table A11: *NMR nuclei and correlated frequency.*

Measured nucleus	Frequency / MHz
¹ H	400.00
¹³ C	100.00
¹⁹ F	376.50

Chemical shifts were listed in parts per million (ppm) according to literature known deuterated solvent residual peaks^[258,259]. Coupling constants (*J*) were specified in Hz. Fluorine spectra were calibrated using an internal, instrument-specific calibration factor of +179.91, estimated with fluorine standard.

ii. Crystal structures:

Crystal structures were measured at the Institute of Inorganic Chemistry, Saarland University (Dr. V. Huch) using X8 ApexII X-ray diffractometer. Crystallographic data for the structure have been deposited with the Cambridge Crystallographic Data Centre, CCDC, 12 Union Road, Cambridge CB21EZ, UK. Copies of the data can be obtained free of charge on quoting the depository numbers CCDC 1010897-1010900.

iii. UV-Vis and fluorescence spectra, lifetime measurement, quantum yields

All spectra were recorded in quartz cuvettes (3 mL content, 1 cm layer thickness, Hellma Analytics 117.11-FQS). UV-Vis spectra were recorded in a Jasco Spectrophotometer V-650 spectrometer, fluorescence spectra in a Jasco Spectrofluorometer FP-6500. The concentrations of all solutions were in the μM range.

Fluorescence lifetime measurements were conducted using a home-built TCSPC setup including a time-correlated single photon counting module (PicoQuant PicoHarp 300). Excitation was established using a pulsed diode laser (LDH-P-C-470B 470 nm, Picoquant) containing a pulse width of 60-120 ps or a fiber laser (FemtoFiber pro TVIS, Toptica). Emission filters with a transmission range of 525/50, 546/20, 590/70 and 585/50 nm (all AHF Analysentechnik) were applied, with respect to the dye's fluorescence signal. A single-photon avalanche device was used (PDM 100ct SPAD, Micron Photo Devices) as detector. Analysis was done with reconvolution fit (PicoQuant Symphotime 64, Picoquant). Lifetime histograms were tail-fitted with Origin Pro 8.6G using exponential function.

Fluorescence quantum yields were estimated using cross calibration method with two references according to table A12:

table A12: *References for estimated QY.*

chromophore	reference 1 - solvent	reference 2 - solvent
α -Br-BODIPY (1)	Rhodamine 123 - ethanol	Fluorescein – basic ethanol
α -TMSAc-BODIPY (4)	Rhodamine 6G - ethanol	Atto 520 - water
α -Ethynyl-BODIPY (6)	Rhodamine 123 - ethanol	Fluorescein – basic ethanol
click product (9b)	Rhodamine 6G - ethanol	Atto 520 - water
β -I-BODIPY (2)	Rhodamine 123 - ethanol	Fluorescein – basic ethanol
β -Ethynyl-BODIPY (7)	Rhodamine 123 - ethanol	Fluorescein – basic ethanol
γ -Br-BODIPY (3)	Rhodamine 123 - ethanol	Fluorescein – basic ethanol
γ -TMSAc-BODIPY (5)	Rhodamine 123 - ethanol	Fluorescein – basic ethanol
γ -Ethynyl-BODIPY (8)	Rhodamine 123 - ethanol	Fluorescein – basic ethanol

ii. Kinetic measurement technique

Kinetic measurements were established using self-manufactured, lockable quartz cuvettes (from type 3/GS/Q/10mm, Starna), designed by M. Wirtz and G. Berlin, Inorganic Chemistry, Saarland University. The measurements were done in a Jasco Spectrofluorometer FP-6500. Data were recorded over a period of 16 h every five minutes using front face excitation in a 30° angle.

For analysis, the product signal intensity was reduced about the relative starting compound ratio. Plotting signal maximum versus measurement time delivers the formation and decay kinetics. These curves were fitted with Origin Pro 8.6G using exponential function

$$y = y_0 + \sum_{n=1}^x A_n * e^{-(x-x_0)/t_n}$$

iii. Microscopy instrumentation

The azide functionalized agarose beads pictures were generated using fluorescence lifetime imaging. The setup components and picture recording specifications are listed in table A13.

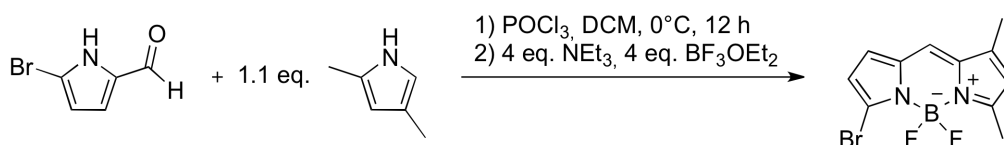
table A13: *Instrumentation for FLIM measurement.*

	green channel	orange channel
<i>excitation</i>		
laser	LDH-P-C-470B	Toptica FemtoFiber pro TVIS
wavelength	470 nm	550 nm
power	3 μW	3 μW
puls frequency	20 MHz	80 MHz
excitation filter		546/20
<i>emission</i>		
dichroitic mirror	F68-544HC Triple Line (AHF Analysentechnik)	
filter	525/50 (AHF Analysentechnik)	585/50 (AHF Analysentechnik)
detector	Perkin Elmer SPCM-AQR-14	
<i>hardware</i>		
microscope	Zeiss Axiovert 200	
objectiv	Zeiss C-Apochromat 63x/1.2 Water corrected for 170 μm cover slide	
TCSPC-system	PicoQuant PicoHarp 300	
piezostage	PI E710.4CL	
laser driver	PicoQuant PDL808	
<i>picture</i>		
aquisition	PicoQuant Symphotime 64 Version	
size	80 μm x 80 μm	
pixel	512x512	
pixel dwell time	3.0 ms	

7.2.6. Synthetic procedures and characterization data

All oxygen and moisture sensitive reactions were carried out under inert gas atmosphere. Glassware was oven-dried and used with Schlenk-technique methods. Reaction progress was controlled using Silica on TLC PET-foils with a layer thickness of 0.250 mm (pore size: 60 Å, Fluka Analytics). Compound screening was done by general column chromatography using silica gel, pore size of 0.040 – 0.063 mm as technical grade (Fluka - Analytics).

Synthesis of 3-Bromo-5,7-dimethyl-4,4'-difluoro-bora-3a,4a-diaza-(s)-indacene - α -Br-BODIPY (1)



5.0 mmol (865.7 mg) 5-bromopyrrole carbaldehyde are dissolved in 250 mL dry dichloromethane. Then, 5.2 mmol (495.0 mg) 2,4-dimethylpyrrole and 5.0 mmol (768.0 mg) phosphorous oxychloride are added at 0°C. After stirring for 12 h, 30.0 mmol (4.5 mL) triethylamine brighten the dark red solution. 4.0 mL boron trifluoride diethyl etherate (48%) are added after stirring for additional 5 min. The reaction mixture is heated to reflux over 5 h. Subsequent to cooling to room temperature, saturated sodium hydrogen carbonate solution quenches the reaction. The phases are separated, the organic layer is washed three times with H₂O and dried over sodium sulfate. Quick filtration with silica gel and dichloromethane - petrol ether (1:1) delivers the crude product. Additional column chromatography using same solvent delivers a red crystalline solid (1270.4 mg, 4.2 mmol, 85%).

¹H-NMR (400.0 MHz, CDCl₃, 298 K):

δ = 7.01 (s, 1 H), 6.75 (d, J = 3.9 Hz, 1 H), 6.34 (d, J = 3.9 Hz, 1 H), 6.13 (s, 1 H), 2.55 (s, 3 H), 2.20 (s, 3H).

¹³C-NMR (100.0 MHz, CDCl₃, 298 K): δ = 163.8, 145.9, 136.4, 133.6, 126.8, 124.8, 123.0, 121.8, 115.8, 15.2, 11.3 ppm.

¹⁹F-NMR (376.5 MHz, CDCl₃, 298 K): δ = -146.63 (q, J = 30.8 Hz, 2 F) ppm.

Crystal structure CCDC 1010897

HRMS (ESI)

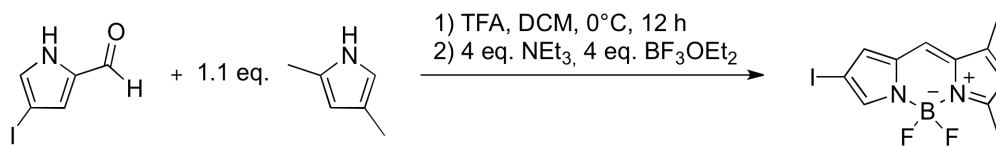
chemical formula	calculated exact mass / Da	measured accurate mass / Da	Error / ppm
$C_{11}^{10} H_{11}^{79} B BrF_2 N_2^+$	298.020303	298.02045	0.5
$C_{11}^{11} H_{11}^{79} B BrF_2 N_2^+$	299.016671	299.01663	-0.1
$C_{11}^{10} H_{11}^{81} B BrF_2 N_2^+$	300.018257	300.01841	0.5
$C_{11}^{11} H_{11}^{81} B BrF_2 N_2^+$	301.014625	301.01475	0.4

Absorbance and Emission: $\lambda_{abs} = 506$ nm, $\lambda_{em} = 516$ nm (DCM)

Lifetime: $\tau_{fl} = 6.5$ ns (DCM)

Quantum Yield: $\Phi = 0.86 \pm 0.01$ (DCM)

The spectra (see spectral data) contain a second, not separable BODIPY fluorophore with identical optical properties, which doesn't affect further synthetic steps. This compound is identified as the corresponding chloride, originating from nucleophilic halogen exchange due to synthesis. 1H -NMR shifts and mass spectra confirm 3-Chloro-5,7-dimethyl-4,4'-difluoro-bora-3a,4a-diaza-(s)-indacene.

Synthesis of 5,7-Dimethyl-2-iodo-4,4'-difluoro-bora-3a,4a-diaza-(s)-indacene - β -I-BODIPY (2)

2.5 mmol (552.0 mg) 4-iodopyrrole carbaldehyde are dissolved in 20 mL dry dichloromethane. Then, 2.6 mmol (247.2 mg) 2,4-dimethylpyrrole and 0.1 mL of trifluoroacetic acid are added at 0°C. After stirring for 12 h, 10.0 mmol (2.0 mL) triethylamine brighten the dark red solution. 2.0 mL boron trifluoride diethyl etherate (48%) are added after stirring for additional 5 min. The reaction mixture was held at 0°C. After 2 hours, the solvent was evaporated and subsequent column chromatography (dichloromethane : petrol ether – 1:1) isolates a red crystalline solid (340.0 mg, 1.0 mmol, 40%).

¹H-NMR (400.0 MHz, CDCl₃, 298 K):

δ = 7.54 (s, 1 H), 7.11 (s, 1 H), 6.95 (s, 1 H), 6.21 (s, 1 H), 2.58 (s, 3 H), 2.26 (s, 3 H).

¹³C-NMR (100.0 MHz, CDCl₃, 298 K): δ = 165.4, 147.2, 141.9, 137.1, 133.4, 130.9, 123.3, 122.2, 99.9, 15.2, 11.3 ppm.

¹⁹F-NMR (376.5 MHz, CDCl₃, 298 K): δ = -146.65 (q, J = 30.5 Hz, 2 F) ppm.

Crystal structure CCDC 1010898

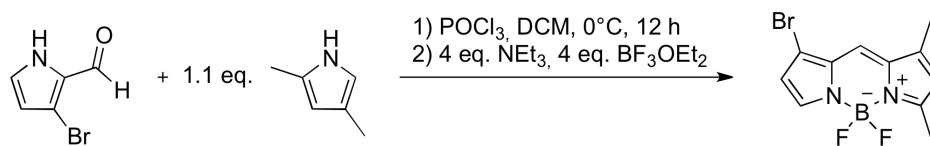
HRMS (ESI)

chemical formula	calculated exact mass / Da	measured accurate mass / Da	Error / ppm
$C_{11}H_{11}BF_2IN_2^+$	346.006439	346.0059	-1.6
$C_{11}H_{11}BF_2IN_2^+$	347.002807	347.00229	-1.5
$C_{10}^{13}CH_{11}BF_2IN_2^+$	348.006162	348.00558	-1.7

Absorbance and Emission: λ_{abs} = 509 nm, λ_{em} = 533 nm (DCM)

Lifetime: $\tau_{fl,1}$ = 3.3 ns, $\tau_{fl,2}$ = 0.6 ns (DCM)

Quantum Yield: Φ = 0.14 \pm 0.02 (DCM)

Synthesis of 1-Bromo-5,7-dimethyl-4,4'-difluoro-bora-3a,4a-diaza-(s)-indacene - γ -Br-BODIPY (3)

This compound was synthesized analogously to the described method for α -Br-BODIPY (1). A red, crystalline solid was yielded (340.0 mg, 1.0 mmol, 40%).

¹H-NMR (400.0 MHz, CDCl₃, 298 K):

δ = 7.64 (s, 1 H), 7.37 (s, 1 H), 6.62 (s, 1 H), 6.36 (s, 1 H), 2.73 (s, 3 H), 2.45 (s, 3H).

¹³C-NMR (100.0 MHz, CDCl₃, 298 K): δ = 167.0, 148.9, 139.4, 139.2, 132.7, 124.1, 123.9, 119.7, 117.0, 17.3, 13.4 ppm.

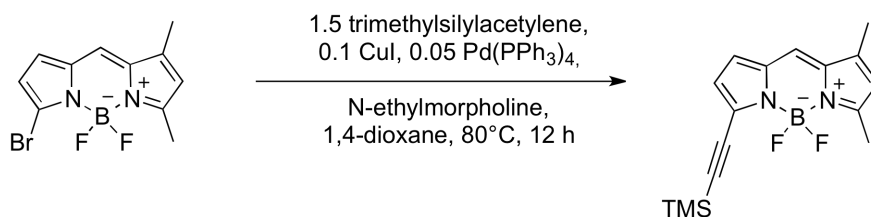
¹⁹F-NMR (376.5 MHz, CDCl₃, 298 K): δ = -146.765 (q, J = 30.7 Hz, 2 F) ppm.

Absorbance and Emission: λ_{abs} = 496 nm, λ_{em} = 506 nm (DCM)

Lifetime: τ_{fl} = <5.0> ns (DCM)

Quantum Yield: Φ = 0.34 \pm 0.01 (DCM)

**Synthesis of 5,7-Dimethyl-3-(trimethylsilyl)-ethynyl-4,4'-difluoro-bora-3a,4a-diaza-(s)-indacene -
 a-TMSAc-BODIPY (4)**



1.00 mmol (300.0 mg) (**1**) and 1.50 mmol (147.1 mg) trimethylsilylacetylene are dissolved in 4.0 mL 1,4-dioxane. Then 4.0 mL N-ethylmorpholine, 0.05 mmol (57.8 mg) tetrakis(triphenyl)palladium(0) and 0.10 mmol (19.0 mg) CuI are added. The mixture is stirred for 12 h at 80°C. The solvent was evaporated and subsequent column chromatography (dichloromethane : petrol ether – 1 : 1 ; ethyl acetate : petrol ether – 1 : 4) yields a shiny pink solid (183 mg, 0.58 mmol, 58%).

¹H-NMR (400.0 MHz, CDCl₃, 298 K):

δ = 7.02 (s, 1 H), 6.80 (d, *J* = 3.9 Hz, 1 H), 6.55 (d, *J* = 3.9 Hz, 1 H), 6.16 (s, 1 H), 2.61 (s, 3 H), 2.25 (s, 3H), 0.29 (s, 3H).

¹³C-NMR (100.0 MHz, CDCl₃, 298 K): δ = 164.9, 146.9, 137.3, 137.2, 134.7, 122.0, 121.7, 120.4, 118.6, 102.3, 97.8, 15.3, 11.5, -0.1 ppm.

¹⁹F-NMR (376.5 MHz, CDCl₃, 298 K): δ = -147.15 (q, *J* = 30.0 Hz, 2 F) ppm.

Crystal structure CCDC 1010899

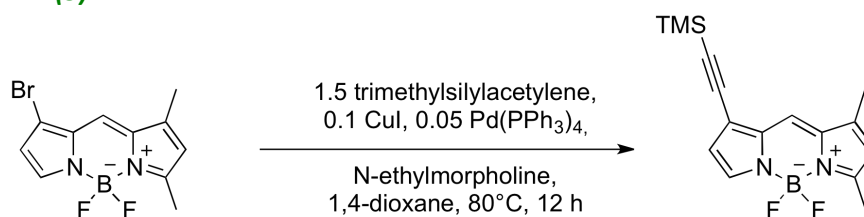
HRMS (ESI)

chemical formula	calculated exact mass / Da	measured accurate mass / Da	Error / ppm
$C_{16}H_{20}BF_2N_2Si^+$	316.149318	316.15028	3.0
$C_{16}H_{20}BF_2N_2Si^+$	317.145686	317.14662	2.9
$C_{15}CH_{20}BF_2N_2Si^+$	318.149041	318.15021	3.7

Absorbance and Emission: λ_{abs} = 529 nm, λ_{em} = 540 nm (DCM)

Lifetime: τ_{fl} = 5.3 ns (DCM)

Quantum Yield: Φ = 1.00 -0.02 (DCM)

Synthesis of 5,7-Dimethyl-1-(trimethylsilyl)-ethynyl-4,4'-difluoro-bora-3a,4a-diaza-(s)-indacene - γ -TMSAc-BODIPY (5)

This compound is synthesized analogously to described method used for α -TMSAc-BODIPY (4). A shiny pink solid (143 mg, 0.45 mmol, 45%) is obtained.

¹H-NMR (400.0 MHz, CDCl₃, 298 K):

δ = 7.49 (s, 1 H), 7.27 (s, 1 H), 6.48 (d, J = 2.0 Hz, 1 H), 6.21 (s, 1 H), 2.60 (s, 3 H), 2.33 (s, 3H), 0.29 (s, 3H).

¹³C-NMR (100.0 MHz, CDCl₃, 298 K): δ = 164.9, 146.9, 137.1, 134.7, 122.0, 121.7, 120.4, 118.7, 110.0, 102.3, 97.8, 15.3, 11.5, -0.1 ppm.

¹⁹F-NMR (376.5 MHz, CDCl₃, 298 K): δ = -146.69 (q, J = 30.7 Hz, 2 F) ppm.

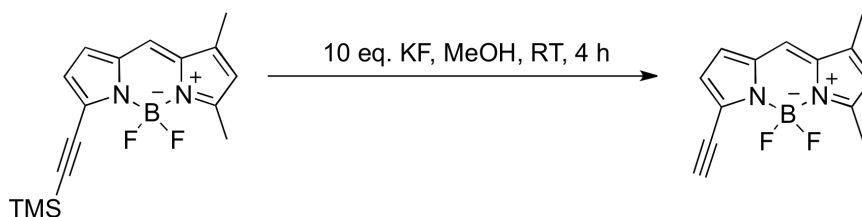
Crystal structure CCDC 1010900

Absorbance and Emission: λ_{abs} = 510 nm, λ_{em} = 520 nm (DCM)

Lifetime: τ_{fl} = 4.9 ns (DCM)

Quantum Yield: Φ = 0.92 \pm 0.04 (DCM)

Synthesis of 3-Ethynyl-5,7-dimethyl-4,4'-difluoro-bora-3a,4a-diaza-(s)-indacene - α -ethynyl-BODIPY (6)



1.00 mmol (316.2 mg) (**4**) is dissolved in 50.0 mL methanol and 10.0 mmol (580.9 mg) potassium fluoride is added. The solution is stirred at room temperature for 4 h. The solvent is evaporated and subsequent column chromatography (dichloromethane : petrol ether – 1 : 1) delivers a red, rapidly decomposing solid (127 mg, 0.52 mmol, 52%).

$^1\text{H-NMR}$ (400.0 MHz, CDCl_3 , 298 K):

δ = 7.08 (s, 1 H), 6.82 (d, J = 3.8 Hz, 1 H), 6.61 (d, J = 3.9 Hz, 1 H), 6.01 (s, 1 H), 3.66 (s, 1 H), 2.64 (s, 3 H), 2.28 (s, 3H).

$^{13}\text{C-NMR}$ (100.0 MHz, CDCl_3 , 298 K): δ = 165.6, 146.4, 137.8, 133.2, 130.8, 125.2, 123.1, 122.3, 122.2, 110.0, 85.7, 14.3, 11.4 ppm.

$^{19}\text{F-NMR}$ (376.5 MHz, CDCl_3 , 298 K): δ = -146.81 (q, J = 30.6 Hz, 2 F) ppm.

HRMS (ESI)

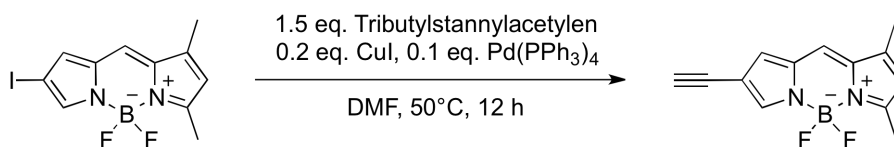
chemical formula	calculated exact mass / Da	measured accurate mass / Da	Error / ppm
$\text{C}_{13}^{10} \text{H}_{12} \text{BF}_2 \text{N}_2^+$	244.109791	244.10911	-2.8
$\text{C}_{13}^{11} \text{H}_{12} \text{BF}_2 \text{N}_2^+$	245.106159	245.10543	-3.0
$\text{C}_{12}^{13} \text{CH}_{12} \text{BF}_2 \text{N}_2^+$	246.109514	246.10883	-2.8

Absorbance and Emission: λ_{abs} = 518 nm, λ_{em} = 529 nm (DCM)

Lifetime: τ_{fl} = 6.5 ns (DCM)

Quantum Yield: Φ = 0.89 \pm 0.02 (DCM)

Synthesis of 2-Ethynyl-5,7-dimethyl-4,4'-difluoro-bora-3a,4a-diaza-(s)-indacene - β -ethynyl-BODIPY (7)



1.00 mmol (345.3 mg) β -iodo-BODIPY (**2**) is dissolved in 10 mL DMF and 0.1 mmol (115.5 mg) tetrakis(triphenyl)palladium(0), 0.2 mmol (38.1 mg) CuI and 1.5 mmol (348.8 mg) tributylstannylacetylene are added and stirred at room temperature for 12 h. The solvent was evaporated and subsequent column chromatography (dichloromethane : petrol ether – 1 : 1) yields a red, rapidly decomposing solid (161.3 mg, 0.66 mmol, 66%).

¹H-NMR (400.0 MHz, CDCl₃, 298 K):

δ = 7.72 (s, 1 H), 7.16 (s, 1 H), 6.97 (s, 1 H), 6.22 (s, 1 H), 3.06 (s, 1 H), 2.61 (s, 3 H), 2.29 (s, 3H).

¹³C-NMR (100.0 MHz, CDCl₃, 298 K): δ = 165.9, 141.2, 137.8, 131.5, 127.4, 125.2, 124.4, 122.3, 110.1, 103.6, 78.3, 15.4, 11.5 ppm.

¹⁹F-NMR (376.5 MHz, CDCl₃, 298 K): δ = -146.62 (q, J = 22.9 Hz, 2 F) ppm.

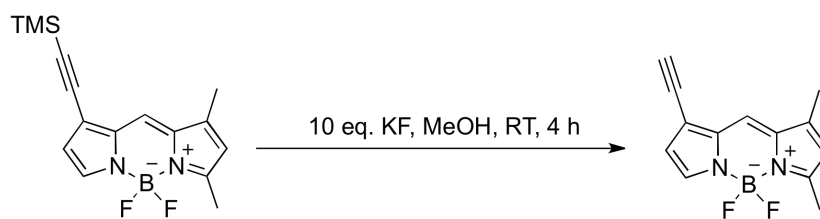
HRMS (ESI)

chemical formula	calculated exact mass / Da	measured accurate mass / Da	Error / ppm
$\text{C}_{13}^{10} \text{H}_{12} \text{BF}_2 \text{N}_2^+$	244.109791	244.10899	-3.2
$\text{C}_{13}^{11} \text{H}_{12} \text{BF}_2 \text{N}_2^+$	245.106159	245.10532	-3.4
$\text{C}_{12}^{13} \text{CH}_{12} \text{BF}_2 \text{N}_2^+$	246.109514	246.10867	-3.4

Absorbance and Emission: λ_{abs} = 509 nm, λ_{em} = 536 nm (DCM)

Lifetime: τ_{fl} = 6.2 ns (DCM)

Quantum Yield: Φ = 0.84 \pm 0.04 (DCM)

Synthesis of 1-Ethynyl-5,7-dimethyl-4,4'-difluoro-bora-3a,4a-diaza-(s)-indacene - γ -ethynyl-BODIPY (8)

(5) is deprotected similarly to the procedure used for α -ethynyl-BODIPY (6). A red, rapidly decomposing solid (124 mg, 0.51 mmol, 51%) is obtained.

$^1\text{H-NMR}$ (400.0 MHz, CDCl_3 , 298 K):

δ = 8.04 (s, 1 H), 7.43 (s, 1 H), 6.74 (s, 1 H), 6.25 (s, 1 H), 3.63 (s, 1 H), 2.61 (s, 3 H), 2.48 (s, 3H).

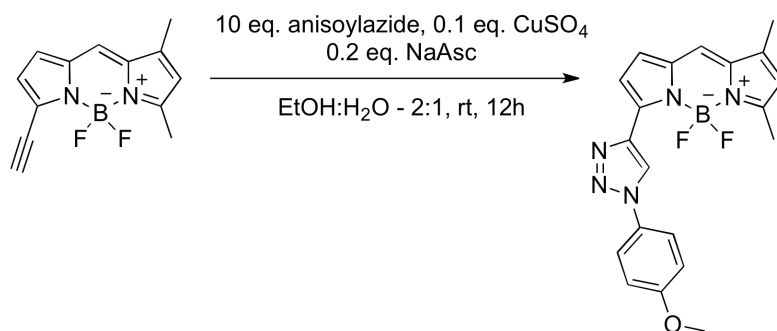
$^{19}\text{F-NMR}$ (376.5 MHz, CDCl_3 , 298 K): δ = -147.36 (q, J = 30.3 Hz, 2 F) ppm.

Absorbance and Emission: λ_{abs} = 510 nm, λ_{em} = 519 nm (DCM)

Lifetime: τ_{fl} = 4.4 ns (DCM)

Quantum Yield: Φ = 0.87 \pm 0.05 (DCM)

Synthesis of 3-(Methoxyphenyl)triazoyl-5,7-dimethyl-4,4'-difluoro-bora-3a,4a-diaza-(s)-indacene – click product (9b)



Triazole formation is achieved using 0.5 mmol (123.6 mg) α -ethynyl-BODIPY (**6**) and 5.0 mmol (50 μ l) of a 1 M anisyl azide solution in *tert.* butyl methyl ether. Both components were dissolved in 20 mL ethanol. CuSO_4 and sodium ascorbate are mixed in 10 mL water and are added to the reaction mixture after catalyst formation. After 12 h at room temperature, the solvent is removed under vacuum and column chromatography (dichloromethane) delivers a purple solid (0.1 mmol, 39.3 mg, 20%).

$^1\text{H-NMR}$ (400.0 MHz, CDCl_3 , 298 K):

δ = 8.83 (s, 1H), 7.74 (d, J = 8.9 Hz, 1 H), 7.36 (d, J = 4.2 Hz, 1 H), 7.17 (s, 1H), 7.06 (d, J = 8.9 Hz, 1 H), 6.17 (s, 1H), 3.89 (s, 3H), 2.63 (s, 3H), 2.30 (s, 3H)

$^{19}\text{F-NMR}$ (376.5 MHz, CDCl_3 , 298 K): δ = -145.91 ppm

HRMS (ESI)

chemical formula	calculated exact mass / Da	measured accurate mass / Da	Error / ppm
$\text{C}_{21}^{\text{10}} \text{H}_{20} \text{BF}_2 \text{N}_4 \text{O}^+$	393.16975	393.16833	-3.6
$\text{C}_{21}^{\text{11}} \text{H}_{20} \text{BF}_2 \text{N}_4 \text{O}^+$	394.166118	394.1647	-3.6
$\text{C}_{20}^{\text{13}} \text{CH}_{20} \text{BF}_2 \text{N}_4 \text{O}^+$	395.169473	395.1681	-3.5

Absorbance and Emission: λ_{abs} = 544 nm, λ_{em} = 555 nm (DCM)

Lifetime: τ_{fl} = 6.1 ns (DCM)

Quantum Yield: Φ = 0.73 \pm 0.05 (DCM)

7.2.7. Spectral data

NMR-spectra

- i. 3-Bromo-5,7-dimethyl-4,4'-difluoro-bora-3a,4a-diaza-(s)-indacene - α -Br-BODIPY (1)

Figure A15: $^1\text{H-NMR}$ (1).

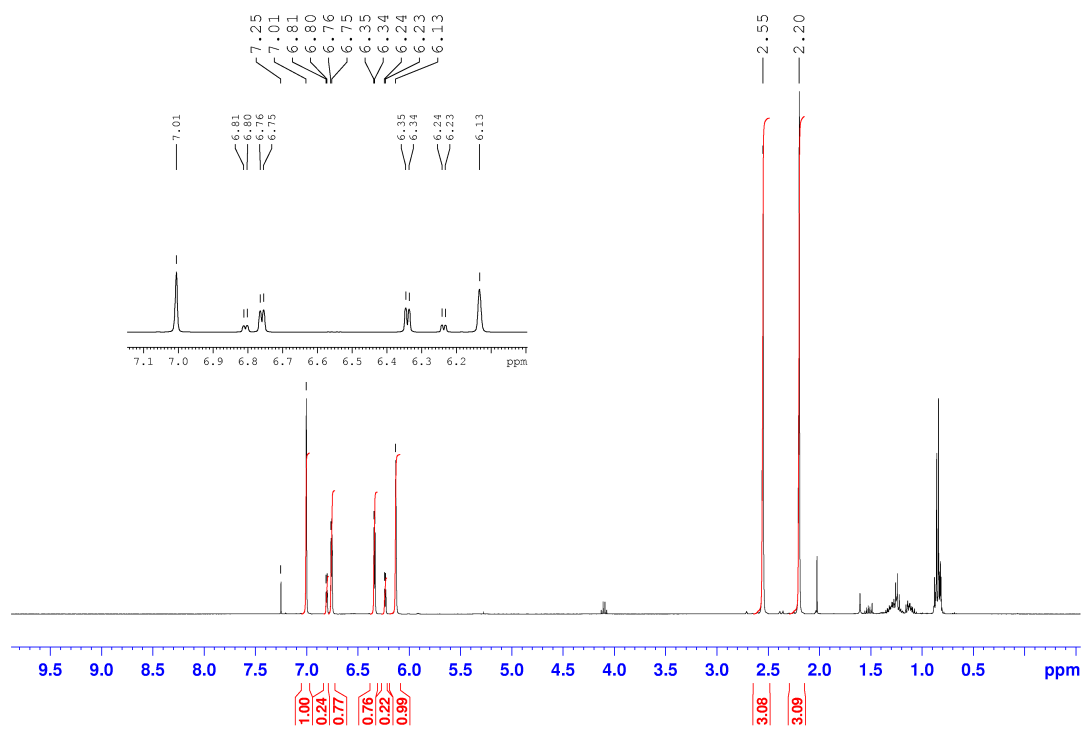


Figure A16: $^{13}\text{C-NMR}$ (1).

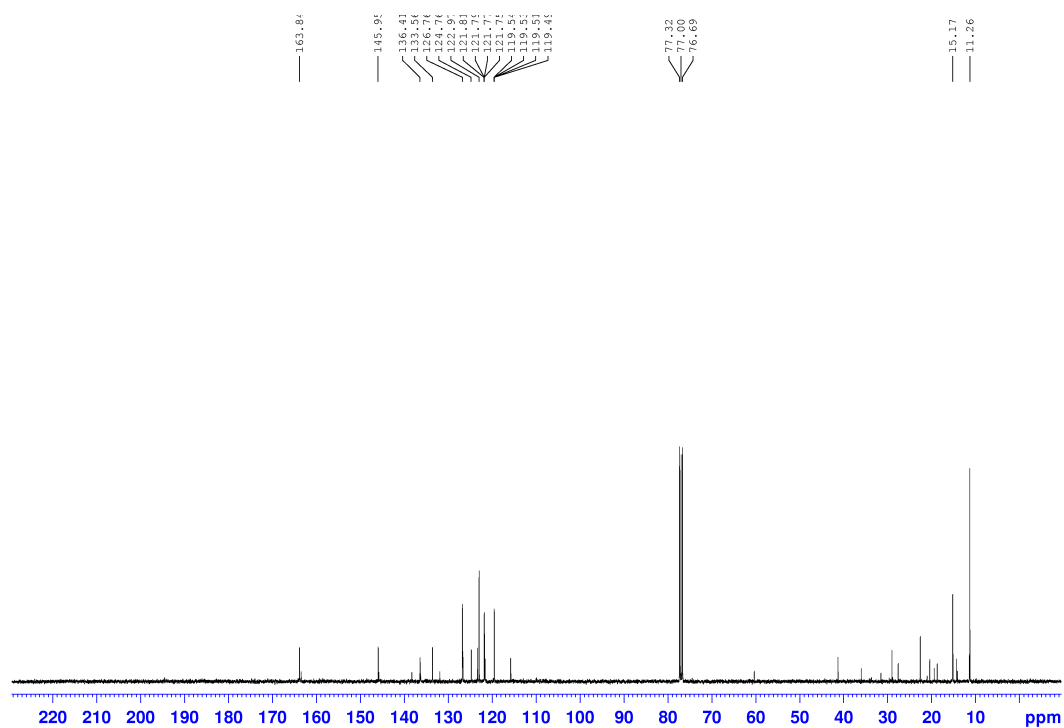


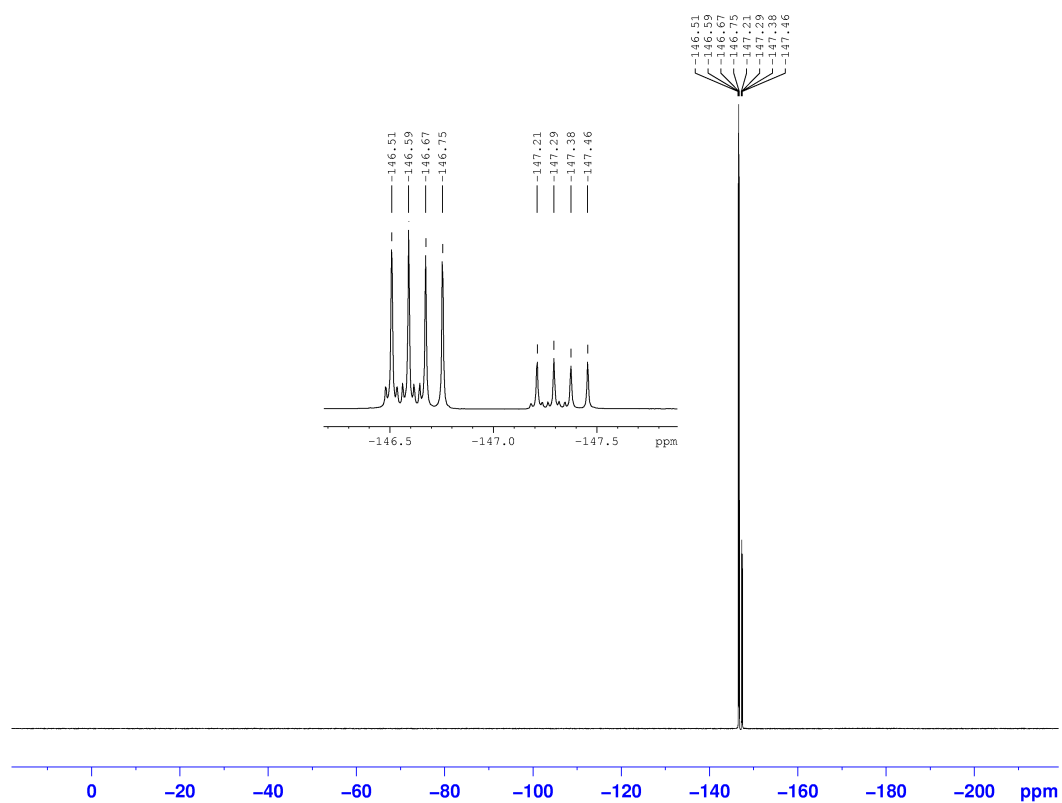
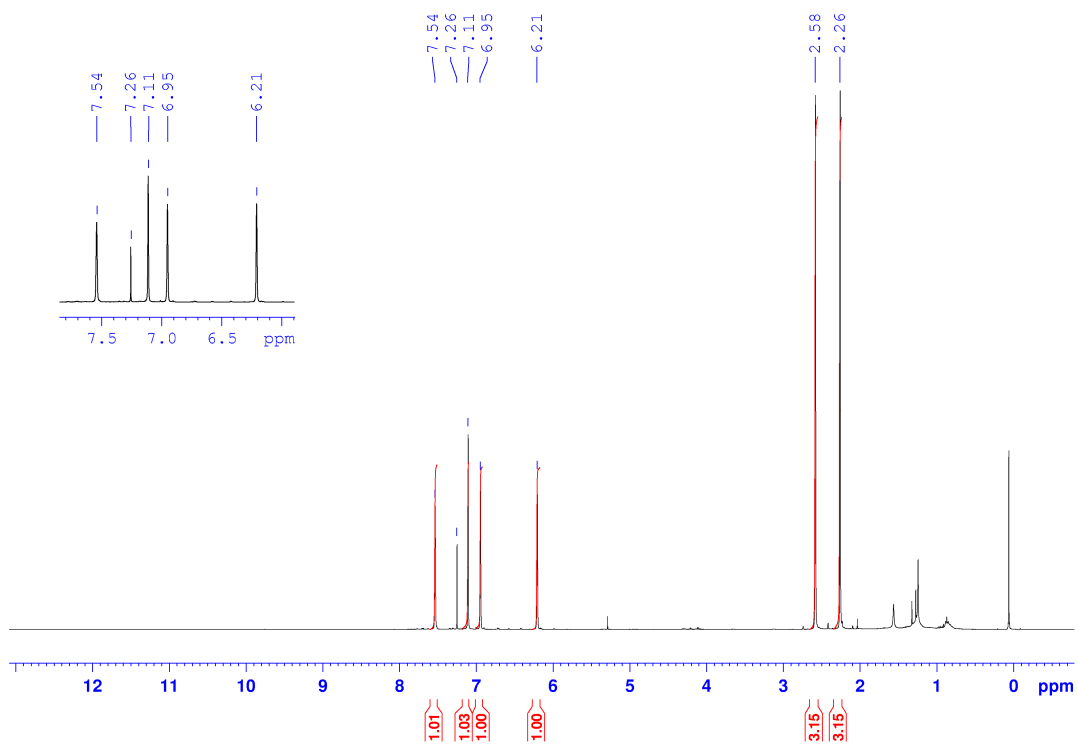
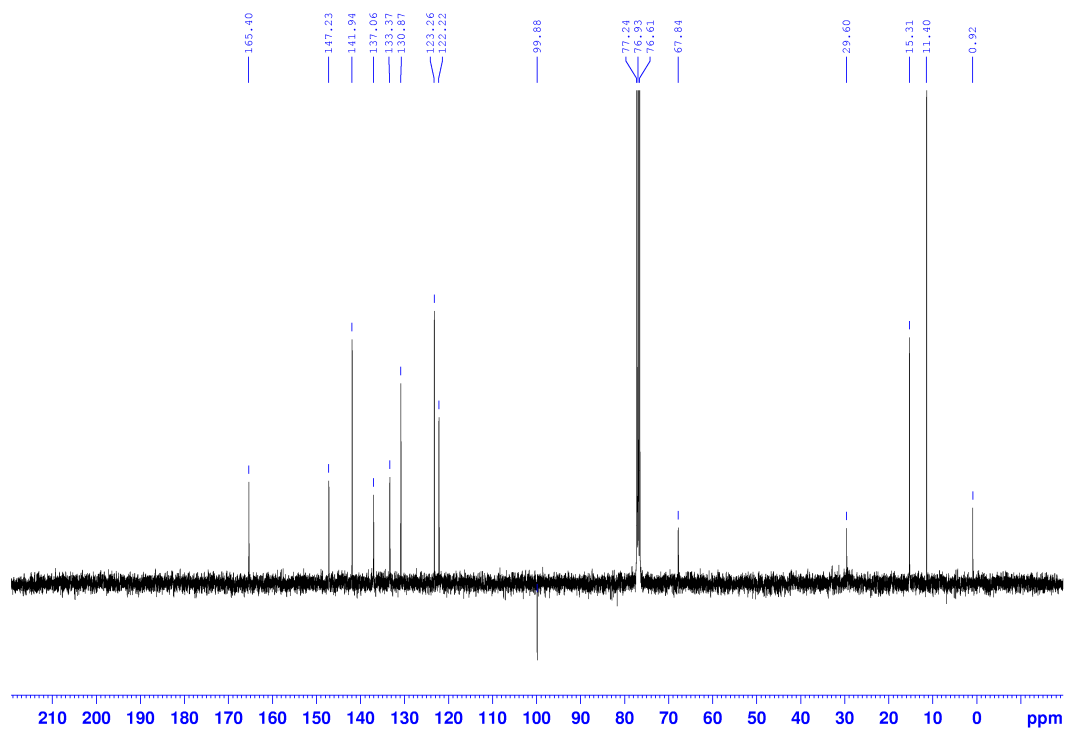
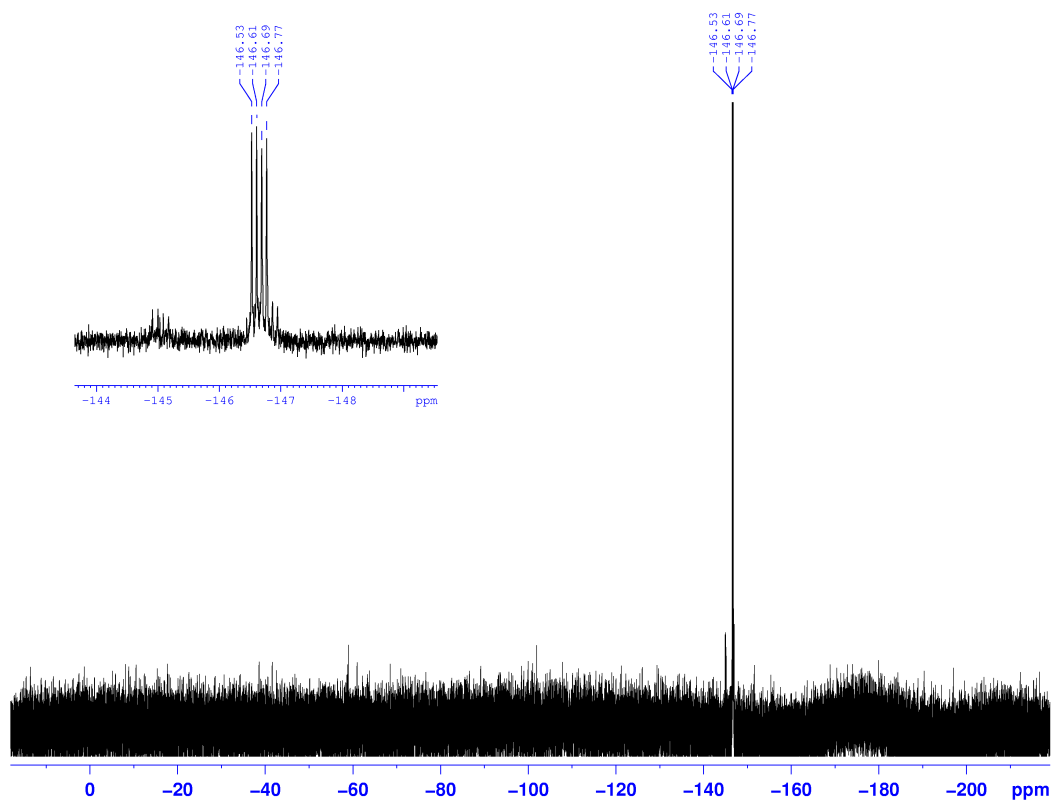
Figure A17: ^{19}F -NMR (**1**).ii. 1,3-Dimethyl-2-iodo-4,4'-difluoro-bora-3a,4a-diaza-(s)-indacene - β -I-BODIPY (**2**)Figure A18: ^1H -NMR (**2**).

Figure A19: $^{13}\text{C-NMR}$ (2).Figure A20: $^{19}\text{F-NMR}$ (2).

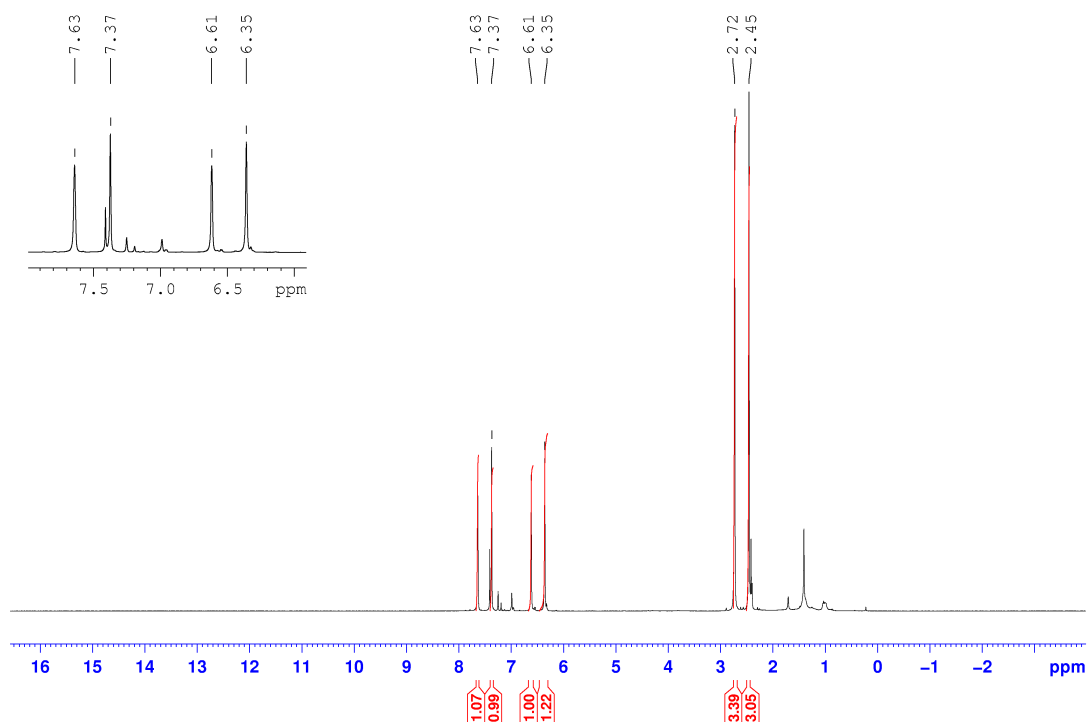
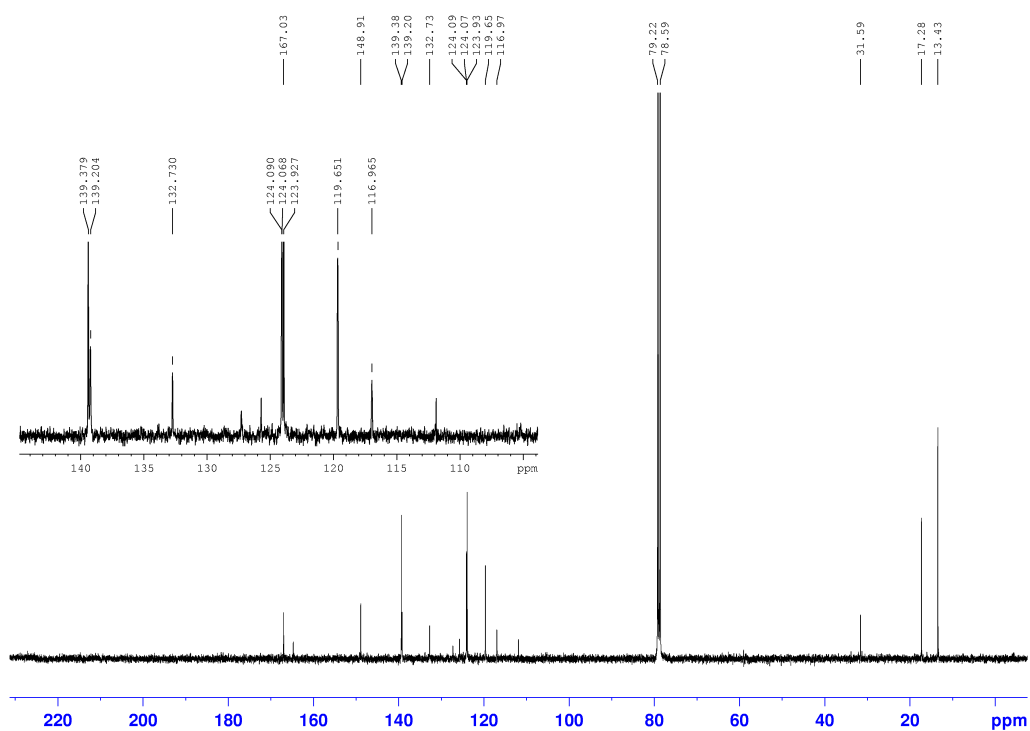
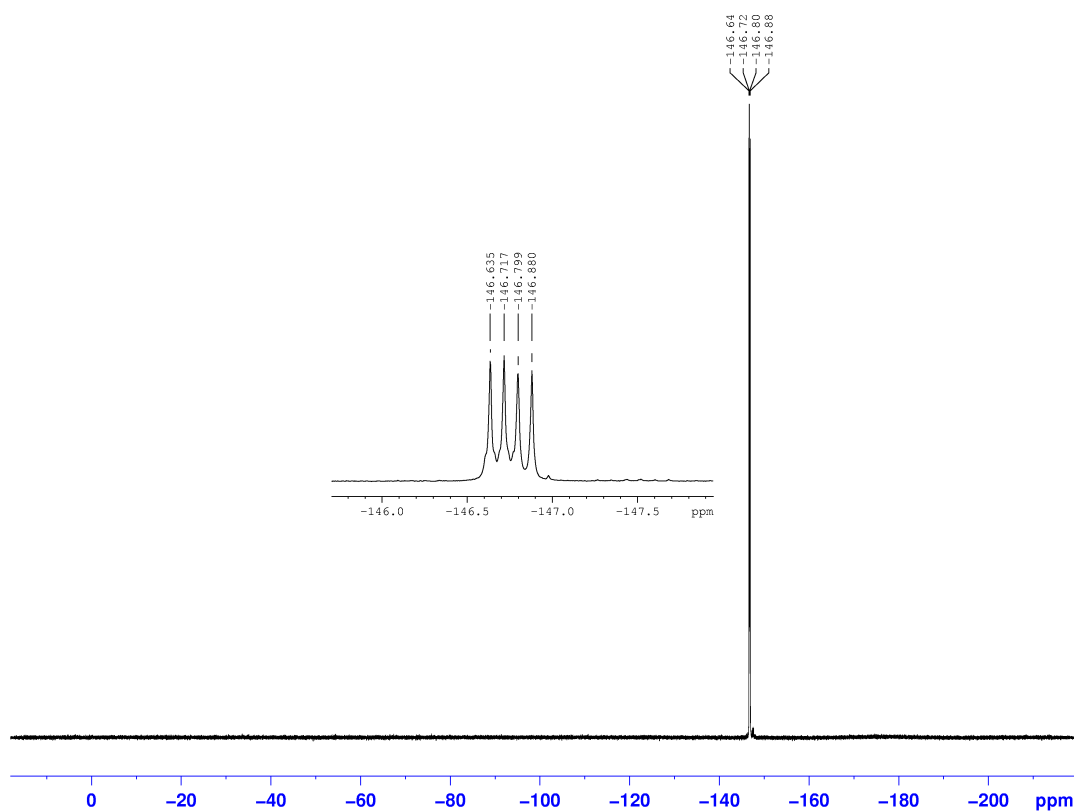
iii. 1-Bromo-5,7-dimethyl-4,4'-difluoro-bora-3a,4a-diaza-(s)-indacene - γ -Br-BODIPY (3)Figure A21: $^1\text{H-NMR}$ (3).Figure A22: $^{13}\text{C-NMR}$ (3).

Figure A23: ^{19}F -NMR (**3**).

- iv. 1,3-Dimethyl-3-(trimethylsilyl)ethynyl-4,4'-difluoro-bora-3a,4a-diaza-(s)-indacene - α -TMSAc-BODIPY (**4**)

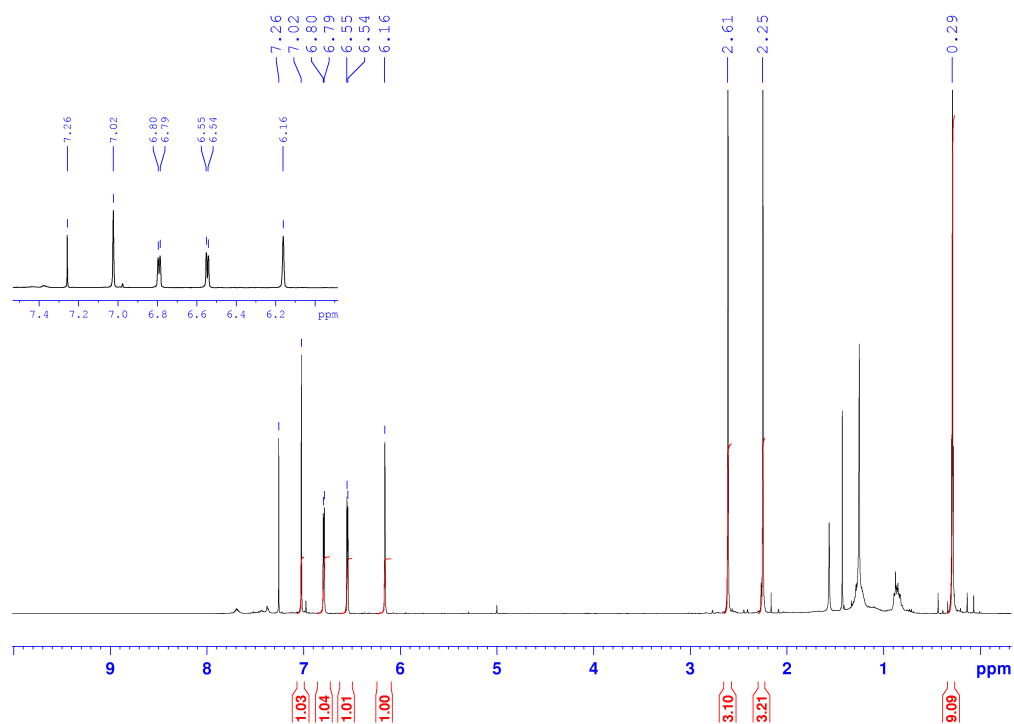
Figure A24: ^1H -NMR (**4**).

Figure A25: $^{13}\text{C-NMR}$ (4).

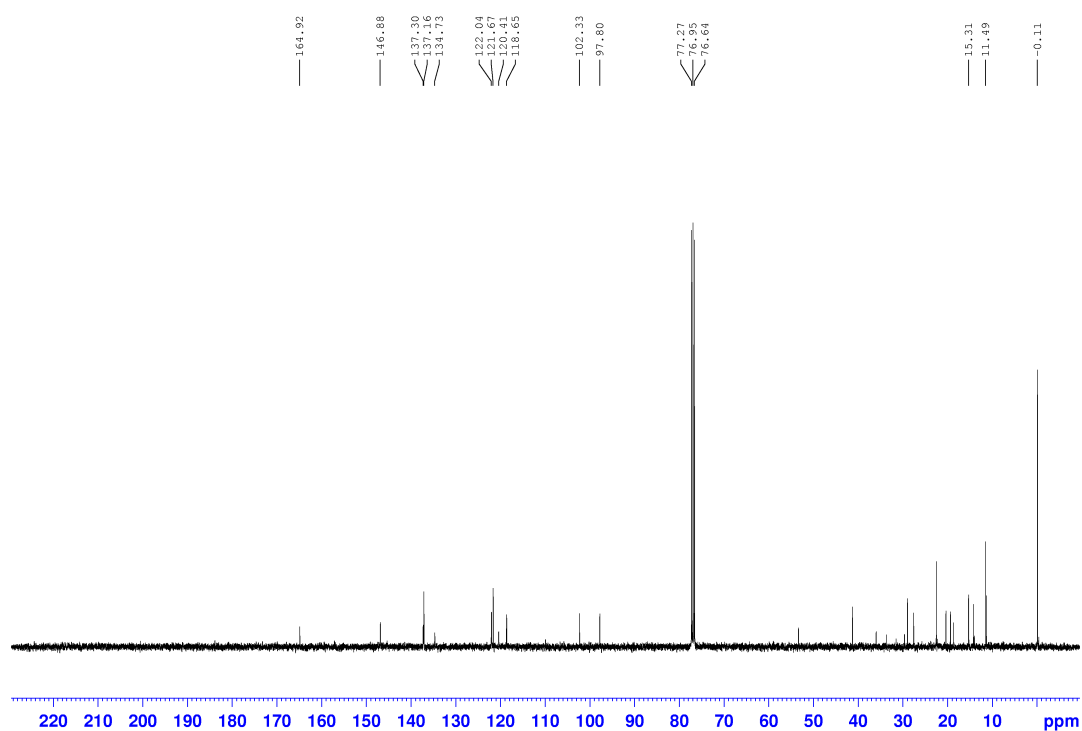
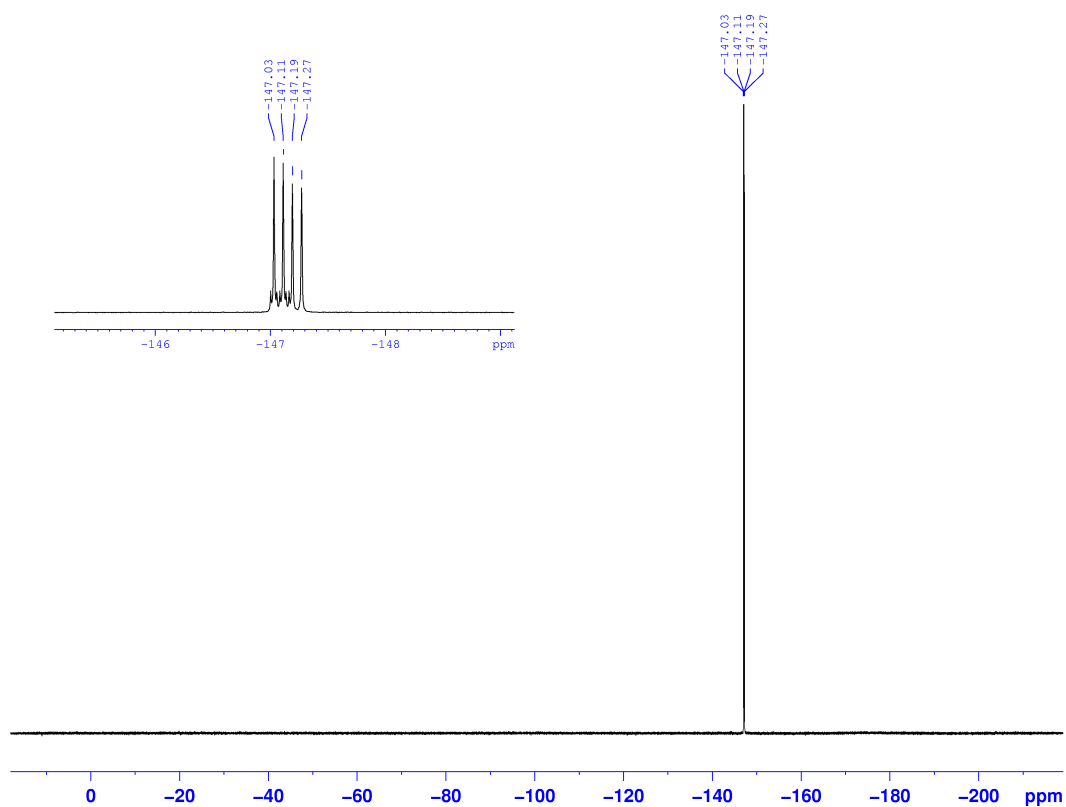


Figure A26: $^{19}\text{F-NMR}$ (4).



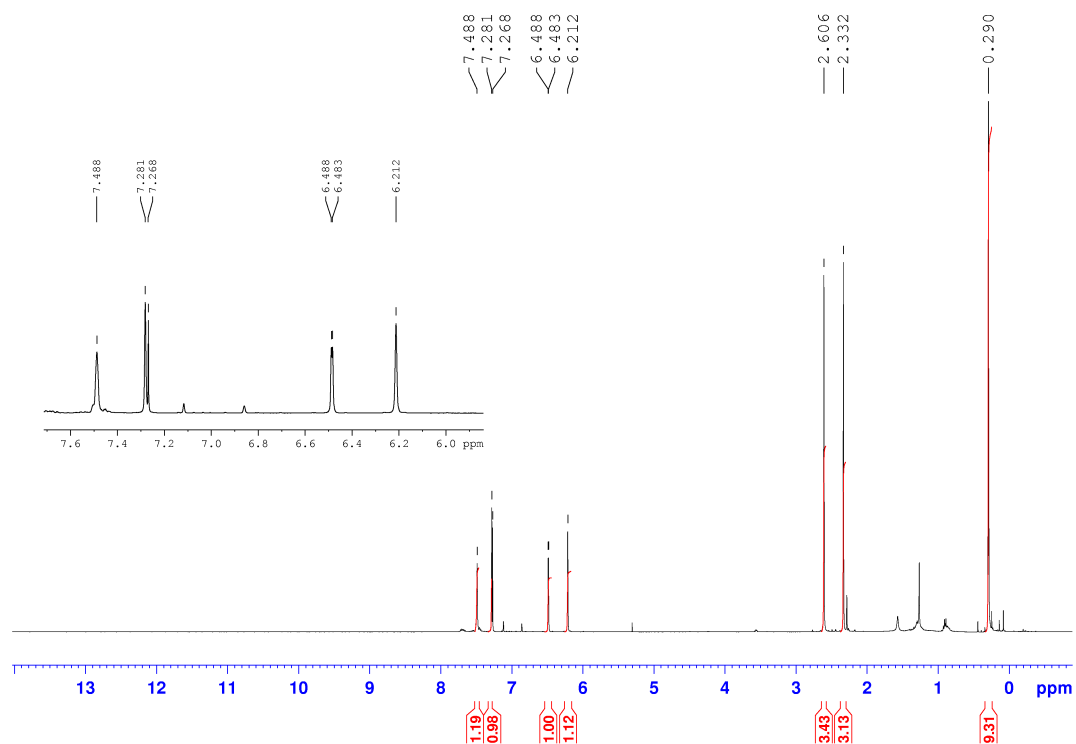
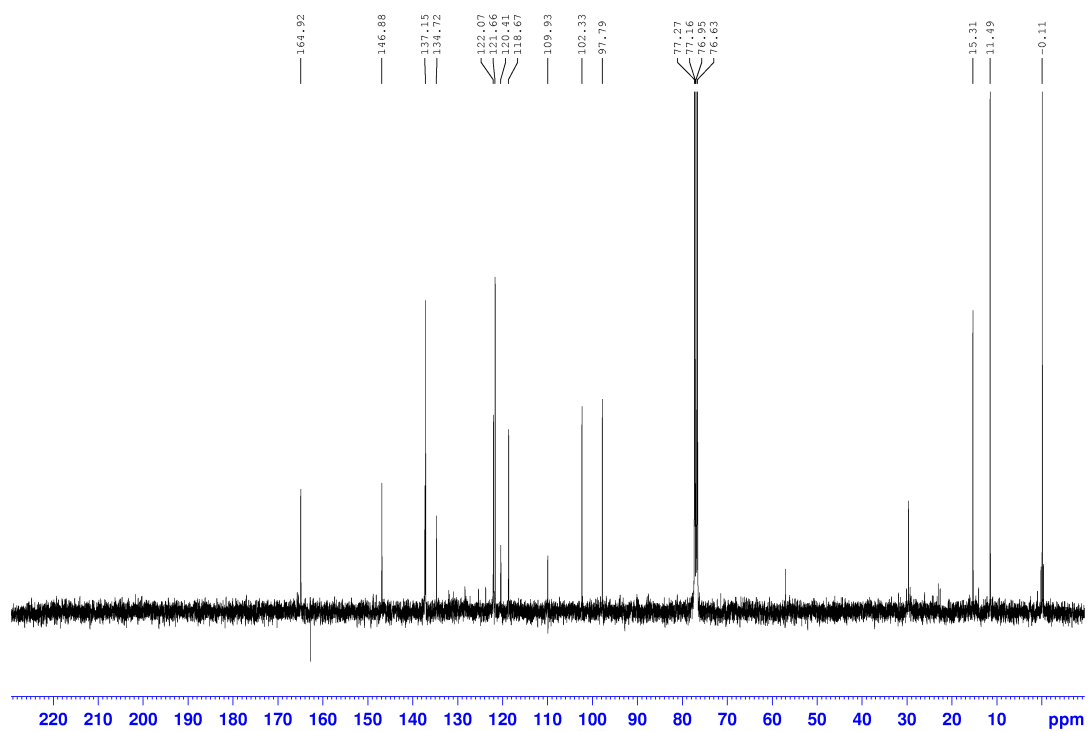
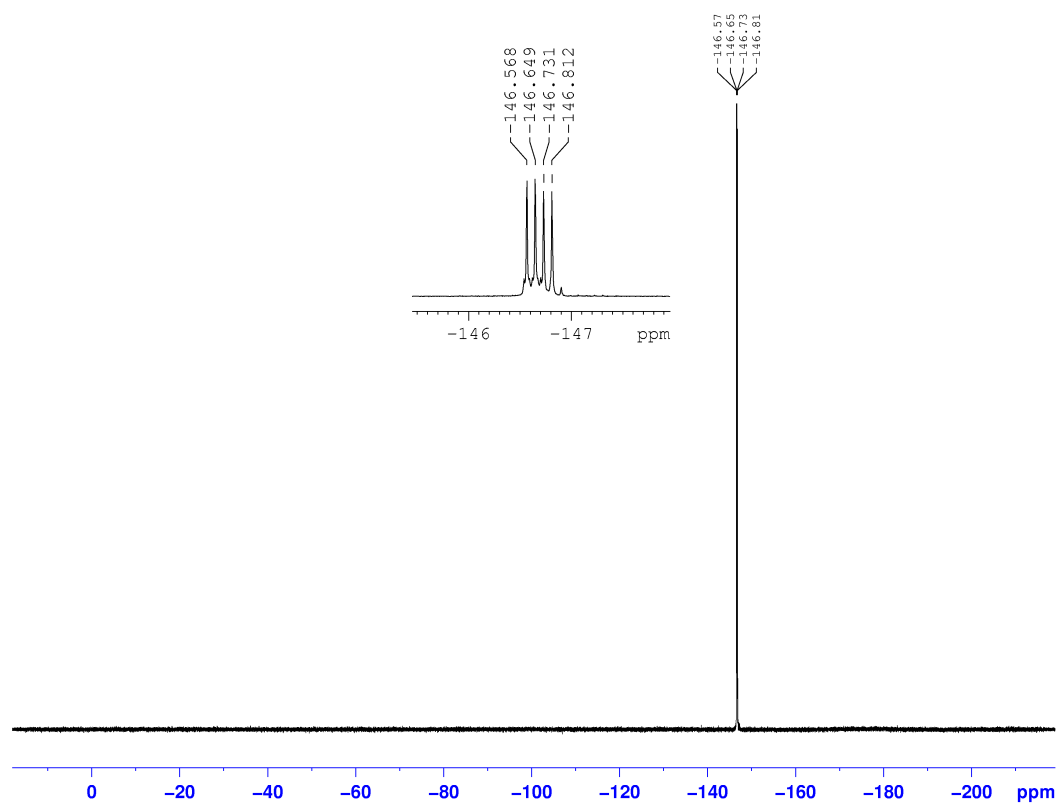
v. 5,7-Dimethyl-1-(trimethylsilyl)ethynyl-4,4'-difluoro-bora-3a,4a-diaza-(s)-indacene - - γ -TMSAc-BODIPY (5)Figure A27: $^1\text{H-NMR}$ (5).Figure A28: $^{13}\text{C-NMR}$ (5).

Figure A29: ^{19}F -NMR (5).

- vi. 3-Ethynyl-5,7-dimethyl-4,4'-difluoro-bora-3a,4a-diaza-(s)-indacene - α -ethynyl-BODIPY (6)

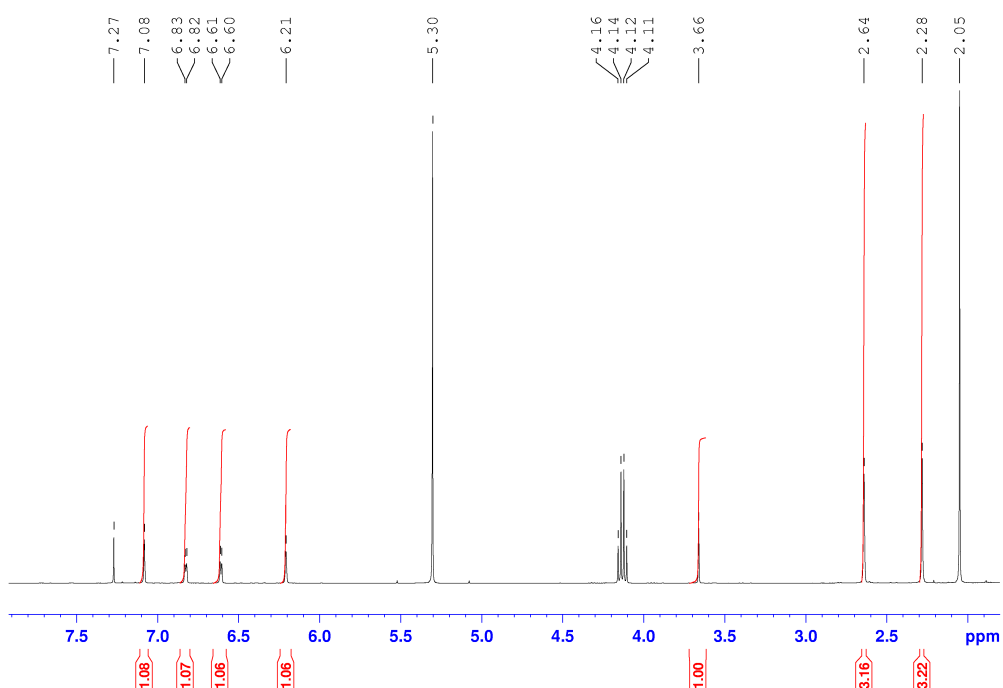
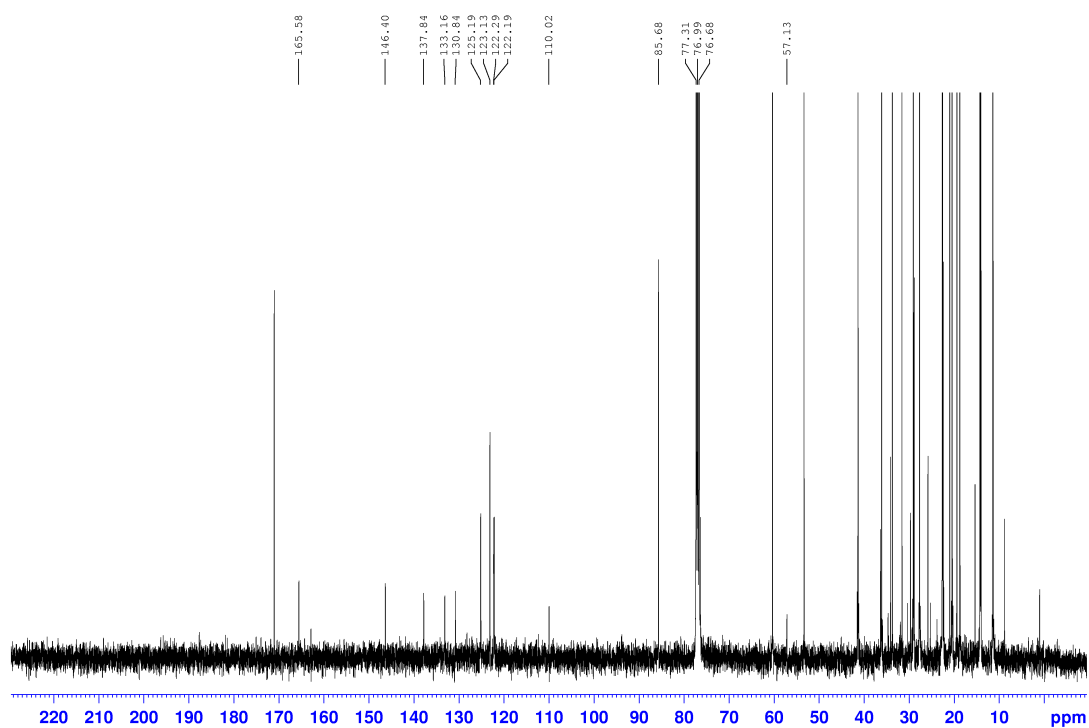
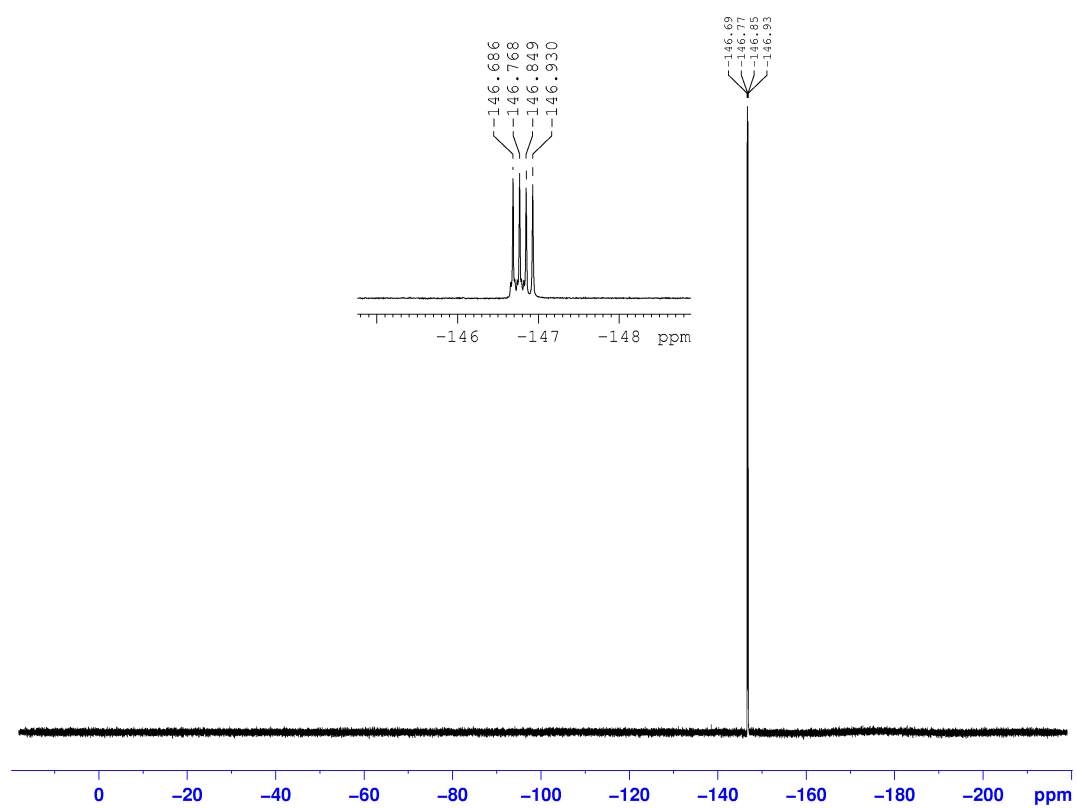
Figure A30: ^1H -NMR (6).

Figure A31: $^{13}\text{C-NMR}$ (6).Figure A32: $^{19}\text{F-NMR}$ (6).

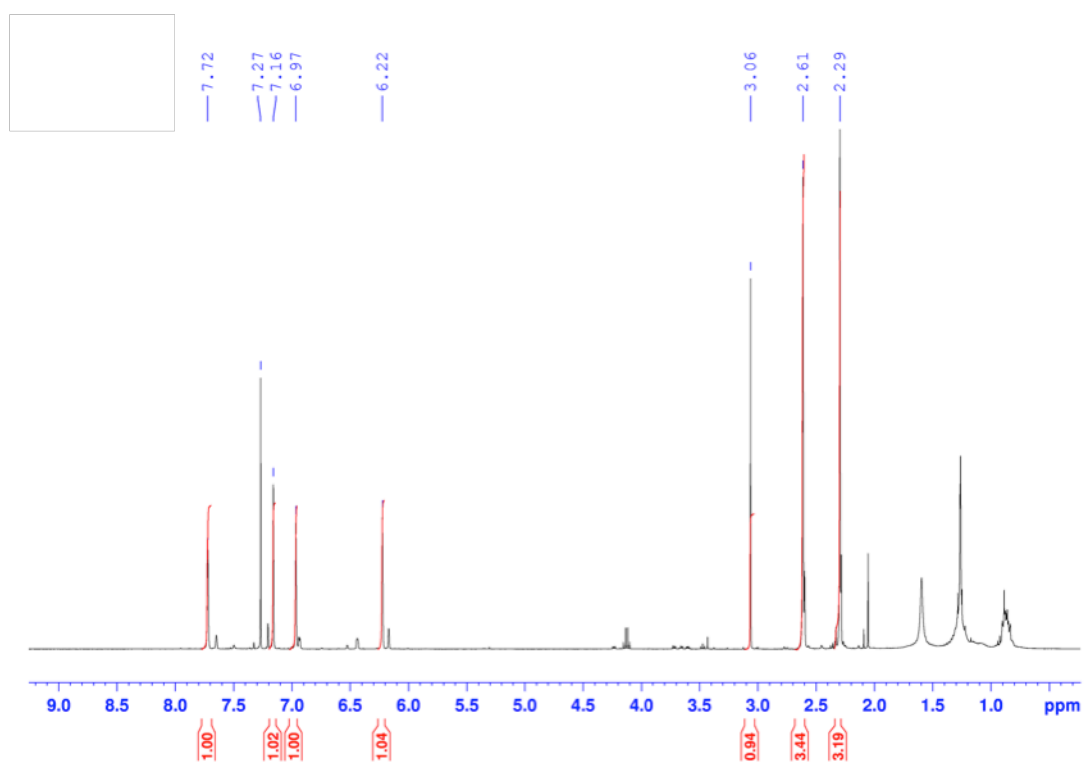
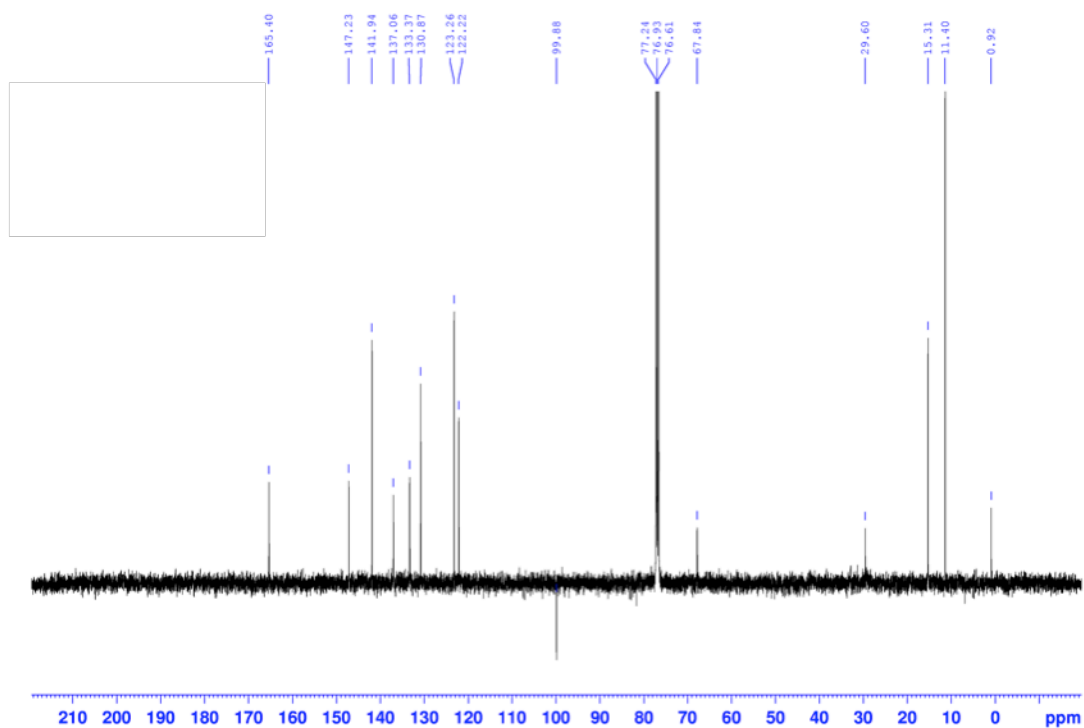
vii. 2-Ethynyl-5,7-dimethyl-4,4'-difluoro-bora-3a,4a-diaza-(s)-indacene - β -ethynyl-BODIPY (7)Figure A33: $^1\text{H-NMR}$ (7).Figure A34: $^{13}\text{C-NMR}$ (7).

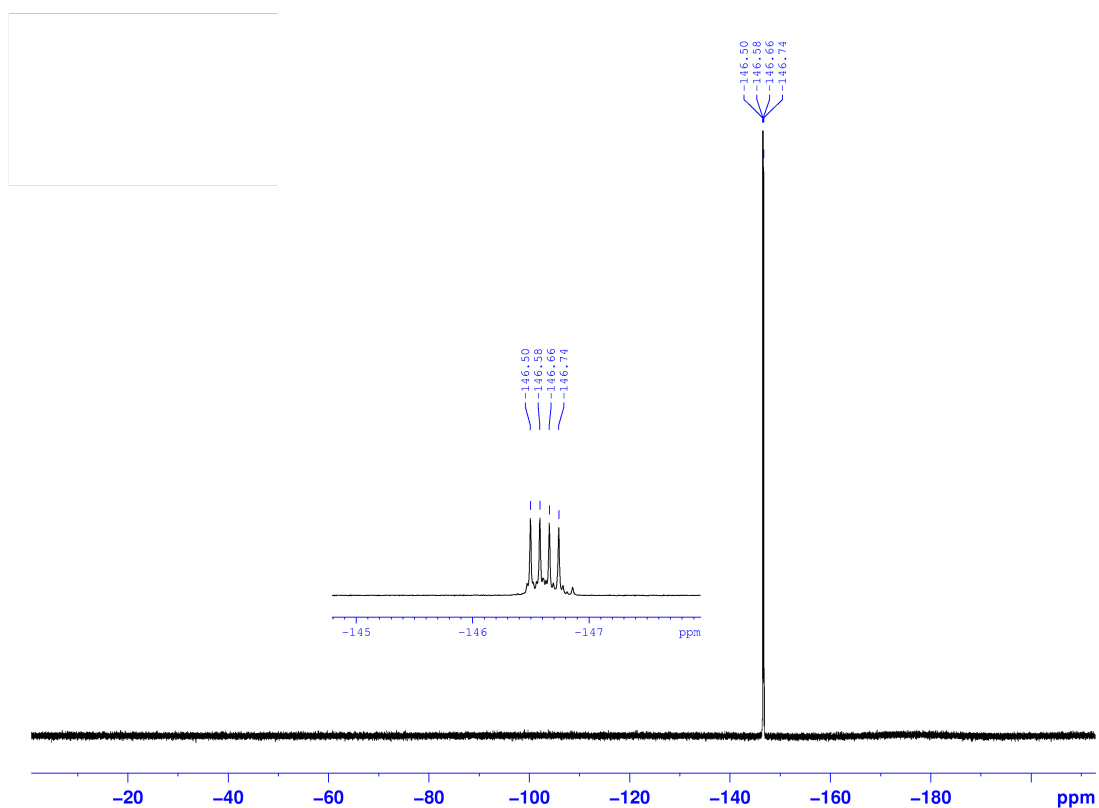
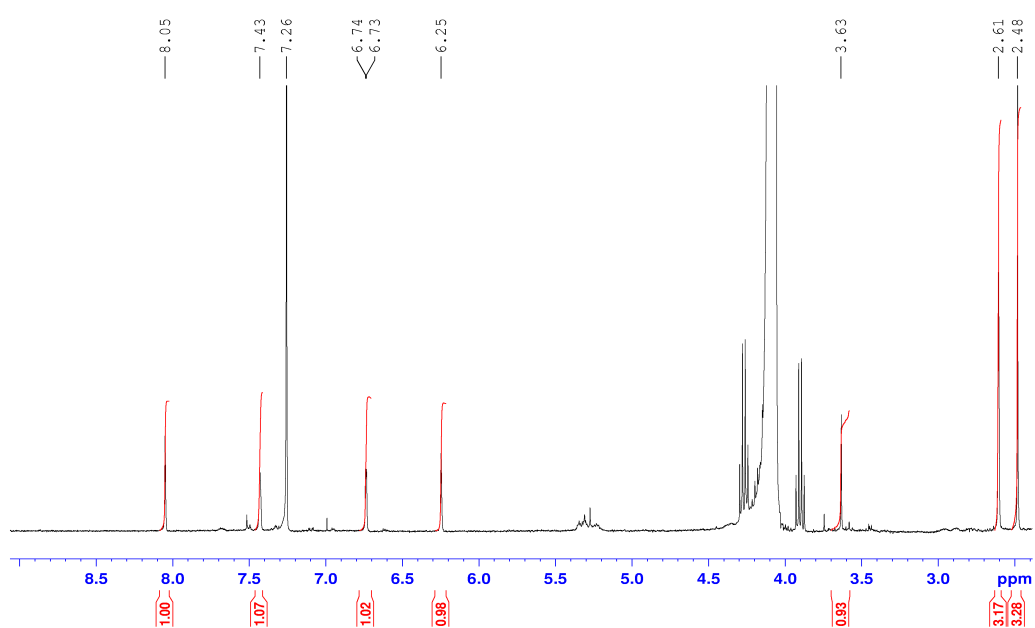
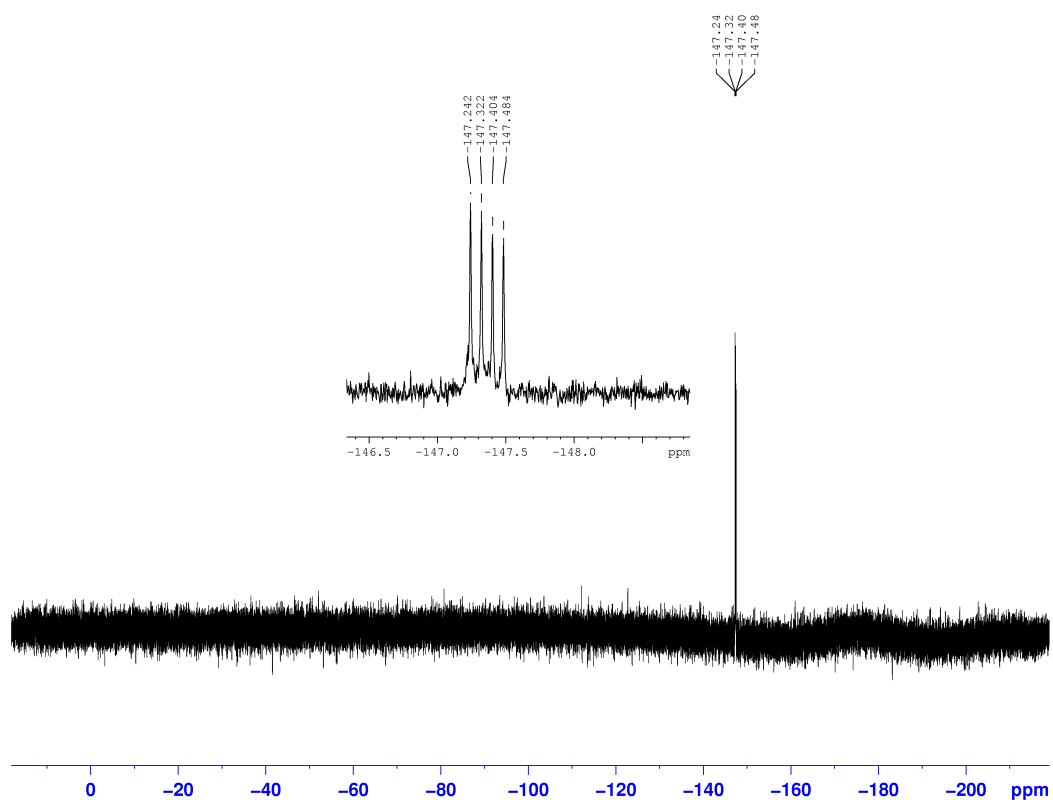
Figure A35: ^{19}F -NMR (**7**).viii. 1-Ethynyl-5,7-dimethyl-4,4'-difluoro-bora-3a,4a-diaza-(s)-indacene - γ -ethynyl-BODIPY (**8**)Figure A36: ^1H -NMR (**8**).

Figure A37: ^{19}F -NMR (**8**).

- ix. [3-\(Methoxyphenyl\)triazol-5,7-dimethyl-4,4'-difluoro-bora-3a,4a-diaza\(s\)-indacene](#) – [click product \(9b\)](#)

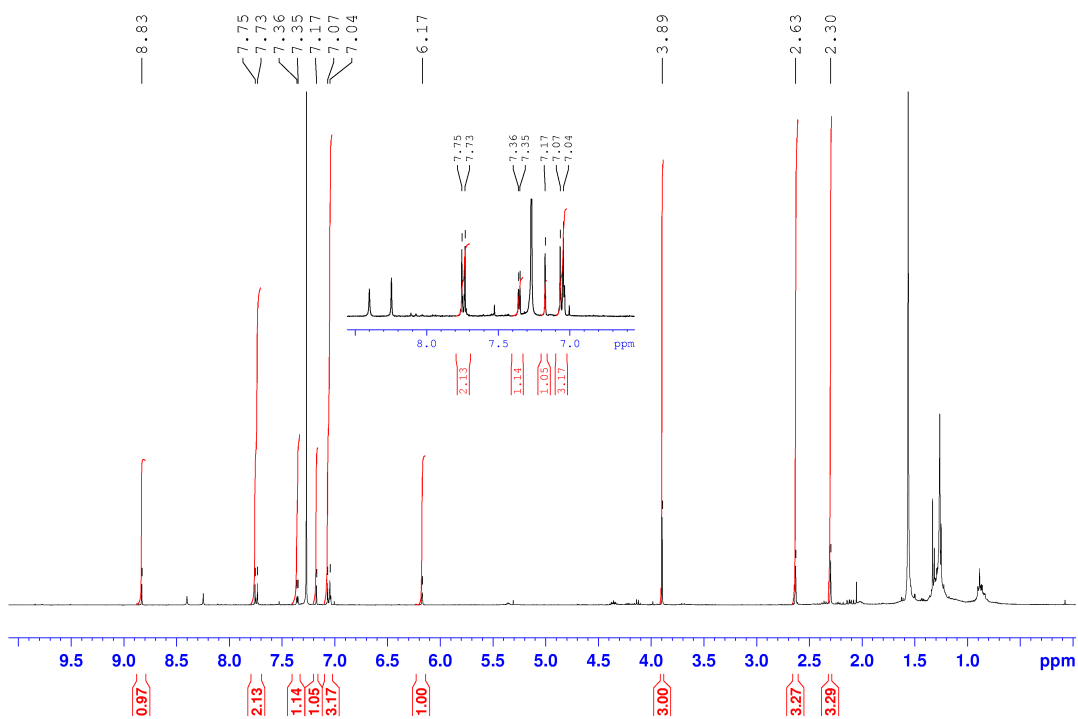
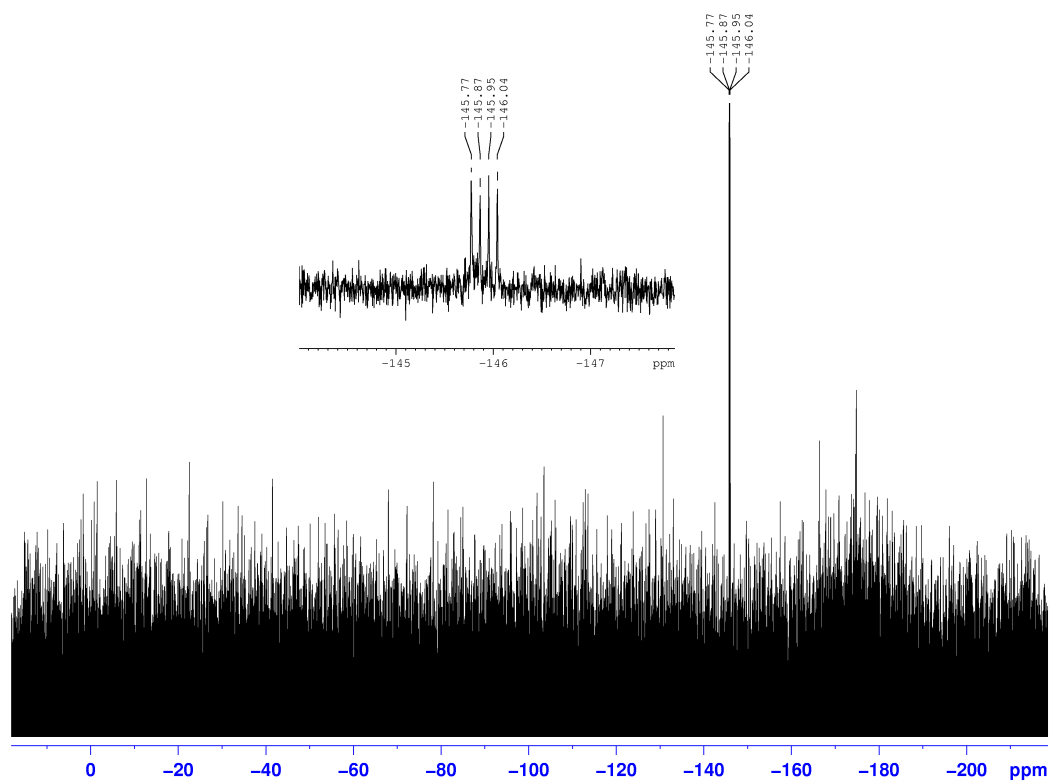
Figure A38: ^1H -NMR (**9b**).

Figure A39: ^{19}F -NMR (**9b**).

iv. Mass spectra

i. 3-Bromo-5,7-dimethyl-4,4'-difluoro-bora-3a,4a-diaza-(s)-indacene - α -Br-BODIPY (1)

Figure A40: mass spectra (1).

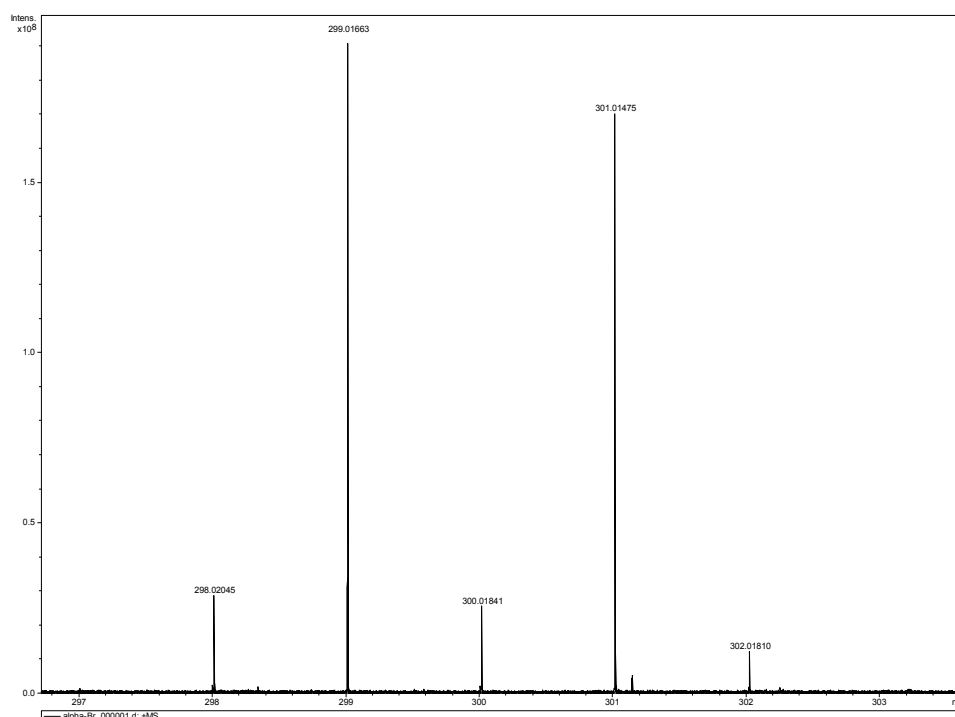
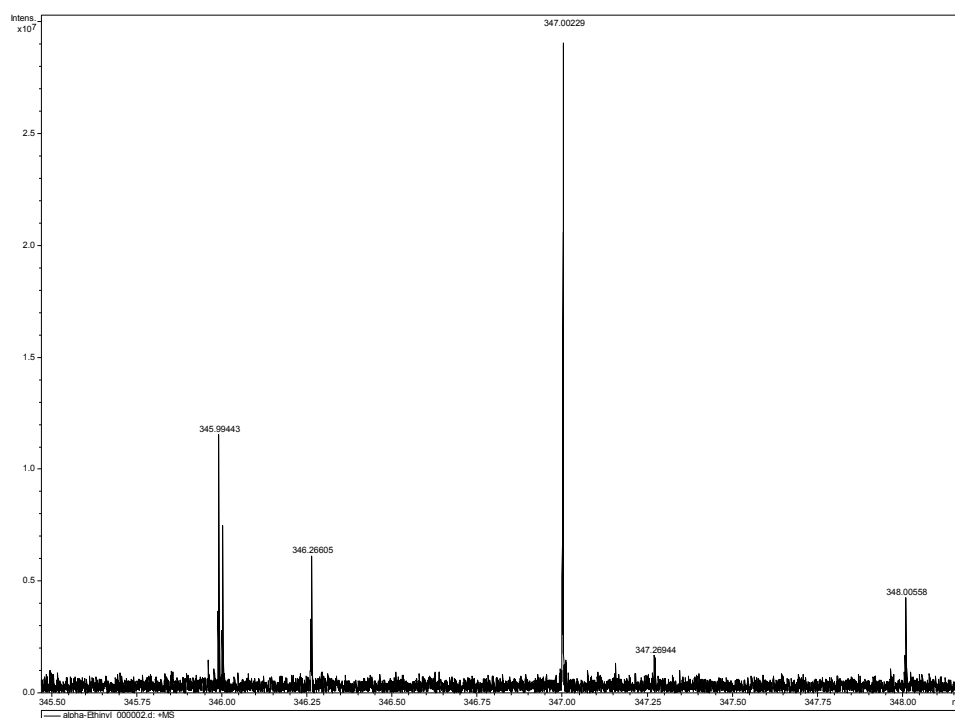
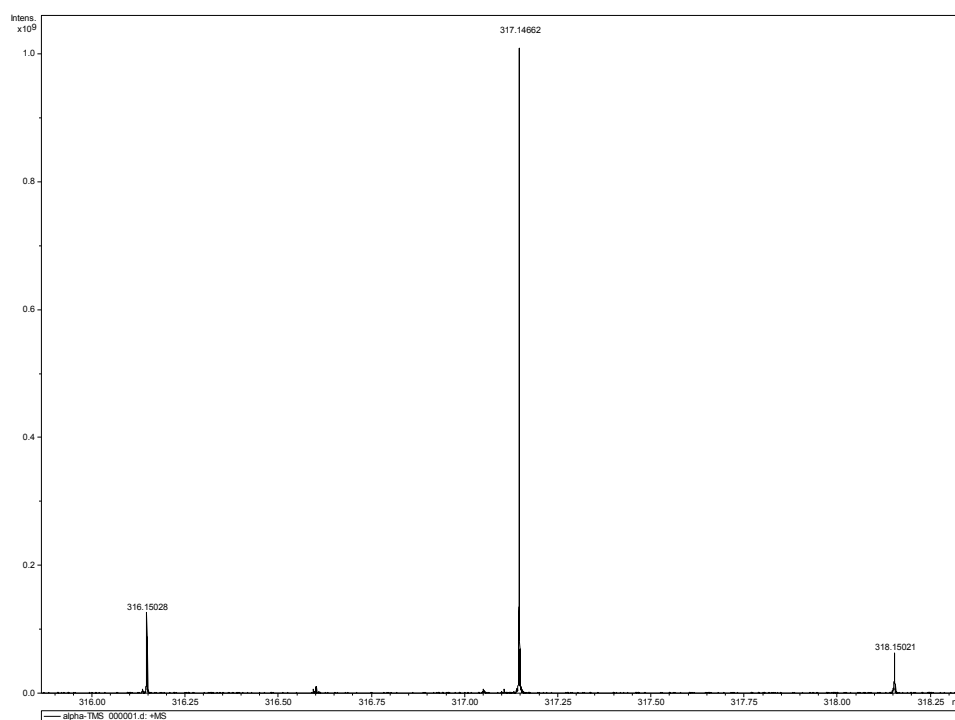
ii. 1,3-Dimethyl-2-iodo-4,4'-difluoro-bora-3a,4a-diaza-(s)-indacene - β -I-BODIPY (2)

Figure A41: mass spectra (2).



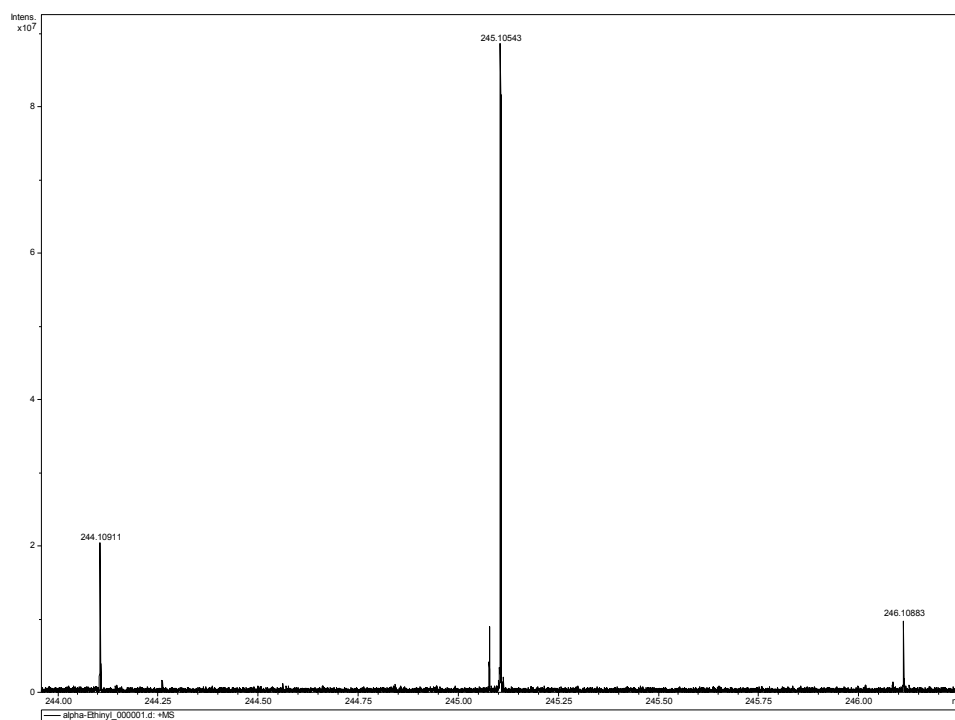
- iii. 5,7-Dimethyl-3-(trimethylsilyl)ethynyl-4,4'-difluoro-bora-3a,4a-diaza-(s)-indacene - α -TMSAc-BODIPY (4)

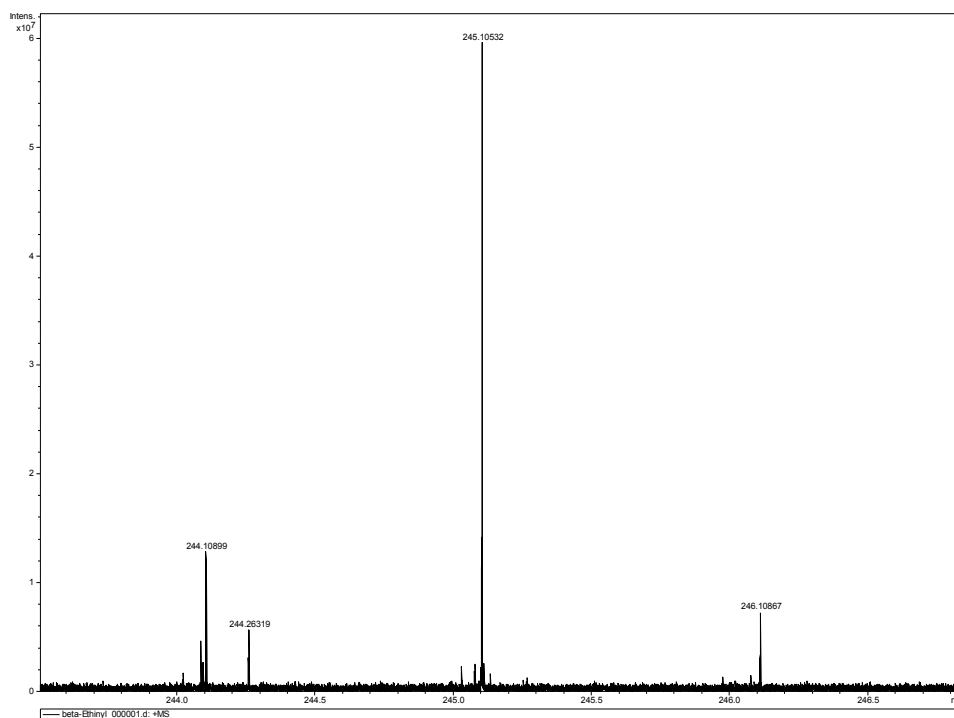
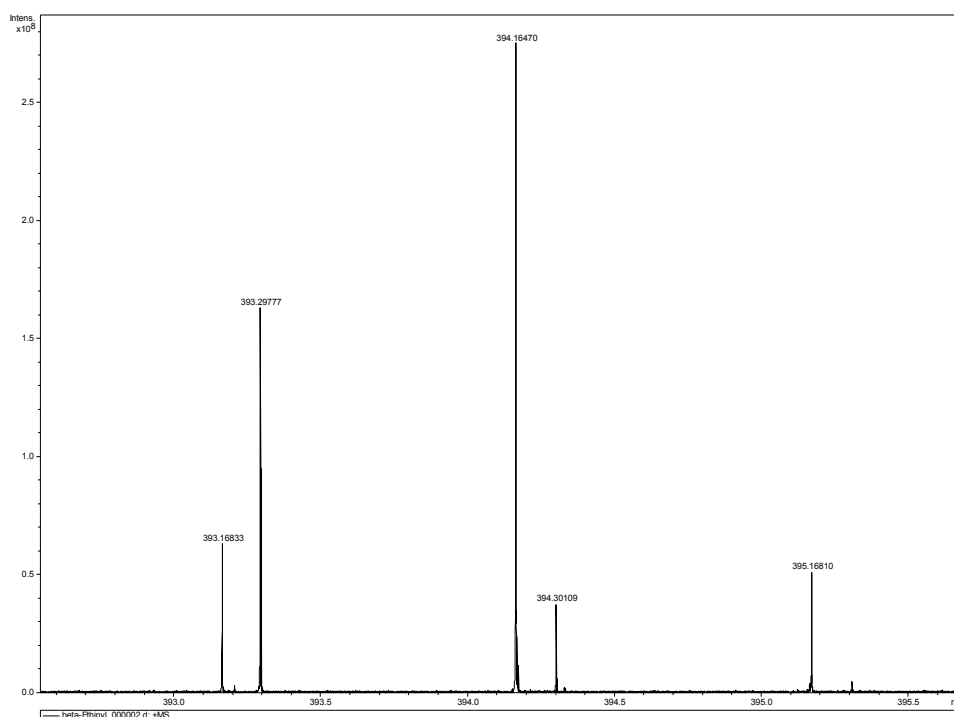
Figure A42: mass spectra (4).



- iv. 3-Ethynyl-5,7-dimethyl-4,4'-difluoro-bora-3a,4a-diaza-(s)-indacene - α -ethynyl-BODIPY (6)

Figure A43: mass spectra (6).



v. 2-Ethynyl-5,7-dimethyl-4,4'-difluoro-bora-3a,4a-diaza-(s)-indacene - β -ethynyl-BODIPY (7)Figure A44: *mass spectra (7)*.vi. 3-(Methoxyphenyl)triazol-5,7-dimethyl-4,4'-difluoro-bora-3a,4a-diaza-(s)-indacene - click product (9b)Figure A45: *mass spectra (9b)*.

7.3. Metathesis reaction

7.3.1. Further reactivity study of BODIPYlidene compound (2)

The multi-color behavior of BODIPYlidene carbene complex (2) was investigated via reaction with different olefins. *Cis*-stilbene was used as second olefin, which only forms one product, (3), during the reaction (figure A46).

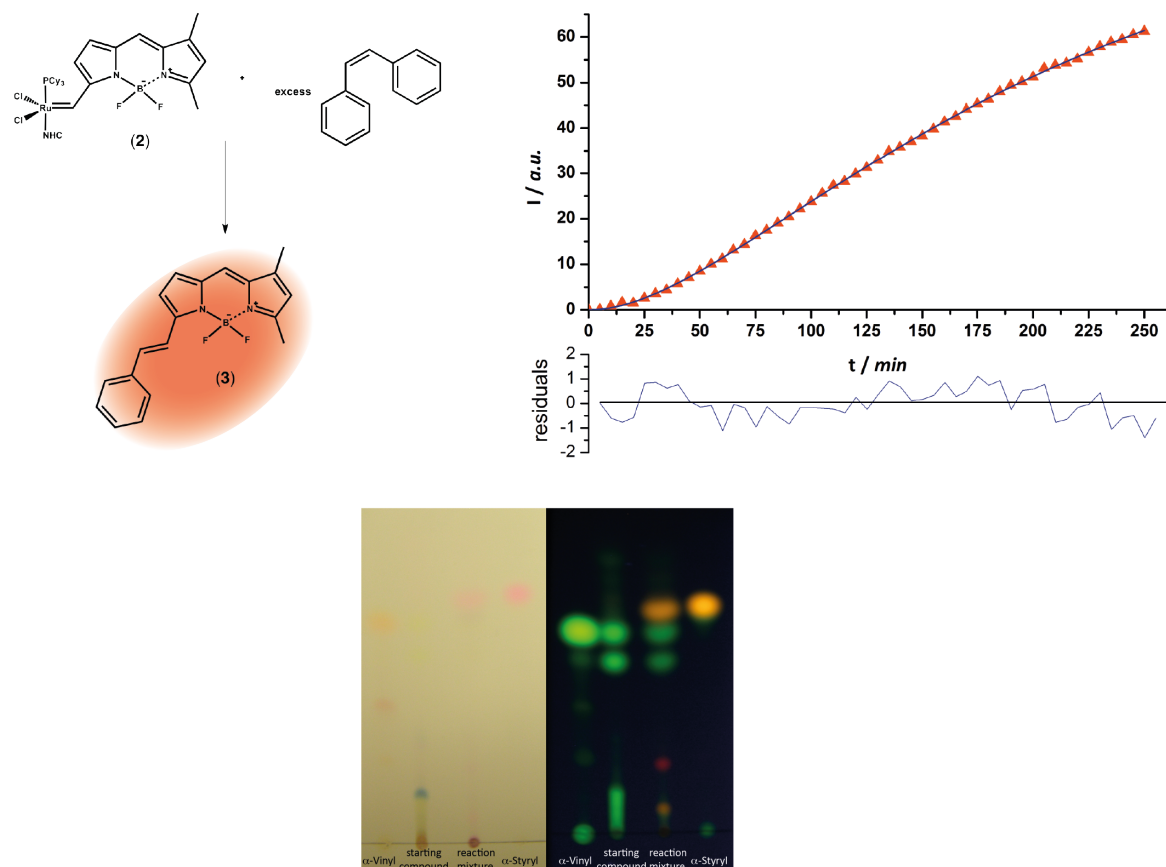


Figure A46: Reactivity study of (2) towards *cis*-stilbene forming α -styryl BODIPY (3) confirmed by thin layer and fluorescence analysis ($k_1 = 1.99 \cdot 10^{-2} \text{ min}^{-1}$; $k_2 = 5.33 \cdot 10^{-2} \text{ min}^{-1}$).

The kinetic data were recorded, using the experimental approach described in 7.3.5. Thin layer chromatography revealed that only one product is formed as expected (figure A46).

Further investigations were established using *trans,trans*-1,4-diphenylbutadiene. The reaction with complex (2) forms two different BODIPY compounds: α -styryl BODIPY (3) and another, literature known BODIPY (5), with extended conjugation, identified by its spectral characteristics ($\lambda_{\text{exc}} = 583 \text{ nm}$; $\lambda_{\text{em}} = 596 \text{ nm}$)^[2].

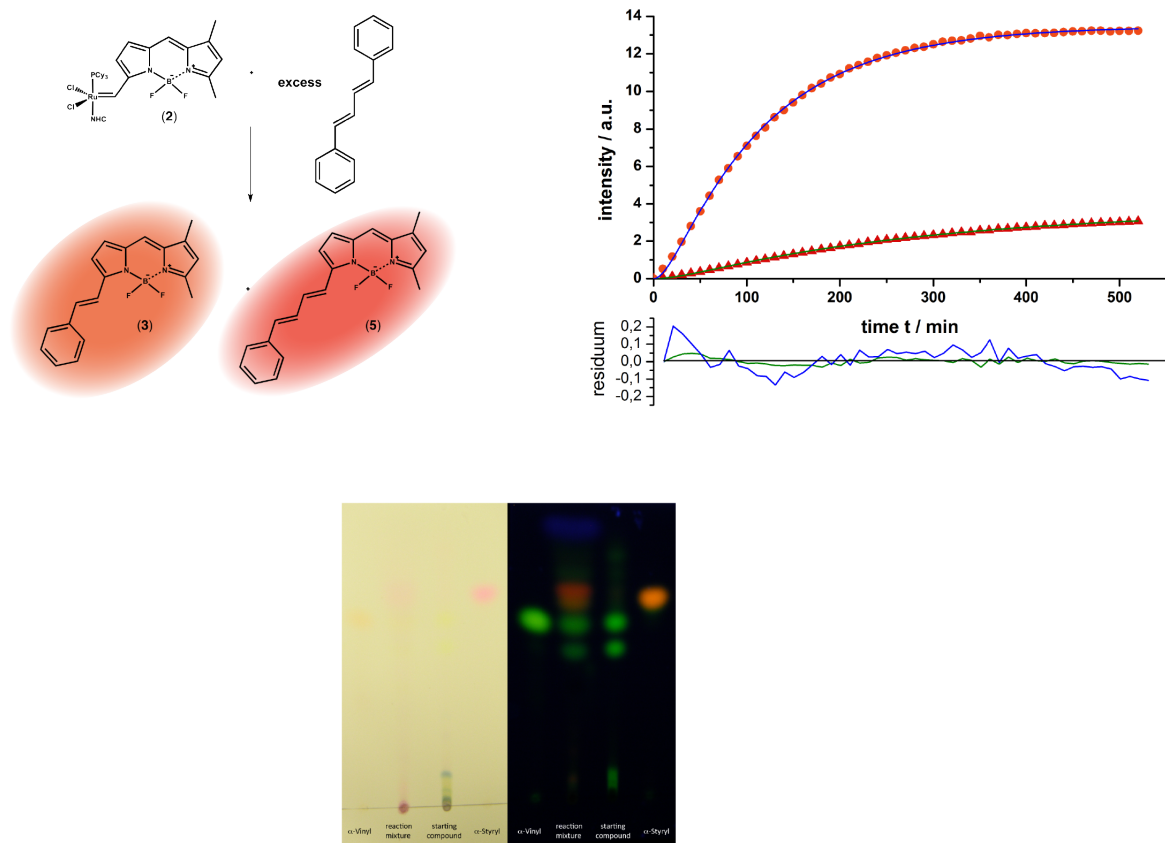


Figure A47: Reactivity study of **(2)** towards *trans,trans*-1,4-diphenylbutadiene forming α -styryl BODIPY **(3)** and a second red-shifted BODIPY **(5)** confirmed by thin layer chromatography and fluorescence analysis ($k_{1-(3)} = 9.09 \cdot 10^{-3} \text{ min}^{-1}$; $k_{2-(3)} = 6.57 \cdot 10^{-2} \text{ min}^{-1}$; $k_{1-(5)} = 3.61 \cdot 10^{-3} \text{ min}^{-1}$; $k_{2-(5)} = 3.97 \cdot 10^{-2} \text{ min}^{-1}$).

In the reaction of **(2)** with four different olefins (ethylene, styrene, *cis*-stilbene, *trans,trans*-1,4-diphenylbutadiene), three chromophores (**(1)**, **(3)**, **(5)**) with different emission properties were formed.

7.3.2. Control experiments revealing reaction selectivity

The reactivity of **(2)** towards olefins is visualized on the single-molecule level (figure 21). To verify that detected single-molecule signals stem from metathesis reaction, blank measurements without addition of **(2)** (figure A48) and a second slide with a dimethyldichlorosilane modified surface were performed (figure A49).

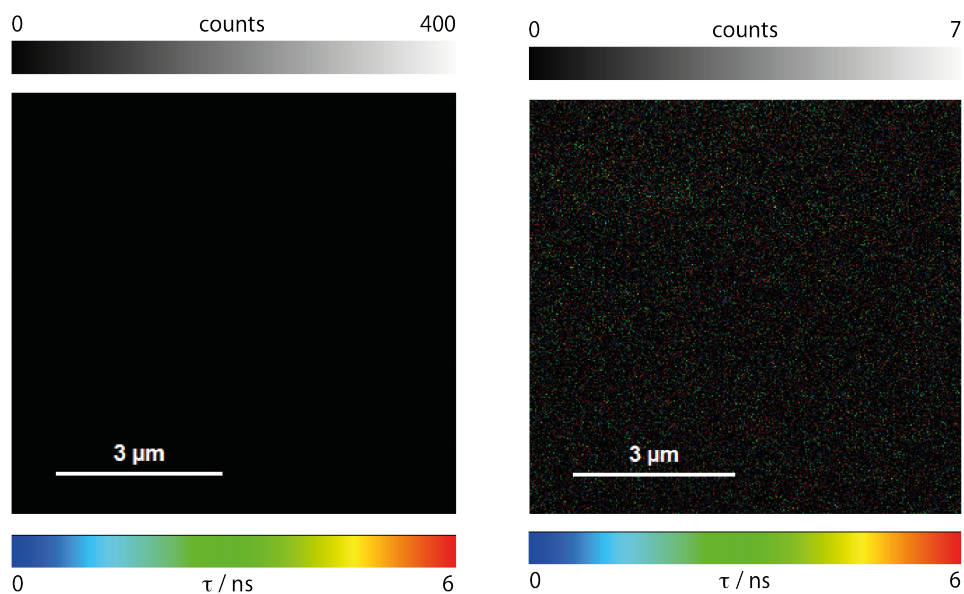


Figure A48: Cover slide from experiment illustrated in figure 21 before treatment with compound (**2**). Left: comparable brightness, right: reduced brightness.

A silylated, non-reactive cover glass was treated with BODIPYlidene Ruthenium reagent (**2**). Spurious fluorescent burst, visible as single or double bright pixels, hint at fluorescent impurities with single-molecule behavior on the glass surface. However, in no case, fluorescence emission as bright and stable as in figure 21 could be recorded. We conclude that no fluorescence could be observed because of missing reactive sides on the cover glass. To summarize figure A49, these single-molecule investigations revealed that compound (**2**) requires double bond containing substrates for generation of fluorescence.

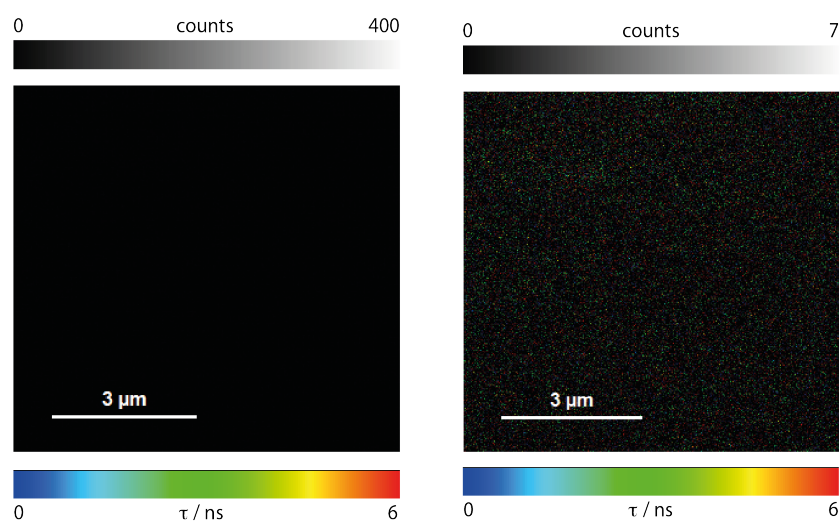
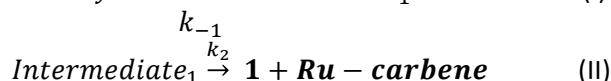


Figure A49: Single-molecule fluorescence analysis after every experimental step.

7.3.3. Detailed description of the used kinetic model

Metathesis is a highly reversible reaction where multiple equilibria have to be considered. In order to keep the kinetic analysis as simple as possible, we focused on the early times (up to 5h), where the whole system mainly consists of compound (**2**) and a reactive counterpart with a double bond. At these early times of the conversion, the formation of (**1**) is composed at least by the following sequence of elementary reactions (I) and (II):



The reversibility of step (II) is not considered here, as styrene **S** is more abundant by a factor > 100 than (**1**). From this follows the description of the kinetics for consumption of substrate (**2**) (eq. III), intermediate (**I**₁) growth and decrease (eq. IV) and formation of product (**1**) (eq. V):

$$\frac{d[\mathbf{2}]}{dt} = -k_1[\mathbf{2}][\mathbf{S}] + k_{-1}[\mathbf{I}_1] \quad (\text{III})$$

$$\frac{d[\mathbf{I}_1]}{dt} = +k_1[\mathbf{2}][\mathbf{S}] - k_{-1}[\mathbf{I}_1] - k_2[\mathbf{I}_1] \quad (\text{IV})$$

$$\frac{d[\mathbf{1}]}{dt} = +k_2[\mathbf{I}_1] \quad (\text{V})$$

The same description applies to the formation of (**3**), although the individual rate constant k_i are likely different, *i.e.* k_i^* . The intermediate, presumably a Ruthena-cyclobutane as well, exhibits a different conformation and is therefore denominated as **I**₂.

Formation of (**1**)

Under the assumption that once the Ruthenacyclobutane **I**₁ (respectively **I**₂) is formed, it decomposes into (**1**) ((**3**), respectively), *i.e.* $k_{-1} \sim 0$. Having excess of styrene **S** in mind, we expect pseudo-first order kinetics for the first steps which leads to an exponential decay of [**2**]. The description for [**I**₁] follows that of the radioactive decay with an intermediate (eq. VI).

$$\frac{d[\mathbf{I}_1]}{dt} = +k'_1[\mathbf{2}] - k_2[\mathbf{I}_1] \quad (\text{VI})$$

The intermediate I_1 decomposes faster into the well-known 2nd-generation Grubbs-catalyst, from which (2) was originally produced (scheme 34), *i.e.* $k_2 \gg k_1$. The rate limiting step is then the formation of the intermediate I_1 . Under these conditions, insertion of (eq. VI) into (V) yields

$$\frac{d[1]}{dt} = +k_1' [2] \Rightarrow [1] = [2]_{t=0} \{1 - \exp(-k_1' t)\} \quad (\text{VII})$$

This behavior describes the formation of the green fluorescent product **1** in ¹⁹F-NMR very well. One should keep in mind that only 80% of [2] are converted to [1]. A matching of the concentrations in optical spectroscopy was not done due the strong coloration of (2) which causes significant reabsorption effects.

Formation of (3) in Fluorescence Spectroscopy

Further following the description of radioactive decay as only (pseudo-)first-order kinetics are involved, we employed a biexponential function to fit the formation of orange fluorescent (3) and other fluorophores with internal double bonds (eq. VIII) (figure 20 and Appendix).

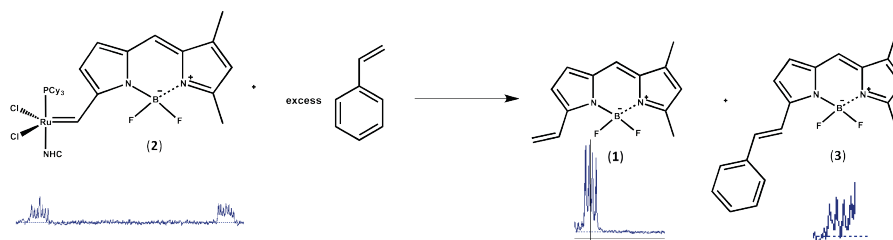
$$[3](t) \propto [2]_{t=0} \{1 + C_1 \exp[-k_1' t] - C_2 \exp[-k_2^* t]\} \quad (\text{VIII})$$

The determination of the pre-exponential factors C_1 and C_2 and, hence, the concentration determination was, again, not attempted by fluorescence spectroscopy. The rate constants were therefore only calculated from the exponentials. An intermediate, although expected, was neither unambiguously detected by UV-VIS nor by ¹⁹F-NMR nor by the more sensitive fluorescence spectroscopy. The latter observation could be due to quenching by the metal center.^[244] We can summarize that the rate-limiting step is reaction (I) in the formation of (1) and (II) in all systems containing internal double bonds.

Although kinetics can be yet brought in line with the experimental observations, more competitive pathways should be considered. Phosphine dissociation might occur before the reaction.^[23] From a kinetic point of view, however, we cannot decide without doubts whether phosphine-Ruthenium dissociation precedes formation of the reactive intermediate, *i.e.* the Ruthena-cyclobutane, as prerequisite activation or whether the phosphine ligand may be expelled by the approaching double bond.

7.3.4. ^{19}F -NMR kinetic analysis of α -vinyl BODIPY (**1**) and α -styryl BODIPY (**3**) formation

The reaction of compound (**2**) (~ 12.0 mM) with freshly distilled styrene (~ 1.3 M) was monitored in CDCl_3 via ^{19}F -NMR for quantification (scheme A1).



Scheme A1: Reaction of (**2**) with styrene and according NMR spectra.

Compared to fluorescence measurements, the acquisition in NMR studies requires more time per spectra (^{19}F : 3.90 min, fluorescence: 0.25 min). For ^{19}F -NMR experiments, the reaction rate had to be reduced diminishing reaction progress during data recording. Different rates were achieved by changed reaction compound ratios of (**2**) and styrene (^{19}F : 1:100, fluorescence 1: ~ 1000). In NMR experiments this ratio could be estimated by comparison of ^1H -NMR signals of carbene-H of (**2**) at 21.70 ppm and the doublet of doublets from styrene at 6.86 ppm (figure A50).

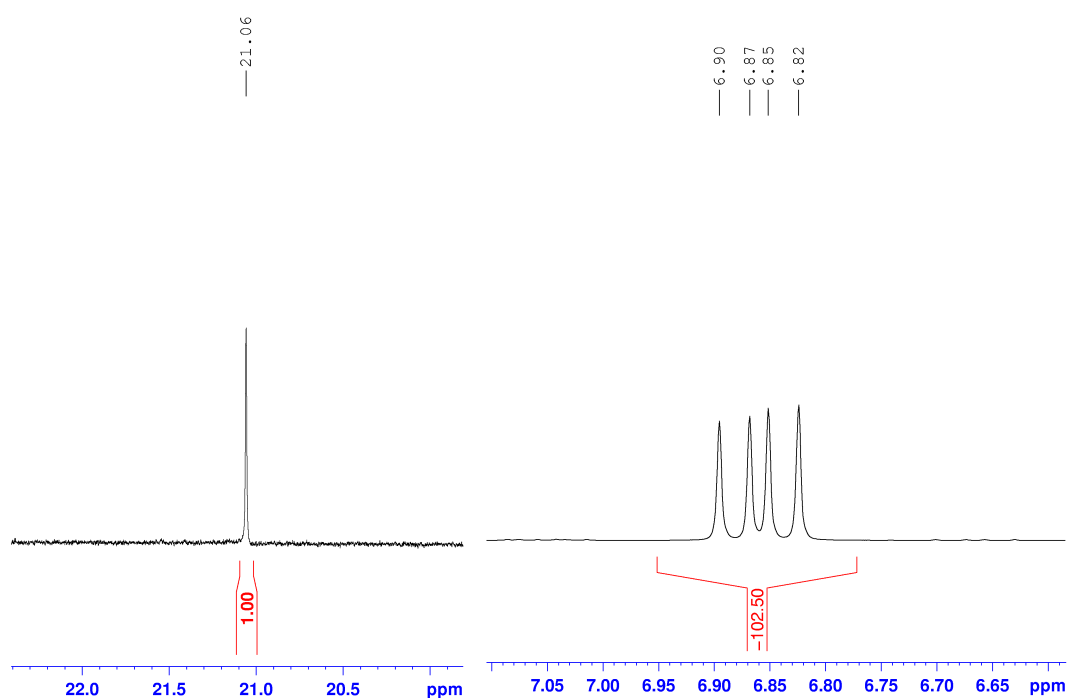


Figure A50: The ratio of starting compounds was estimated by integration of carbene-H of compound (**2**) and doublet of doublets from styrene. The concentration of styrene was about 100 times higher as compound (**2**).

Furthermore, the scan parameters (number of scans and dummy scans) of the single spectra were optimized to achieve a better signal-to-noise ratio. Subsequent NMR spectra enabled kinetic data extraction (Bruker Dynamics Center V2.2.4). The data revealed similar tendency as the fluorescence measurements (figure A51).

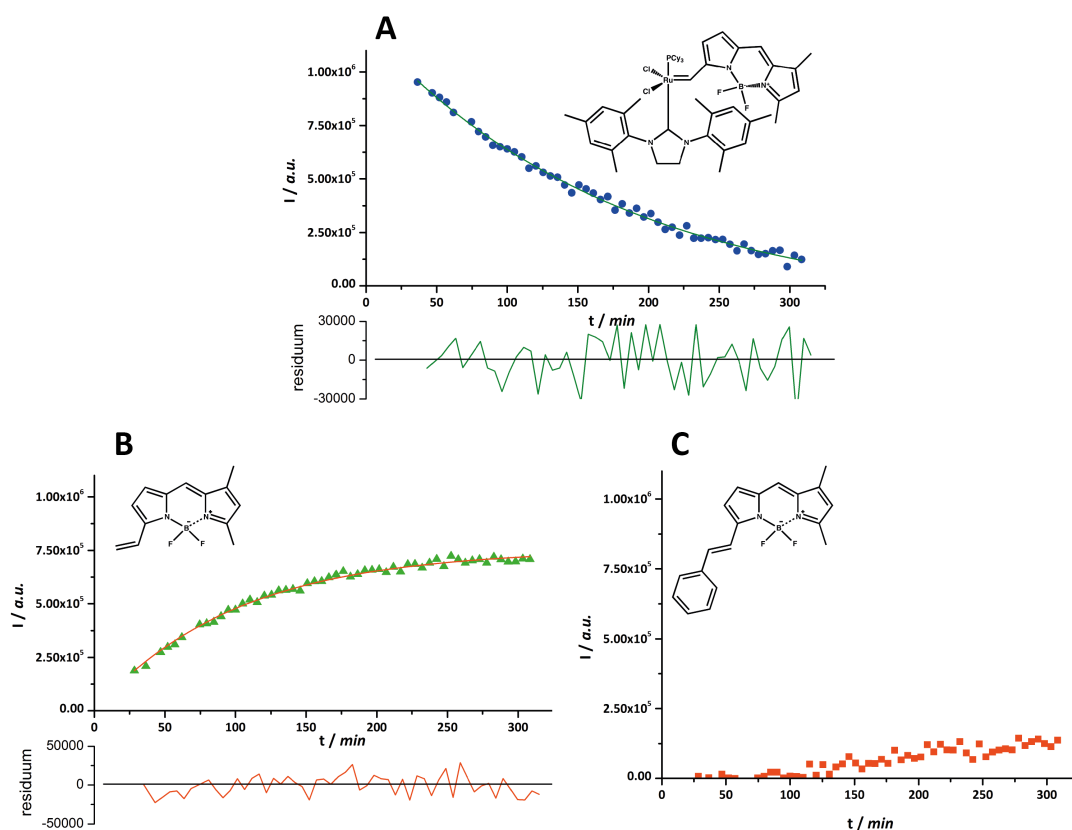


Figure A51: ^{19}F -NMR kinetics extracted out of recorded spectra. **A**: decomposition of (2), $k_1 = 5.55 * 10^{-3} \text{ min}^{-1}$; **B**: formation of (1), $k_1 = 1.00 * 10^{-2} \text{ min}^{-1}$; **C**: formation of (3), no fit was possible because of widely noisy data in spectra.

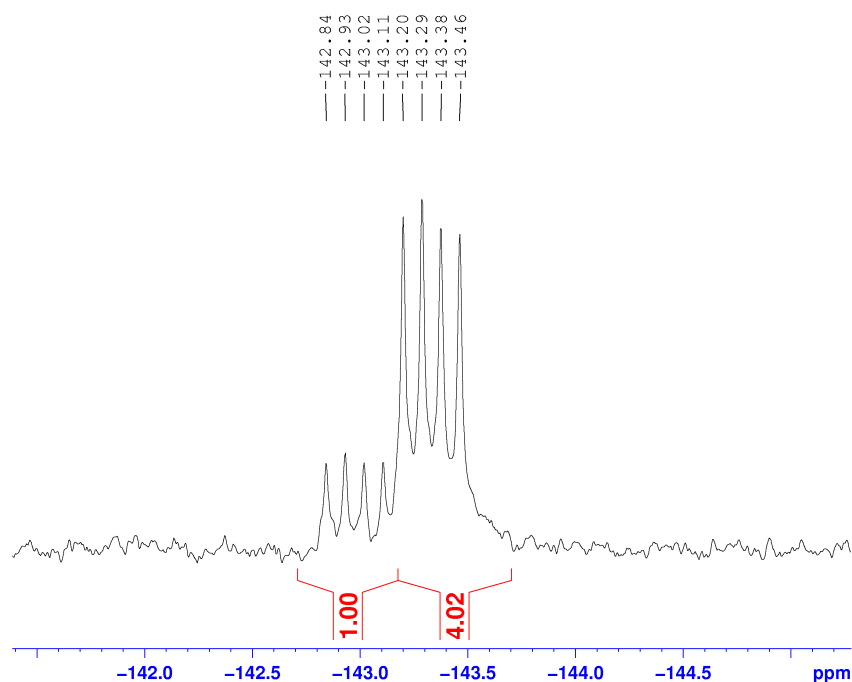


Figure A52: Integration of the two formed products out of reaction showed in scheme A1. In these spectra, the product ratio could be estimated by integration of the two product signals.

Furthermore, the product ratio was estimated after complete transformation (figure A52). The yield of α -vinyl BODIPY (**1**) was four times higher compared to α -styryl BODIPY (**3**).

7.3.5. General Experimental

Chemicals and solvents

All chemicals and solvents were purchased from various suppliers and directly used without further purification (Sigma-Aldrich, Acros Organics, Alfa-Aesar, Apollo Scientific, TCI). Solvents for spectroscopy investigations were used in HPLC or spectroscopic grade. Anhydrous solvents were prepared under literature-known procedures^[256,257].

Analytical instruments and measurement techniques

NMR-spectra:

NMR spectra were recorded in deuterated solvents as noted in experimental procedures using a Bruker Avance 400 (400 MHz) and Bruker Avance 500 (500 MHz) spectrometer according (nucleus frequency see table A14). ¹³C NMR of compound (**1**) was measured with a Bruker Avance 500 at 263 K preventing decomposition during NMR experiment.

table A14: NMR nuclei and correlated frequency.

Measured nucleus	Frequency / MHz
¹ H	400.0
¹³ C	100.0 / 125.0
¹⁹ F	376.5
³¹ P	162.0

Chemical shifts were listed in parts per million (ppm) according to literature known deuterated solvent residual peaks^[258,259]. Coupling constants (*J*) were specified in Hz. Fluorine and phosphorous spectra were calibrated using an internal, instrument-specific calibration factor of +179.91 for ¹⁹F and -111.43 for ³¹P, estimated with appropriate standards.

Crystal structures:

Crystal structures were measured at the Institute of Inorganic Chemistry, Saarland University (Dr. V. Huch) using X8 ApexII X-ray diffractometer. Crystallographic data for the structure have been deposited with the Cambridge Crystallographic Data Centre, CCDC, 12 Union Road, Cambridge CB21EZ, UK. Copies of the data can be obtained free of charge on quoting the depository numbers CCDC 1028352-1028354.

UV-Vis and fluorescence spectra, kinetic data

All spectra were recorded in Hellma quartz cuvettes (3 ml content, 1 cm layer thickness, Hellma Analytics 117.11-FQS). UV-Vis spectra were recorded in a Jasco Spectrophotometer V-650 spectrometer, fluorescence spectra in a Jasco Spectrofluorometer FP-6500. The concentrations of all solutions were in the μ molar range.

Kinetic measurements were established using self-manufactured, lockable quartz cuvettes. For the simultaneous measurement of absorption and emission spectroscopy, two identical lockable cuvettes were filled at the same time with identical compositions. Emissive data were recorded over a period of 10 h every ten minutes using front face excitation in a 30° angle. This detection geometry was chosen to suppress reabsorption effects during reaction monitoring due to the strong coloration by **(2)**. The intensity progress at the wavelength of the emission maximum was used for kinetic data analysis. In the case of overlapping emission bands, *e.g.* see the emission spectra of **(1)** and **(3)** in figure 20 A, the signal intensity of the long-wavelength product was corrected for the contribution from the intensity of the more blue-shifted species. The similar rate constants for the formation of **(3)** in the three analyzed reactions confirmed the validity of this procedure. Kinetic data were fitted

using exponential function (Origin Pro 8.6G, Origin Labs) according to the described kinetic model (Appendix 7.3.3).

Fluorescence lifetime measurement

Fluorescence lifetime measurements were conducted using a home-built TCSPC setup including a time-correlated single photon counting module (PicoHarp 300, PicoQuant). Excitation was established using a pulsed diode laser (LDH-P-C-470B 470 nm, Picoquant) containing a pulse width of 60-120 ps or a fiber laser (FemtoFiber pro TVIS, Toptica). Emission filters with a transmission range of 525/50, 546/20, 590/70 and 585/50 nm (center wavelength λ / transmission band $\Delta\lambda$; all AHF Analysentechnik) were employed, with respect to the dye's fluorescence signal. A single-photon avalanche device was used (PDM 100ct SPAD, Micron Photo Devices) as detector.

Microscopy instrumentation

The single-molecule pictures were generated using fluorescence lifetime imaging. The setup components and picture recording specifications are listed in table A15.

table A15: *Instrumentation for FLIM single-molecule measurement.*

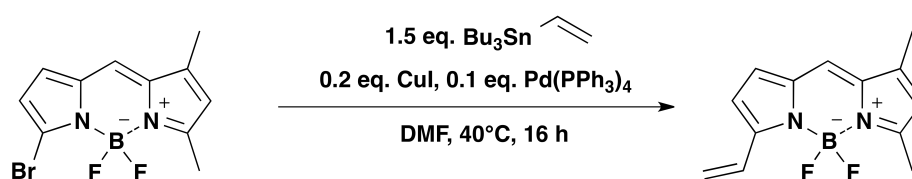
	green channel	orange channel
<i>excitation</i>		
laser	Toptica FemtoFiber pro TVIS	Toptica FemtoFiber pro TVIS
wavelength	500 nm	550 nm
power	0.68 kW*cm ⁻²	1.41 kW*cm ⁻²
puls frequency	80 MHz	80 MHz
excitation cleanup filter	500/10	546/20
<i>emission</i>		
dichroitic mirror	F68-544HC Triple Line (AHF Analysentechnik)	
filter	525/50 (AHF Analysentechnik)	585/50 (AHF Analysentechnik)
detector	Perkin Elmer SPCM-AQR-14	
<i>hardware</i>		
microscope	Zeiss Axiovert 200	
objectiv	Zeiss α Plan Fluor 100x / 1.45 oil	
TCSPC-system	PicoQuant PicoHarp 300	
piezostage	PI E710.4CL	
laser driver	PicoQuant PDL808	
<i>picture</i>		
aquisition	PicoQuant Symphotime 64 Version	
size	8 μ m x 8 μ m	
pixel	256x256	
pixel dwell time	4.0 ms	

It should be mentioned that no integratable data were obtained from single-molecule FLIM which were not known before from the ensemble.

7.3.6. Synthetic procedures and characterization data

All oxygen and moisture sensitive reactions were carried out under inert gas atmosphere. Glassware was oven-dried and used with Schlenk-technique methods. Reaction progress was controlled using Silica on TLC PET-foils with a layer thickness of 0.25 mm (pore size: 60 Å, Fluka Analytics). Compound screening was done by general column chromatography using silica gel, pore size of 0.040 – 0.063 mm as technical grade (Fluka - Analytics).

Synthesis of 3-Vinyl-5,7-dimethyl-4,4'-difluoro-bora-3a,4a-diaza-(s)-indacene - α -Vinyl-BODIPY (1)



1.00 mmol (300.00 mg) 3-Brom-5,7-dimethyl-4,4'-difluoro-bora-3a,4a-diaza-(s)-indacene is dissolved in 20 ml dimethylformamide. 0.20 mmol (19.05 mg) CuI and 0.10 mmol (115.56 mg) tetrakis(triphenylphosphin)palladium(0) are added. After five minutes, 1.50 mmol (475.65 mg) tributyl(vinyl)tin were adjoined. After stirring for 16 h, a dark red solution was obtained. Removing solvent, the mixture was separated by column chromatography using silica gel, and dichloromethane – petrol ether (1:1) and toluene – petrol ether (1:1) as eluent. A red compound was received (209.00 mg, 0.85 mmol, 85%).

$^1\text{H-NMR}$ (400.0 MHz, CDCl_3 , 298 K):

δ = 7.38 (dd, J = 8.0 Hz, 16.0 Hz, 1 H), 7.24 (s, 1 H), 7.08 (d, J = 4.0 Hz, 1 H), 6.88 (d, J = 4.0 Hz, 1 H), 6.29 (s, 1H), 6.11 (d, J = 16.0 Hz, 1H), 5.73 (d, J = 8.0 Hz, 1H), 2.74 (s, 3 H), 2.42 (s, 3H) ppm.

$^{13}\text{C-NMR}$ (125.0 MHz, CDCl_3 , 263 K): δ = 160.2, 152.5, 143.5, 135.2, 133.9, 128.9, 127.7, 123.0, 120.6, 120.3, 114.2, 14.9, 11.2 ppm.

$^{19}\text{F-NMR}$ (376.5 MHz, CDCl_3 , 298 K): δ = -144.00 (q, J = 30.1 Hz, 2 F) ppm.

Crystal structure: CCDC 1028352

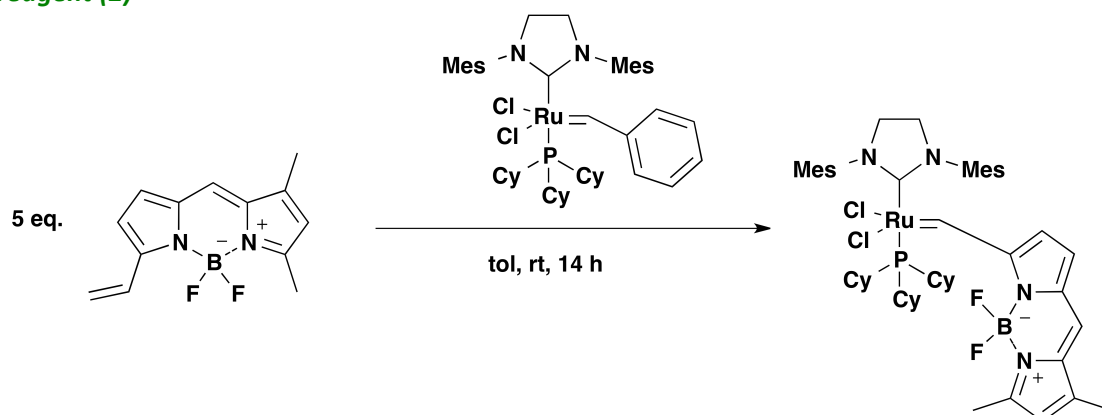
HRMS (ESI)

chemical formula	calculated exact mass [Da]	measured accurate mass [Da]	Error [ppm]
$\text{C}_{13}^{10} \text{H}_{14} \text{BF}_2 \text{N}_2^+$	246.125441	246.1248	-2.6
$\text{C}_{13}^{11} \text{H}_{14} \text{BF}_2 \text{N}_2^+$	247.121809	247.12117	-2.6

Absorbance and Emission: $\lambda_{\text{abs}} = 527 \text{ nm}$, $\lambda_{\text{em}} = 536 \text{ nm}$ (toluene)

Lifetime: $\tau_{\text{fl}} = 5.1 \text{ ns}$ (CHCl_3)

Synthesis of (3-Vinyl-5,7-dimethyl-4,4'-difluoro-bora-3a,4a-diaza-(s)-indacenyliден)[1,3-bis(2,4,6-trimethylphenyl)-2-imidazolidinyliden]dichloro(tricyclohexylphosphin)ruthenium – BODIPYlidene Ru reagent (2)



Benzyliden[1,3-bis(2,4,6-trimethylphenyl)-2-imidazolidinyliden]dichloro(tricyclohexylphosphin) ruthenium (1.0 mmol, 849.0 mg) is dissolved in 50 ml of toluene. 5.0 mmol (1230.3 mg) 3-vinyl-5,7-dimethyl-4,4'-difluoro-bora-3a,4a-diaza-(s)-indacene were added and reaction mixture is stirred for 14 h. Every half hour, solvent is removed and fresh, dry toluene is added. After last solvent removal, column chromatography at 0°C using petrol ether – ethyl acetate (2:1) delivers compound (**3**) (598.4 mg, 0.6 mmol, 60 %).

¹H-NMR (400.0 MHz, CDCl₃, 298 K):

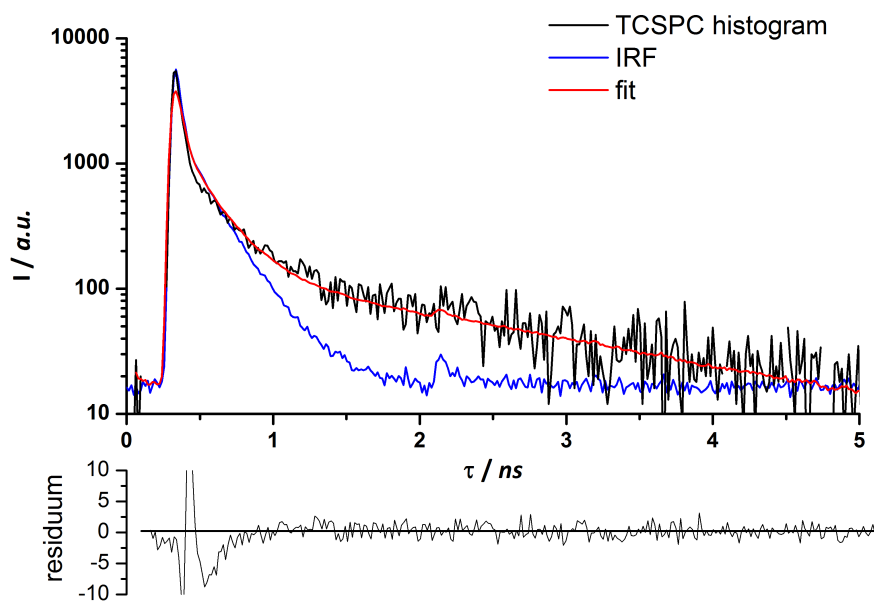
δ = 21.7 (s, 1 H), 8.48 (s, 1 H), 6.95-6.92 (m, 4 H), 6.82 (s, 1 H), 6.30 (s, 1H), 6.16 (s, 1 H), 5.57 (s, 1 H), 3.37 (s, 4 H), 2.87 (s, 3 H), 2.84 (s, 3 H), 2.67 (s, 3 H), 2.47 (s, 1 H), 2.21 (s, 3 H), 2.00-1.50 (s, 39 H) ppm.

¹⁹F-NMR (376.5 MHz, CDCl₃, 298 K): δ = -134.55 (dq, 1 F, ¹J_{F-F} = 102 Hz, ²J_{19F-11B} = 34 Hz), -140.73 (dq, 1 F, ¹J_{F-F} = 102 Hz, ²J_{19F-11B} = 30 Hz) ppm.

³¹P-NMR (162.0 MHz, CDCl₃, 298 K): δ = 32.34 (s) ppm.

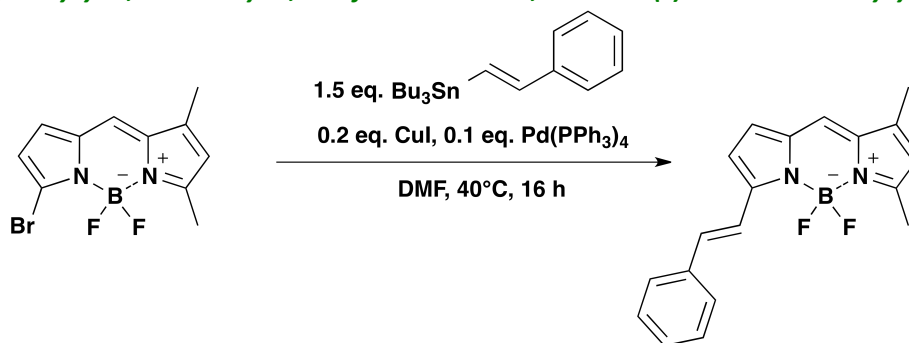
Crystal structure: CCDC 1028353

Absorbance and Emission: λ_{abs} = 612 nm, λ_{em} = -/- nm (toluene)

Lifetime: *biexponential reconvolution fit*

Fit results:

$\tau_1 = 0.030$ ns	$A1 = 8914.09$ kCnts	compound (2)
$\tau_2 = 3.010$ ns	$A2 = 0.1265$ kCnts	decomposition of (2)

Synthesis of 3-Styryl-5,7-dimethyl-4,4'-difluoro-bora-3a,4a-diaza-(s)-indacene - α -styryl-BODIPY (3)

3-Styryl-5,7-dimethyl-4,4'-difluoro-bora-3a,4a-diaza-(s)-indacene was synthesized analog to compound (1) using *trans*-tributyl(2-phenylethenyl)stannane as organo-tin reagent. Isolation of 225.5 mg (0.70 mmol, 70%) of a red crystalline solid was possible.

¹H-NMR (400.0 MHz, CDCl₃, 298 K):

δ = 7.65-7.58 (m, 3 H), 7.39-7.28 (m, 4 H), 7.05 (s, 1 H), 6.94 (d, J = 4.0 Hz, 1 H), 6.85 (d, J = 4.0 Hz, 1 H), 6.21 (s, 1 H), 2.60 (s, 3 H), 2.26 (s, 3H) ppm.

¹³C-NMR (100.0 MHz, CDCl₃, 298 K): δ = 162.9, 159.3, 153.4, 142.7, 136.5, 135.6, 135.3, 134.8, 129.0, 128.8, 128.2, 125.3, 122.0, 120.1, 119.3, 115.2, 110.0, 15.0, 11.3 ppm.

¹⁹F-NMR (376.5 MHz, CDCl₃, 298 K): δ = -143.63 (q, J = 33.9 Hz, 2 F) ppm.

Crystal structure: CCDC 1028354

HRMS (ESI)

chemical formula	calculated exact mass [Da]	measured accurate mass [Da]	Error [ppm]
C ₁₉ H ₁₈ ¹⁰ BF ₂ N ₂ ⁺	322.156741	322.15633	-1.3
C ₁₉ H ₁₈ ¹¹ BF ₂ N ₂ ⁺	323.153109	323.15263	-1.5

Absorbance and Emission: λ_{abs} = 563 nm, λ_{em} = 572 nm (DCM)

Lifetime: τ_{fl} = 4.9 ns (CHCl₃)

7.3.7. Spectra

NMR-spectra

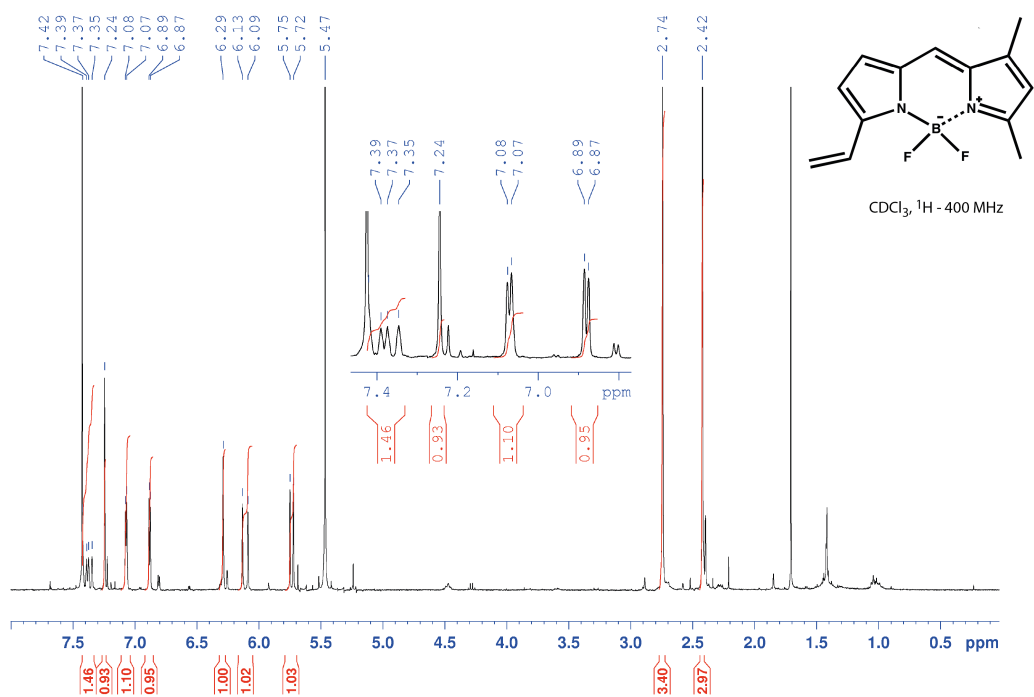
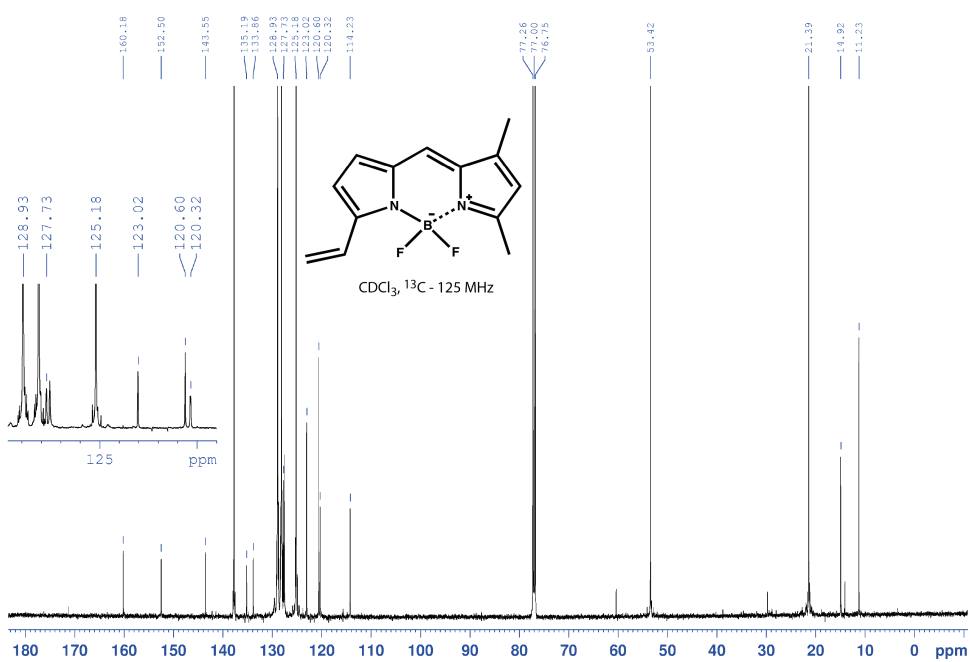
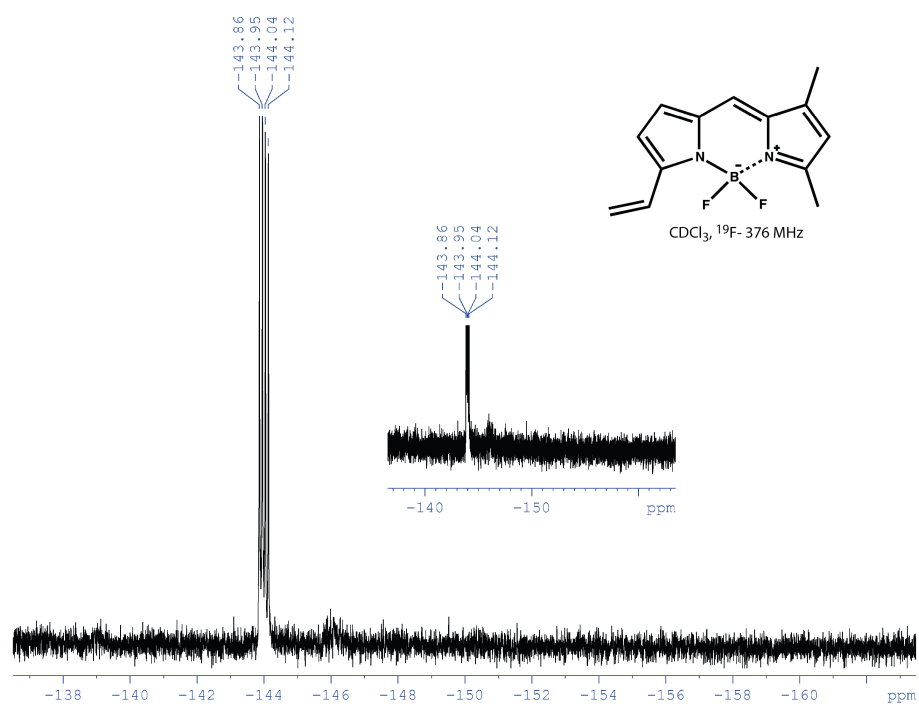
3-Vinyl-5,7-dimethyl-4,4'-difluoro-bora-3a,4a-diaza-(s)-indacene - α -Vinyl-BODIPY (**1**)Figure A53: $^1\text{H-NMR}$ (**1**).Figure A54: $^{13}\text{C-NMR}$ (**1**).

Figure A55: ^{19}F -NMR (1).

(3-Vinyl-5,7-dimethyl-4,4'-difluoro-bora-3a,4a-diaza-(s)-indacenylyden)[1,3-bis(2,4,6-trimethylphenyl)-2-imidazolidinyliden]dichloro(tricyclohexylphosphin)ruthenium – BODIPYlidene Ru catalyst (2)

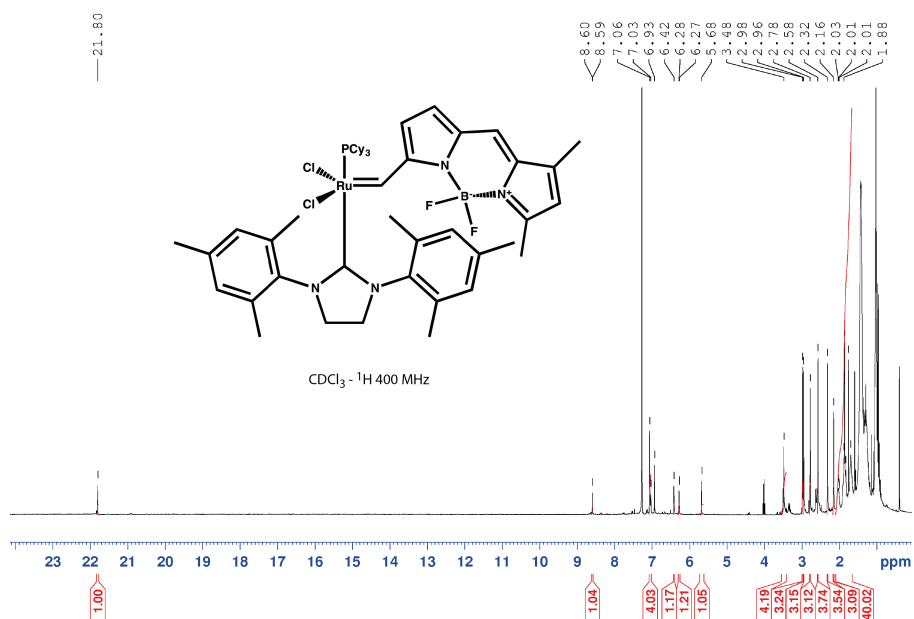
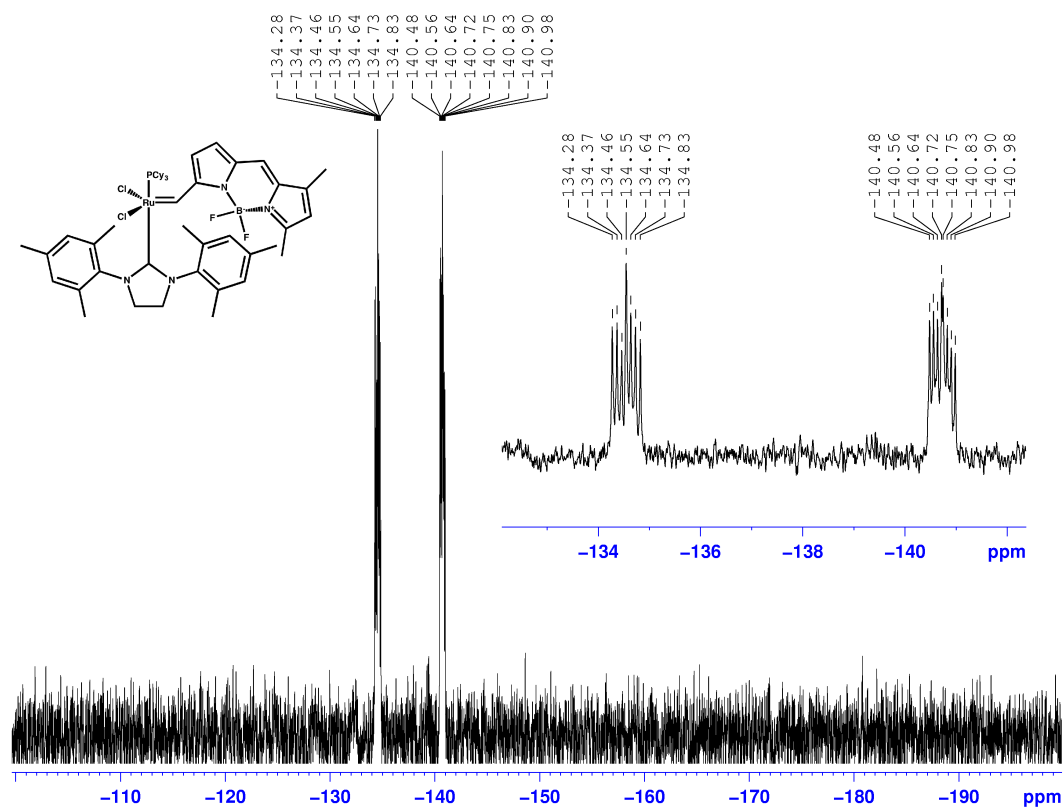
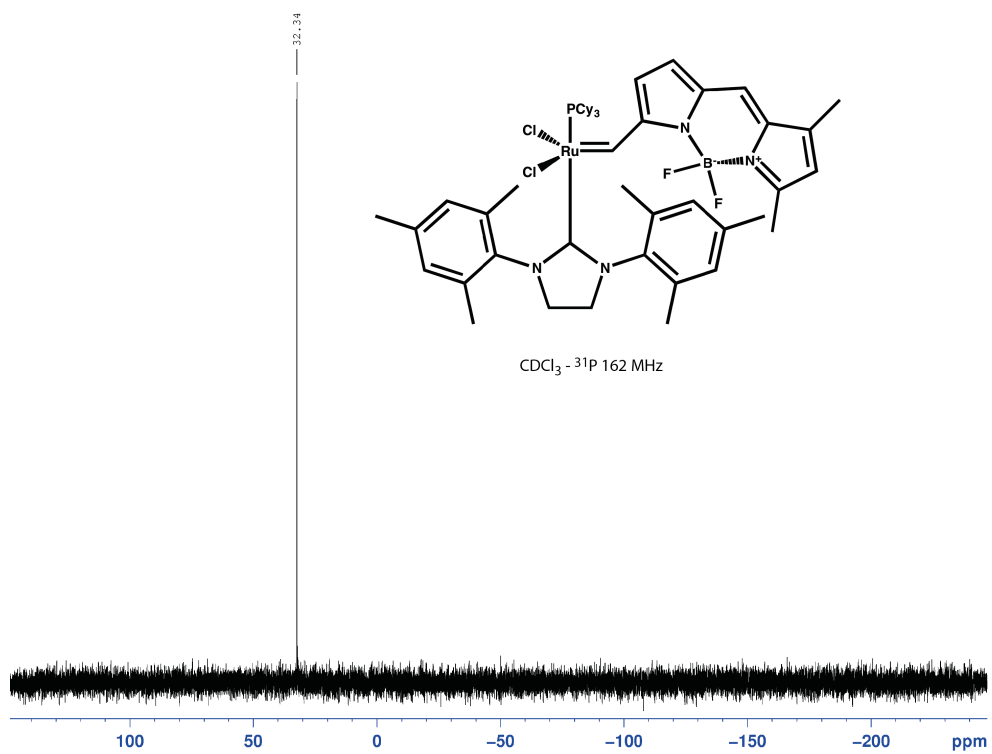
Figure A56: ^1H -NMR (2).

Figure A57: ^{19}F -NMR (2).Figure A58: ^{31}P -NMR (2).

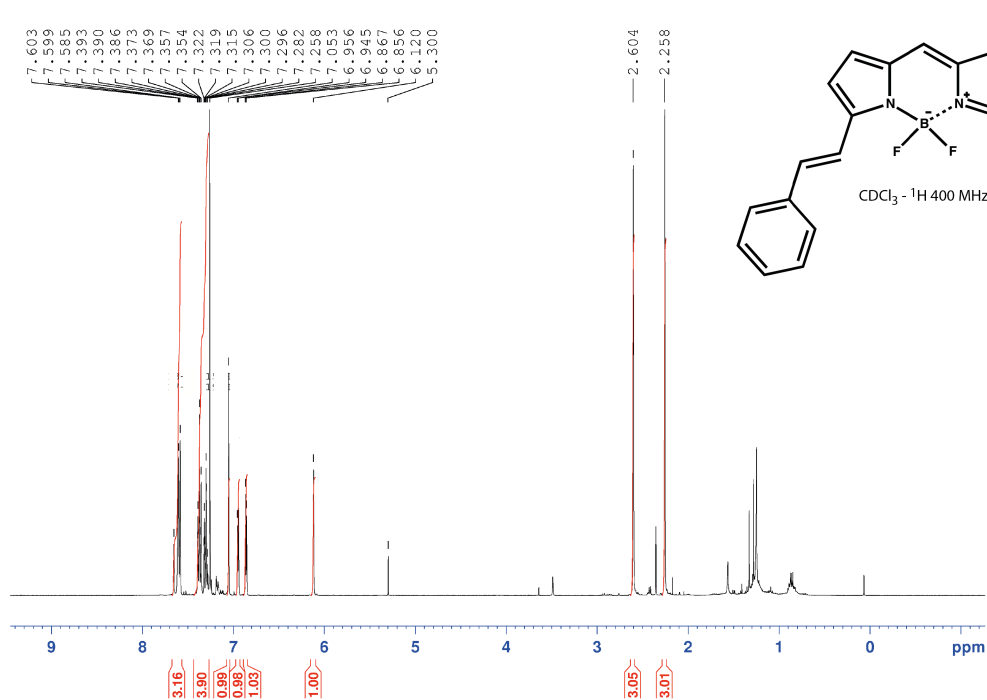
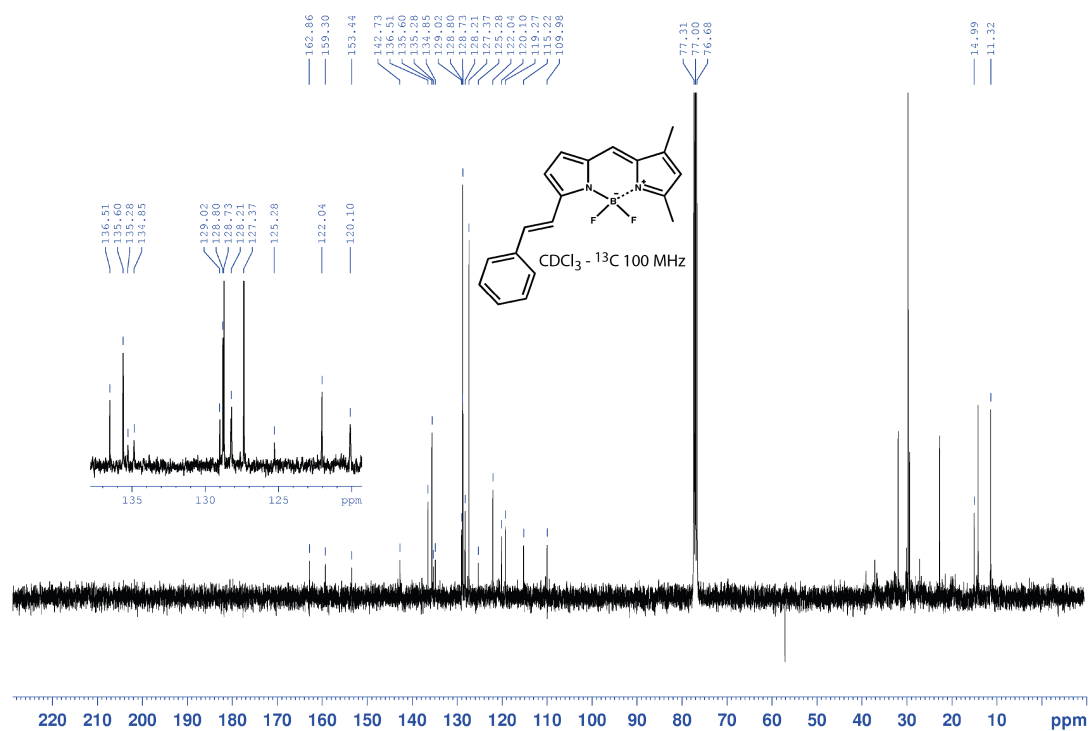
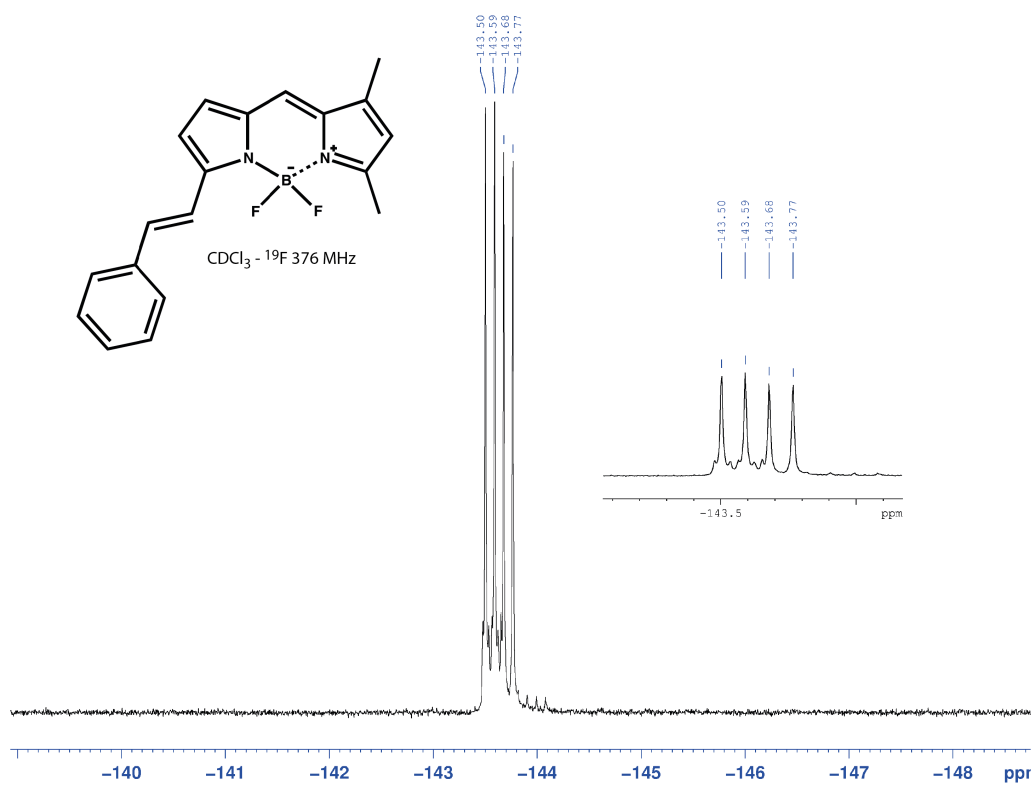
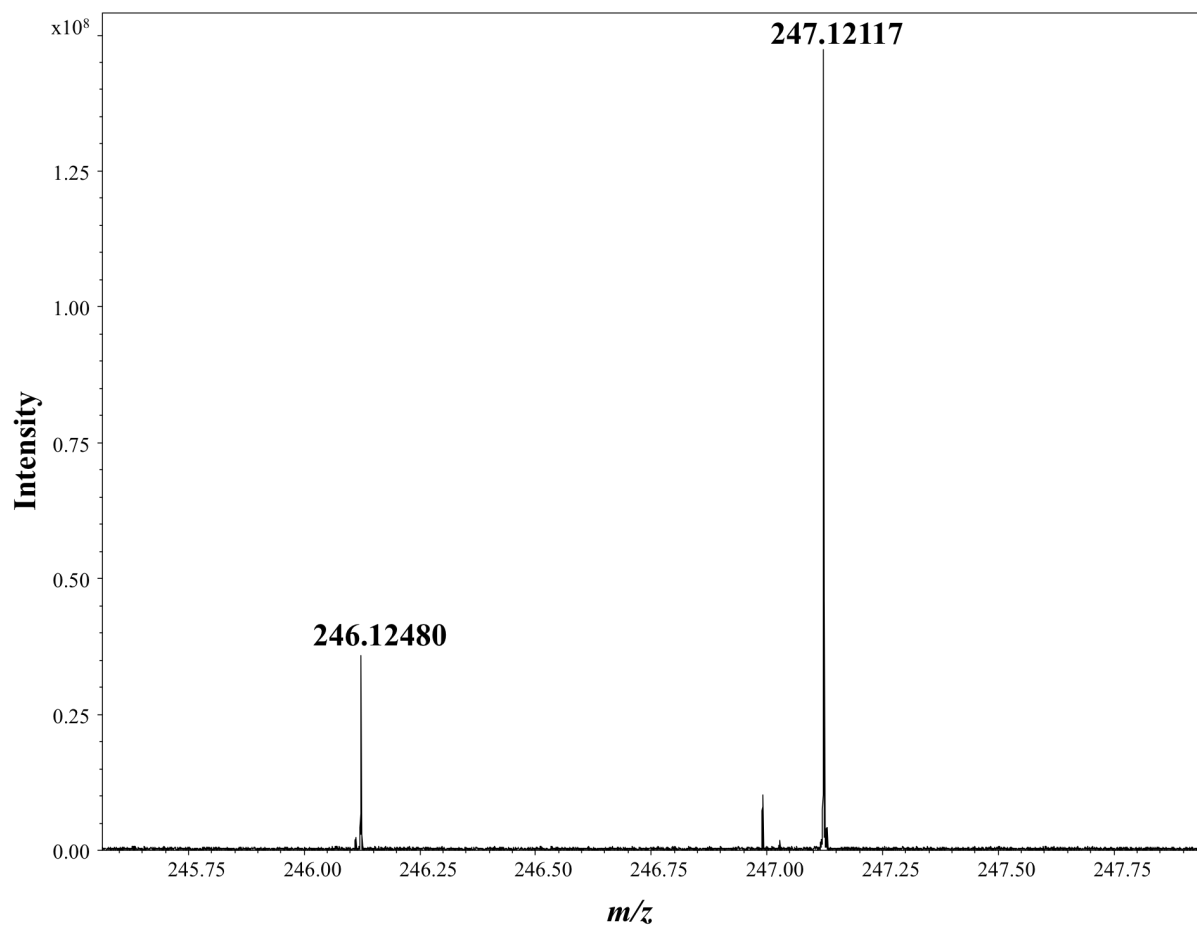
3-Styryl-5,7-dimethyl-4,4'-difluoro-bora-3a,4a-diaza-(s)-indacene - α -styryl-BODIPY (**3**)Figure A59: $^1\text{H-NMR}$ (**3**).Figure A60: $^{13}\text{C-NMR}$ (**3**).

Figure A61: ^{19}F -NMR (**3**).

Mass spectra

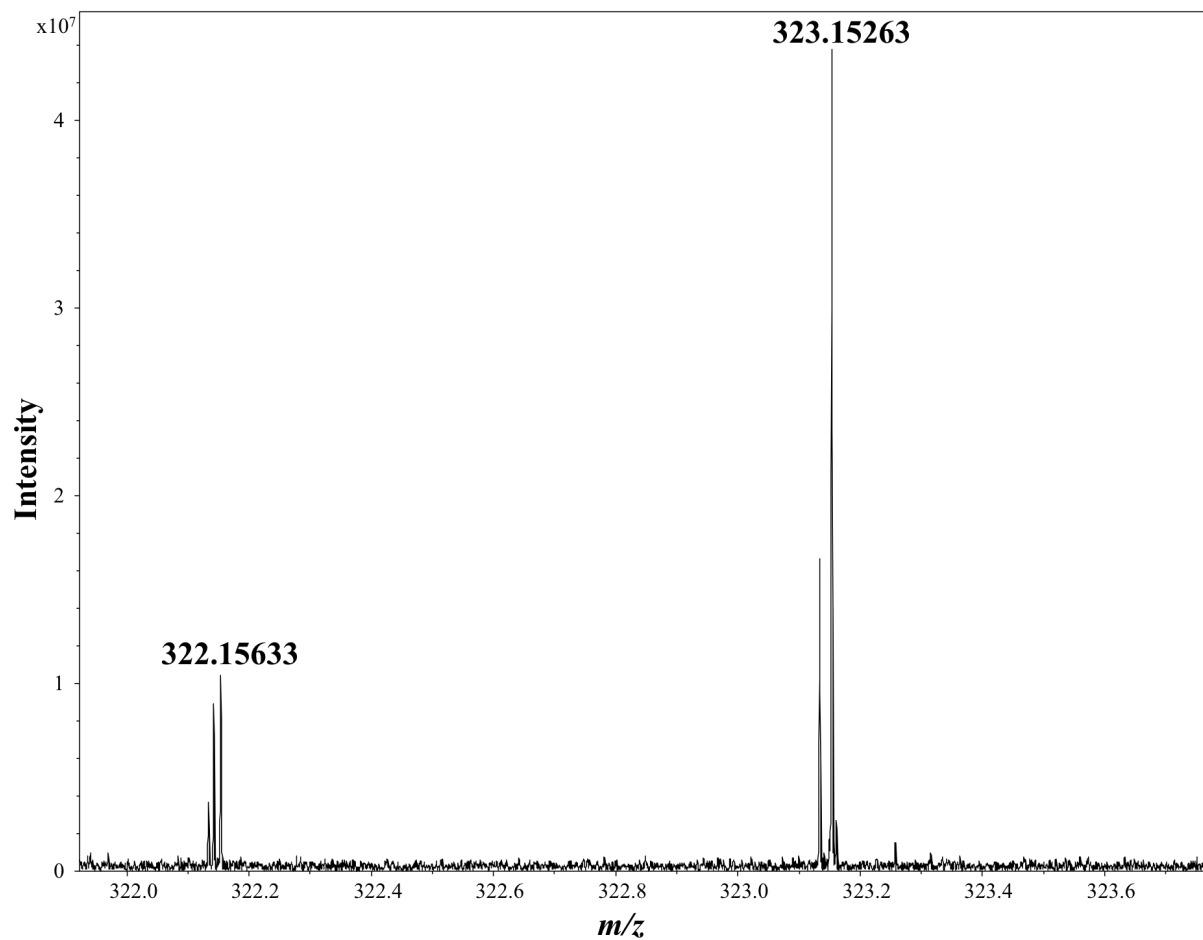
3-Vinyl-5,7-dimethyl-4,4'-difluoro-bora-3a,4a-diaza-(s)-indacene - α -Vinyl-BODIPY (**1**)

Figure A62: mass spectra (**1**).



3-Styryl-5,7-dimethyl-4,4'-difluoro-bora-3a,4a-diaza-(s)-indacene - α -styryl-BODIPY (3)

Figure A63: mass spectra (3).



8. Literature

- [1] A. Rybina, C. Lang, M. Wirtz, K. Größmayer, A. Kurz, F. Maier, A. Schmitt, O. Trapp, G. Jung, D.-P. Hertzen, *Angew. Chem., Int. Ed. Engl.* **2013**, *52*, 6322–6325.
- [2] G. De Cremer, M. B. J. Roeffaers, E. Bartholomeeusen, K. Lin, P. Dedecker, P. P. Pescarmona, P. A. Jacobs, D. E. De Vos, J. Hofkens, B. F. Sels, *Angew. Chem. Int. Ed. Engl.* **2010**, *49*, 908–911.
- [3] T. Cordes, S. A. Blum, *Nat. Chem.* **2013**, *5*, 993–999.
- [4] M. Wirtz, A. Grüter, P. Rebmann, T. Dier, D. A. Volmer, V. Huch, G. Jung, *Chem. Commun.* **2014**, *50*, 12694–12697.
Reproduced by permission of The Royal Society of Chemistry
- [5] M. Wirtz, A. Grüter, F. Heib, V. Huch, J. Zapp, M. Schmitt, D.-P. Hertzen, G. Jung, *submitted* **2015**.
- [6] C. Amatore, A. Jutand, *Acc. Chem. Res.* **2000**, *33*, 314–321.
- [7] E. Jiménez-Núñez, A. M. Echavarren, *Chem. Rev.* **2008**, *108*, 3326–3350.
- [8] D. G. Blackmond, *Angew. Chem. Int. Ed. Engl.* **2005**, *44*, 4302–4320.
- [9] L. S. Santos, *European J. Org. Chem.* **2008**, *2008*, 235–253.
- [10] M. R. Chierotti, R. Gobetto, *Eur. J. Inorg. Chem.* **2009**, *2009*, 2581–2597.
- [11] Y. Wang, C. Wöll, *Surf. Sci.* **2009**, *603*, 1589–1599.
- [12] P. Schwille, J. Bieschke, F. Oehlenschläger, *Biophys. Chem.* **1997**, *66*, 211–228.
- [13] P. Hervés, M. Pérez-Lorenzo, L. M. Liz-Marzán, J. Dzubiella, Y. Lu, M. Ballauff, *Chem. Soc. Rev.* **2012**, *41*, 5577–5587.
- [14] S. R. Crouch, T. F. Cullen, A. Scheeline, E. S. Kirkor, *Anal. Chem.* **1998**, *70*, 53–106.
- [15] W. Dang, N.-H. Sung, *Polym. Eng. Sci.* **1994**, *34*, 707–715.
- [16] J. Zielonka, J. Joseph, A. Sikora, B. Kalyanaraman, *Methods Enzymol.* **2013**, *526*, 145–157.
- [17] A. Miki, S. Ye, M. Osawa, *Chem. Commun.* **2002**, 1500–1501.

-
- [18] J. A. Haber, N. S. Lewis, *J. Phys. Chem. B* **2002**, *106*, 3639–3656.
- [19] J. Mijović, S. Andjelić, J. M. Kenny, *Polym. Adv. Technol.* **1996**, *7*, 1–16.
- [20] K. Grabow, U. Bentrup, *ACS Catal.* **2014**, *4*, 2153–2164.
- [21] B. M. Weckhuysen, *Chem. Commun.* **2002**, 97–110.
- [22] M. L. McKelvy, T. R. Britt, B. L. Davis, J. K. Gillie, F. B. Graves, L. A. Lentz, *Anal. Chem.* **1998**, *70*, 119–178.
- [23] M. S. Sanford, J. a Love, R. H. Grubbs, *J. Am. Chem. Soc.* **2001**, *123*, 6543–6554.
- [24] P. Schwab, R. H. Grubbs, J. W. Ziller, *J. Am. Chem. Soc.* **1996**, *118*, 100–110.
- [25] A. G. Wenzel, R. H. Grubbs, *J. Am. Chem. Soc.* **2006**, *128*, 16048–16049.
- [26] F. Benito-Lopez, W. Verboom, M. Kakuta, J. H. G. E. Gardeniers, R. J. M. Egberink, E. R. Oosterbroek, A. van den Berg, D. N. Reinhoudt, *Chem. Commun.* **2005**, 2857–2859.
- [27] H. Lu, M. Gratzl, *Anal. Chem.* **2000**, *72*, 1569–1575.
- [28] L. Tröger, N. Hilbrandt, M. Epple, *Le J. Phys. IV* **1997**, *7*, C2–323–C2–324.
- [29] N. Esfandiari, Y. Wang, T. McIntire, S. Blum, *Organometallics* **2011**, 2901–2907.
- [30] S.-G. Lim, S. A. Blum, *Organometallics* **2009**, *28*, 4643–4645.
- [31] M. Heilemann, *J. Biotechnol.* **2010**, *149*, 243–251.
- [32] T. Christ, F. Kulzer, P. Bordat, T. Basché, *Angew. Chemie Int. Ed.* **2001**, *40*, 4192–4195.
- [33] I. L. C. Buurmans, B. M. Weckhuysen, *Nat. Chem.* **2012**, *4*, 873–886.
- [34] N. M. Esfandiari, S. A. Blum, *J. Am. Chem. Soc.* **2011**, *133*, 18145–18147.
- [35] M. Schwering, A. Kiel, A. Kurz, K. Lympelopoulos, A. Sprödefeld, R. Krämer, D.-P. Hertel, *Angew. Chem. Int. Ed. Engl.* **2011**, *50*, 2940–2945.
- [36] M. B. J. Roeffaers, B. F. Sels, H. Uji-i, F. C. De Schryver, P. A. Jacobs, D. E. De Vos, J. Hofkens, *Nature* **2006**, *439*, 572–575.
- [37] E. Haustein, P. Schwille, *Curr. Opin. Struct. Biol.* **2004**, *14*, 531–540.
- [38] B. Schuler, *Chemphyschem* **2005**, *6*, 1206–1220.

- [39] A. E. Speers, B. F. Cravatt, *Chem. Biol.* **2004**, *11*, 535–546.
- [40] M. B. J. Roeffaers, G. De Cremer, H. Uji-i, B. Muls, B. F. Sels, P. A. Jacobs, F. C. De Schryver, D. E. De Vos, J. Hofkens, *Proc. Natl. Acad. Sci. U. S. A.* **2007**, *104*, 12603–12609.
- [41] B. Z. Shang, J.-W. Chu, *ACS Catal.* **2014**, *4*, 2216–2225.
- [42] C. R. Pudney, R. S. K. Lane, A. J. Fielding, S. W. Magennis, S. Hay, N. S. Scrutton, *J. Am. Chem. Soc.* **2013**, *135*, 3855–3864.
- [43] S. Lata, M. Gavutis, R. Tampé, J. Piehler, *J. Am. Chem. Soc.* **2006**, *128*, 2365–2372.
- [44] M. Rashidian, J. K. Dozier, M. D. Distefano, *Bioconjug. Chem.* **2013**, *24*, 1277–1294.
- [45] K. Lymperopoulos, A. Kiel, A. Seefeld, K. Stöhr, D.-P. Hertzen, *ChemPhysChem* **2010**, *11*, 43–53.
- [46] M. A. Fourati, C. Pellerin, C. G. Bazuin, R. E. Prud'homme, *Polymer (Guildf)*. **2013**, *54*, 730–736.
- [47] A. Cyphersmith, A. Maksov, R. Hassey-Paradise, K. D. McCarthy, M. D. Barnes, *J. Phys. Chem. Lett.* **2011**, *2*, 661–665.
- [48] M. Schmitt, R. Hempelmann, S. Ingebrandt, W. M. Munief, D. Durneata, K. Groß, F. Heib, *Int. J. Adhes. Adhes.* **2014**, *55*, 123–131.
- [49] T. Ha, P. Tinnefeld, *Annu. Rev. Phys. Chem.* **2012**, *63*, 595–617.
- [50] P. S. Dittrich, P. Schwille, *Appl. Phys. B Lasers Opt.* **2001**, *73*, 829.
- [51] M. F. Juette, D. S. Terry, M. R. Wasserman, Z. Zhou, R. B. Altman, Q. Zheng, S. C. Blanchard, *Curr. Opin. Chem. Biol.* **2014**, *20C*, 103–111.
- [52] L. D. Lavis, R. T. Raines, *ACS Chem. Biol.* **2014**, *9*, 855–866.
- [53] N. Boens, V. Leen, W. Dehaen, *Chem. Soc. Rev.* **2012**, *41*, 1130–1172.
- [54] A. Loudet, K. Burgess, *Chem. Rev.* **2007**, *107*, 4891–4932.
- [55] G. Ulrich, R. Ziessel, A. Harriman, *Angew. Chem. Int. Ed. Engl.* **2008**, *47*, 1184–1201.
- [56] V. Leen, T. Leemans, N. Boens, W. Dehaen, *European J. Org. Chem.* **2011**, *2011*, 4386–4396.

- [57] V. Leen, V. Z. Gonzalvo, W. M. Deborggraeve, N. Boens, W. Dehaen, *Chem. Commun.* **2010**, 46, 4908–4910.
- [58] V. Leen, E. Braeken, K. Luckermans, C. Jackers, M. Van der Auweraer, N. Boens, W. Dehaen, *Chem. Commun.* **2009**, 4515–4517.
- [59] G. Ulrich, A. Haefele, P. Retailleau, R. Ziessel, *J. Org. Chem.* **2012**, 77, 5036–5048.
- [60] A. Schmitt, Reactive Fluorescent Dye Systems for Single-Molecule Studies, Dissertation, Saarland University, **2009**.
- [61] J. Eid, A. Fehr, J. Gray, K. Luong, J. Lyle, G. Otto, P. Peluso, D. Rank, P. Baybayan, B. Bettman, et al., *Science* **2009**, 323, 133–138.
- [62] M. Tokunaga, K. Kitamura, K. Saito, A. H. Iwane, T. Yanagida, *Biochem. Biophys. Res. Commun.* **1997**, 235, 47–53.
- [63] X. Shen, G. Zhang, D. Zhang, *Org. Lett.* **2012**, 14, 1744–1747.
- [64] D. Xiao, M. M. F. Choi, *Anal. Chem.* **2002**, 74, 863–870.
- [65] Y. He, M. Lu, H. P. Lu, *Phys. Chem. Chem. Phys.* **2013**, 15, 770–775.
- [66] Y. Kurishita, T. Kohira, A. Ojida, I. Hamachi, *J. Am. Chem. Soc.* **2010**, 132, 13290–13299.
- [67] Y. He, Y. Li, S. Mukherjee, Y. Wu, H. Yan, H. P. Lu, *J. Am. Chem. Soc.* **2011**, 133, 14389–14395.
- [68] K. Blank, G. De Cremer, J. Hofkens, *Biotechnol. J.* **2009**, 4, 465–479.
- [69] H. W. Lee, C. H. Heo, D. Sen, H.-O. Byun, I. H. Kwak, G. Yoon, H. M. Kim, *Anal. Chem.* **2014**, 86, 10001–10005.
- [70] L. Chen, W. Sun, J. Li, Z. Liu, Z. Ma, W. Zhang, L. Du, W. Xu, H. Fang, M. Li, *Org. Biomol. Chem.* **2013**, 11, 378–382.
- [71] K. P. F. Janssen, G. De Cremer, R. K. Neely, A. V. Kubarev, J. Van Loon, J. A. Martens, D. E. De Vos, M. B. J. Roeffaers, J. Hofkens, *Chem. Soc. Rev.* **2014**, 43, 990–1006.
- [72] S. N. Goonewardena, P. R. Leroueil, C. Gemborys, P. Tahiliani, S. Emery, J. R. Baker, H. Zong, *Bioorg. Med. Chem. Lett.* **2013**, 23, 2230–2233.
- [73] W. H. Binder, R. Sachsenhofer, *Macromol. Rapid Commun.* **2007**, 28, 15–54.
- [74] O. S. Wolfbeis, *Angew. Chem. Int. Ed. Engl.* **2007**, 46, 2980–2982.

- [75] C. Le Droumaguet, C. Wang, Q. Wang, *Chem. Soc. Rev.* **2010**, 39, 1233 – 1239.
- [76] M. Sawa, T.-L. Hsu, T. Itoh, M. Sugiyama, S. R. Hanson, P. K. Vogt, C.-H. Wong, *Proc. Natl. Acad. Sci.* **2006**, 103, 12371–12376.
- [77] A. T. J. Dirks, J. J. L. M. Cornelissen, R. J. M. Nolte, *Bioconjug. Chem.* **2009**, 20, 1129–1138.
- [78] C. Wang, F. Xie, N. Suthiwangcharoen, J. Sun, Q. Wang, *Sci. China Chem.* **2011**, 55, 125–130.
- [79] T. Vorfalt, K. J. Wannowius, V. Thiel, H. Plenio, *Chemistry* **2010**, 16, 12312–12315.
- [80] S. B. Garber, J. S. Kingsbury, B. L. Gray, A. H. Hoveyda, *J. Am. Chem. Soc.* **2000**, 122, 8168–8179.
- [81] E. Bordes-Richard, E. M. Gaigneaux, A. Löfberg, E. Payen, P. Ruiz, G. De Cremer, E. Bartholomeeusen, P. P. Pescarmona, K. Lin, D. E. De Vos, et al., *Catal. Today* **2010**, 157, 236–242.
- [82] B. Scheinhardt, J. Trzaskowski, M. C. Baier, B. Stempfle, A. Oppermann, D. Wöll, S. Mecking, *Macromolecules* **2013**, 46, 7902–7910.
- [83] J. R. Lakowicz, Springer Science & Business Media B.V., New York, **2006**, p. 954.
- [84] F. Ciruela, K. A. Jacobson, V. Fernández-Dueñas, *ACS Chem. Biol.* **2014**, 9, 1918–1928.
- [85] C.-W. Chang, M. Wu, S. D. Merajver, M.-A. Mycek, *J. Biomed. Opt.* **2009**, 14, 060502.
- [86] A. Miyawaki, *Dev. Cell* **2003**, 4, 295–305.
- [87] K. Truong, M. Ikura, *Curr. Opin. Struct. Biol.* **2001**, 11, 573–578.
- [88] R. Roy, H. Sungchul, H. Taekjip, *Nat. Meth.* **2008**, 5, 507–516.
- [89] Z. Hu, J. Hu, Y. Cui, G. Wang, X. Zhang, K. Uvdal, H.-W. Gao, *J. Mater. Chem. B* **2014**, 2, 4467.
- [90] S. Tyagi, E. A. Lemke, *Methods Cell Biol.* **2013**, 113, 169–187.
- [91] J. Schoch, M. Staudt, A. Samanta, M. Wiessler, A. Jäschke, *Bioconjug. Chem.* **2012**, 23, 1382–1386.
- [92] E. M. Hensle, N. M. Esfandiari, S.-G. Lim, S. A. Blum, *European J. Org. Chem.* **2014**, 3347–3354.

- [93] S. M. Brombosz, A. L. Appleton, A. J. Zappas, U. H. F. Bunz, *Chem. Commun.* **2010**, 46, 1419–1421.
- [94] Z. Liao, E. N. Hooley, L. Chen, S. Stappert, K. Müllen, T. Vosch, *J. Am. Chem. Soc.* **2013**, 135, 19180–19185.
- [95] B. Finkler, C. Spies, M. Vester, F. Walte, K. Omlor, I. Riemann, M. Zimmer, F. Stracke, M. Gerhards, G. Jung, *Photochem. Photobiol. Sci.* **2014**, 13, 548–562.
- [96] C. Spies, B. Finkler, N. Acar, G. Jung, *Phys. Chem. Chem. Phys.* **2013**, 15, 19893–19905.
- [97] C. Spies, S. Shomer, B. Finkler, D. Pines, E. Pines, G. Jung, D. Huppert, *Phys. Chem. Chem. Phys.* **2014**, 16, 9104–9114.
- [98] H. Zollinger, *Color Chemistry - Syntheses, Properties, and Applications of Organic Dyes and Pigments*, Wiley-VCH Verlag GmbH & Co. KGaA, Weinheim, Germany, **2003**.
- [99] A. Rybina, M. Wirtz, D. Brox, R. Krämer, G. Jung, D.-P. Herten, *Toward Single-Molecule Catalysis*, Wiley-VCH Verlag GmbH & Co. KGaA, Weinheim, Germany, **2014**.
- [100] D. D. Nolting, J. C. Gore, W. Pham, *Curr. Org. Synth.* **2011**, 8, 521–534.
- [101] J. Tanaka, *Bull. Chem. Soc. Jpn.* **1963**, 36, 1237–1249.
- [102] H. Langhals, *Chem. Ber.* **1985**, 118, 4641–4645.
- [103] A. Rademacher, S. Märkle, H. Langhals, *Chem. Ber.* **1982**, 115, 2927–2934.
- [104] T. Maki, S. Hashimoto, *J. Soc. Chem. Ind. Japan* **1951**, 54, 544–546.
- [105] U. Guhathakurta-Ghosh, R. Aroca, R. O. Loutfy, Y. Nagao, *J. Raman Spectrosc.* **1989**, 20, 795–800.
- [106] Y. Nagao, *Prog. Org. Coatings* **1997**, 31, 43–49.
- [107] S. R. Trenor, A. R. Shultz, B. J. Love, T. E. Long, *Chem. Rev.* **2004**, 104, 3059–3077.
- [108] W.-C. Sun, K. R. Gee, R. P. Haugland, *Bioorg. Med. Chem. Lett.* **1998**, 8, 3107–3110.
- [109] K. R. Gee, W. C. Sun, M. K. Bhalgat, R. H. Upson, D. H. Klaubert, K. A. Latham, R. P. Haugland, *Anal. Biochem.* **1999**, 273, 41–48.
- [110] N. Sekar, *Colourage* **1999**, 46, 55.
- [111] X. Jin, C. Uttamapinant, A. Y. Ting, *Chembiochem* **2011**, 12, 65–70.

- [112] S. Nizamov, K. I. Willig, M. V Sednev, V. N. Belov, S. W. Hell, *Chemistry* **2012**, *18*, 16339–16348.
- [113] H. v. Pechmann, J. B. Cohen, *Berichte der Dtsch. Chem. Gesellschaft* **1884**, *17*, 2187–2191.
- [114] D. J. Maly, F. Leonetti, B. J. Backes, D. S. Dauber, J. L. Harris, C. S. Craik, J. A. Ellman, *J. Org. Chem.* **2002**, *67*, 910–915.
- [115] A. Waggoner, *Methods Enzymol.* **1995**, *246*, 362–373.
- [116] A. Toutchkine, D.-V. Nguyen, K. M. Hahn, *Org. Lett.* **2007**, *9*, 2775–2777.
- [117] R. B. Altman, D. S. Terry, Z. Zhou, Q. Zheng, P. Geggier, R. A. Kolster, Y. Zhao, J. A. Javitch, J. D. Warren, S. C. Blanchard, *Nat. Meth.* **2012**, *9*, 68–71.
- [118] E. J. Adie, S. Kalinka, L. Smith, M. J. Francis, A. Marenghi, M. E. Cooper, M. Briggs, N. P. Michael, G. Milligan, S. Game, *Biotechniques* **2002**, *33*, 1152–4, 1156–1157.
- [119] R. Sjöback, J. Nygren, M. Kubista, *Spectrochim. Acta Part A Mol. Biomol. Spectrosc.* **1995**, *51*, L7–L21.
- [120] G. R. Fleming, A. W. E. Knight, J. M. Morris, R. J. S. Morrison, G. W. Robinson, *J. Am. Chem. Soc.* **1977**, *99*, 4306–4311.
- [121] T. Egawa, Y. Koide, K. Hanaoka, T. Komatsu, T. Terai, T. Nagano, *Chem. Commun.* **2011**, *47*, 4162–4164.
- [122] D. Warther, F. Bolze, J. Léonard, S. Gug, A. Specht, D. Puliti, X.-H. Sun, P. Kessler, Y. Lutz, J.-L. Vonesch, et al., *J. Am. Chem. Soc.* **2010**, *132*, 2585–2590.
- [123] A. H. Coons, M. H. Kaplan, *J. Exp. Med.* **1950**, *91*, 1–13.
- [124] L. D. Lavis, T. J. Rutkoski, R. T. Raines, *Anal. Chem.* **2007**, *79*, 6775–6782.
- [125] W.-C. Sun, K. R. Gee, D. H. Klaubert, R. P. Haugland, *J. Org. Chem.* **1997**, *62*, 6469–6475.
- [126] J. B. Grimm, A. J. Sung, W. R. Legant, P. Hulamm, S. M. Matlosz, E. Betzig, L. D. Lavis, *ACS Chem. Biol.* **2013**, *8*, 1303–1310.
- [127] L. D. Lavis, T.-Y. Chao, R. T. Raines, *ACS Chem. Biol.* **2006**, *1*, 252–260.
- [128] M. Beija, C. A. M. Afonso, J. M. G. Martinho, *Chem. Soc. Rev.* **2009**, *38*, 2410–2433.

- [129] N. Panchuk-Voloshina, R. P. Haugland, J. Bishop-Stewart, M. K. Bhalgat, P. J. Millard, F. Mao, W. Y. Leung, *J. Histochem. Cytochem.* **1999**, *47*, 1179–1188.
- [130] Y. Koide, Y. Urano, K. Hanaoka, W. Piao, M. Kusakabe, N. Saito, T. Terai, T. Okabe, T. Nagano, *J. Am. Chem. Soc.* **2012**, *134*, 5029–5031.
- [131] K. Kolmakov, V. N. Belov, J. Bierwagen, C. Ringemann, V. Müller, C. Eggeling, S. W. Hell, *Chemistry* **2010**, *16*, 158–166.
- [132] J. Karolin, L. B.-A. Johansson, L. Strandberg, T. Ny, *J. Am. Chem. Soc.* **1994**, *116*, 7801–7806.
- [133] E. V. de Wael, J. A. Pardoën, J. A. van Koeveringe, J. Lugtenburg, *Recl. des Trav. Chim. des Pays-Bas* **2010**, *96*, 306–309.
- [134] B. Hinkeldey, A. Schmitt, G. Jung, *ChemPhysChem* **2008**, *9*, 2019–2027.
- [135] J.-S. Lee, N. Kang, Y. K. Kim, A. Samanta, S. Feng, H. K. Kim, M. Vendrell, J. H. Park, Y.-T. Chang, *J. Am. Chem. Soc.* **2009**, *131*, 10077–10082.
- [136] M. Kamiya, K. Johnsson, *Anal. Chem.* **2010**, *82*, 6472–6479.
- [137] W. Zhao, E. M. Carreira, *Angew. Chem. Int. Ed. Engl.* **2005**, *44*, 1677–1679.
- [138] A. Loudet, R. Bandichhor, K. Burgess, A. Palma, S. O. McDonnell, M. J. Hall, D. F. O'Shea, *Org. Lett.* **2008**, *10*, 4771–4774.
- [139] I. D. Johnson, H. C. Kang, R. P. Haugland, *Anal. Biochem.* **1991**, *198*, 228–237.
- [140] H.-F. Ji, R. Majithia, X. Yang, X. Xu, K. More, *J. Am. Chem. Soc.* **2008**, *130*, 10056–10057.
- [141] A. Treibs, F.-H. Kreuzer, *Justus Liebigs Ann. Chem.* **1968**, *718*, 208–223.
- [142] Y. Cakmak, S. Kolemen, S. Duman, Y. Dede, Y. Dolen, B. Kilic, Z. Kostereli, L. T. Yildirim, a L. Dogan, D. Guc, et al., *Angew. Chem. Int. Ed. Engl.* **2011**, *50*, 11937–11941.
- [143] S. Duman, Y. Cakmak, S. Kolemen, E. U. Akkaya, Y. Dede, *J. Org. Chem.* **2012**, *77*, 4516–4527.
- [144] K. Umezawa, D. Citterio, K. Suzuki, *Anal. Sci.* **2014**, *30*, 327–349.
- [145] A. D. Laurent, C. Adamo, D. Jacquemin, *Phys. Chem. Chem. Phys.* **2014**, *16*, 14334–56.
- [146] X. Qian, Y. Xiao, Y. Xu, X. Guo, J. Qian, W. Zhu, *Chem. Commun.* **2010**, *46*, 6418–6436.

- [147] J. Kurlach, P. Schwille, W. W. Webb, G. W. Feigenson, *Proc. Natl. Acad. Sci.* **1999**, *96*, 8461–8466.
- [148] X. Li, S. Zhang, J. Cao, N. Xie, T. Liu, B. Yang, Q. He, Y. Hu, *Chem. Commun.* **2013**, *49*, 8656–8658.
- [149] N. Kaur, P. Kaur, K. Singh, *RSC Adv.* **2014**, *4*, 29340.
- [150] W. Wu, J. Zhao, H. Guo, J. Sun, S. Ji, Z. Wang, *Chemistry* **2012**, *18*, 1961–1968.
- [151] Y. Jeong, J. Yoon, *Inorganica Chim. Acta* **2012**, *381*, 2–14.
- [152] R. Ziessel, G. Ulrich, A. Harriman, *New J. Chem.* **2007**, *31*, 496.
- [153] J. Banuelos, F. L. Arbeloa, T. Arbeloa, V. Martinez, I. L. Arbeloa, in *Appl. Sci. Innov. Pvt. Ltd.*, **2012**, 641–677.
- [154] F. Arbeloa, J. Banuelos, V. Martnez, T. Arbeloa, I. Arbeloa, *Trends Phys. Chem.* **2008**, *13*, 101 – 122.
- [155] M. Shah, K. Thangaraj, M.-L. Soong, L. T. Wolford, J. H. Boyer, I. R. Politzer, T. G. Pavlopoulos, *Heteroat. Chem.* **1990**, *1*, 389–399.
- [156] A. B. Nepomnyashchii, M. Bröring, J. Ahrens, A. J. Bard, *J. Am. Chem. Soc.* **2011**, *133*, 8633–8645.
- [157] Y. Chen, J. Zhao, H. Guo, L. Xie, *J. Org. Chem.* **2012**, *77*, 2192–2206.
- [158] A. B. Nepomnyashchii, A. J. Bard, *Acc. Chem. Res.* **2012**, *45*, 1844–1853.
- [159] L. Gai, J. Mack, H. Lu, H. Yamada, D. Kuzuhara, G. Lai, Z. Li, Z. Shen, *Chemistry* **2014**, *20*, 1091–1102.
- [160] L. Wu, K. Burgess, *Chem. Commun.* **2008**, 4933–4935.
- [161] W. Qin, T. Rohand, W. Dehaen, J. N. Clifford, K. Driesen, D. Beljonne, B. Van Averbeke, M. Van der Auweraer, N. Boens, *J. Phys. Chem. A* **2007**, *111*, 8588–8597.
- [162] V. Leen, V. Z. Gonzalvo, W. M. Deborggraeve, N. Boens, W. Dehaen, *Chem. Commun.* **2010**, *46*, 4908–4910.
- [163] T. Rohand, W. Qin, N. Boens, W. Dehaen, *European J. Org. Chem.* **2006**, *2006*, 4658–4663.
- [164] N. Miyaura, A. Suzuki, *Chemistry* **1995**, *95*, 2457–2483.

- [165] K. C. Nicolaou, P. G. Bulger, D. Sarlah, *Angew. Chem. Int. Ed. Engl.* **2005**, *44*, 4442–4489.
- [166] L. Jiao, W. Pang, J. Zhou, Y. Wei, X. Mu, G. Bai, E. Hao, *J. Org. Chem.* **2011**, *76*, 9988–9996.
- [167] H. M. Gilow, D. E. Burton, *J. Org. Chem.* **1981**, *46*, 2221–2225.
- [168] L. Bonardi, G. Ulrich, R. Ziessel, *Org. Lett.* **2008**, *10*, 2183–2186.
- [169] T. Yogo, Y. Urano, Y. Ishitsuka, F. Maniwa, T. Nagano, *J. Am. Chem. Soc.* **2005**, *127*, 12162–12163.
- [170] R. a. Davis, A. R. Carroll, R. J. Quinn, P. C. Healy, A. R. White, *Acta Crystallogr. Sect. E Struct. Reports Online* **2007**, *63*, o4076–o4076.
- [171] A. Poirel, A. De Nicola, P. Retailleau, R. Ziessel, *J. Org. Chem.* **2012**, *77*, 7512–25.
- [172] J. M. Muchowski, D. R. Solas, *Tetrahedron Lett.* **1983**, *24*, 3455–3456.
- [173] C. Bonnier, D. D. Machin, O. Abdi, B. D. Koivisto, *Org. Biomol. Chem.* **2013**, *11*, 3756–3760.
- [174] C. Thivierge, R. Bandichhor, K. Burgess, *Org. Lett.* **2007**, *9*, 2135–2138.
- [175] G. Jung, A. Schmitt, M. Jacob, B. Hinkeldey, *Ann. N. Y. Acad. Sci.* **2008**, *1130*, 131–137.
- [176] S. van de Linde, M. Heilemann, M. Sauer, *Annu. Rev. Phys. Chem.* **2012**, *63*, 519–440.
- [177] M. A. Thompson, M. D. Lew, W. E. Moerner, *Annu. Rev. Biophys.* **2012**, *41*, 321–342.
- [178] D. Wöll, E. Braeken, A. Deres, F. C. De Schryver, H. Uji-i, J. Hofkens, *Chem. Soc. Rev.* **2009**, *38*, 313–328.
- [179] G. De Cremer, B. F. Sels, D. E. De Vos, J. Hofkens, M. B. J. Roeffaers, *Chem. Soc. Rev.* **2010**, *39*, 4703–4717.
- [180] F. Kulzer, T. Xia, M. Orrit, *Angew. Chemie* **2010**, *122*, 866–879.
- [181] S. Manley, J. M. Gillette, G. H. Patterson, H. Shroff, H. F. Hess, E. Betzig, J. Lippincott-Schwartz, *Nat. Methods* **2008**, *5*, 155–157.
- [182] H. P. Lu, L. Xun, X. S. Xie, *Science* **1998**, *282*, 1877–1882.
- [183] Y. Jiang, N. R. Douglas, N. R. Conley, E. J. Miller, J. Frydman, W. E. Moerner, *Proc. Natl. Acad. Sci. U. S. A.* **2011**, *108*, 16962–16967.

- [184] L. C. Tabares, D. Kostrz, A. Elmalk, A. Andreoni, C. Dennison, T. J. Aartsma, G. W. Canters, *Chemistry* **2011**, *17*, 12015–12019.
- [185] M. B. J. Roeffaers, G. De Cremer, J. Libeert, R. Ameloot, P. Dedecker, A.-J. Bons, M. Bückins, J. A. Martens, B. F. Sels, D. E. De Vos, et al., *Angew. Chem. Int. Ed. Engl.* **2009**, *48*, 9285–9289.
- [186] K. Velonia, O. Flomenbom, D. Loos, S. Masuo, M. Cotlet, Y. Engelborghs, J. Hofkens, A. E. Rowan, J. Klafter, R. J. M. Nolte, et al., *Angew. Chem. Int. Ed. Engl.* **2005**, *44*, 560–564.
- [187] P. Chen, W. Xu, X. Zhou, D. Panda, A. Kalininskiy, *Chem. Phys. Lett.* **2009**, *470*, 151–157.
- [188] T. Tachikawa, S. Yamashita, T. Majima, *Angew. Chem. Int. Ed. Engl.* **2010**, *49*, 432–435.
- [189] S. M. Canham, J. Y. Bass, O. Navarro, S.-G. Lim, N. Das, S. A. Blum, *Organometallics* **2008**, *27*, 2172–2175.
- [190] A. Kiel, J. Kovacs, A. Mokhir, R. Krämer, D.-P. Hertel, *Angew. Chemie* **2007**, *119*, 3427–3430.
- [191] R. Ameloot, M. Roeffaers, M. Baruah, G. De Cremer, B. Sels, D. De Vos, J. Hofkens, *Photochem. Photobiol. Sci.* **2009**, *8*, 453–456.
- [192] P. D. Bartlett, *Rec. Chem. Prog.* **1950**, *11*, 47–51.
- [193] A. Schmitt, B. Hinkeldey, B. Hötzer, G. Jung, *J. Phys. Org. Chem.* **2009**, *22*, 1233–1238.
- [194] H. Cousin, O. Trapp, V. Peulon-Agasse, X. Pannecoucke, L. Banspach, G. Trapp, Z. Jiang, J. C. Combret, V. Schurig, *European J. Org. Chem.* **2003**, *2003*, 3273–3287.
- [195] C. Lang, U. Gärtner, O. Trapp, *Chem. Commun.* **2011**, *47*, 391–393.
- [196] R. D. Bach, C. Canepa, J. E. Winter, P. E. Blanchette, *J. Org. Chem.* **1997**, *62*, 5191–5197.
- [197] H. Shi, Z. Zhang, Y. Wang, *J. Mol. Catal. A Chem.* **2005**, *238*, 13–25.
- [198] H. C. Kolb, M. G. Finn, K. B. Sharpless, *Angew. Chem. Int. Ed. Engl.* **2001**, *40*, 2004–2021.
- [199] R. Huisgen, L. Möbius, G. Müller, H. Stangl, G. Szeimies, J. M. Vernon, *Chem. Ber.* **1965**, *98*, 3992–4013.
- [200] C. W. Tornøe, C. Christensen, M. Meldal, *J. Org. Chem.* **2002**, *67*, 3057–3064.

- [201] V. V Rostovtsev, L. G. Green, V. V Fokin, K. B. Sharpless, *Angew. Chem. Int. Ed. Engl.* **2002**, *41*, 2596–2599.
- [202] M. Meldal, C. W. Tornøe, *Chem. Rev.* **2008**, *108*, 2952–3015.
- [203] K. Ding, L.-X. Dai, Eds., *Organic Chemistry - Breakthroughs and Perspectives*, Wiley-VCH Verlag GmbH & Co. KGaA, Weinheim, Germany, **2012**.
- [204] C. R. Becer, R. Hoogenboom, U. S. Schubert, *Angew. Chem. Int. Ed. Engl.* **2009**, *48*, 4900–4908.
- [205] M. A. Tasdelen, Y. Yagci, *Angew. Chem. Int. Ed. Engl.* **2013**, *52*, 5930–5938.
- [206] E. M. Sletten, C. R. Bertozzi, *Acc. Chem. Res.* **2011**, *44*, 666–676.
- [207] C. Le Droumaguet, C. Wang, Q. Wang, *Chem. Soc. Rev.* **2010**, *39*, 1233–1239.
- [208] S. Lepthien, L. Merkel, N. Budisa, *Angew. Chem. Int. Ed. Engl.* **2010**, *49*, 5446–5450.
- [209] B. B. Kasten, X. Ma, H. Liu, T. R. Hayes, C. L. Barnes, S. Qi, K. Cheng, S. C. Bottorff, W. S. Slocumb, J. Wang, et al., *Bioconjug. Chem.* **2014**, *25*, 579–592.
- [210] A. A. H. Ahmad Fuaad, F. Azmi, M. Skwarczynski, I. Toth, *Molecules* **2013**, *18*, 13148–13174.
- [211] H. Wang, J. He, M. Zhang, Y. Tao, F. Li, K. C. Tam, P. Ni, *J. Mater. Chem. B* **2013**, *1*, 6596.
- [212] L.-T. T. Nguyen, J. Devroede, K. Plasschaert, L. Jonckheere, N. Haucourt, F. E. Du Prez, *Polym. Chem.* **2013**, *4*, 1546.
- [213] X.-L. Sun, C. L. Stabler, C. S. Cazalis, E. L. Chaikof, *Bioconjug. Chem.* **2005**, *17*, 52–57.
- [214] R. Manova, T. A. van Beek, H. Zuilhof, *Angew. Chem. Int. Ed.* **2011**, *50*, 5428–5430.
- [215] L. Jia, Z. Cheng, L. Shi, J. Li, C. Wang, D. Jiang, W. Zhou, H. Meng, Y. Qi, D. Cheng, et al., *Appl. Radiat. Isot.* **2013**, *75*, 64–70.
- [216] L. Liang, D. Astruc, *Coord. Chem. Rev.* **2011**, *255*, 2933–2945.
- [217] E. Ganapathi, S. Madhu, M. Ravikanth, *Tetrahedron* **2014**, *70*, 664–671.
- [218] K. Sivakumar, F. Xie, B. M. Cash, S. Long, H. N. Barnhill, Q. Wang, *Org. Lett.* **2004**, *6*, 4603–4606.
- [219] V. Hornillos, E. Carrillo, L. Rivas, F. Amat-Guerri, A. U. Acuña, *Bioorg. Med. Chem. Lett.* **2008**, *18*, 6336–6339.

- [220] E. M. Hensle, S. A. Blum, *J. Am. Chem. Soc.* **2013**, *135*, 12324–12328.
- [221] L.-Y. Niu, Y.-S. Guan, Y.-Z. Chen, L.-Z. Wu, C.-H. Tung, Q.-Z. Yang, *Chem. Commun.* **2013**, *49*, 1294–1296.
- [222] L.-Y. Niu, Y.-S. Guan, Y.-Z. Chen, L.-Z. Wu, C.-H. Tung, Q.-Z. Yang, *J. Am. Chem. Soc.* **2012**, *134*, 18928–18931.
- [223] J. Shang, N. M. Gallagher, F. Bie, Q. Li, Y. Che, Y. Wang, H. Jiang, *J. Org. Chem.* **2014**, *79*, 5134–5144.
- [224] D. Elson, J. Requejo-Isidro, I. Munro, F. Reavell, J. Siegel, K. Suhling, P. Tadrus, R. Benninger, P. Lanigan, J. McGinty, et al., *Photochem. Photobiol. Sci.* **2004**, *3*, 795–801.
- [225] J.-L. Chen, X.-F. Cao, J.-Y. Wang, L.-H. He, Z.-Y. Liu, H.-R. Wen, Z.-N. Chen, *Inorg. Chem.* **2013**, *52*, 9727–9740.
- [226] N. Lucchetti, S. Lancianesi, M. Petrini, *European J. Org. Chem.* **2014**, 5433–5441.
- [227] L. W. K. Moodie, D. S. Larsen, *European J. Org. Chem.* **2014**, *2014*, 1684–1694.
- [228] A. M. Zaed, M. W. Grafton, S. Ahmad, A. Sutherland, *J. Org. Chem.* **2014**, *79*, 1511–1515.
- [229] R. R. Schrock, *J. Organomet. Chem.* **1986**, *300*, 249–262.
- [230] J.-L. Hérisson, Y. Chauvin, *Die Makromol. Chemie* **1970**, *141*, 161–176.
- [231] M. R. Gagne, R. H. Grubbs, J. Feldman, J. W. Ziller, *Organometallics* **1992**, *11*, 3933–3935.
- [232] M. Scholl, S. Ding, C. W. Lee, R. H. Grubbs, *Org. Lett.* **1999**, *1*, 953–956.
- [233] R. Grubbs, S. Chang, *Tetrahedron* **1998**, *54*, 4413 – 4450.
- [234] C. Bielawski, R. Grubbs, *Angew. Chemie* **2000**, *39*, 2903–2906.
- [235] P. Schwab, M. B. France, J. W. Ziller, R. H. Grubbs, *Angew. Chemie Int. Ed.* **1995**, *34*, 2039–2041.
- [236] M. Scholl, T. M. Trnka, J. P. Morgan, R. H. Grubbs, *Tetrahedron Lett.* **1999**, *40*, 2247–2250.
- [237] M. Scholl, S. Ding, C. W. Lee, R. H. Grubbs, *Org. Lett.* **1999**, *1*, 953–956.

- [238] T. M. Trnka, J. P. Morgan, M. S. Sanford, T. E. Wilhelm, M. Scholl, T.-L. Choi, S. Ding, M. W. Day, R. H. Grubbs, *J. Am. Chem. Soc.* **2003**, *125*, 2546–2558.
- [239] W. Zhang, J. S. Moore, *Adv. Synth. Catal.* **2007**, *349*, 93–120.
- [240] A. H. Hoveyda, A. R. Zhugralin, *Nature* **2007**, *450*, 243–251.
- [241] J. Huang, E. D. Stevens, S. P. Nolan, J. L. Petersen, *J. Am. Chem. Soc.* **1999**, *121*, 2674–2678.
- [242] E. L. Dias, S. T. Nguyen, R. H. Grubbs, *J. Am. Chem. Soc.* **1997**, *119*, 3887–3897.
- [243] P. Schwab, R. Grubbs, J. Ziller, *J. Am. Chem. Soc.* **1996**, *118*, 100–110.
- [244] P. Kos, H. Plenio, *Chem. - A Eur. J.* **2014**, *21*, 1088–1095.
- [245] M. B. Dinger, J. C. Mol, *Organometallics* **2003**, *22*, 1089–1095.
- [246] S. H. Hong, A. G. Wenzel, T. T. Salguero, M. W. Day, R. H. Grubbs, *J. Am. Chem. Soc.* **2007**, *129*, 7961–7968.
- [247] R. Kadyrov, A. Rosiak, *Beilstein J. Org. Chem.* **2011**, *7*, 104–110.
- [248] Y. Han, D. Mayer, A. Offenhäusser, S. Ingebrandt, *Thin Solid Films* **2006**, *510*, 175–180.
- [249] R. Roy, S. Hohng, T. Ha, *Nat. Meth.* **2008**, *5*, 507–516.
- [250] A. M. van Oijen, *Curr. Opin. Biotechnol.* **2011**, *22*, 75–80.
- [251] H. P. Latscha, U. Kazmaier, H. Klein, *Organische Chemie*, Springer Science & Business Media B.V., Heidelberg, **2008**.
- [252] J. Clayden, N. Greeves, S. Warren, *Organic Chemistry*, Oxford University Press, Oxford, **2012**.
- [253] J. M. Baskin, J. A. Prescher, S. T. Laughlin, N. J. Agard, P. V Chang, I. A. Miller, A. Lo, J. A. Codelli, C. R. Bertozzi, *Proc. Natl. Acad. Sci. U. S. A.* **2007**, *104*, 16793–16797.
- [254] M. Hesse, H. Meier, B. Zeeh, *Spektroskopische Methoden in Der Organischen Chemie*, Georg Thieme Verlag, Stuttgart, **2005**.
- [255] L. Ghosez, C. Franc, F. Denonne, C. Cuisinier, R. Touillaux, *Can. J. Chem.* **2001**, *79*, 1827–1839.
- [256] T. Eicher, S. Hauptmann, A. Speicher, *The Chemistry of Heterocycles*, Wiley-VCH Verlag GmbH & Co. KGaA, Weinheim, Germany, **2012**.

- [257] L. F. Tietze, T. Eicher, U. Diederichsen, A. Speicher, *Reactions and Syntheses*, Wiley-VCH Verlag GmbH & Co. KGaA, Weinheim, Germany, **2007**.
- [258] G. R. Fulmer, A. J. M. Miller, N. H. Sherden, H. E. Gottlieb, A. Nudelman, B. M. Stoltz, J. E. Bercaw, K. I. Goldberg, *Organometallics* **2010**, *29*, 2176–2179.
- [259] H. E. Gottlieb, V. Kotlyar, A. Nudelman, *J. Org. Chem.* **1997**, *62*, 7512–7515.

9. List of abbreviations

abs	Absorption
a.u.	augmented unit
Bodipy	Boron dipyrromethen
bs	broad singlet
Bu	Butyl
ⁿ Bu	normal Butyl
^t Bu	tertiary Butyl
cat.	catalytic amounts
CM	cross metathesis
Cy	cyclohexyl
d	doublet
dd	doublet of doublets
δ	chemical shift
dest.	distilled
DCM	methylene chloride
DMF	Dimethylformamide
em	Emission
exc	Excitation
fl	fluorescence
Et	ethyl
Hz	hertz
J	coupling constant
chap.	chapter
m	multipllett
mL	milliliter
Me	methyl
Mes	mesityl
NBS	N-bromosuccinimid
NHC	N-heterocyclic carbene
nm	nanometer
NMR spectroscopy	nuclear magnetic resonance spectroscopy
p.	page
Ph	phenyl
ppm	parts per million
ⁱ Pr	iso-propyl
q	quartet
RCM	ring closing metathesis
ROM(P)	ring opening metathesis (polymerisation)
tert.	tertiary
THF	tetrahydrofuran
UV-Vis	Ultra-violet to visible light spectra

10. Scientific contributions

Scientific journals

“Distinguishing Alternative Reaction Pathways by Single-Molecule Fluorescence Spectroscopy” - A. Rybina, C. Lang, M. Wirtz, K. Großmayer, A. Kurz, F. Maier, A. Schmitt, O. Trapp, G. Jung, D.-P. Hertel, *Angew. Chem. Int. Ed.* **2013**, *52*, 6322–6325.

<http://onlinelibrary.wiley.com/doi/10.1002/anie.201300100/abstract>

“Direkte Beobachtung alternativer Reaktionswege durch Einzelmolekülfluoreszenzspektroskopie” - A. Rybina, C. Lang, M. Wirtz, K. Großmayer, A. Kurz, F. Maier, A. Schmitt, O. Trapp, G. Jung, D.-P. Hertel, *Angew. Chem.* **2013**, *125*, 6445–6449.

<http://onlinelibrary.wiley.com/doi/10.1002/ange.201300100/abstract>

“Toward Single-Molecule Catalysis” – A. Rybina, M. Wirtz, D. Brox, R. Krämer, G. Jung, D.-P. Hertel, *Molecular Catalysts: Structure and Functional Design* - L. H. Gade, P. Hofmann, **Wiley VCH**, Juli 2014, Weinheim, ISBN: 978-3-527-33521-3.

<http://onlinelibrary.wiley.com/doi/10.1002/9783527673278.ch3/summary>

“Two-Color Emissive Probes for Click Reactions” – M. Wirtz, A. Grüter, P. Rebmann, T. Dier, D. A. Volmer, V. Huch, G. Jung, *Chem. Comm.* **2014**, *50*, 12694 – 12697.

<http://pubs.rsc.org/en/content/articlelanding/2014/cc/c4cc05288a - !divAbstract>

“A Two-Color Fluorogenic Carbene-Complex for Metathesis Reaction” – M. Wirtz, A. Grüter, F. Heib, V. Huch, J. Zapp, D.-P. Hertel, M. Schmitt, G. Jung, *submitted*.

Scientific conferences

Poster presentations

"Spectroscopic Investigations of Fluorescent Dyes and their Chemical Reactions", N. Baltes, M. Wirtz, G. Nürnberg, G. Jung, 12th Methods and Applications of Fluorescence, 2011, Strasbourg, France.

"Fluorophors for Investigating Organic Reactions on a Single-Molecule Level", M. Wirtz, A. Rybina, C. Lang, O. Trapp, D.-P. Herten and G. Jung, 4th EuCheMS Chemistry Congress, 2012, Prague, Czech Republic.

"Fluorophors for Investigating Organic Reactions on a Single-Molecule Level", M. Wirtz, A. Rybina, C. Lang, O. Trapp, D.-P. Herten and G. Jung, Tag der Chemie – Universität des Saarlandes, 2012, Saarbrücken, Germany.

"Mechanistic Investigations by Single-Molecule Spectroscopy – An Approach to the Metathesis Reaction", M. Wirtz, A. Rybina, J. Menges, C. Lang, O. Trapp, D.-P. Herten and G. Jung, Heidelberg Forum of Molecular Catalysis – Universität Heidelberg, 2013, Heidelberg, Germany.

"Mechanistic Investigations by Single-Molecule Fluorescence Spectroscopy – An Approach to the Metathesis Reaction", M. Wirtz, A. Rybina, J. Menges, C. Lang, O. Trapp, D.-P. Herten and G. Jung, Tag der Chemie – Universität des Saarlandes, 2013, Saarbrücken, Germany.

"Mechanistic Investigations by Single-Molecule Fluorescence Spectroscopy – An Approach to the Metathesis Reaction", M. Wirtz, A. Rybina, J. Menges, C. Lang, O. Trapp, D.-P. Herten and G. Jung, Trends in Molecular Catalysis – Universität Heidelberg, 2013, Heidelberg, Germany.

Oral presentations

„Mechanistic Investigations by Single-Molecule Fluorescence Spectroscopy – From Epoxidation to the Metathesis Reaction", M. Wirtz, A. Rybina, J. Menges, D.-P. Herten, G. Jung, 13th Methods and Applications of Fluorescence, 2013, Genova, Italy.